Experimental Investigations of Residual Strength and Repaired Strength of Corrosion Damaged Prestressed Bridge Beams

Ali Alfailakawi

Dissertation submitted to the faculty of the Virginia Polytechnic Institute and State University in partial fulfillment of the requirements for the degree of

Doctor of Philosophy

in

Civil Engineering

Matthew H. Hebdon, Chair

Carin L. Roberts-Wollmann, Co-Chair

Ioannis Koutromanos

David W. Mokarem

June 13, 2022

Blacksburg, Virginia

Keywords: Corrosion Damage, Flexural strength, Prestressed concrete girders, Bridges, Forensic engineering, Residual flexural strength

Experimental Investigations of Residual Strength and Repaired Strength of Corrosion Damaged Prestressed Bridge Beams

Ali Alfailakawi

Abstract

The durability of infrastructure components, such as prestressed concrete bridge beams, can be significantly affected by long-term deterioration associated with corrosion. Corrosion is a major concern for bridges in Virginia, due to the frequent use of deicing salts during the winter, as well as the number of structures in marine environments. The residual capacity of corrosion damaged prestressed I-beams and box beams needs to be accurately estimated to determine if damaged bridges need to be posted, and to help with making informed decisions related to repair, rehabilitation and replacement of damaged bridges.

The initial stage of the research investigated the ability to determine the in-situ strength of members that have visible corrosion-related damage. In this stage, six corrosion-damaged beams were investigated. Prior to testing, the beams were visually inspected and damage was documented. The beams were then tested in the lab to determine their flexural strength. Following testing, samples of strands were removed and tested to determine their tensile properties while cores were taken to determine compressive strength. Powdered concrete samples were removed to perform chloride concentration tests. The tested strengths of the beams were compared to calculated strengths using two methods for damage estimation and two different calculation approaches.

Two repair methods were then evaluated through large-scale experimental testing, aimed at restoring the strength of deteriorated prestressed concrete beams. The investigated repairs

included External Post-Tensioning (PT) and Carbon Fiber Reinforced Polymer (CFRP) laminates applied to the bottom flange of beams for flexural strengthening. A total of five full-scale bridge members were tested to failure throughout this stage. All beams were subjected to monotonically increasing loads until failure. For beams repaired with external PT, the experimental test was accompanied by a detailed approach for determining the ultimate failure load, the ultimate stress in the external tendons, and the location of the failure. For beams repaired with CFRP, the experimental test was accompanied by a parametric study that was performed to determine the maximum reduction in flexural strength for which CFRP can be considered as a viable repair method to restore the lost capacity.

This dissertation provides additional information on estimating the residual capacity of corrosion-damaged beams and shows the types of repair that can restore their original strength. With this information, Departments of Transportation (DOT) can properly determine what types of repair are a suitable for the damaged girders based on their level of corrosion.

Experimental Investigations of Residual Strength and Repaired Strength of Corrosion Damaged Prestressed Bridge Beams

Ali Alfailakawi

General Audience Abstract

Many bridges in the United States were built using longitudinal members, called girders, made of prestressed concrete. In prestressed concrete, because concrete cannot resist high tensile forces, tensioned steel cables, called strands, are used to produce compression on the concrete member to improve its behavior when it is in service. Corrosion induces cracks in the concrete superstructure which accelerates the deterioration rate and can result in a partial loss of the concrete body and exposure of the embedded steel. This causes degradation in the load-carrying capacity of the bridge girders which raises a danger to vehicles, passengers, and pedestrians. The residual capacity of corrosion damaged prestressed I-beams and box beams needs to be accurately estimated to determine if damaged bridges need to be posted, and to help with making informed decisions related to repair, rehabilitation and replacement of damaged bridges.

The initial stage of the research investigated the ability to determine the in-situ strength of members that have visible corrosion-related damage. In this stage, six corrosion-damaged beams were investigated. Prior to testing, the beams were visually inspected, and damage was documented. The beams were then tested in the lab. Following testing, samples of strands were removed and tested to determine their tensile properties while cores were taken to determine compressive strength. Powdered concrete samples were removed to perform chloride concentration tests. The tested strengths of the beams were compared to calculated strengths.

Two repair methods were then evaluated through large-scale experimental testing, aimed at restoring the strength of deteriorated prestressed concrete beams. The investigated repairs included External Post-Tensioning (PT) and Carbon Fiber Reinforced Polymer (CFRP) sheets applied to the bottom of beams for flexural strengthening. A total of five full-scale bridge members were tested to failure throughout this stage. All beams were subjected to monotonically increasing loads until failure. For beams repaired with external PT, the experimental test was accompanied by a detailed approach for determining the ultimate failure load, the ultimate stress in the external tendons, and the location of the failure. For beams repaired with CFRP, the experimental test was accompanied by a parametric study that was performed to determine the maximum reduction in flexural strength for which CFRP can be considered as a viable repair method to restore the lost capacity.

This dissertation provides additional information on estimating the residual capacity of corrosion-damaged beams and shows the types of repair that can restore their original strength. With this information, Departments of Transportation (DOT) can properly determine what types of repair are a suitable for the damaged girders based on their level of corrosion.

To my parents, Shareefa Burabee and Hussain Alfailakawi, there are no words that can truly express the level of gratitude and appreciation I have for you. You are the best parents a son could ask for. I would not be where I am today without your constant love and encouragement. As you like to remind me: “Nothing good comes easily”.

Acknowledgments

Firstly, I would like to thank God for the opportunity to pursue my studies at Virginia Tech. Secondly, I would like to thank my government for supporting me during my educational journey.

I would like to express my gratitude to my advisor, Dr. Roberts-Wollmann (or mom as we called her behind her back), for providing me with this great opportunity to learn and grow as a structural engineer. Dr. Wollmann has been an amazing mentor, guide, and support throughout my time at Virginia Tech. Her insight, knowledge, and expertise were invaluable. Also, I would like to thank Dr. Matthew Hebdon for being my advisor and for his continuous encouragement and motivation throughout my journey at Virginia Tech. I also appreciate Dr. Ioannis Koutromanos and Dr. David Mokarem for serving on my graduate committee, and providing valuable feedback and suggestions throughout my time at Virginia Tech.

I would like to thank Virginia Tech for welcoming me and providing me with the environment to pursue my studies. I would also like again to thank Dr. David Mokarem and lab technicians Brett Farmer and Garrett Blankenship at the Thomas M. Murray Structures Laboratory, for their help throughout the project. It was great having you around to assist me anytime and anywhere. I thankfully acknowledge the support of the Virginia Department of Transportation (VDOT) and the Virginia Transportation Research Council (VTRC) to this project which I had the advantage to be part of.

A special thanks to my friend Abdullah Al Rufaydah, who never fails to make me smile, and for his support and kindness during the lab's long days and nights. This project would not have been possible without your constant help and assistance at every step. A special thanks to my friends at Tech: Samuel Sherry, Rashed Alarrak and Japsimran Singh.

A special thanks to my brothers, Abdullah, Meshari and Essa, and my sister Mariam for their constant love, care, and support. Lastly, a very special thank you to my wife, Shatha Alhouli whose constant love and support was integral in my success.

TABLE OF CONTENTS

LIST OF FIGURES

LIST OF TABLES

CHAPTER 1: Introduction

1.1 Motivation and Overview

Corrosion in concrete bridge girders is a concern that impacts bridge strength and durability, as well as passenger and vehicle safety. Many bridges were built in the United States throughout the 1950s and 1960s. According to (Naito et al., 2011), the majority of wearing surfaces were built directly on the superstructure without the use of waterproofing barriers. While the concrete cover is intended to protect the reinforcing steel, chloride accumulation to a certain limit might cause corrosion in the embedded reinforcement. Bridge collapses and shutdowns due to corrosion have generated concerns about the durability of other bridges that are still in operation. Deicing chemicals are commonly used in Virginia to keep roadways safe during the winter season. Through concrete cracks and expansion joints, these chemicals may seep and reach the reinforcing steel. Furthermore, bridges erected in coastal locations are vulnerable to corrosion due to saltwater spray. Even though bridges are examined and load rated on a regular basis, corrosion damage may not be evident on the concrete surface until it has progressed to an advanced degree. The techniques and instruments used to identify corrosion damage in concrete bridges are advancing. Recently, a nondestructive corrosion detection approach based on magnetic flux leakage has shown promise for identifying corrosion damage in box girders at an early stage. This equipment is inexpensive and may be used in the bridge inspection procedure (Chase & Balakumaran, 2020).

There is currently only a small amount of experimental study on bridge girders affected by corrosion. (Naito et al., 2010a) conducted a thorough research program to investigate corrosion-damaged precast, prestressed adjacent box beams with the goal of providing

recommendations for calculating residual strength based on visual inspections. They gathered beams from demolished bridges and conducted forensic examinations. Although a prior study effort (Harries, 2009) assessed two beams from an adjacent box beam bridge, no physical tests were undertaken as part of this program to determine real flexural strength.

This present research is part of a larger initiative at Virginia Tech that is supported by the Virginia Department of Transportation (VDOT) and the Virginia Transportation Research Council (VTRC) to examine and repair bridges in Virginia that are deteriorating due to corrosion. External post-tensioning reinforcement, CFRP, and other repair procedures are available. For this study, eighteen beams were retrieved from three different bridges in Virginia and sent to Virginia Tech's Thomas Murray Structures Lab for destructive testing. These girders display varied degrees of degradation. The present work assesses the existing state of these corroded damaged prestress concrete girders and develops a procedure for calculating residual strength. It also demonstrates the impact of selected repair procedures on capacity restoration.

1.2 Dissertation Organization

This dissertation is organized as a manuscript format, where traditional chapters are replaced by manuscripts. Each manuscript has been, or will shortly be submitted to a peer-reviewed journal. Each of the manuscripts in this dissertation appear in their most refined format, either as the submitted version or based on improvements made during the peer-review process. Three journal papers are presented, of which a majority of the research and primary authorship was completed by the author of this dissertation.

Chapter 1 provides an introduction, motivation, and overview of the research to this dissertation. Chapter 2 provides a literature review comprised of relevant topics about corroded

damaged prestressed girder and methods for repairment. A historical look at the corrosion effects on the girders and strength capacity will be examined. This will be followed by a review of more contemporary research findings that investigated research topics and how different variables, (e.g., type of structure, element age, traffic flow, and environmental exposure) can affect the overall behavior of a girder. The literature review was conducted for applications relating to flexural retrofits either by using external post tensioning or CFRP. Analytical prediction models were reviewed for external post tensioning repair.

Chapter 3 presents the journal article titled "Experimental and Analytical Evaluation of Residual Capacity of Corrosion-Damaged Prestressed Concrete Bridges Girders".

Chapter 4 presents the journal article titled "Flexural Strengthening Repair of Corroded Damaged Bridge Girders Using External Post-Tensioning Method".

Chapter 5 presents the journal article titled "Flexural Strengthening Repair of Corroded Damaged Bridge Girders Using CFRP Method".

Chapter 6 provides recommendations, conclusions, potential areas for future work relating to the research project and Ph.D. contributions.

1.3 Attributions

The research reported in this dissertation was supported and funded by the Virginia Transportation Research Council (VTRC). These research project titles and grant numbers is "Experimental and Analytical Evaluation of Residual Capacity and Repair Methods for Corrosion-Damaged Prestressed Concrete Bridge Girders (Grant No. VTRC XXXXX)."

1.4 Research Purpose and Scope

To provide guidance for bridge inspectors in rating deteriorated girders for flexural strength, some uncertainties regarding flexural strength of girders that show signs of corrosion must be alleviated. Therefore, this study aims to:

- Compare the flexural strength of girders that have different levels of deterioration.
- Investigate the flexural behavior and the failure modes of girders that have different levels of deterioration.
- Evaluate the adequacy of bridges constructed in the 1960's and 1970's in light of the current design codes.
- Evaluate previous recommendations for flexural strength calculation of corrosion damaged prestressed concrete girders.
- Add new full-scale test results to the limited database of flexural strength of corrosion damaged prestressed concrete girders.
- Determine the effect of FRP and external post tensioning as repair methods to restore the flexural strength capacity for the damaged beams.
- Develop a new calculation procedure to determine the ultimate stress in the external post tensioning tendons in order to evaluate the flexural strength capacity.

To achieve the study goals, a comprehensive evaluation of the current literature on the flexural strength of deteriorating bridge girders was done. For flexural testing in the lab, eighteen prestressed concrete bridge girders recovered from decommissioned bridges in Virginia with varying degrees of corrosion damage were chosen. In this work, girders and test configurations were chosen to enable a head-to-head comparison of the flexural strength of damaged and

undamaged, or less damaged, beams. Then, destructive investigation and material tests were carried out to learn more about the girders' in-situ state. The girders' flexural strengths were anticipated using several methodologies from the 2017 AASHTO LRFD and the ACI318-19 codes. These calculations were refined using actual material properties, measurable parameters during physical testing, and literature recommendations. Evaluation of these methods, analyses, and comparisons with the experimental results were performed to reach conclusions. Computer software used to aid in this research were Microsoft Excel, Mathcad prime 6.0 and Response 2000.

CHAPTER 2: Literature Review

The first prestress concrete bridge in the US was built in 1950 and since then this construction technology accelerated rapidly. Nowadays, most of the concrete bridges all around US are built in that fashion. Many research programs have been conducted to study the effect of prestress concrete technology and on methods to maintain and improve this technology (Ciolko, 2005). In order to have a guideline to determine the residual capacity of deteriorated girders and a best-fit repair technique, we need to have a good understanding of how to evaluate the corrosion-damaged girders. Included in this chapter are inspection methods used to assess the types of damage in girders, a summary of published reports and refereed journal papers, and a description of various repair methods.

2.1 Damage of Prestressed Girders

Corrosion of reinforcing steel can cause buildings in harsh environments to exhibit reduced serviceability or safety far sooner than expected, requiring replacement, rehabilitation, or strengthening. Winter snow and ice result in the need for the use of road salts on a regular

basis in order to maintain safe driving conditions. As a consequence, large amounts of chloride are absorbed into concrete bridge decks and beams, resulting in corrosion. The chlorides cause an ionic defect in the passive layer of protection around the steel, resulting in the development of corrosion. The corrosion process causes a volume increase of up to 6.5 times the initial strand size. A radial compression force is generated on the surrounding concrete as the strands corrode and grow in size. Because of the hoop stress or Poisson effect, a tensile stress occurs perpendicular to the compression force, circumferentially to the strand, according to mechanics. A crack forms when the tensile stress exceeds the tensile capacity of the concrete. These cracks can appear horizontally as delamination or vertically as longitudinal cracks. Delamination form when corrosion occurs in multiple strands, and the volumetric expansion of the individual strands work together to split a horizontal section. The cracking mechanism is shown schematically In Figure 2.1.

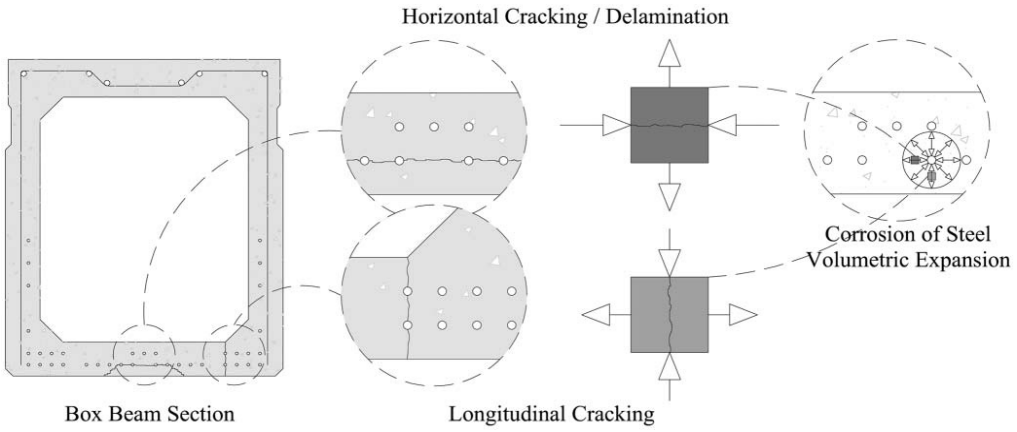

Figure 2.1 Corrosion induced cracking and delamination (Naito et al., 2011)

With that stated, past research on how to assess the status of corroded beams and measure their strength is presented in the following sections.

2.1.1 Non-Destructive Test

Non-destructive testing (NDT) procedures have been developed to assess girder degradation without causing structural damage. NDT assessments are typically based on a variety of techniques, including acoustic, ultrasonic, electromagnetic, and electrochemical methods (Zou, 2014). This section will describe methods including visual inspection, half-cell potential, and resistivity.

2.1.1.1 Visual Inspection

To document the type and extent of the deterioration in the concrete girders, visual inspection is considered as the first step in assessing the concrete girders' conditions (Manning & National, 1985) (Heejeong & D., 2003). Visual inspection of girders can be performed easily since it does not require a lot of specialized equipment. It is required to chip unsound concrete to evaluate the actual condition of the girder. When performing a visual inspection, all types of deterioration should be documented. There are many types of deterioration, such as cracks, section loss, delamination, and exposed strands. Length, width, and orientation of cracks should be noted (Manning & National, 1985). Concrete spalling is easy to measure along with the level of corrosion in the exposed strands, if any. Delamination can be detected by tap testing using a hammer. However, visual inspection is a subjective method since the accuracy depends on the inspector's experience (Shubinsky & Northwestern University (Evanston, 1994)).

2.1.1.2 Half-Cell potential

The half-cell potential approach predicts corrosion in concrete in a rapid, cost-effective, and non-destructive manner by mapping the potential corrosion of the strands and mild reinforcement along the beam. The half-cell measures the potential difference on the concrete

surface between the steel and a standard copper sulfate electrode (Elsener et al., 2003). The electrode should be placed on the embedded steel under the concrete cover to get this measurement. A voltmeter is used to show the potential difference measurement. The lower the voltage, the more likely corrosion is present at the tested location. The procedures and measurements are based on (ASTM-C876, 2015). Potential mapping is the most generally accepted and standardized non-destructive approach for measuring the corrosion condition of reinforcing bars in concrete buildings today (Kiviste et al., 2019).

2.1.1.3 Resistivity

The concrete resistivity is primarily affected by two factors: the concrete quality and moisture content. The higher the moisture content is, the lower the resistivity is. Results obtained from the resistivity test do not indicate whether the reinforcing steel is corroded or not. Rather, they give additional information about the locations which exhibit the conditions that may result in a high corrosion rate. The concrete resistivity is determined using a four-point Wenner probe as per (AASHTO, 2011), in which a current is applied to the two outer probes, and the potential difference is measured between the two inner probes.

2.1.2 Previous Research on Evaluating Corrosion Damage

Corrosion is the main cause for the premature deterioration of concrete structures, and it can effect performance by increasing deflection under service loads and decrease the ultimate capacity of the structure (Rodriguez et al., 1997). A 2.5% corrosion rate can lead to 17% - 25 % reduction in the ultimate strength capacity (Imam et al., 2018), since the deterioration leads to a loss in the cross section of the reinforcing bars (Dasar et al., 2017). (Moawad et al., 2018) noted that prestressed beams can resist the corrosion more than convectional concrete beams, because

they are considered to be crack-free as a result of prestressing. Therefore this section presents a summary of published reports and journal papers discussing the effect of the corrosion on the performance of structures and its correlation with NDT and destructive tests results, if any.

2.1.3.1 (Harries, 2009)

Figure 2.2. Collapse of Lake View Drive Bridge

Two full-scale corroded prestressed adjacent box beams were tested in flexural, and forensically examined afterward. They were recovered from the partially collapsed Lake View Drive Bridge, which failed as a result of dead load only (see Figure 2.2). The main cause of the collapse was a large loss in the section of the prestressing strands (see Figure 2.3). This loss was underestimated by inspectors because it is difficult to visually inspect the box girder at the site.

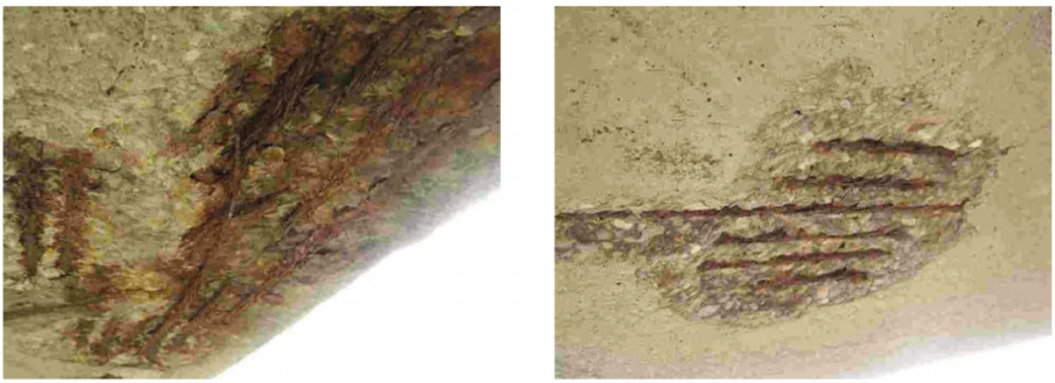

Figure 2.3. Loss and corrosion in the strands (Harries, 2009)

During testing, trapped water was discovered in the voids of the girder. This trapped water raises the possibility of deterioration and corrosion of the top strands in the bottom flange. The two beams were tested under four point loading and failed with rupturing in the strands with 20% and 50% capacity of the original beam, respectively. From the forensic examination, it was observed that the top layer of strands in the bottom flange was corroded, which add more credence to the idea of the effect of the trapped water Figure 2.4.

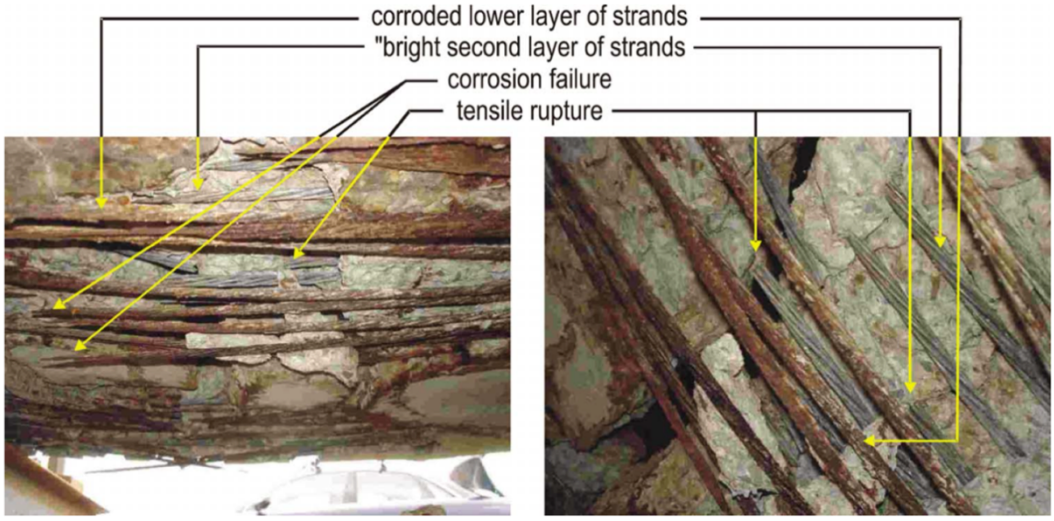

Figure 2.4. Condition of the strands after the test (Harries, 2009)

Furthermore, the concrete cover was less than prescribed in the design drawings, which may have an impact on the strands' durability, limit their protection, and accelerate damage caused by both environmental exposure and mechanical damage. The authors recommended that if a strand is found to be corroded or damaged anywhere along the span, its contribution to flexural strength along the length of the girder should be ignored. However, if the strand loss happens at a specific small location away from the midspan, redevelopment of this strand near the midspan can be assumed. Besides that, transverse cracking indicates significant prestressing loss in the girder, whereas longitudinal cracking should disqualify any strands at that location from being considered in the load rating procedure.

2.1.3.2 (Naito et al., 2010a)

Following the above-mentioned research done by (Harries, 2009), (Naito et al., 2010b) conducted another posttest forensic examination. The authors stated that the main issue in bridge failure was that the concrete cover was less than 1.5 in., and the stirrups were placed on top of the bottom layer of prestressing strand, resulting in even less concrete cover. Furthermore, the vent hole at the top of the beams allowed water to be trapped in the beams, leading to an increase in chloride concentration. The initiation of corrosion was determined by a threshold of 0.032% chloride by mass of concrete. The chloride concentration was higher on the sides of the beams due to water leakage through the shear key as compared to the chloride concentration on the bottom of the beams from salt spray from the road surface. Longitudinal hairline cracks are evidence that there may be an impact on the cross-sectional area of the strands along that crack as well as adjacent strands. As a result, the cross section of the strands should be reduced in flexural strength calculations.

The strands were classified into three corrosion levels and tension tested until failure (see Figure 2.5). The ultimate load capacities of 16 wires were measured. The wires with light corrosion had a tensile strength of 288 ksi, the wires with pitting had a tensile strength of 230 ksi, and the wires with heavy pitting had a tensile strength of 206 ksi.

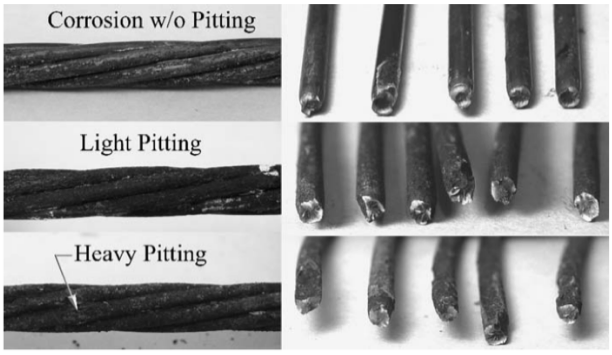

Figure 2.5. Three levels of corrosion (Naito et al., 2010b)

Finally, the authors made load rating recommendations for bridges with moderate damage that are still in use, and main points can be summarized as follow:

- Subtract 100% of all exposed strands plus an additional 25% of these exposed strands, the resulted number of strands should be deducted from the total number of strands and excluded from capacity calculations.
- Strands adjacent to or intersecting a crack are ineffective in the region immediately adjacent to the crack.
- Action must be taken by bridge owners if significant strand loss which is defind as more than 20% of the total number of beam strands, is observed, particularly in fascia beams. Also, action must be taken in the case of beams with no exposed strands but visible internal damage, such as bottom flange cracking with rust and/or delamination.

2.1.3.3 (Naito et al., 2011) *and* (Naito et al., 2010a) *ATLSS REPORT*

Based on visual examination, this investigation was conducted on seven corroded segments of adjacent box girders to assess their flexural strength. These girders were recovered from three different Pennsylvania bridges that had been in use for more than 50 years. To develop a nondestructive approach for determining the remaining flexural strength of corroded girders based on surface degradation, a probabilistic-based research and quantification of corrosion in strands adjacent to longitudinal cracks was conducted. Inspections of all types of degradation, such as spalling, delamination, longitudinal cracks, and exposed strands, as well as half-cell potential and material tests, were conducted as part of the investigation. The study's findings revealed that the fabrication processes used for box-beam construction in the 1950s and 1960s allowed for significant variances in internal void geometries and strand positions. Due to inconsistent strand placement and the fact that stirrups were placed on top of the lower level of

strands, 92 percent of all strands had less cover than required. Next, the cover concrete was removed and strands were exposed. Each degree of corrosion in strands was assigned an index based on sectional loss, as shown in Figure 2.6. The damage indexes were (0) no corrosion, (1) light corrosion, (2) pitting, (3) heavy pitting, (4) wire loss, and (5) fracture.

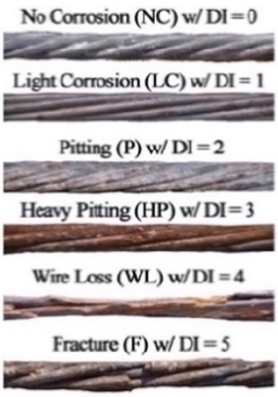

Figure 2.6. Strand damage conditions (Naito et al., 2011)

Furthermore, A chloride level of 0.0130 % by mass of concrete separated the region between light corrosion and no corrosion of prestressing strands; heavy pitting of the strands was possible with chloride levels of 0.005 % and no corrosion with chloride levels of 0.082 %. The use of chloride levels alone was not a reliable indicator of strand corrosion based on the fluctuations and outliers found. According to the probabilistic research, the corrosion degree of strands along the girder is related to the type and location of deterioration. (Naito et al., 2010a) presented guidelines for determining residual flexural strength based on this probabilistic analysis and the observed reduction in tensile strength of corroded strands (see Figure 2.6), which are presented in Table 2.1.

Table 2.1 Damage estimation for strands to calculate flexural capacity for corrodion damaged box beams (Naito et al., 2010a)

Percentage of original cross-sectional area of strands to be included in the strength calculations	**Strand condition**
0%	- All exposed strands
75%	- Strands, in all layers, in line with a longitudinal crack - Exterior strands adjacent to a longitudinal crack located no more than 3 in. from the crack
95%	- All other strands in a longitudinally cracked beam

It is worth noting that Naito et al. proposed that all damage within an inspection window length of two development lengths should be considered to be present at the same section under evaluation simultaneously. The authors concluded that longitudinal cracks were shown to be more effective than half-cell potential and chloride level approaches in identifying corrosion in strands.

2.1.3.3 (Papé & Melchers, 2011)

Three prestressed post-tensioned concrete beams were tested to failure, followed by a close inspection of the condition of the strands and concrete. The I-beams were from a 45-year-old bridge in Australia called the Sorell Causeway Bridge. Because it was exposed to a harsh marine environment, the bridge had suffered significant degradation. Based on the degree of degradation, beams were classified as being in good, moderate, or bad condition. A good beam was considered as the base beam, and the test results revealed that moderate and poor condition beams failed at 70% and 51%, respectively, compared to the good condition beam. The corrosion in the strands was caused mostly by longitudinal cracking along the path of the post-tensioning. Corrosion caused between 75% and 100% loss in the region of the strands, which explained the

test findings. XRD (X-ray diffraction spectroscopy) and SEM (scanning electron microscopy) were used to determine the presence of chloride in the strands, which was most likely affected by the surrounding concrete. Furthermore, there was evidence of the presence of bacteria in several exposed strand locations, which increases the likelihood of corrosion in the steel.

2.1.3.4 (Pape & Melchers, 2013)

Following the above-mentioned study, (Pape & Melchers, 2013) examined three more corroded prestressed beams from the same bridge. The corrosion damage on the tested girders was classified as minor, medium, and heavy. After destructive analysis, the cross-sectional area losses of the tendons at the failure locations due to corrosion were evaluated to be 0%, 57%, and 64%, respectively. Some of these losses had apparent indications of damage on the exterior of the beams, such as rust or cracks, while others had no visible evidence of damage at all. The purpose of this research was to investigate the influence of corrosion damage on failure mode and residual strength. Girders were subjected to four-point loading tests. All of them failed due to wire rupturing. The light, medium, and severe corrosion-damaged girders failed at loads that were 89 %, 61 %, and 45 % of their corresponding undamaged-condition design capacities, respectively. Results showed that the percentage loss of cross-sectional area of the tendon correlated with the residual strength. However, the strength correlation did not apply directly to the girder with minor corrosion since there was no reduction in the cross-sectional area of the tendon at the failure location, even though only 89% of the design capacity was reached.

2.2 Repair Methods

Over the last decades, there has been a rapid increase in the volume and weight of heavy vehicles all over the world. In addition to that, many bridges are more than 50 years old. Thus,

the rate of deterioration in existing bridges is increasing and become a major problem nowadays, due to high traffic, exposure to marine environment, deicing salts and structure aging. Studies showed that external post-tensioning (PT) and Carbon Fiber Reinforced Polymer (CFRP) can be considered as a good option for repairing deteriorated structures. In this section, these types of repairs will be discussed.

2.2.1 External Post-Tensioning

External post-tensioning (PT) can be used as a method of repair to restore the capacity of any structural element. It can increase the strength and serviceability of deteriorated structures (Harajli, 1993). In addition to that, it is considered an economical solution instead of demolishing and rebuilding the structure. Engineers prefer this type of repair because of the speed of construction, minimal disruption to traffic flow and ease to monitor and maintain (Suntharavadivel & Aravinthan, 2005). The repair system includes attaching external tendons to end of the beams by anchorage systems, which leads to an increase in flexural strength (Nassif et al., 2003). The external tendons can be made of steel or CFRP (Bennitz et al., 2012), (Heo et al., 2013). The tendons can follow a straight, harped, or draped path along the length of the beam through a duct which is filled either with grout or flexible fillers (see Figure 2.7 and Figure 2.8).

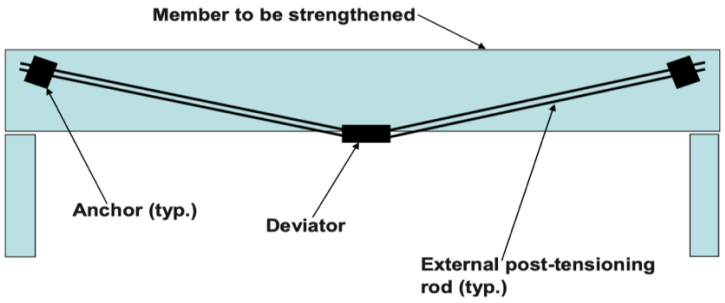

Figure 2.7. Schematic of external post-tensioning using draped profile tendons (Khudeira, 2010)

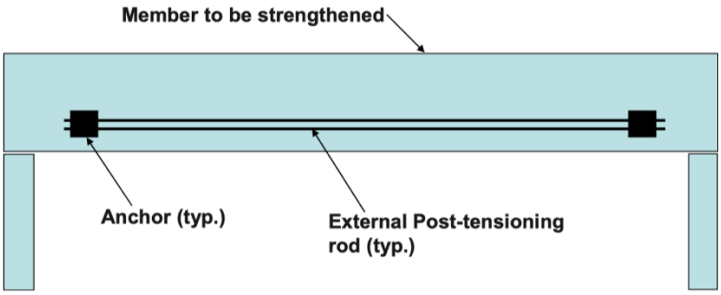

Figure 2.8. Schematic of external post-tensioning using straight profile tendons (Khudeira, 2010)

The external PT system is placed outside the beam section by anchoring the tendons, which can be single (Tao & Du, 1985) or multi strands, at the ends of the beam by two anchors blocks on each side and attaching the deviator points near the mid-span by saddles. The design of the anchorage is crucial to transfer the prestressing force to the beam. There are many types of anchorage and deviation systems that have been used, such as reinforced concrete blocks (Zhang et al., 2020) (Leicht et al.,) (see

Figure 2.9), anchor pins (Lee et al. 2018) (see Figure 2.10), or steel bracket anchorage systems (Sayed-Ahmed et al., 2004) (see Figure 2.10).

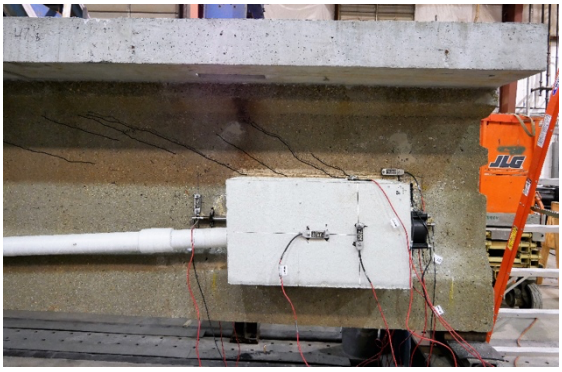

Figure 2.9. Reinforced concrete block anchorage (Leicht et al., 2022)

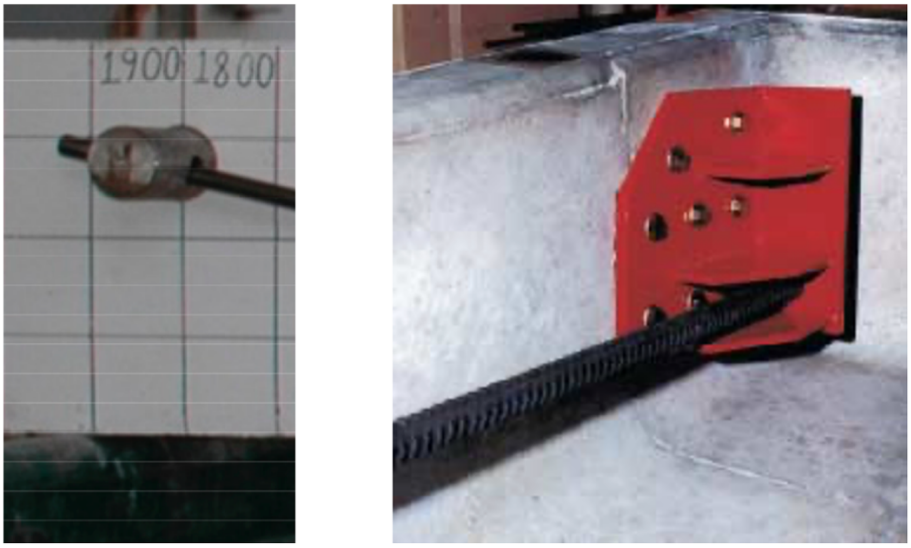

Figure 2.10. Anchor pins and steel bracket anchorage systems (Lee et al., 2018) (Sayed-Ahmed et al., 2004)

(Sayed-Ahmed et al., 2004) tested six corrosion-damaged beams taken from a decommissioned bridge in Alberta (Canada). Two beams were tested with no repair to be considered as an initial state condition, two with CFRP strips and sheets, and two with external post-tensioning repair. A new system with steel anchorage brackets was used for these inverted U-shaped beams. The external PT is introduced through Dywidag bars, which have been anchored at the ends of the beam and deviated at the third points of the beam. The experiment showed external PT repair as an effective repair method increasing the capacity by 20%.

(Bennitz et al., 2012) tested seven reinforced concrete T-beams, one with no repair and six with straight external unbonded CFRP tendons. Initial tendon depth, prestressing force, and the presence of deviators were the varying factors between the six beams. The CFRP tendons were anchored at the end of the beams using external steel brackets. Eventually, all the repaired beams exhibited an increase in strength of more than 17%.(Lee et al., 2018) tested nine pre-damaged beams, three as reference beams and six as post-tensioned beams. Drilled holes in the beams were made and a repetitive loading prior to loading was programmed to imitate a real-life

damaged condition. External PT repair was applied after reaching the yield point and introduced by a high-strength steel rod with a harped V-shaped profile that was deviated at the mid-span with an external saddle. The steel rods were connected to the beam with anchor pins through drilled holes in the beam. (Lee et al., 2018) concluded that the external PT increased the strength and stiffness by 40% and 28%, respectively. Also, he mentioned that the increase in the stiffness of the beams was observed through the reduction of the width in the cracks.

Research has also been done on the repair of existing bridges. (Khudeira, 2010) selected on external PT system as a repair method for the rehabilitation of an existing corrosion-damaged reinforced concrete bridge in Chicago. 150-grade steel threaded bars were anchored to the web at the end of the beams by stiff steel brackets. The brackets were connected to the beam by post-tensioning rods through a drilled holes to ensure sufficient friction between the brackets and the concrete. (Khudeira, 2010) concluded that this method improved the strength, service performance, and durability.

(Zhang et al., 2020) conducted a forensic examination of an existing PT box-girder bridge in China that had been repaired 14 years earlier. The investigation showed many types of deterioration in the bridge, such as vertical deflection, cracking, prestressing loss, and damaged slab. Therefore, he presented a new plan to repair the bridge and improve its capacity, stiffness and reduce the deflection. The plan included a replacement of the concrete deck, additional external post-tensioning tendons, sealing cracks, and patching the spalleed areas. The static loading tests show a reduction in the strains and vertical deflections by 17% and 19%, respectively. The tests verified that the capacity, stiffness, and integrity of the bridge were improved after using this type of repair.

2.2.1.1 Prediction of ultimate stress in unbonded prestressed tendons

External prestressing has seen substantial changes in application, technology, and research since its start in the early 1950s. The approach is particularly suitable for new structure development as well as strengthening and rehabilitation of existing structures. External prestressing allows to decrease web thickness in new bridge construction, whereas external prestressing allows for a considerable increase in the load bearing capacity of older bridges during rehabilitation.

The researchers concentrated on developing reasonable equations for the ultimate stress in unbonded tendons, f_{ps}. Numerous studies and substantial discussion among researchers have been conducted on the prediction of f_{ps} (Roberts-Wollmann et al., 2005) (Naaman & Alkhairi, 1992). The great majority of these research attempted to improve upon previously established prediction equations based on rational techniques in order to make it easier to compute the nominal bending resistance at ultimate, M_n.

It is necessary to investigate calculation of the stress in the tendons at ultimate state. The change in stress in the prestressing steel in bonded prestressed beams can be determined from the strain compatibility between concrete and steel. This indicates that this analysis is section dependent. However, structural analysis of beams with unbonded internal and/or exterior tendons presents multiple issues that have been addressed by several researchers. The fundamental difficulty arises when the perfect bond assumption generally employed for beams with bonded tendons cannot be used, making sectional analysis impossible (Harajli & Naaman, 1985) (Collins & Mitchell, 1987). This is because the strain in the concrete at the level of the prestressed unbonded tendon cannot be expected to be equal to the tendon's strain at that level. This is

mainly because the stress in unbonded tendons is distributed (i.e., averaged) across the member because of the lack of bond between the tendon and the surrounding concrete. Therefore, in the case of beams with unbonded tendons, the global deformation compatibility between the tendons' anchorages must be calculated. The initial cable profile, span to depth ratio, deflection shape of the structure, and beam end characteristics all influence the stress change in tendon (Hussien et al., 2012). As a result, beams with unbonded tendons are more difficult to analyze. Many experimental and analytical studies have been undertaken to measure the stress at ultimate in unbonded tendons. This section discusses previous research that has been conducted to develop prediction equations for the calculation of f_{ps}, according to the date of its publication.

(Harajli, 1990) investigated the influence of member span–depth ratio on f_{ps} and identified it as an independent design parameter. A small number of experimental beam tests were used to validate the analytical findings. The author stated that there was a lack of clarity on the way through which this specific parameter affects f_{ps}.

(Naaman & Alkhairi, 1991) conducted a review of numerous prediction equations used to predict f_{ps} in unbonded tendons, based on existing experimental and analytical research dealing with f_{ps} for studies conducted between 1950 and 1990. The literature study was advanced by comparing predicted to experimental values for the prediction equations for both f_{ps} and Δf_{ps}. The experimental findings were derived from nine separate studies including a total of 143 beams experiments. While the majority of prediction equations produced conservative findings, the authors concluded that there was still space for improvement in accounting for the factors found to have the largest influence on the value of f_{ps}. In general, they found that f_{ps} remains

constrained in unbonded tendons by a lower bound (i.e., the effective prestress, f_{pe}) and an upper bound (i.e., the steel yield strength, f_{py}).

(Naaman & Alkhairi, 1992) introduced a new rational approach for determining the f_{ps} of internally unbonded tendons. To begin, a comprehensive examination of stress expressions in tendons was provided using a bond reduction coefficient, assuming elastic cracking analysis for a variety of loading configurations and tendon profiles. The authors then suggested the idea of the bond reduction coefficient at ultimate nominal resistance Ω_u, as a function of the ratio of the strain increase beyond f_{ps} in unbonded to bonded prestressing steel. The value of Ω_u was determined using the 143 test beams collected in the first portion of the investigation (see equation (1) and (2)). They then employed the factor Ω_u and the ratio c/d_{ps} in their suggested f_{ps} equation (3), which was based on rational beam theory and linear strain distribution assumptions. When compared to previously studied prediction equations, the predicted versus experimental results for f_{ps} and Δf_{ps} indicated exceptional accuracy.

$$\Omega_u = \frac{2.6}{\left(\frac{L}{d_{ps}}\right)} \qquad (1)$$

$$\Omega_u = \frac{5.4}{\left(\frac{L}{d_{ps}}\right)} \qquad (2)$$

$$f_{ps} = f_{pe} + \left(\Delta f_{psu}\right)_m = f_{pe} + \Omega_u E_{ps} \epsilon_{cu} \left(\frac{d_{ps}}{c} - 1\right) \qquad (3)$$

(Lee et al., 1999) proposed a new design equation that takes global compatibility into account as well as the plastic hinge length (see equation (4)). The suggested design equation was generated under the assumption that the primary parameters were determined rationally. Certain coefficients in their equation were found by regression analysis of historical test data.

Additionally, they compared predicted and experimental data using the stress fps specified in the ACI and AASHTO LRFD codes, as well as their own suggested equation. The suggested equation agreed well with the test data, although the codes were little conservative.

$$f_{ps} = 70 + 0.8f_{se} + \frac{1}{15}\frac{(A_s' - A_s) * f_y}{A_{ps}} + 80 \times \sqrt{\frac{d_s * f_c'}{d_p * \rho_{ps}} * \left[\frac{1}{f} + \frac{1}{\left(\frac{L}{d_p}\right)}\right]} \qquad (4)$$

By including the influence of plastic hinges on f_{ps}, (Roberts-Wollmann et al., 2005) established an equation based on test findings and the mechanics of simple collapse mechanisms for predicting the stress in externally unbonded tendons at ultimate. Their model was based on loading either the outer or middle span of a three-span member and on the assumption that "rotation at a support hinge is only half that of a midspan hinge" in agreement with MacGregor's findings (MacGregor, 1989). The authors developed an equation for f_{ps} as a function of $f_{pe,}$ the length of the tendon between anchorages, the number of support hinges needed to establish a mechanism crossed by the tendon, the depth of the neutral axis, assuming yielding of the tensile prestressing steel within the section, and d_{ps} (see equation (5) and (6)). The predicted values of f_{ps} were compared to a comprehensive database of results from previous testing on beams and slabs with unbonded tendons. The equation gave conservative estimates of ultimate stresses and a reasonable approach for forecasting stresses in continuous tendons with several spans. In 1998, their equation was integrated into the AASHTO LRFD specifications (AASHTO, 1998).

$$f_{ps} = f_{pe} + 900\left(\frac{d_p - c}{l_e}\right) \leq f_{py} \qquad (5)$$

$$l_e = \left(\frac{2l_i}{2 + N_s}\right) \qquad (6)$$

The AASHTO LRFD Bridge Design Specifications, (AASHTO, 2017), provide instructions for analyzing beams with bonded and unbonded tendons. Section 5.7.3.1.3 describes two techniques for analyzing such a beam: Detailed Analysis and Simplified Analysis. The detailed analysis considers the strain compatibility between the section and the bonded prestressing steel, while also considering the global displacement compatibility, across bonded tendon sections within the span, to determine the stress in the unbonded prestressing steel. As mentioned in section 5.7.3.1.3b, the simplified analysis uses a more conservative effective stress to calculate the depth of the neutral axis. The simpler technique, as illustrated in equations (7) and (8), employs semiempirical equations to compute the depth of the neutral axis, c, for T-beams and rectangular beams, respectively. Equation specifies the stress in the bonded prestressing steel (9).

$$c = \frac{A_{psb}f_{pu} + A_{psu}f_{pe} + A_s f_s - A'_s f'_s - 0.85 f'_c (b - b_w) h_f}{0.85 f'_c \beta_1 b_w + k A_{ps} \frac{f_{pu}}{d_p}} \tag{7}$$

$$c = \frac{A_{psb}f_{pu} + A_{psu}f_{pe} + A_s f_s - A'_s f'_s}{0.85 f'_c \beta_1 b + k A_{psb} \frac{f_{pu}}{d_p}} \tag{8}$$

$$f_{ps} = f_{pu}\left(1 + 2\left(1.04 - \frac{f_{py}}{f_{pu}}\right)\frac{c}{d_p}\right) \tag{9}$$

The ACI 381 Building Code and Commentary (American Concrete Institute, 2019) has no advice on how to compute ultimate tendon stresses in systems with bonded and unbonded tendons. The Code does provide empirical formulae for the ultimate stress on bonded tendons and a separate equation for unbonded tendons. These are given in the equations (10), (11) and (12) below.

$$f_{ps} = f_{pu}\left\{1 - \frac{\gamma_p}{\beta_1}\left[\rho_p \frac{f_{pu}}{f_c'} + \frac{d}{d_p}\frac{f_y}{f_c'}(\rho - \rho')\right]\right\} \quad (10)$$

$$f_{ps} = Least\ of\left(f_{se} + 10000 + \frac{f_c'}{100\rho_p}, f_{se} + 60000, f_{py}\right)\ if\ \frac{l_n}{h} \leq 35 \quad (11)$$

$$f_{ps} = Least\ of\left(f_{se} + 10000 + \frac{f_c'}{300\rho_p}, f_{se} + 30000, f_{py}\right)\ if\ \frac{l_n}{h} > 35 \quad (12)$$

The equation for unbonded tendons was created using test data, with all experiments used either unbonded tendons alone or unbonded tendons in conjunction with bonded non-prestressed reinforcement. Thus, it is uncertain how the existence of bonded prestressing affects the ultimate stress in unbonded tendons.

2.2.1.2 Basis of corbel design

A corbel is a reinforced concrete component that consists of a short-haunched cantilever that is used to support a reinforced concrete beam element. Corbel is a structural element that is used to support precast structural systems such as precast beams and pre-stressed beams. With the column or wall element, the corbel is cast monolithically. Because the corbel is cast separately from the column part, cracks develop at the intersection between the corbel and the column. To prevent cracks, we must install shear friction reinforcement perpendicular to the direction of the cracks. Also, corbels may collapse due to yielding of the tension tie, crushing or splitting of the compression strut, or localized bearing or shearing failure under the loading plate. Figure 2.11 shows these failure modes (American Concrete Institute, 2019). Section 16.5 in (American Concrete Institute, 2019) provides detailed instructions for designing this type of structural element.

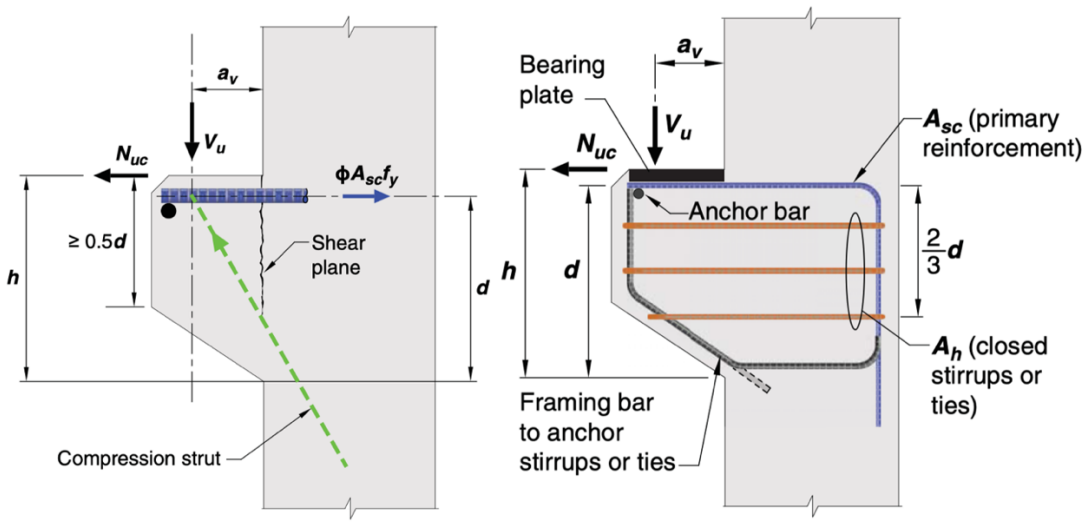

Figure 2.11. Design of corbels (American Concrete Institute, 2019)

Moreover, (American Concrete Institute, 2019) section 23.2.9 allows corbel to be designed using strut-and-tie models. Figure 2.12 illustrates a strut-and-tie model of a corbel supported by a column (Wight, 2013). The structural action inside the corbel is provided by an inclined compression strut, A–C, and a tension tie, A–B. Tension in the column bars and ties, as well as compression forces in struts between the ties, resist shear forces generated in the columns above and below the corbel.

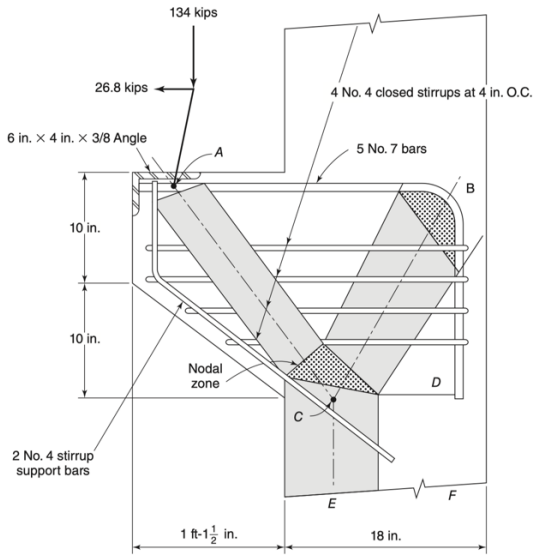

Figure 2.12. Strut-and-tie model for a corbel (Wight, 2013)

2.2.2 Repair with Carbon Fiber Reinforced Polymer (CFRP)

Even with recommendations and precautions given in current codes to prevent corrosion in structure, evidences of corrosion of steel are still reported in many publications. Many research programs, as mentioned in the above sections, carried out investigations into the condition of damaged corroded concrete beams. several strategies can be used to restore the capacity of a damaged beam such as external post tensioning, internal strand splices and welded steel jackets, but the main problem with all these types of repairs that they are labor intensive and can be exposed again for future corrosion (Klaiber et al., 2003). So, the best alternative to these methods is FRP (Fiber Reinforced Polymer) laminates. This repair type is suggested because of the high strength to weight ratio material, excellent resistance to corrosion, fatigue properties and ease of installation (Ali et al., 2014) (Klaiber et al., 2003). The cost-effective point can be explained as CFRP can be transferred using smaller equipment and effort than external post tensioning. In addition to that, CFRP laminates and fabric can be customized to the desired length which is easier compared to welded steel plates. CFRP does not exhibit plastic yielding as steel does instead, it behaves elastically up to the ultimate strain, and this is one of its disadvantages. A brittle behavior with CFRP rupture must be included in the design of the structure. Many research projects have been conducted and proved that FRP can increase the capacity of concrete structures, reduce deflection and add more confinement to the concrete which delays concrete spalling and cracking caused by the expansive forces of the corrosion (Rose et al., 2009) (Duthinh & Starnes, 2004) (Soudki, 2006) (Balasubramaniam et al., 2011).

The anchorage system plays a main role in the CFRP repair system. The most important goal for the anchorage system is to delay or prevent the debonding from occurring in the longitudinal CFRP laminates. This is considered to be one of the main challenges with external

CFRP repair methods (Ali et al., 2014) (Ceroni et al., 2008). Also, anchorage systems can provide a stress transfer mechanism if no bond length is available beyond the critical portion of the member. There are many systems such as anchor spikes, transverse wrapping, U-Anchors, longitudinal chases, FRP strips, plate anchors, bolted angles, cylindrical hollow sections, ductile anchoring systems, and other miscellaneous systems are also available (Grelle & Sneed, 2013).

Each of these anchoring systems has its own set of geometrical restrictions, installation constraints, and force (stress) transfer characteristics (Grelle & Sneed, 2013). For example, anchor spikes are strands of bundled fibers, one end of which is inserted in the composite matrix and the other in the concrete substrate. They are often positioned orthogonally to or in-plane with FRP, and they can be oriented at any angle (see Figure 2.13) (Ozbakkaloglu & Saatcioglu, 2009). This type is often utilized for anchoring along the length of the FRP laminate or towards its end.

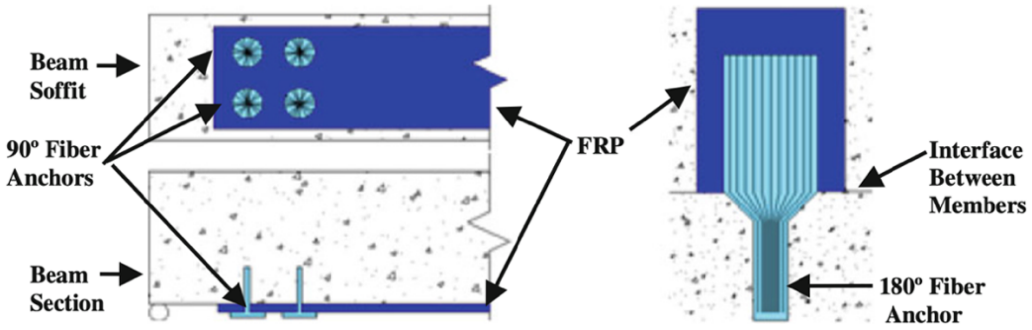

Figure 2.13. Comparison between 90° and 180° anchor spikes (Grelle & Sneed, 2011)

Another anchoring system, transverse wrapping, may be discrete strips positioned at the end of the CFRP sheet or along its length, or it can be continuous throughout its length Figure 2.14. Fiber orientation might be perpendicular to or angled with respect to the longitudinal axis of the member. This type is similar to the anchor spikes in term of the installation's location.

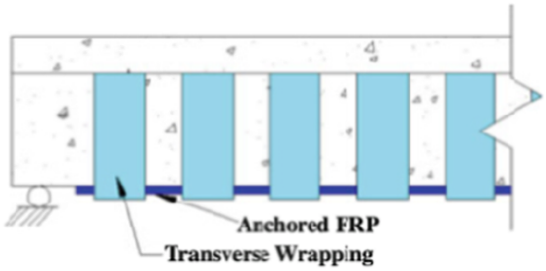

Figure 2.14. Example of transverse wrapping anchorage (Grelle & Sneed, 2013)

The use of FRP strips is another type of anchorage system, and it is the simplest one. It consists of one or more strips installed on the top of the reinforced FRP sheets (see Figure 2.15). They are normally positioned perpendicular to the direction of force in the FRP sheet and in the plane of the FRP sheet. FRP anchoring systems have been found to be not as successful when compared to other anchorage methods, limiting the number of studies in which they have been used. As a result, the behavior of FRP strip anchoring has received little attention (Grelle & Sneed, 2013).

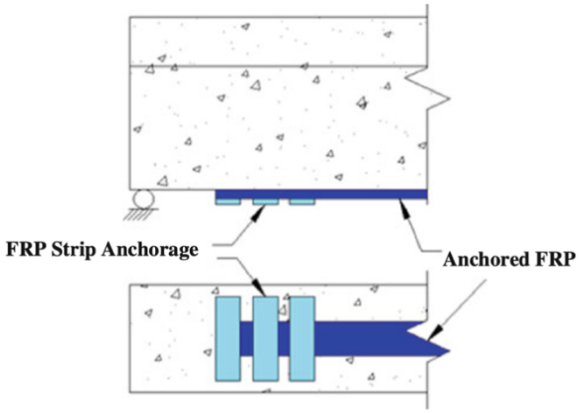

Figure 2.15. FRP strip anchorage (Grelle & Sneed, 2013)

In order to get the maximum benefit from the FRP repair, a high level of care in the installation must be expended. (Ali et al., 2014) summarized the procedure of installing this type of repair. The authors mentioned that surface preparation by grinding, application of a priming adhesive layer, bonding of the CFRP laminates and sheets, and insertion of the CFRP anchors

into the drilled holes were all part of the strengthening method. Figure 2.16 shows steps of installation of the CFRP (Pino et al., 2017). The surface preparation was given considerable attention prior to bonding. The outside weak surface of the concrete was removed using uniform mechanical grinding until the particles were revealed. Following that, the beams' surfaces were washed with water, and any loose particles were removed using compressed air. Holes for CFRP anchors were bored at the suitable spacing, according to the prescribed arrangements, and at the required depth for each specimen using a small-job electrical driller. A pressured air blower and a tiny steel grinder were also used to clean and remove dust as well as any fine or loose particles from within the holes. After the surface had been prepped to the required quality, the epoxy resins were mixed according to the manufacturer's instructions until the mixture was uniform in color.

CFRP sheets and plates were precisely cut to the appropriate dimensions and attached to the beam specimens. After filling the holes approximately halfway with epoxy resin and applying an initial layer of epoxy resin to the surface of the RC beams, the CFRP anchors were inserted into the holes and rolled in the longitudinal direction of the fibers using an air removal roller and by hand to remove any trapped air bubbles and to firmly impregnate the fibers. The CFRP sheet was then applied after a high solids saturant was applied. After allowing the saturant to soak the carbon fiber sheet and embedded CFRP anchors for a period of time, a second application of epoxy resin layer was applied to the top of the CFRP sheet and the splayed CFRP anchor fibers to guarantee that the two components are linked together during curing. Hand rolling was then used to eliminate any trapped air bubbles from the interior. Before testing, the adhesive was cured at room temperature for at least 7 days in the laboratory.

Figure 2.16. Procedure of installing CFRP sheets (Pino et al., 2017)

Many experiments have tested the effect of the CFRP laminates. For example, Isakveien Bridge in Oslo was demolished, after 35 years in service, and four prefabricated prestressed concrete T-beams were preserved for testing (Takács & Kanstad, 2000). Two beams were used to obtain the base capacity and CFRP plates were installed in the other two. One and two CFRP layers were used at the bottom side of the beams and were attached using epoxy-based adhesive. The flexural capacity increased by 28% and 37% in the beams with one and two CFRP layers, respectively. The authors concluded that CFRP repair is cost effective, non-corrosive and can add a considerable strength to structures. Also, (Klaiber et al., 2003) tested the four-span in-situ Altoona Bridge, which is in Iowa. The bridge was damaged due to overhigh vehicle and a CFRP repair was suggested to strengthen the bridge. Only one damaged prestressed beam was tested and analyzed in this study. The spalling in concrete and exposed strands were observed in the damaged beam (see Figure 2.17).

Figure 2.17. Signs of damage in the tested beam (Klaiber et al., 2003)

One layer of four strips of CFRP laminates were installed to the soffit of the beam using epoxy-resin (see Figure 2.18). Two trucks (rear tandem) were used in the testing of the bridge (see Figure 2.19).

Figure 2.18. CFRP sheets attached to the repaired beam

The authors concluded that flexural strengthening is feasible if 15% or less of the strands are damaged. Also, they mentioned that the use of transverse CFRP sheets can prevent debonding of the longitudinal CFRP laminates.

Figure 2.19. Trucks used in the loading test

Some studies have investigated the relationship between CFRP and the amount of internal steel. Seven beams, reinforced internally with different amount of steel and externally with CFRP laminates, were tested to evaluate the effectiveness of the CFRP on strength and ductility (Duthinh & Starnes, 2004). Clamps and wraps were the two types of anchorage systems that were been used. The CFRP laminates were installed after reaching various percentages of the cracking moment for each specimen. With all these combinations and taking one beam as a reference beam, the authors concluded that CFRP is effective in increasing the strength of these beams and confirm the previous findings in some studies that limiting the increase in strength to 20% is reasonable for CFRP repair. Also, using mechanical clamps or wraps with FRP fabric and adhesive increased the capacity of the anchorage more than using adhesive only.

Ninety-four reinforced concrete beams were tested at the University of Waterloo to identify the effectiveness of two types of FRPs, which are glass and carbon fiber sheets (Soudki, 2006). All the specimens were subjected to an accelerated corrosion process which led to an approximately 15% loss in the steel. There were many test variables, such as the level of corrosion, the location of the FRP repair and the type of loading. Tests showed that at the end of the corrosion process, FRP reduced the cracks opening by 88% (see Figure 2.20). The study

concluded that FRP repair systems can recover the losses due to the corroded steel and can restore the strength, integrity, and serviceability of the structure.

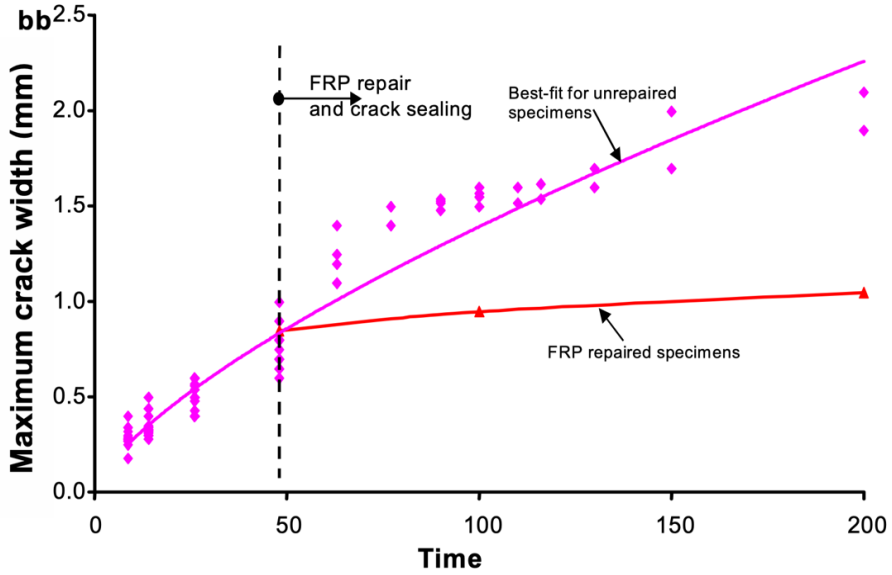

Figure 2.20. Crack width vs time (Soudki, 2006)

(Lee et al., 1997) tested four RC beams to verify the effectiveness of CFRP repair. One beam was used as a reference beam while others were exposed to accelerated corrosion to have different levels of deterioration. Only two out of the three corroded beams were repaired with CFRP sheets. The non-repaired beam had 10% loss in the steel cross section and failed at ultimate strength of 85% of the strength of the reference beam. While the two repaired beams failed with rupturing the CFRP sheets with an increase of 40% in the strength compared to the reference beam.

In experiments done in India, five damaged HSC beams with varied degrees of corrosion were repaired with GFRP (Balasubramaniam et al., 2011). As a reference beam, one specimen was left uncorroded and undamaged. A reinforcement mass loss of 10% and 25% was applied to two beams as corroded control. The last two beams were corroded and reinforced with GFRP.

Compared with the reference beam, the repaired beams had an increase in the ultimate strength of 35% and 5% for the 10% and 25% loss in the steel cross section, respectively.

(Nguyen et al., 2013) tested a total of 12 pretensioned concrete beams. The specimens were divided into three groups. In first group, there were three beams, one with no strands damaged and the other two with 25% and 50% strands damage. In second group, four specimens with 25% loss in the strands were reinforced with one layer of CFRP but with different length along the soffit of the beam (0.3, 0.5 and full beam length). While the third group, consisted of five beams with 50% loss in the stands, which were repaired with different numbers of CFRP layers (1 to 5 layers). Results showed that the length of the sheets increased the stiffness by 10%, but the ultimate loads were not affected by increasing the sheet lengths. However, the cracking load was significantly increased with the increase in number of CFRP layers. Hence, the initial stiffness was enhanced. However, the beam with three CFRP layers recovered strength to 91.5% of the controlling beam's strength. The trend of increasing strength did not continue with the beams that have four and five layers. The ultimate load for the beams strengthened with more than three layers shows a reduction compared to the one repaired with three layers. The debonding of CFRP sheets occurred earlier with these specimens. The cracks at midspan were well restrained and became smaller with the larger number of CFRP sheet layers (see Figure 2.21).

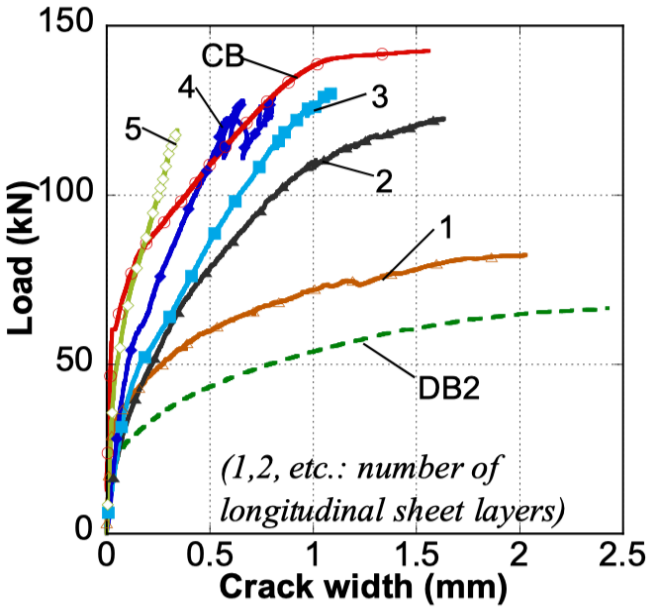

Figure 2.21. Effect of number of layers on flexural crack widths

The larger number of CFRP layers the less strain in the strands at the same level, since the CFRP sheets contribute to carrying the tensile stress with the strands. When the number of bonded sheets was increased, the critical sections in the prestrssed beams changed from the constant moment area to the region near the sheet ends, where the importance of the type of anchorage is presented. The study mentioned that the existing equations in the guidelines of ACI are insufficient to predict the debonding from the ends of bonded sheets since the ACI method overestimates the calculation of the flexural capacity. So, CFRP repair with a large number of sheets, sufficient length and type of anchorage needs to be further investigated.

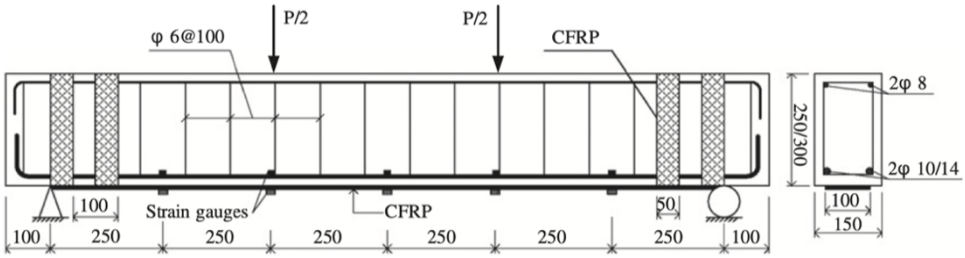

Figure 2.22. Flexural repair with CFRP

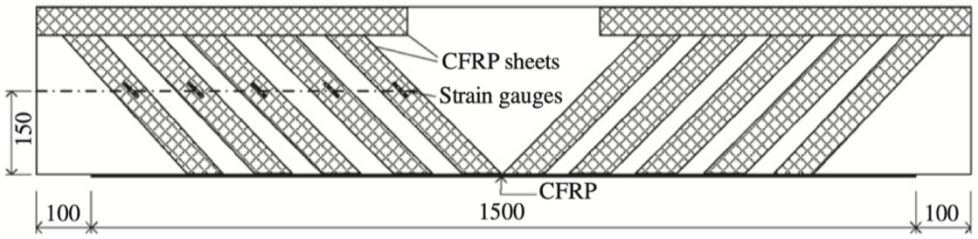

Figure 2.23. Flexural-shear repair with CFRP

(Dong et al., 2013) tested fourteen specimens to study the behavior of reinforced beams repaired with external flexural and flexural-shear CFRP (see Figure 2.22 and Figure 2.23). The variables in this study were number of CFRP sheets, concrete cover, reinforcement ratio, stirrup ratio, concrete strength, and pre-crack width. The increase in the flexural capacity of the CFRP reinforced beams varied between 41% and 125% over the control beam, while the increase in shear capacity varied between 31% and 74% over the control beam.

Another study done by (Pino et al., 2017), showed the difference between fiber-reinforced polymer (FRP) and fabric-reinforced cementitious matrix (FRCM) systems. Three full-scale AASHTO Type III girders were extracted from a demolished bridge. One girder served as the reference specimen, while the other two girders were damaged by cutting four strands at two different locations along the girder length and repaired with FRP and FRCM, respectively. Results showed that both composite methods restored the original capacity of the beam. On the other hand, authors stated that ACI 440.2 R proved to have a conservative estimate of design strengthened capacity when compared with the experimental results.

Many other studies like (Kim et al., 2008) agreed with all the previous researchers mention above, that the FRP can increase stiffness, strength capacity and deflection. Also, it can control development of cracks and increase ductility of the beams.

Literature Review Summary

As shown in the previous sections, some research projects have been conducted to evaluate corroded damaged girder using non-destructive and destructive tests. A comprehensive research program was carried out by (Naito et al., 2010a) to study corrosion damaged precast, prestressed adjacent box beams with the objective of developing guidelines for the calculation of residual strength based on visual inspections. They collected beams from demolished bridges and performed forensic investigations. No physical tests were performed to determine actual flexural strength. Based on excavating strands from the beams and its proximity to cracks or spalls, they made recommendations for a reduced cross-sectional area to be used in strength calculations. Therefore, there is a need to collect more data to enhance the statistical analysis done by (Naito et al., 2010a), but also testing beams to failure to validate the approach. Also, check whether the approach is valid for different types of beams or only for box beams. If not, new recommendations are required.

Furthermore, some studies test different types of methods to increase the strength of deteriorated girders. The capacity of prestressed concrete beams which have experienced corrosion damage and have subsequently been repaired requires additional study. Also, there is a need to understand the correlation between the condition of the damaged corroded beams and either the CFRP or external PT repair methods. So, more data with detailed non-destructive test for deteriorated girders are required in order to decide the best type of repair to restore the original strength capacity.

The AASHTO LRFD Bridge Design Specifications, (AASHTO, 2017), provide instructions for analyzing beams with bonded and unbonded tendons. Section 5.7.3.1.3 describes

two techniques for analyzing such a beam: Detailed Analysis and Simplified Analysis. The detailed analysis considers the strain compatibility between the section and the bonded prestressing steel, while the part of stress in the unbonded prestressing steel in the calculations is not clear. Therefore, a detailed analysis showing clearly both bonded and unbonded tendons is required to know the capacity of the repaired girder.

This current research looks to collect test data to address all the above requirements and make provisions in the ACI 318 code where possible.

CHAPTER 3: Large Scale Laboratory Testing – Unrepaired Corrosion Damaged Girders

Chapter 3 consists of the manuscript: "Experimental and Analytical Evaluation of Residual Capacity of Corrosion-Damaged Prestressed Concrete Bridges Girders" This paper is currently in preparation for submission to journal.

Experimental and Analytical Evaluation of Residual Flexural Strength of Corrosion-Damaged Prestressed Concrete Bridges Girders

Ali Alfailakawi[1]; Carin L. Roberts-Wollmann[2]; Matthew H. Hebdon, [3]; Ioannis Koutromanos, [4]

Virginia Tech, Blacksburg, VA

3.1 Abstract:

This paper presents the results of testing of six corrosion-damaged prestressed beams which had been removed from existing bridges during their demolition. Three beams were Type II AASHTO I-beams and three were box beams. Prior to testing, the beams were visually inspected. The beams were then tested in the lab to determine their flexural strength. Following testing, samples of strands were removed and tested to determine their tensile properties while cores were taken to determine compressive strength. Powdered concrete samples were removed to perform chloride concentration tests.

The tested strengths of the beams were compared to calculated strengths using two methods for damage estimation and two different calculation approaches. The methods for damage estimation relied exclusively on visual inspections; one was the method recommended

by Naito et al., (2011), while the second was a modified method developed in this study from the current tests. The two calculation approaches were the strain compatibility method and the AASHTO LRFD method. Overall, the results yielded reasonable estimates of residual strength, except for one of the box beams that was discovered to have considerable water within the hollow cells. The final recommendations are that bridge inspectors develop detailed damage maps of corrosion-damaged beams and that load raters use the Naito et al. method to get a conservative estimate of damage for both box beams and I-beams. Either method for calculating strength is valid, however, the AASHTO LRFD method is simpler.

3.2 Introduction

3.2.1 Background

The durability of infrastructure components, such as bridges, is significantly affected by long-term deterioration associated with corrosion. The transport of agents and the chemical processes associated with corrosion lead to cracking in the concrete, which then accelerates the corrosion process. Corrosion is a significant concern for bridges, due to the frequent use of deicing salts during the winter, as well as the number of structures in marine environments. Over time, the exposure of prestressing steel to corrosive agents can lead to complete loss of strands and, in extreme circumstances, to complete failure of bridge beams (Naito et al., 2010b). Research is necessary to assess the impact of corrosion on the local and global behavior of bridges and to establish mitigation techniques to ensure long-term durability.

At present, there is a relatively limited amount of experimental research on bridge girders damaged by corrosion. Researchers in New Zealand and Pennsylvania have conducted destructive tests on decommissioned prestressed beams (Rogers et al., 2012), (Harries, 2009). A

comprehensive research program was carried out by Naito et al., (2010a) to study corrosion-damaged precast, prestressed adjacent box beams with the objective of developing guidelines for the calculation of residual strength based on visual inspections. They collected beams from demolished bridges and performed forensic investigations. No physical tests were performed as part of this program to determine actual flexural strength, although a previous research program Harries, (2009) tested two beams from an adjacent box beam bridge. Based on excavating strands from the beams, Naito et al., (2010a) determined that the probability of corrosion damage was highest for strands located beneath a longitudinal crack. There was also a higher probability of corrosion for strands immediately adjacent to the strand beneath the crack. Based on proximity to cracks or spalls, they made recommendations for a reduced cross-sectional area to be used in strength calculations. In the paper presented herein, additional data was collected to enhance the recommendations made by Naito et al., (2010a), and go a step further by testing the beams to failure to validate the approach.

3.2.2 Problem Statement

A method to determine the flexural strength of prestressed concrete members with section loss and corrosion of prestressing strands is not well-established. The understanding of the residual capacity is critical for the evaluation of bridges with advanced levels of deterioration.

3.2.3 Purpose and Scope

The overall purpose of this study was to conduct tests to determine the remaining capacity of prestressed concrete members, which have localized regions of deterioration, and to develop a method that can be used to determine the residual flexural strength of prestressed concrete bridge beams based primarily on visual inspections. These tests should aid in the

development of guidelines for inspectors to ensure they collect the necessary data on damage to aid in the calculation of strength for load rating.

In order to achieve the objective of this project, three adjacent prestressed concrete box beams, and three prestressed I-beams were tested to failure to determine their residual flexural capacity after many years of service. These beams, retrieved from bridges that were being demolished, had varying degrees of deterioration, ranging from delaminated concrete to strands with severe section loss. Prior to testing, the damage was mapped, and non-destructive evaluations were performed. After testing, samples of strands, concrete cores, and powdered concrete samples were removed and tested.

3.3 Description of Specimens

3.3.1 Lesner Bridge Beams

The westbound lanes of the Lesner Bridge, also known as the Lynnhaven Inlet Bridge, were constructed in 1967. The structure comprised prestressed concrete beams in the approaches and steel beams for the main spans. The beams in the approach spans were 49 ft – 9 in. long, 36 in. deep prestressed I-beams. The beams were specified to have 5000 psi concrete and were prestressed with 22–7/16-in. Grade 270 stress-relieved prestressing strands. There were seven beams in each span, spaced at 5 ft – 2.5 in, center-to-center.

After almost 50 years of service, the bridge was demolished and replaced beginning in 2016. In the spring of 2017, nine beams were retrieved during the demolition process and delivered to Virginia Tech for testing. The slab between the beams was saw-cut to allow for the retrieval of beams to include a section of their cast-in-place composite deck. Figure 3.1 is a

photograph of Span 7, showing the extent of deterioration in typical beams. The Lesner Bridge was repaired several times over the years, so patching is evident in many locations. The retrieved Lesner Bridge beams are referenced by the names I-Beam 1 through I-Beam 9, and only I-beams 3,6 and 7 are presented in this paper and will be referenced as I-Beam 1, I-Beam 2 and I-Beam 3, respectively. The cross-section of the Lesner Bridge I-beams is shown in Figure 3.1. More details about the beam locations can be found in (Alfailakawi et al., 2020).

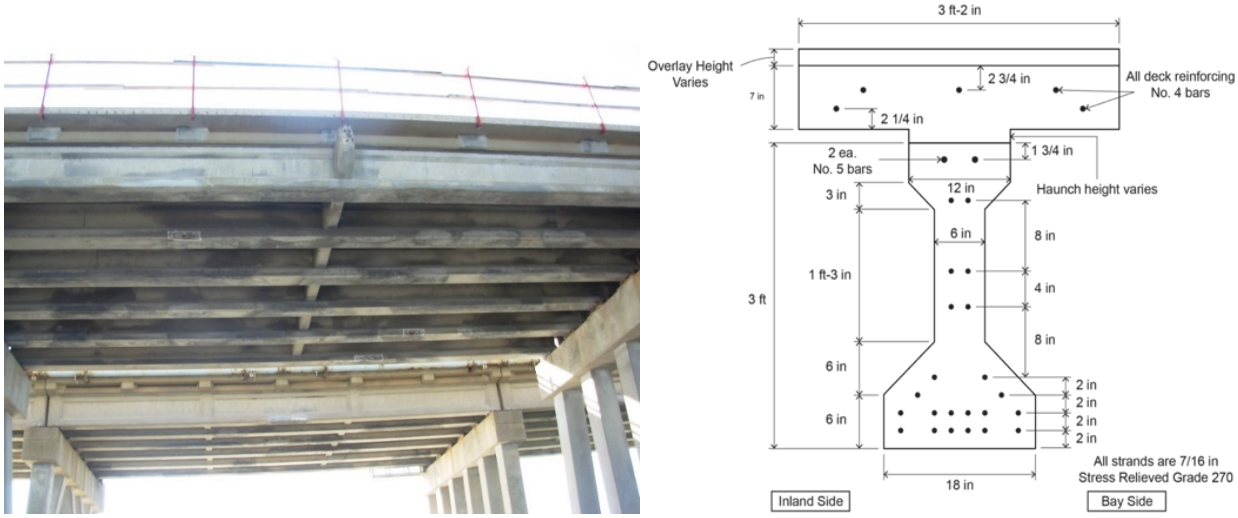

Figure 3.1. Typical Deterioration on the Lesner Bridge (left) Cross-section of Lesner Bridge I-Beams (Right)

3.3.2 Aden Road Bridge Beams

The Aden Road Bridge was constructed in 1979. It was a three-span bridge with nine prestressed box beams per span. The fascia beams were 3 ft – 0 in. wide by 27 in. deep, and the seven interior beams were 4 ft – 0 in. wide by 27 in deep. Only interior beams were used in this project. The beams were 55 ft long and were prestressed with 33–7/16-in. diameter Grade 270 stress relieved strands. The beams were connected transversely with grouted 12-in. deep shear keys and ½-in diameter Grade 270 prestressing strands at each quarter point of each span. The

bridge had an asphalt wearing surface applied directly to the top of the box beams, which was removed prior to demolition of the bridge.

After slightly over 30 years of service, the joints had failed, and the bridge was showing signs of severe deterioration, including exposed and fractured prestressing strands (Figure 3.2). In 2013, the bridge was demolished and replaced. During demolition, six of the interior beams were transported to Virginia Tech for future testing, three of which were tested in this project. The Aden Road Bridge beams are referenced by the names Box Beam 1 through Box Beam 6, and only Box Beams 1,2 and 4 are presented in this paper and will be referenced as Box Beam 1, Box Beam 2 and Box Beam 3, respectively.. Figure 3.2 shows the cross-section of the Aden Road Bridge box beams.

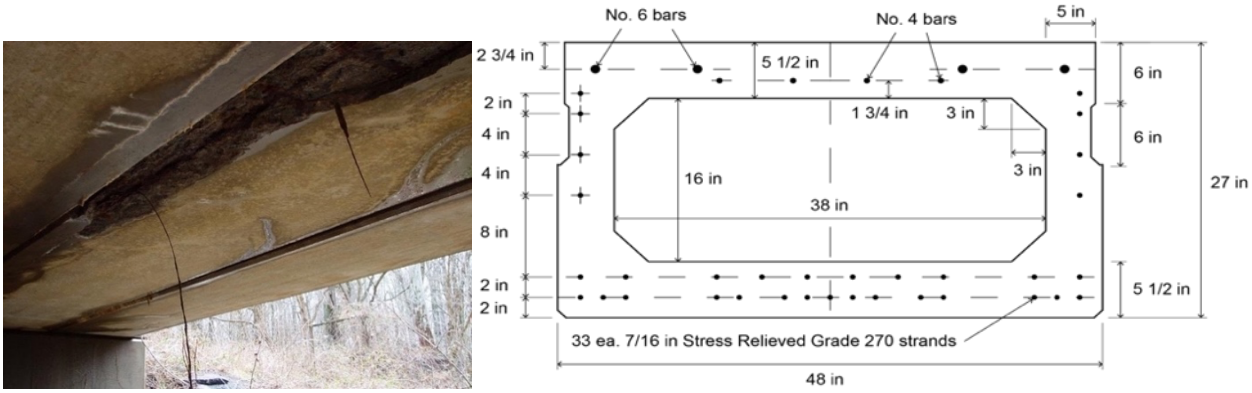

Figure 3.2. Typical corrosion damage on Aden Road Bridge (left), Cross-section of Aden Road Bridge Box Beams (right)

3.4 Corrosion Damage Assessment

This section presents the methodology used to assess the condition of the beams in this study. This includes only visual inspection. Half-cell potential testing was performed but it did not add valuable information for the corrosion damage assessment and strength capacity

calculations. More information about the damaged maps for each beam and heat maps showing the finding from half-cell tests can be found in Alfailakawi et al., (2020).

3.4.1 Visual Inspection

All of the beams in the study were thoroughly examined and detailed damage maps were created. Figure 3.3 presents a typical damage map for three sides of I-Beam 2. The bay side, which is facing the Chesapeake Bay, is more damaged than the inland side. The top sketch is one side, oriented right-side-up, the middle sketch is the bottom of the beam, and the bottom sketch is the other side of the beam, oriented up-side-down. This allows the reader to see how side damage and bottom face damage are related to each other spatially. Visual inspection maps for the other beams can be found in Alfailakawi et al., (2020).

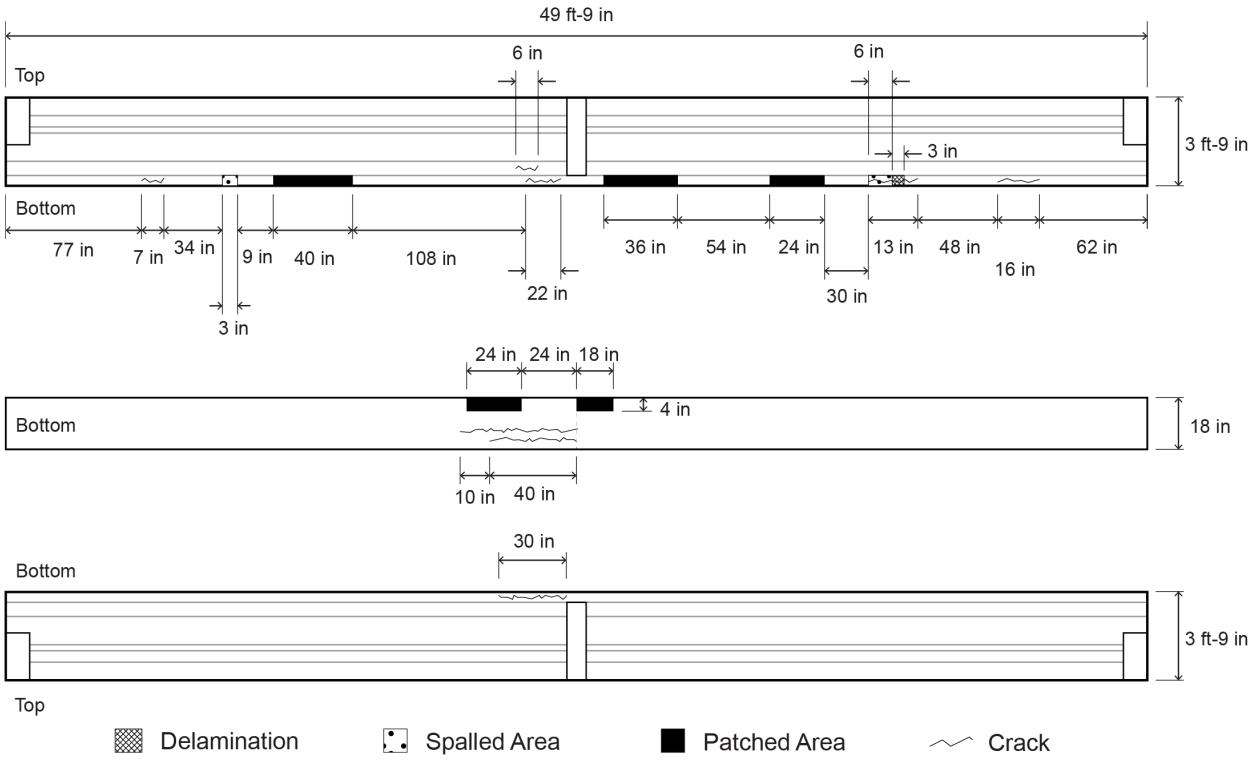

Figure 3.3. I-Beam 2 - Medium condition

3.4 Experimental Test Methods

3.5.1 Test setup

All six of the selected beams were tested in a simple-span configuration with a roller support at one end and a pin support at the opposite end. Loads were applied with a 400-kip hydraulic ram and a spreader beam, so two equal loads were applied 8 ft apart, centered at the mid-span of the beam. Preliminary strength calculations were performed for each beam prior to testing to confirm a flexural failure would occur prior to a shear failure. Figure 3.4 presents a schematic of the test setup for the Lesner Bridge I-beams and Figure 3.5 shows the setup for the Aden Road Bridge box beams.

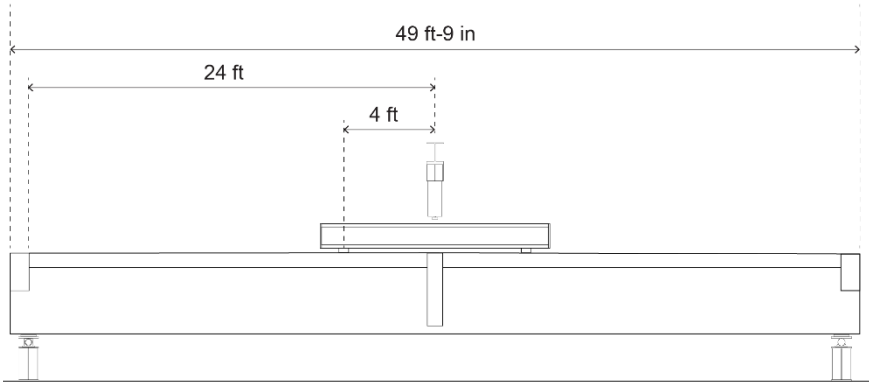

Figure 3.4. Flexural Testing Setup for Lesner Bridge I-Beams

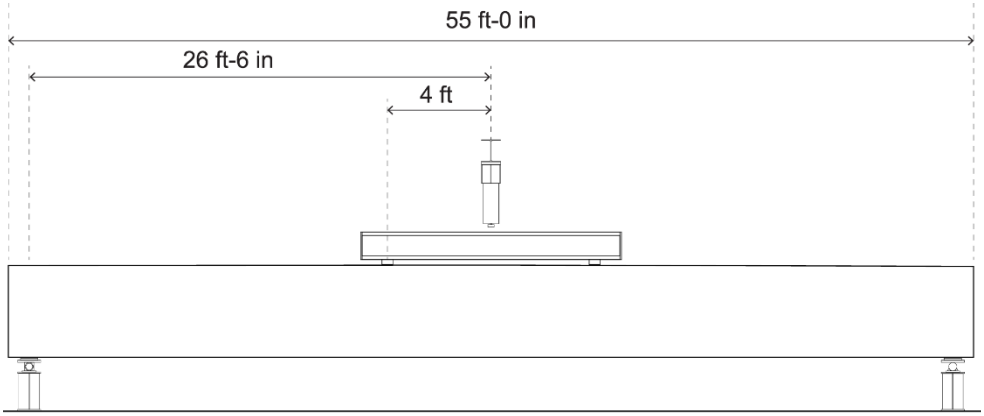

Figure 3.5. Flexural Testing Setup for the Aden Road Bridge Box Beams

3.5.2 Instrumentation

Each flexural test had similar instrumentation. Wire pots were used to measure the vertical deflections at the mid-span and quarter points. BDI (Bridge Diagnostics, Inc) gages were used to measure longitudinal strains at several locations along the length of the beam. At each location, an array of BDI gages was installed vertically, through the depth of the beam, to investigate strain distributions and to determine the location of the centroid of the cross-section. A load cell was placed between the hydraulic ram and the cross-head of the loading frame. The load cell, wire potentiometers and the BDI strain transducers were connected to a wireless BDI data acquisition system. The system sampled the data at a rate of 33 HZ throughout testing. A schematic of the BDI gage arrangement for the Lesner Bridge I-beams and for the Aden Road Bridge box beams can be found in Alfailakawi et al., (2020).

3.5.3 Test Procedure

For each beam, an expected cracking load was calculated prior to testing. During testing, the load was increased in 5- or 10-kip increments to slightly below this expected load. After each subsequent load increment, all cracks were marked, and photographs taken. After the beam began to exhibit signs that the prestressing was yielding and the load was not increasing significantly, loading protocol was changed to a manual deflection control. An increment of deflection was chosen based on the load-deflection behavior at that point of the testing. At each increment, the load was paused, and the beam was examined. When failure appeared imminent, the researchers did not continue to approach the beam to look for new cracks or crack propagation. Loading continued until failure occurred, due either to top flange crushing or due to the beam continuing to deform without resisting any additional load. After failure, the load was removed, and the beam was carefully examined to determine the number of prestressing

strands that either showed evidence of having been fractured due to corrosion prior to testing or had failed during testing.

3.6 Description, observation, and results of tests

3.6.1 I-Beam 3 – Base Beam

This beam represented an undamaged control test to provide a baseline for comparison with subsequent tests. The beam was tested over two days; on the first day, cracks were first observed at 85 kips. At a load of 179 kips, an unexpected inclination of the actuator was observed, so the test had to be stopped until the issue could be fixed.

One week later, the beam was re-tested. The load was applied in increments of 20 kips until reaching 140 kips, at which point 10-kip increments were applied until the failure load of 188 kips with a deflection of 8.93 in. The failure was caused by crushing of the top slab.

The load-deflection plot is shown in Figure 3.9 for first day and second day. On the first day of testing, a slight change in the slope of the line can be seen at around 80 kips, confirming the first cracking load determined visually at 85 kips. For the second day test, at around 186 kips the load deflection curve begins to plateau, indicating the strands were yielding, and the beam failed at 188 kips.

After testing, the concrete cover over the bottom strands was chipped to expose the strands. As can be seen in Figure 3.6, all strands were bright and shiny, showing no signs of corrosion.

Figure 3.6. Bottom of I-Beam 7 after Testing

3.6.2 I-Beam 2

This beam was considered to be in moderately deteriorated condition. Near the mid-span on the bay side of the bridge there was a patch on the bottom flange that extended a few feet on either side of the mid-span diaphragm of the beam. The opposite side of the beam showed very little sign of corrosion damage, except for one 8-in. long hairline crack 2 in. up on the bottom flange. As testing progressed, a spall occurred at the crack, revealing the corroded strand beneath. Also rust staining could be seen on the bottom flange; a post-test autopsy confirmed that the chairs supporting the reinforcement during concrete placement were, in fact, corroded.

During the load test, the first crack was visually observed at 50 kips; however, there was no noticeable change in the slope of the load displacement plot at that load (see Figure 9). At around 105 kips, the load deflection plot began to plateau. The beam failed at an applied load of 118 kips and a deflection of 4.46 in, due to crushing of the top flange.

After testing was completed, the concrete on the bottom flange was removed to investigate the condition of the strands. Upon careful inspection, it was determined that five of

the six bottom row strands showed signs of severe corrosion with most wires broken, apparently due to the aforementioned corrosion. A few wires appeared to have broken during testing and showed a shiny surface. Interestingly, the fourth strand, counting from the top of Figure 3.7, showed no evidence of corrosion damage. The bottom strand in the photo, still embedded in a piece of the patch material, showed evidence of being broken before testing, and was most likely broken at the time the patch was applied. The strand in the same position, but in the second row, also in the patch, was in similar condition.

Figure 3.7. Bottom Flange of I-Beam 2 after Testing

3.6.3 I -Beam 1

This beam was considered to be in poor condition, with considerable patching and spalling all along the bay side of the bottom flange. During testing, the first flexural crack was observed at a load of 80 kips and confirmed by the change in the slope of the load deflection plot in Figure 3.9. The slope of the plot began to plateau at around 155 kips and the beam ultimately failed due to crushing of the top flange, with an applied load of 166 kips and a deflection of 8.19 in.

Close to failure, the bottom flange exhibited significant cracking associated with the corroded strands and patching. After testing, the bottom flange was examined, and it was determined that the strand in the patch and the strand directly above it in the original concrete were both badly damaged and fractured from corrosion (Figure 3.8). In addition, a second bottom-row strand in the patch was damaged. The remainder of the strands were in relatively undamaged condition.

Figure 3.8. Corrosion-Damaged Strands in and above Patch in I-Beam

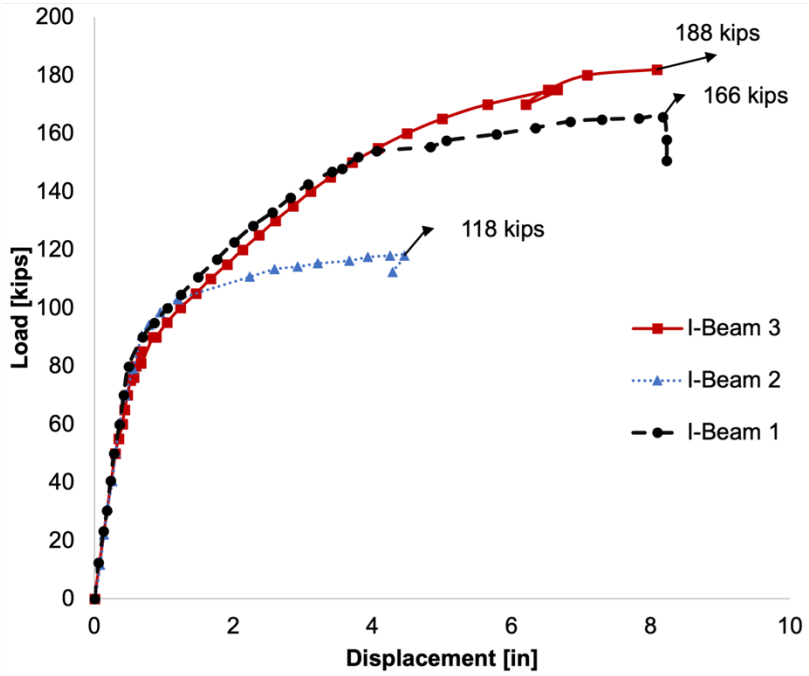

Figure 3.9. Load Versus Displacement Plot for All I-Beams

3.6.4 Box Beam 1

The beam showed signs of significant corrosion damage. Before the test, severe corrosion was observed in the three bottom strands on the west side of the beam near mid-span (see Figure 3.10). On the opposite side of the beam there were longitudinal cracks along the bottom soffit and the side of the beam about 2 in. up from the bottom. This indicated that the nearby strands were also, most probably, corroding.

First cracking was observed at a load of 50 kips, and confirmed with a change in the load deflection plot in Figure 12. At a load of about 90 kips, the load deflection plot began to plateau. The test was terminated at 90.3 kips, when the deflection reached 16.99 in without any further increase in load.

Figure 3.10. Three corroded strands in Box Beam 1

3.6.5 Box Beam 3

Box Beam 3 had a small spall on the west side, with a longitudinal crack about 2 in. up from the bottom of the beam that ran almost the entire length of the beam. There was also an almost full length longitudinal crack on the bottom soffit. The east side of the beam had two short longitudinal cracks.

During testing, first cracking was visually observed at a load of 45 kips, as confirmed by the change in slope of the load-deflection plot in Figure 3.12. During the test and at high deflection, considerable water began leaking from the void in the beam. At that point, the load was held constant, and buckets were used to collect the leaking water. The beam failed when the corroded strands ruptured at an applied load of 83.8 kips.

Upon examination after the test, strands along east side did not show significant corrosion, but the strands had yielded. The strands on the west side were heavily corroded (see Figure 3.11). The edge strands in the lowest level had severe corrosion, possibly exacerbated by the water that had been trapped in the beam. After the bottom concrete cover had spalled off, it was apparent that the three outermost bottom layer strands were severely corroded.

Figure 3.11. Box Beam 3 West Side After Testing

3.6.6 Box-Beam 2

Box Beam 2 had evidence of significant corrosion on the east side of the beam. A large spall near mid-span exposed two corroded strands. There was also a longitudinal crack, about 2 in. up from the bottom soffit, that ran most of the length of the beam.

During testing, cracking in the concrete was first visually observed at a load of 49 kips, which is confirmed by the change in slope of the load deflection plot in Figure 12. Around 90

kips, the load deflection plot began to plateau until failure, which was crushing in the top concrete, occurred at an applied load of 91.6 kips and a deflection of 17.2 in.

Figure 3.13 shows the severely corroded lower strand on the east side, which was observed before the test. After testing, the researchers found that the other strands were relatively undamaged.

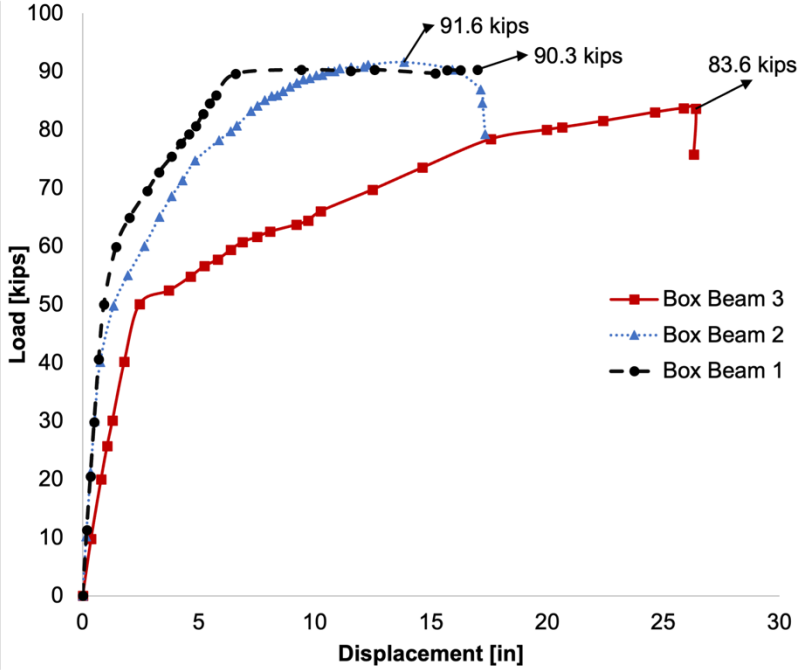

Figure 3.12. Load versus Displacement Plot for All Box Beams

Figure 3.13. Corroded Strand on Bottom of Box Beam 2

3.6.7 Summary of Test Results

Table 3.1 summarizes the experimental results such as the first crack, ultimate load, ultimate deflection, and failure mode of all the specimens.

Table 3.1 Summary of measured results of beams

Beam	First Crack (kips)	Ultimate Load (kips)	Ultimate Deflection (in.)	Failure Mode
I-Beam 3	85	190	8.93	Concrete crushing at the top
I-Beam 2	50	118	4.46	Concrete crushing at the top
I-Beam 1	80	166	8.19	Concrete crushing at the top
Box Beam 1	50	90.3	16.99	Excessive deflection
Box Beam 3	45	83.8	N.A	Strands rupturing
Box Beam 2	49	91.6	17.2	Concrete crushing at the top

3.7 Post-Test Destructive Testing

After each test, destructive tests have been conducted on the beams. These included extracting concrete powder samples, concrete cores and strands. In addition, concrete was chipped off near the failure location, and strand condition was investigated. This section presents the results of these tests.

3.7.1 Total Chloride Evaluation

This section presents the results of the chloride concentration tests on powdered samples obtained from the tested beams. For comparison to the test results, the criteria for corrosion risk compared to chloride content are given in Table 3.2.

Table 3.2. Risk of Corrosion Compared to Chloride Content (Balakumaran, 2010)

% Chloride by mass of sample (concrete)	Risk	Chloride content per volume of concrete (lb/yd^3)
<0.03	Negligible	<1.17
0.03-0.06	Low	1.17-2.35
0.06-0.14	Medium	2.35-5.48
>0.14	High	>5.48

For each beam, the worst-case chloride concentration was compared to the risk of corrosion as presented in Table 3.2 and the assessed condition of the beams based on visual inspections. The comparison is presented in Table 3.3.

Table 3.3. Comparison of Chloride Tests and Visual Inspection Evaluations

Beam Designation	Assessed Condition from Visual Inspection	Chloride Concentration at Strand Level, lb/yd^3	Risk of Corrosion
I-Beam 3	Good	4.39	Medium
I-Beam 2	Medium	5.01	Medium
I-Beam 1	Bad	5.40	Medium
Box Beam 1	Good	1.45	Low
Box Beam 3	Medium	1.14	Negligible
Box Beam 2	Bad	0.67	Negligible

The chloride concentrations from all the I-Beams indicate a medium risk of corrosion, and yet they had very different levels of corrosion damage to their strands. I-Beam 3, which had the lowest concentration, had almost no evidence of corrosion of the strands. I-Beams 1 and 2, had higher chloride concentrations, and more evidence of corrosion damage. The Box Beams also gave odd results. The chloride concentrations indicated a low to negligible risk of corrosion, and yet all three beams showed evidence of significant corrosion of the strands. These results indicate that collecting field samples to evaluate chloride concentrations may not be valuable in the corrosion assessment of damaged beams.

3.7.2 Compression Strength Testing

The compressive strength was measured for each concrete core sample. The results are presented in Table 3.4. The average concrete strength of the deck after nearly 50 years of service was slightly lower than that specified in the plans, with the exception of I-beam 3, which was relatively high at 7.2 ksi. All the cores indicated that the original deck included river gravel, and a later overlay was made from latex modified concrete. It is unknown why the core from the

deck of I-beam 3 was so much stronger than the others. Regarding the I-beams, the concrete strength was higher than the original plan strength by 45%. Similarly, the 33-year-old box beams had a compressive strength that was 40% higher than the 5-ksi design strength.

Table 3.4. Compressive strength for concrete cores

Beam/Sample	Average Factored Compressive Strength (psi)
I-Beam 2 slab	2860
I-Beam 2 web	6100
I-Beam 1 slab	3500
I-Beam 1 web	5600
I-Beam 3 slab	7230
I-Beam 3 web	5870
Box-Beam 1	7300
Box-Beam 2	7200
Box-Beam 3	6630

3.7.3 Tension Tests of Retrieved Strands

The condition of the strands varied from beam to beam. Some of them were heavily damaged, such as the strand from I-beam 2 and all box beams, while strands from I-beam 1 and I-Beam 3 were in a good condition. Table 3.5 shows the yield and ultimate tensile strengths of the prestressing strands that were extracted from the end of each beam. More information can be found in Alfailakawi et al., (2020).

Table 3.5. Tensile Test Results

Girder Designation	Elastic Modulus, ksi	Yield Strength, ksi	Ultimate Strength, ksi
I-Beam 3	31,000	243.5	261.5
I-Beam 2	27,500	N.A	188.5
I-Beam 1	34,000	252	272
Box Beam 1	33,000	257	269
Box Beam 2	30,000	N.A	224
Box Beam 3	N.A	90	191

3.8 Analysis of Data and Development of Method for Residual Strength Calculation

This section presents the results of the calculations performed to predict the flexural strength of each beam using four approaches for each beam. Two methods were used to determine a reduced area of prestressing strand to use in the calculations to reflect the corrosion damage. The two methods were the recommendations of Naito et al., (2010a), and a modified method described below. With each reduced prestressing area, strength was calculated once using a strain compatibility approach, and again using the simplified method from the AASHTO LRFD Bridge Design Specifications (AASHTO, 2020).

3.8.1 Modified Method for Estimating Strength of Corrosion Damaged I-Beams

The modified method developed in this study and used to calculate strength of each beam is presented in this section. Types of damage to be considered in this method included longitudinal cracking, delamination, patching, exposed strands, and spalled sections. This method was obtained by relating the visually inspected I-beams to the flexural test results from this study. All types of damage that were within a distance of a strand's development length away from the section being evaluated were considered for calculation of flexural strength. The AASHTO development length equation was used as a reference. Based on comparisons to tests, it was found that the Naito et al. recommendations were somewhat conservative for I-beams. The modified method provides slightly less conservative results.

Table 3.6 presents differences between Naito et al. (2010) approach and the modified method. For the I-beams, the modified method was used to determine the residual capacity. While for the box beams, the modified method closely resembled the results using the Naito et

al., (2010a) recommendations, but did not match the test results as well. Therefore, only the recommendations of Naito et al., (2010a) were used for analyzing the box beams.

Table 3.6. Damage estimation for strands to calculate flexural capacity

Percentage of original cross-sectional area of strands to be included in strength calculations		Strand condition
Naito et al., (2011)	Modified	
0%	0%	All exposed strands, with a heavily corroded condition as fracture or wire loss
0%	20%	All exposed strands, with a moderate condition as heavy pitting
N.A.	10%	Strands in the patched area
75%	60%	Strand closest to a longitudinal crack and in the layer closest to the surface (Figure 3.14)
75%	80%	Strands adjacent to a longitudinal crack, spalled area or patched area, in the layer closest to the surface, located no more than 3 in from the deterioration type (Figure 3.14)
N.A.	80%	Strands, in the layer closest to the surface, within delaminated areas
95%	100%	All other strands in a longitudinally cracked beam

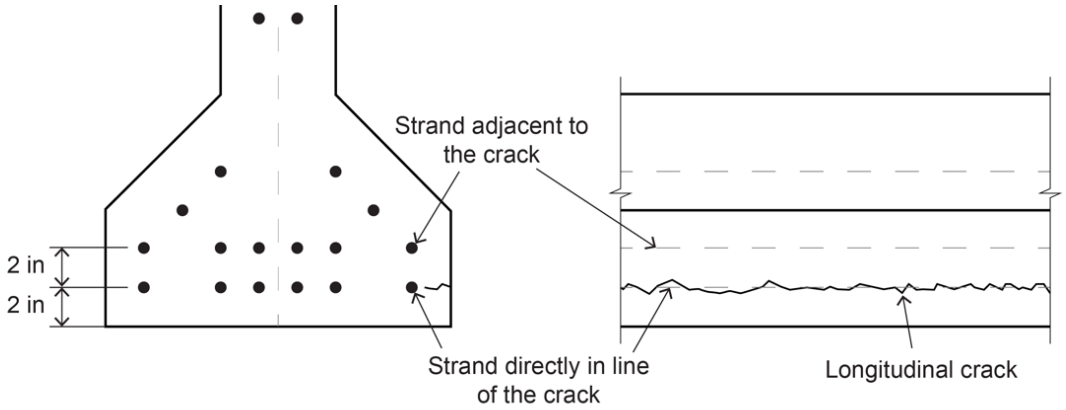

Figure 3.14. Cross-section and elevation view for I-Beam

3.8.2 Comparison of Calculation Methods to Test Results

3.8.2.1 I-Beam 3 – Base Beam

Based on all observations and non-destructive tests, this beam appeared to be in very good condition, with no visible corrosion damage to any strands. Therefore, the strength was

calculated using the cross-section shown in Figure 3.15. The haunch at mid-span was 1.5 in. The results of the strength calculations using strain compatibility and the AASHTO method are shown Table 3.8 and Table 3.9. The analysis validated the methods and material properties used for the calculation of strength and confirmed that this beam did not have any strength degradation due to corrosion damage. Also, the effective prestress calculated from the observed actual cracking load (85 kips) was 147 ksi using the modified method calculations, which was close to the 149 ksi AASHTO-based effective prestress.

3.8.2.2 I-Beam 2

The strength for this beam was also calculated using two methods to account for the damage: the recommendations of Naito et al. (2010a), and the modified method. The damage inferred from the pre-test visual inspection is presented in Figure 3.15. The haunch at mid-span was 1.5 in. The calculations using strain compatibility and the AASHTO method are presented in Table 3.8 and Table 3.9. Based on the damage maps, two out of six strands in the first lower level were in a patched area, and the other two had longitudinal cracks. Additionally, one strand out of six in the second lower level was in the patched area. In order to calculate the flexural strength using strain compatibility, the effective prestress was calculated to be 149 ksi by assuming prestress losses as prescribed by AASHTO. From the test, the effective prestress calculated from the observed actual cracking load (50 kips) was 148 ksi using the modified calculations, which was close to the 149 ksi AASHTO-based effective prestress.

The Modified method provided an exact prediction of the residual strength, while the Naito et al., (2010a) method provided slightly conservative estimates of residual strength using the strain compatibility method.

3.8.2.3 I-Beam 1

The Naito et al. (2010a) approach and the modified method were used to account for the damage in I-Beam 3 (see Figure 3.15). Prior to testing, there was one exposed strand in the first lower level. The beam was not chipped to expose the bottom strands after the test, but damage could be observed based on lost cover during testing. The haunch at mid-span was 1.5 in. The effective prestress calculated using the AASHTO method of prestress losses was 150 ksi; this value was used in both the strain compatibility calculating the flexural strength for each damage estimation method (see Table 3.8 and Table 3.9). The effective prestress calculated from the observed actual cracking load (80 kips) was 162 ksi using the modified calculations, which was above 9% above the AASHTO-based effective prestress.

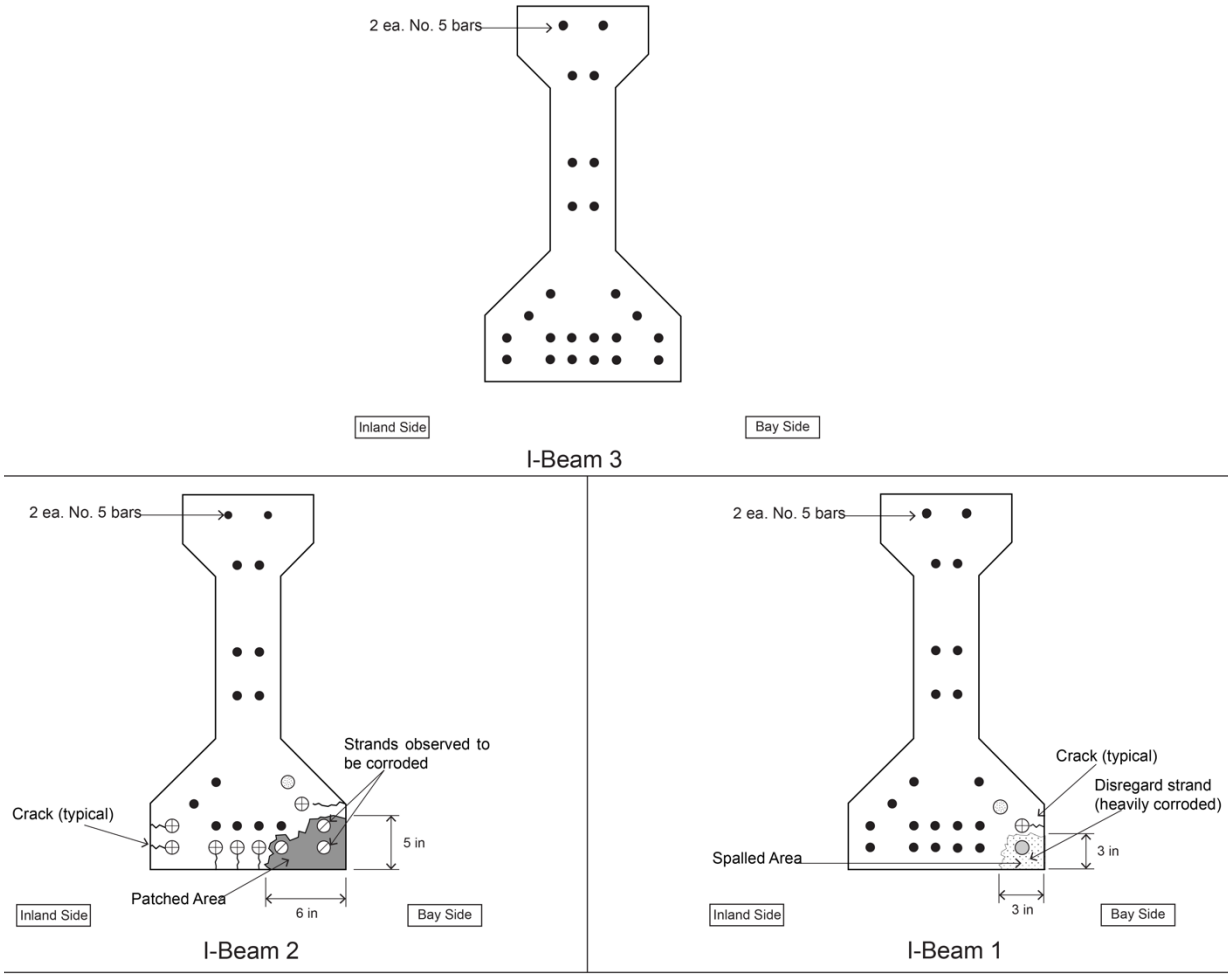

% Cross-Sectional Area

Symbol	●	⊕	○	⊘	◍
Naito et al.	95%	75%	75%	0%	0%
Modified	100%	60%	80%	10%	0%

Figure 3.15. Damage Estimated from Visual Inspection for I-Beam specimens

3.8.2.4 Box Beam 1

The cross-sectional area of the strands in Box Beam 1 to be used for calculations were assumed using the recommendations of Naito et al. (2010a). Based on visual inspection, three exposed strands in the first lower level were heavily corroded (see Figure 3.16). Those assumptions resulted in estimated flexural strengths that were within about 1% the actual strength determined from load testing. Note that the effective prestress calculated from the

AASHTO method was 156 ksi. On the other hand, the effective prestress calculated from the observed 50-kip cracking load and the Naito et al., (2010a) recommendations was 128 ksi, which was about 18% below the AASHTO-based effective prestress.

3.8.2.5 Box Beam 3

Box Beam 3 had different conditions than the other two box beams, with water trapped in the beam leading to a lower strength. The recommendations of Naito et al., (2010a) were used with a small modification to account for the trapped water, where a 15% reduction was applied to the two lower strands levels (see Figure 3.16). This percentage reduction gave reasonable calculated results. The calculations using strain compatibility and the AASHTO method are presented in Table 3.7. Note that the actual cracking load of 50 kips resulted in an effective prestress equal to 167 ksi. The effective prestress calculated from the AASHTO method was 156 ksi. This latter value for effective prestress was used in both calculation methods for flexural strength.

Table 3.7. Estimates of Strength Considering Damage of Box Beam 3

Method to Estimate Damage	Method to Calculate Strength	Flexural Strength, k-ft
Test		1196
(Naito et al., 2010a)	AASHTO	1325
	Strain Compatibility	1332
(Naito et al., 2010a) (trapped water reduction is included)	AASHTO	1168
	Strain Compatibility	1165

3.8.2.6 Box Beam 2

The residual capacity for Box Beam 2 was calculated using the recommendations of Naito et al., (2010a) to estimate the remaining cross-sectional area of the strands. Three exposed strands were disregarded in the calculation of the flexural strength (see Figure 3.16). The Naito et al., (2010a) recommendation provided a close prediction of the residual strength capacity.

Also, the effective prestress calculated from the observed actual cracking load (49 kips) was 139 ksi using the modified calculations, which was 11% below the AASHTO-based effective prestress.

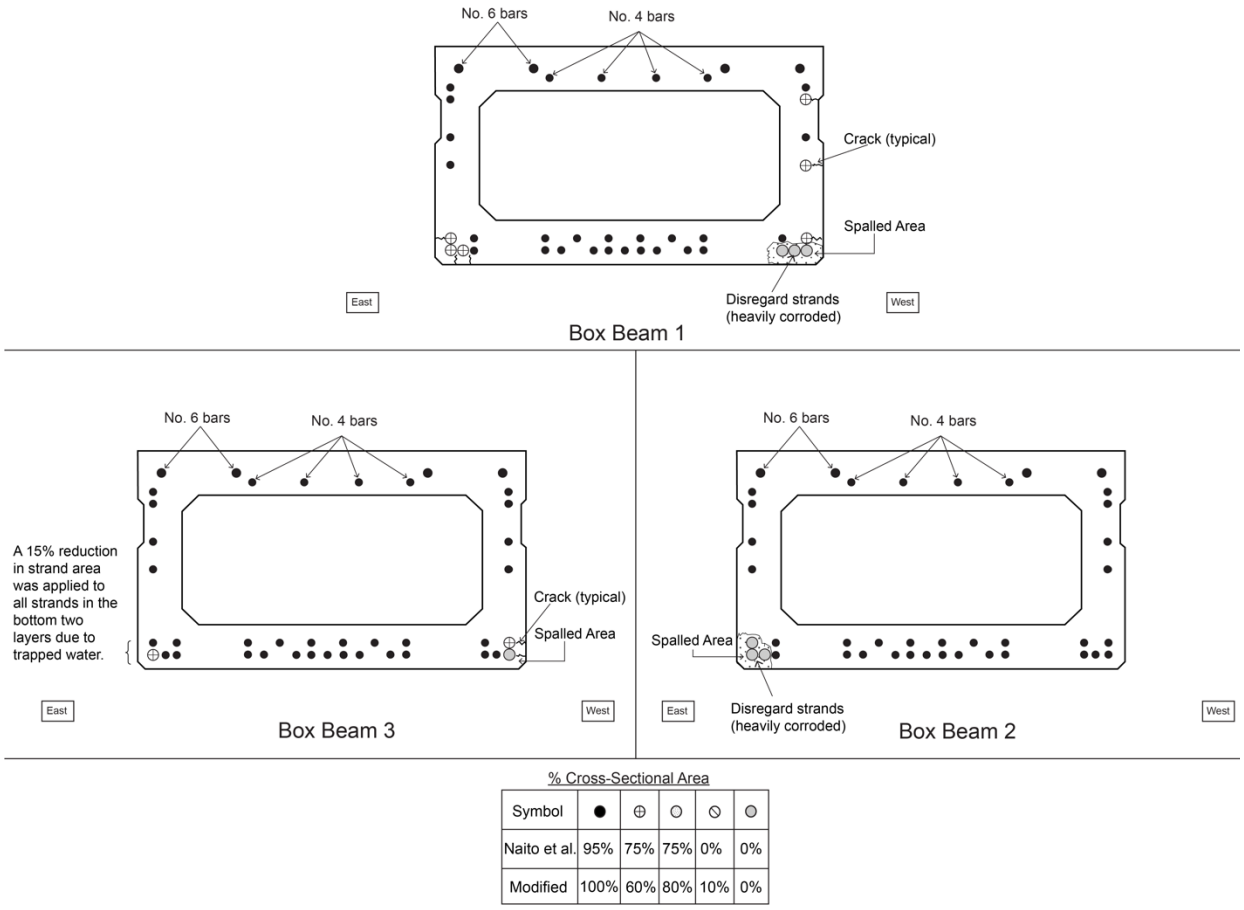

Figure 3.16. Damage Estimated from Visual Inspection for Box Beam specimens

3.8.2.7 Summary of Performance of Damage Assessments

For all of the beams in this study, Table 3.8 compares the results of assuming reduced cross-sectional areas of prestressing steel, as dictated by the Naito et al., (2010a) and the modified method, when calculating the flexural strength using the strain compatibility method.

Table 3.9 makes the same comparisons, except using the AASHTO method for the calculation of the stress in the strands at ultimate. From the tables, all methods provided

reasonable estimates of residual flexural strength, with the Naito et al. method being more conservative for the I-beams as compared to the modified method. The Naito et al. method provided very accurate estimates of residual strength for Box Beam 2 and Box Beam 1 but was unconservative for Box Beam 3. As discussed previously, the water trapped inside of Box Beam 3 contributed to additional unseen corrosion damage and associated loss of strength.

Table 3.8. Comparison of Methods to Tests Using Strain Compatibility

Beam	Tested Strength k-ft	Naito et al. (2010)		Modified Method	
		Estimated Strength, k-ft	M_{test} / $M_{estimated}$	Estimated Strength, k-ft	M_{test} / $M_{estimated}$
I-Beam 3	2038	2034	1.00	2034	1.00
I-Beam 2	1393	1366	1.02	1391	1.00
I-Beam 1	1873	1699	1.10	1762	1.06
Box Beam 1	1269	1253	1.01	N/A	N/A
Box Beam 3	1196	1332	0.89	N/A	N/A
Box Beam 3 - with water effect	1196	1168	1.02	N/A	N/A
Box Beam 2 - Bad	1284	1292	0.99	N/A	N/A

Table 3.9. Comparison of Methods to Tests Using AASHTO Strength Calculations

Beam	Tested Strength k-ft	Naito et al. (2010)		Modified Method	
		Estimated Strength, k-ft	M_{test} / $M_{estimated}$	Estimated Strength, k-ft	M_{test} / $M_{estimated}$
I-Beam 3	2038	2017	1.01	2017	1.01
I-Beam 2	1393	1342	1.04	1365	1.02
I-Beam 1	1873	1675	1.12	1735	1.08
Box Beam 1	1269	1251	1.01	N/A	N/A
Box Beam 3	1196	1325	0.9	N/A	N/A
Box Beam 3 - with water effect	1196	1165	1.03	N/A	N/A
Box Beam 2 - Bad	1284	1289	0.99	N/A	N/A

3.9 Alternative Method – Strain limitation

Naito et al., (2011) and Alfailakawi et al., (2020) provides recommendation for calculating the residual strength for damaged beams based on reduced cross-sectional area, assuming crushing strength of concrete as a failure mode by reaching the maximum strain on the top of the beam. Al Rufaydah, (2021) performed a shear test for Box Beam specimen which

failed by strand's rupturing, not concrete crushing, at total moment of 890 k-ft. during the test strands started rupturing and the load carrying capacity degraded until the test was called off. Therefore, there is a need for an alternative method to estimate the residual flexural capacity of damaged beams that takes into account the fact that strands may rupture before top concrete crushes.

This section provides a guidance to estimate the flexural strength by limiting the strain at the bottom most layer. When the layer of strands reaches this limiting strain, it is assumed that the most damaged strand will rupture. Based on a study conducted by Alfailakawi et al., (2022) the condition of the most damaged strands and its corresponding strain can be obtained from the visual inspection (see Figure 3.17). Therefore, neutral axis location, strain at the top and moment capacity can be calculated. After that, the most damaged strands will be eliminated, and a new sectional analysis is performed to estimate the flexural strength based on crushing failure. If the flexural strength determined by strand rupture is greater than the flexural strength determined by concrete crushing, then the flexural strength determined by strand rupture will be the maximum flexural strength; otherwise, the flexural strength determined by concrete crushing will be the maximum flexural strength.

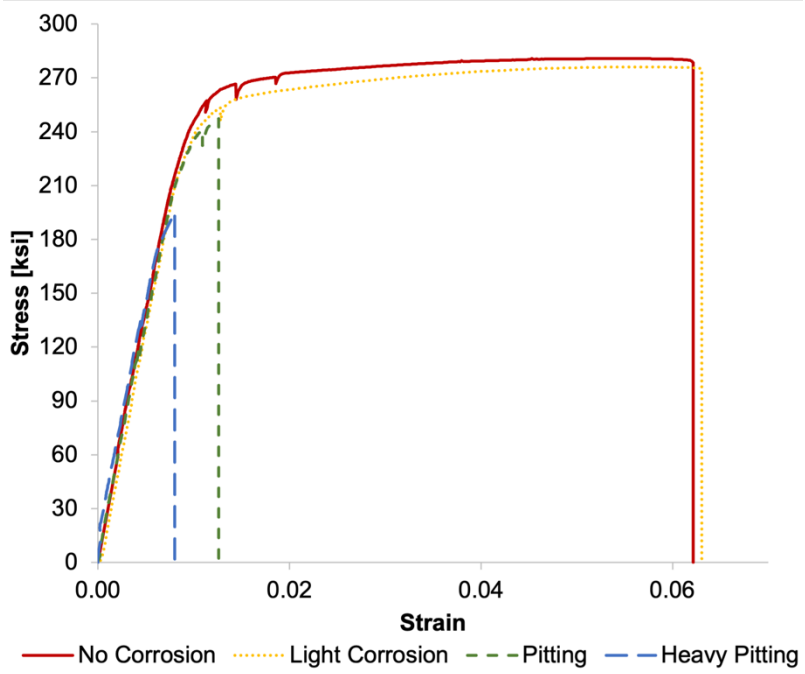

Figure 3.17. Stress-Strain Curves of Prestressing Strand with Various Levels of Damage

3.8.1 Example for Box Beam Failed by Strand's Rupturing

the box beam tested in Al Rufaydah (2021) is a good example to illustrate the use of the proposed method. Figure 3.18 shows the anticipated cross section with the damage assessment based on visual inspection. Table 3.10 shows the three failure modes calculations to show the procedure of this alternative method.

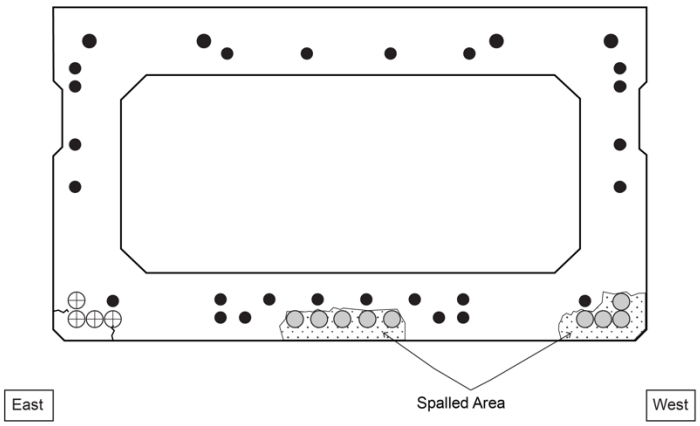

Figure 3.18. Damage Assessment for Box Beam

First, the moment capacity will be calculated based on the current condition of the beam. The full area of strands will be included unless the strand is fractured. So, 8 strands will be eliminated from the calculation at the bottom most layer while 7 strands will be included despite the level of damage. With limiting the strain at the top of the beam to 0.003, the total moment capacity is 1002 kip-ft.

Second, the same configuration of strands used in the first failure mode. As per Figure 3.17, the strain at the bottom most layer will be limited to 0.008 since there are strands aligned with a very wide crack. Based on that, the total strength capacity is 810 k-ft.

Finally, the strands which reached the limit in the second failure mode will be eliminated and the strength capacity will be calculated with 0.003 as a strain limit in the concrete at the top of the beam. Based on that, the calculated flexural moment is 799 k-ft.

Table 3.10. Failure Modes Calculation

Failure Mode		Neutral Axis Depth, in	Strain at the Top of Concrete	Strain at the Level of Bottom Most Layer	Total Moment Capacity, k-ft
First	Concrete Crushing	3.81	**0.003**	0.0225	1002
Second	Strand's Rupturing	7.13	0.001	**0.008**	810
Third	Concrete Crushing	3.31	**0.003**	0.025	799

So, since the second and third failure modes were less than the first one, and the second failure mode is higher than the third failure mode, 810 k-ft is the ultimate moment capacity for this example. The tested total moment strength was 890 k-ft which is higher than the excepted capacity by 9%.

3.9 Discussion

The primary input required to calculate a reasonable estimate of residual strength of corrosion-damaged prestressed bridge beams is a good map of the damage observed during a detailed safety inspection. Previous patching, longitudinal cracking along the strands, delamination, and concrete spalls are all excellent evidence that strand corrosion has progressed to a point where the strand in the deteriorated region cannot be completely counted on to contribute to flexural strength. Moreover, the half-cell potential measurements were performed for all the specimens, however it did not provide any additional information to inform the calculation of strength. This is in agreement with the findings of Naito et al., (2010a), which found that there was some correlation between half-cell results and corrosion of strands, but the coefficient of variation of tests was very high.

The post-test destructive evaluations were valuable to determine concrete strength and strand stress-strain properties. However, the chloride concentration results were mixed. As shown in Table 3.3, the results showed only negligible to low probability of corrosion in the box beams, while in reality they all had at least a few exposed and broken strands. Chloride concentrations also indicated that all of the I-beams had a medium probability of corrosion, but I-beam 3 showed almost no evidence of active corrosion. So, this type of tests is not valuable for evaluating damage for a strength estimation.

To provide the engineer the required information for an accurate estimate of residual strength, bridge inspectors need to develop detailed damage maps, such as those shown in Figure 3.3. The locations of the various types of damage need to be carefully documented so the load

rater can employ the damage estimation recommendations in their strength calculations. Many inspectors already provide these types of detailed maps.

3.10 Summary and Conclusions

The following conclusions can be drawn based on the results of this testing program.

- For prestressed I-beams, with the Naito et al., (2010a) method of damage estimation, either the AASHTO simplified method or strain compatibility approach can be used to calculate conservative estimates of flexural strength. The modified method for damage estimation, as presented in this paper, provides slightly more accurate estimates of residual strength compared to the Naito et al., (2010a) method.
- The Naito et al., (2010a) recommendations to estimate the residual cross-sectional area of prestressed strands in adjacent box beams result in reasonably accurate estimates of strength.
- The alternate method, which is based on strain limitation, produces satisfactory results and accurately captures the failure mechanism.
- Poor drainage of water from the inside of box beams can lead to hidden damage, resulting in overly optimistic predicted flexural strength. Therefore, weep holes should be cleared to allow proper drainage of water.
- Data collected from visual inspections are the best inputs and are sufficient for estimating the remaining cross-sectional area of strands in prestressed concrete flexural members. For unknown reasons, half-cell potentials and chloride concentration testing did not provide consistent results in this study.

3.11 References

AASHTO, L. R. F. D. (2020). Bridge design specifications.

AASHTO, L. R. F. D. (2017). Specifications. *American Association of State Highway and*.

AASHTO, T. P. (2011). 95-11 "Standard Method of Test for Surface Resistivity Indication of Concrete's Ability to Resist Chloride Ion Penetration.". *AASHTO Provisional Standards, 2011 Edition*.

Alfailakawi, A., Roberts-Wollmann, C. L., Hebdon, M., & Koutromanos, I. (2020). Experimental and Analytical Evaluation of Residual Capacity of Corrosion-Damaged Prestressed Concrete Bridge Girders.

Al Rufaydah, A. *Shear Strength Assessment of Corrosion Damaged Prestressed Concrete Girders*. Masters Thesis, Virginia Tech, Blacksburg, VA. 2020.

American Concrete Institute, A. C. I. C. (2019). *Building code requirements for structural concrete (ACI 318-19) : an ACI standard; Commentary on building code requirements for structural concrete (ACI 318R-19)*.

ASTM-C876. (2015). Test Method for Corrosion Potentials of Uncoated Reinforcing Steel in Concrete.

Balakumaran, S. S. G. (2010). *Influence of Bridge Deck Concrete Parameters on the Reinforcing Steel Corrosion*. Virginia Tech].

Harries, K. A. (2009). Structural testing of prestressed concrete girders from the Lake View Drive Bridge. *Journal of Bridge Engineering*, *14*(2), 78-92.

Naito, C., Jones, L., & Hodgson, I. (2010). Inspection methods & techniques to determine non visible corrosion of prestressing strands in concrete bridge components: task 3, forensic evaluation and rating methodology.

Naito, C., Jones, L., & Hodgson, I. (2011). Development of Flexural Strength Rating Procedures for Adjacent Prestressed Concrete Box Girder Bridges. *Journal of Bridge Engineering*, *16*(5), 662-670.

Naito, C., Sause, R., Hodgson, I., Pessiki, S., & Macioce, T. (2010). Forensic Examination of a Noncomposite Adjacent Precast Prestressed Concrete Box Beam Bridge. *Journal of Bridge Engineering*, *15*(4), 408-418.

Rogers, R., Wotherspoon, L., Scott, A. N., & Ingham, J. M. (2012). Residual strength assessment and destructive testing of decommissioned concrete bridge beams with corroded pretensioned reinforcement.

Rose, A. L., Suguna, K., & Ragunath, P. N. (2009). Strengthening of corrosion-damaged reinforced concrete beams with glass fiber reinforced polymer laminates. *Journal of Computer Science*, *5*(6), 435.

CHAPTER 4: Large Scale Laboratory Testing – External Post-Tensioning Repair Method

Chapter 3 consists of the manuscript: "Flexural Strengthening Repair of Corrosion Damaged Bridge Girders Using External Post-Tensioning Method" This paper is currently in preparation for submission to journal.

Flexural Strengthening Repair of Corrosion Damaged Bridge Girders Using External Post-Tensioning Method

Ali Alfailakawi[1]; Carin L. Roberts-Wollmann[2]; Matthew H. Hebdon, [3]; Ioannis Koutromanos, [4]

Virginia Tech, Blacksburg, VA

4.1 Abstract:

The results of testing two 54-year-old, corrosion-damaged Type II AASHTO I-Beams that were repaired with external post-tensioning are presented in this paper. The specific retrofit can be utilized to restore the flexural strength of corrosion-damaged prestressed beams. Two beams with similar levels of corrosion damage were obtained from a Virginia bridge during demolition and the residual strength was determined using a modified approach established by Alfailakawi et al., (2020), which evaluates the effects of corrosion damage based on visual inspection. Repairs were designed and implemented using external post-tensioning to restore the flexural strength based on the damage estimation. Following that, the beams were tested in the laboratory to evaluate their moment capacity. Both beams were subjected to monotonically increasing loads until a concrete crushing failure mode occurred at the top of the beams. The experimental test was accompanied by a detailed approach for determining the ultimate failure load, the ultimate stress in the external tendons, and the location of the failure. Simplified

calculations based on design code guidelines were performed and it was determined that they resulted in overly conservative failure load estimates.

4.2 Introduction

4.2.1 Background

External post-tensioning (PT) can be used as a method of repair to restore the capacity of any structural element. It can increase the strength and serviceability of deteriorated structures (Harajli, 1993). In addition, it is considered an economical solution compared to demolishing and rebuilding the structure. Engineers prefer this type of repair because of the speed of construction, minimal disruption to traffic flow, and ease of monitoring and maintenance (Suntharavadivel & Aravinthan, 2005). The repair system includes attaching external tendons to the ends of the beams by anchorage systems (Nassif et al., 2003). The external tendons can be made of steel or CFRP (Bennitz et al., 2012), (Heo et al., 2013). The design of the anchorage is crucial to transfer the prestressing force to the beam. There are many types of anchorage and deviation systems that have been used, such as reinforced concrete blocks (Zhang et al., 2020) (Leicht et al., 2020), anchor pins (Lee et al. 2018), or steel bracket anchorage systems (Sayed-Ahmed et al., 2004).

Sayed-Ahmed et al., (2004) tested two corrosion-damaged beams taken from a decommissioned bridge in Alberta (Canada). A system with steel anchorage brackets was used for these inverted U-shaped beams. The external PT was introduced through Dywidag bars, which were anchored at the ends of the beam and deviated at the third points of the beam. The experiment showed external PT repair was an effective repair method, increasing the capacity by 20%.

Bennitz et al., (2012) tested seven reinforced concrete T-beams, one with no repair and six with straight external unbonded CFRP tendons. All the repaired beams exhibited an increase in strength of more than 17%. Lee et al., (2018) tested nine pre-damaged beams, three as reference beams and six as strengthened post-tensioned beams. They concluded that the external PT increased the strength and stiffness by 40% and 28%, respectively. Also, they mentioned that the increase in the stiffness of the beams was observed through the reduction of the width in the cracks.

Research has also been done on the repair of existing bridges. Khudeira, (2010) selected an external PT system as a repair method for the rehabilitation of an existing corrosion-damaged reinforced concrete bridge in Chicago. Grade 150 steel threaded bars were anchored to the web at the end of the beams by stiff steel brackets. The brackets were connected to the beam by post-tensioning rods through drilled holes to ensure sufficient friction between the brackets and the concrete. Khudeira, (2010) concluded that this method improved the strength, service performance, and durability.

4.2.2 Problem Statement

The calculation of the flexural capacity of prestressed concrete beams, which have corrosion damage and are subsequently repaired, requires additional study. The research presented in this paper first evaluated damaged beams using the method presented in Alfailakawi et al., (2020). Then the researchers developed external post tensioning repair schemes, repaired the beams, and tested the repaired beams. Improvements in methods to estimate the residual capacity and the repaired capacity of corrosion-damaged beams will help bridge engineers

develop effective repairs in the future. In addition, a detailed approach is presented in this paper to calculate the ultimate stress in the external tendons.

4.2.2 Purpose and Scope

The overall purpose of this research was to evaluate recommendations for methods to calculate residual strength and to evaluate the repaired strength of corrosion damaged beams using external post-tensioning. The capacities of repaired corrosion-damaged prestressed beams were determined using large-scale experimental tests. External post-tensioning was used as a repair method and was evaluated to determine the resulting restoration of structural capacity. Two beams retrieved from the Lesner Bridge, which was demolished and rebuilt in 2016 were tested to achieve the purpose of this research.

4.3 Description of Specimens

4.3.1 Lesner Bridge Beams

The west bound lanes of the Lesner Bridge, also known as the Lynnhaven Inlet Bridge, were built in 1967. The approach spans were constructed using prestressed concrete beams, whereas the main spans were constructed with steel beams. The beams in the approach spans were 49 ft – 9 in. long, 36 in. deep prestressed I-beams (AASHTO Type II). The beams were specified to have 5000 psi concrete strength and were prestressed with 22 - 7/16-in. Grade 270 stress-relieved prestressing strands. Each span included seven beams spaced 5 ft – 2.5 in. center-to-center.

The bridge was demolished and rebuilt in 2016 after almost 50 years of service. Nine beams were recovered during the demolition phase and sent to Virginia Tech for testing. The

slab between the beams was saw-cut to enable the beams to be retrieved, together with a part of their cast-in-place composite deck. Figure 4.1 illustrates the level of degradation in typical beams. The Lesner Bridge was repaired several times over the years, so patching is evident in many locations. The cross-section of the Lesner Bridge I-beams is also shown also Figure 4.1. Note that the sides of the beam are labeled as “bay side” and “inland side.” As this suggests, when the beams were in-situ, the “bay side” faced the Chesapeake Bay, and the “inland side” faced the Lynnhaven Inlet. The bay side of the beams always exhibited a higher level of corrosion damage.

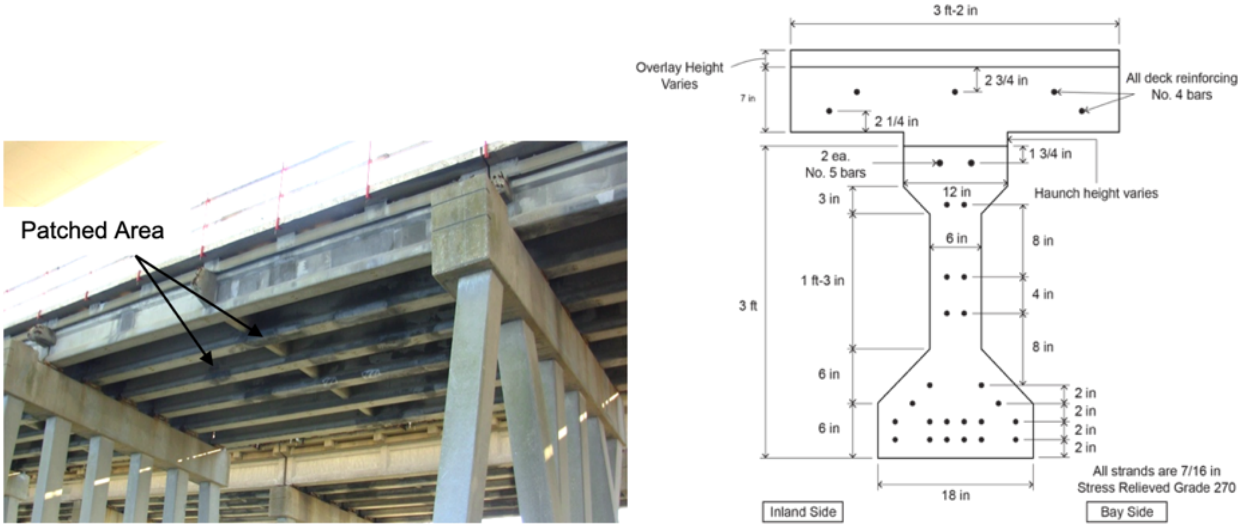

Figure 4.1. Typical Deterioration on the Lesner Bridge (left) Cross-section of Lesner Bridge I-Beams (Right)

For simplification purposes, the Lesner Bridge beams in this paper will be referenced as I-Beam 1 and I-Beam 5 which correspond to Alfailakawi et al., (2022). More information regarding beam designations and the original locations can be found in Alfailakawi et al., (2022).

4.4 Evaluation of Corrosion Damage

Prior to developing the repair plans for the beams, they were examined to determine the level of corrosion and the resulting with loss of the flexural strength. Visual inspection and half-

cell testing were used to create damage maps and half-cell contour maps, respectively. Additionally, after the flexural strength testing, powdered concrete samples from the beams were obtained to determine chloride contents.

4.3.1 Visual Inspection

The beams were examined, and each beam's existing condition was thoroughly documented. The documentation included the location of damage such as cracks, delaminations, spalling, patching, and strand exposure. Delaminations were located by tapping the sides of the beams with a hammer and recording locations that had a hollow or dead sound. Detailed damage maps were created for each beam, indicating the size and location of each defect. Figure 4.2 and Figure 4.3 present damage maps for I-Beam 1 and I-Beam 5, respectively.

In Figure 4.2 and Figure 4.3, the top sketch is one side, oriented right-side-up, the middle sketch is the bottom of the beam, and the bottom sketch is the other side of the beam, oriented up-side-down. This allows the reader to see how side and bottom face damage are related spatially.

4.3.2 Half-Cell Potential Tests

Half-cell readings were taken at 1525 points on all the sides of both beams. Figure 4.2 and Figure 4.3 illustrate the potential mapping of I-Beam 1 and I-Beam 5. The figures reveal both beams have a low likelihood of corrosion in general. However, the beams have a high

chance of corrosion at the middle of the beam on the bay side, quite similar to the damage maps generated.

As per ASTM C876, Table 4.1 shows the probability of corrosion for both beams. For instance, 288 half-cell readings were taken from the bay side of I-Beam 1, 64 of which were more than -200mV, showing that 28% of the readings indicate that the probability of corrosion is less than 10%. In addition, 66% A readings indicate uncertainty (between -200mV and -350mV) and 6% of readings indicate 90% probability of corrosion (less than -350mV).

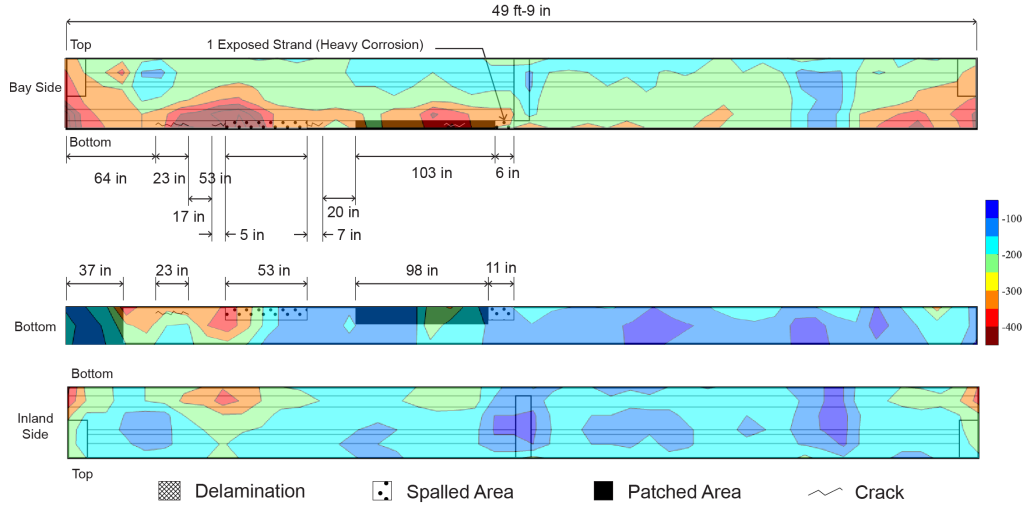

Figure 4.2. Heat Map for Half-Cell - I-Beam 1 (in millivolts)

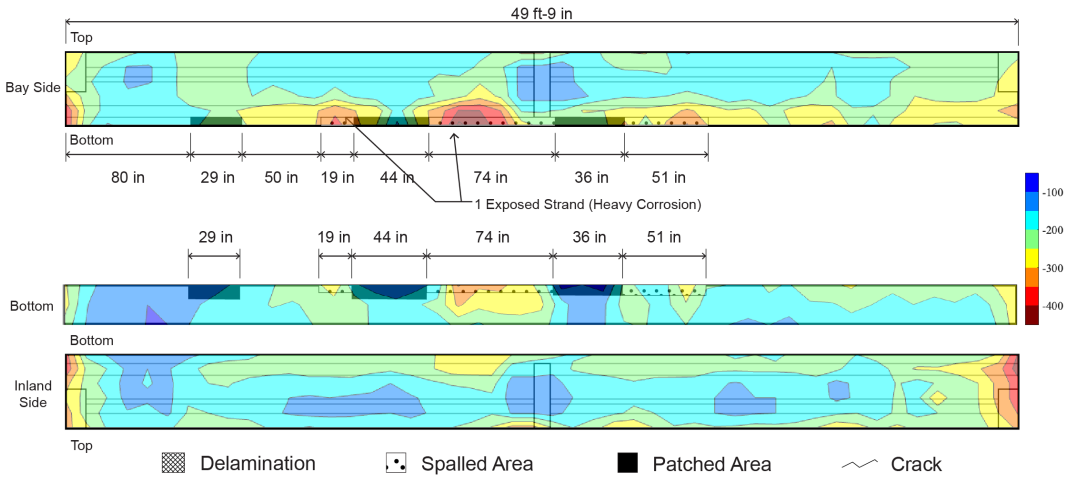

Figure 4.3. Heat Map for Half-Cell - I-Beam 5 (in millivolts)

Table 4.1. Probability of Corrosion in the Beams

Beam	Side	10% Corrosion	Uncertain	90% Corrosion
I-Beam 1	Bay	28%	66%	6%
	Bottom	86%	13%	1%
	Inland	82%	17%	1%
I-Beam 5	Bay	44%	52%	4%
	Bottom	65%	34%	1%
	Inland	54%	43%	3%

4.4.3 Total Chloride Evaluation

This section summarizes the chloride concentration measurements performed on powdered samples taken from the tested beams. The threshold for corrosion risk due to chloride contents are given in Table 4.2.

Table 4.2. Risk of Corrosion Compared to Chloride Content (Balakumaran, 2010)

% Chloride by mass of sample (concrete)	Risk	Chloride content per volume of concrete (lb/yd3)
<0.03	Negligible	<1.17
0.03-0.06	Low	1.17-2.35
0.06-0.14	Medium	2.35-5.48
>0.14	High	>5.48

Figure 4.4 illustrates the chloride content testing results for the beams. For I-Beam 1, the 1-in. penetration depth contained more chloride than the 0.5-in. starting depth on the inland and bay sides. This might be because water or rain rinsed chloride off the concrete's surface, while the beam sat in storage outside of the lab for over three years, resulting in a low value. In general, the chloride concentration dropped as the depth of the sample increased. At each depth point, the chloride content on the bay side was much larger than on the inland side, most likely due to the bay side being exposed to a harsher environment. According to Table 4.2, I-Beam 1 had a medium risk of corrosion on the inland side and a high risk of corrosion on the bay side. The chloride content values for I-Beam 5 indicated that the beam had a moderate risk of corrosion on the bay side and a negligible risk of corrosion on the inland side.

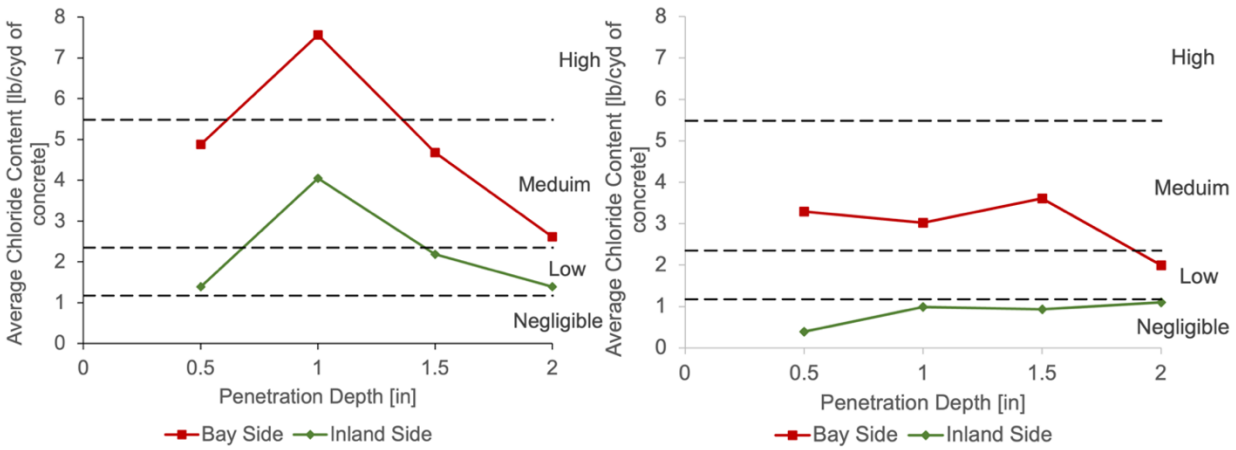

Figure 4.4. Results of Chloride Testing for I-Beam 1 (Left) and I-Beam 5 (Right)

4.4.4 Discussion

The damage maps for both beams reveal similarities in the center of the beams, which is the section of interest for flexural analysis, and this is in accordance with the results obtained from the half-cell heat maps provided. However, based on the chloride content tests results I-Beam 1 was considered to have a medium to high risk of corrosion, while I-Beam 5 had a negligible to medium risk of corrosion. These forensic investigations offered a general idea of the likelihood of corrosion in the beams, but they cannot be used as a quantification approach to be incorporated in the calculation to determine the residual flexural strength.

4.5 Residual and Undamaged Strength Calculations

To design the necessary repairs, first the original undamaged strength and the residual flexural strength for each beam was calculated. The damage maps and the method presented in Alfailakawi et al., (2020) was used to account for the damage.

4.5.1 Tested Material Properties

The calculations presented in this section were performed using material properties based on samples taken from the beams after testing (see Table 4.3)

Table 4.3. Material Properties Based on Extracted Samples

Specimen	Beam Concrete Compressive Strength, psi	Deck Concrete Compressive Strength, psi	Prestressing Steel Breaking Strength, ksi
I-Beam 1	7455	6030	276
I-Beam 5	5990	5660	280

4.5.2 Evaluation of Corrosion Damage

Figure 4.5 shows cross-sections of the two beams that were repaired with external PT. Each cross-section presents the damage that was present within one development length on each side of the beam's midspan. Additionally, the expected condition of strands is shown in this picture depending on their proximity to damage, such as a longitudinal crack, spall, or patch. The table in the figure present reduced cross-sectional area of the strands utilized in the strength calculations.

The residual strength of the beams was determined assuming that the repair would need to extend the beam's service life by another 20 years. Thus, in addition to the damage already detected, it was expected that corrosion would continue to degrade strands throughout the remaining 20 years of the beam's operating life. If just cosmetic repairs, such as patching, are made to the beams during a repair, the corrosion will continue within the beam. For instance, Figure 4.5 shows the cross-section of beams with the present degree of damage estimated by visual inspection. After a further 20 years of service, it was conservatively estimated that the four

inner strands next to the damaged region, within 2 in. of the current spall or patch, would likewise corrode.

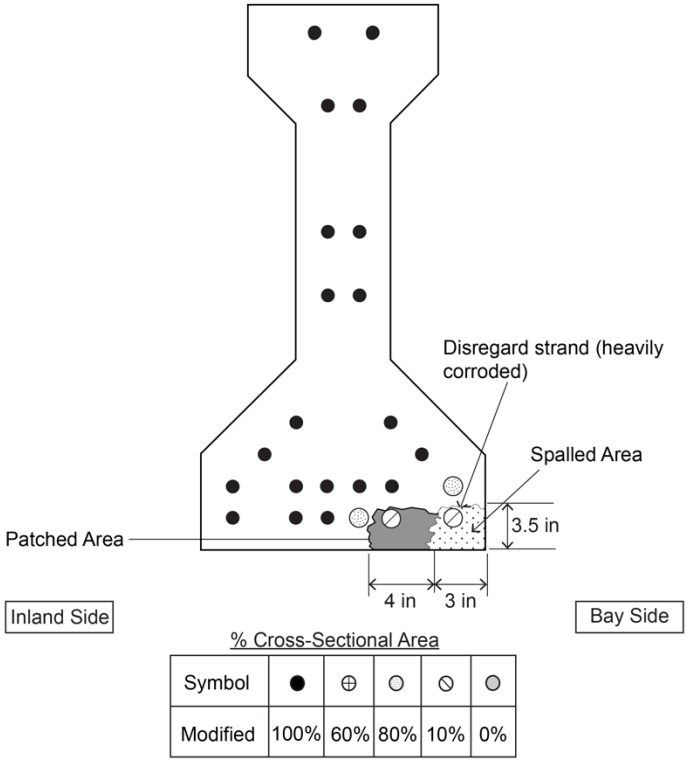

Figure 4.5. Damage Estimation for Both Beams

To calculate the residual strength of a beam with corrosion damage, a modified approach described in Alfailakawi et al., (2020) was utilized to assess damage to the I-Beam using visual inspection records. The estimated residual strengths of the beams were determined using this approach and are shown in Table 4.4. These calculations were initially performed using a 20-year damage prediction and then redone using the beams' current condition. A strain compatibility technique was employed to account for each layer of prestressing as well as the compression reinforcing in the deck for all unrepaired beams.

Table 4.4. Estimated Strength Capacity of the Beams

Specimen	Undamaged Strength k-ft	Strength with Current Corrosion Damage k-f	Strength with Assumed Corrosion Damage after an Additional 20 years k-ft
I-Beam 1	1901	1797	1345
I-Beam 5	1901	1787	1378

4.5.3 Repair of the I-Beams

The two Lesner Bridge I-Beams were repaired to restore flexural strength using external PT. One external tendon with four 0.6-in diameter strands was added to each side of the beam's web. The tendons were attached to each end of each beam by concrete anchor blocks. The anchor blocks were designed as corbels using section 16.5 in The ACI 318 Building Code Requirements for Structural Concrete and Commentary, (ACI, 2019), which provides detailed instructions for designing this type of structural element to prevent any type of failure either in the anchor block or at the interface between anchor block and the web. The required steel reinforcement including shear friction reinforcement and flexural reinforcement is five No. 5 bars and four No. 4 bars spaced as shown in Figure 4.6. Also, prior to placing the concrete for the anchor blocks, the surface of the beam's web was lightly chipped to create a roughened surface to improve the bond between the anchor block and the web. The required reinforcement was threaded through holes, which were drilled through the webs, and anchored in the concrete in the block on the opposite side of the web.

The blocks included PT anchorage devices for the tendons. The anchorage device was designed to accommodate seven 0.6-in. strands but only four strands were used. As a result, the plate was sufficiently large and the factored force ($1.2\ P_{jack}$) could be safely transmitted to the concrete without the need for spiral reinforcing.

In addition to casting the anchor blocks on the webs of the beams, additional concrete was cast at the bottom of the mid-span diaphragm wall to accommodate a deviation saddle so the

tendon could have a single-point harping pattern. Figure 4.6 presents other details of the external PT repair, while Figure 4.7 presents an elevation view of the repaired beam.

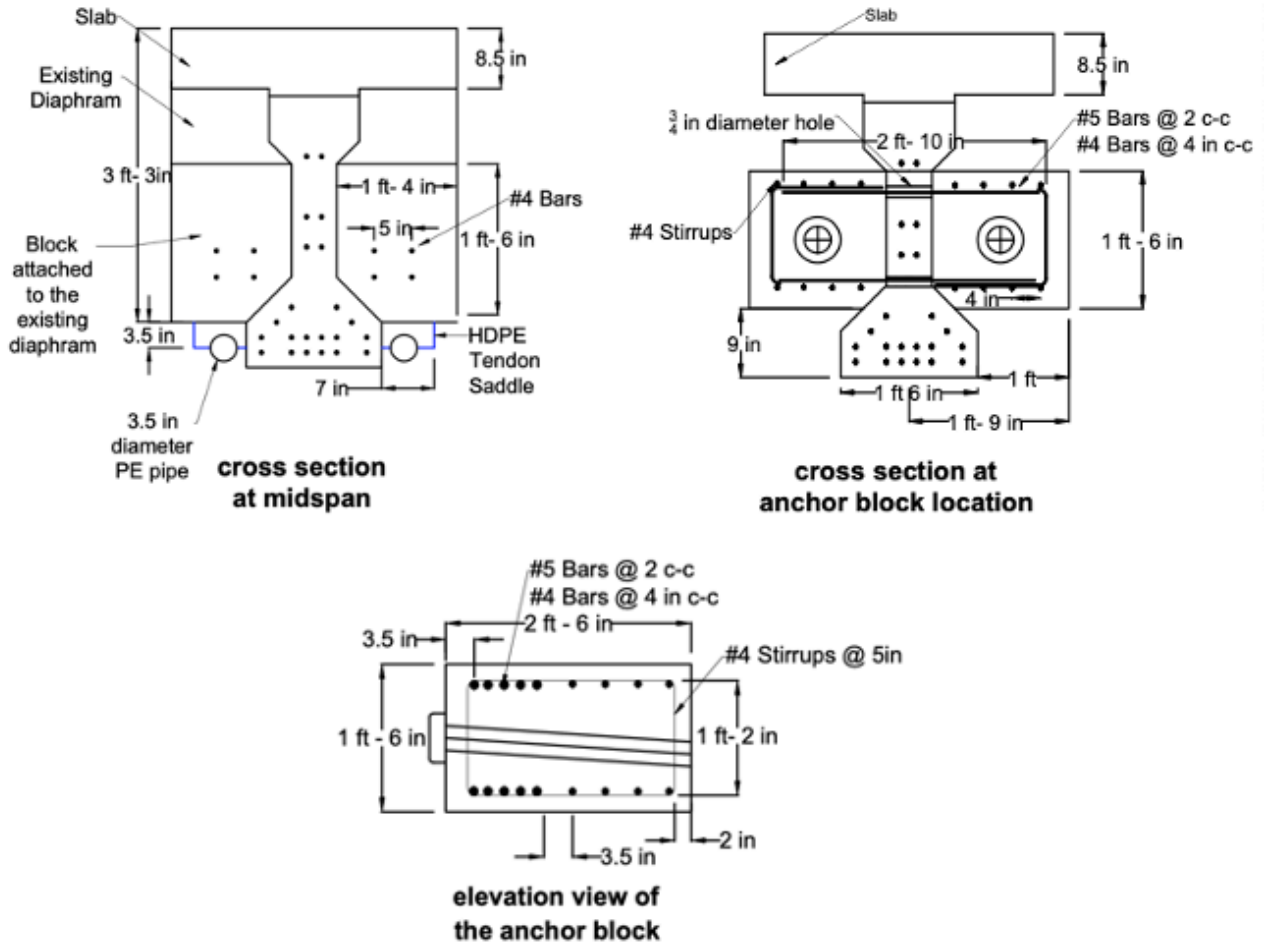

Figure 4.6. External PT Details for the Lesner Bridge Beams

After the new concrete components reached the desired strength of 5000 psi, high density polyethylene (HDPE) duct was installed between the anchor blocks, and the four 0.6-in. diameter strands were placed in the ducts. The strands were anchored at the dead end anchor block and stressed at the live end to a jacking stress of 216 ksi which is 80% of the ultimate stress of the strands. After the stressing operations were completed, the ducts were filled. In one of the beams, conventional grout was pumped into the ducts; in the other, heated wax was injected. Figure 4.8 presents photos of the duct filling processes.

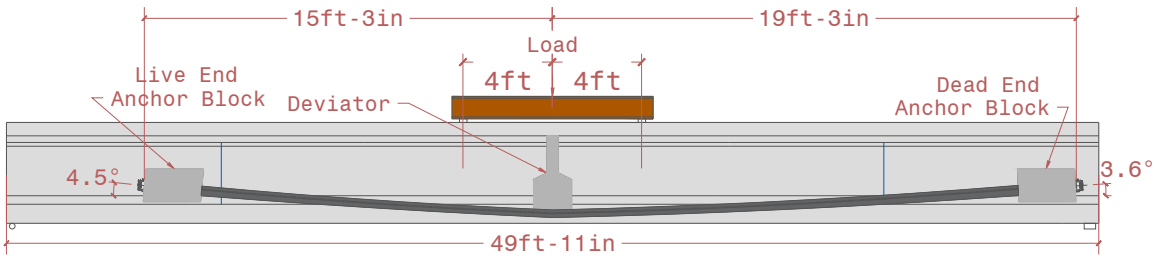

Figure 4.7. Elevation View of External PT Repair on Lesner Bridge Beam

4.5.3.1 Application of External Post-tensioning

Prior to stressing the external PT, strain gauges and LVDTs were installed at various locations on the beam. The external tendons were stressed to 80% of the guaranteed ultimate tensile strength. The stress in the strands between the anchor blocks, after losses caused by friction at the deviator and seating of the tendon on the live end, was calculated to be (180 ksi).

The PT process for each beam began by stressing the strands on the Bay side to 20% of the 80% of the ultimate stress. Then, on the inland side, the same stress percentage was applied. Following that, the inland side was increased to 60% of the ultimate stress, followed by the bay side. Then the bay side stressed to 100% as well as the inland side. Figure 9 illustrates the locations of the LVDTs behind the anchor blocks during the stressing process. Table 4.5 shows the LVDT readings after stressing all the strands. All the readings were quite small, so these negligible movements proved the efficiency of the anchor block design.

Table 4.5. LVDT Readings after Stressing

Specimen	END	LVDTs Readings after Stressing, in.		Midspan Upward Deflection, in.
		Transverse	Longitudinal	
I-Beam 1	Live	0.013	0.010	0.17
	Dead	0.016	0.000	
I-Beam 5	Live	0.014	0.006	0.28
	Dead	0.017	0.000	

Figure 4.8. External Post-Tensioning Repair

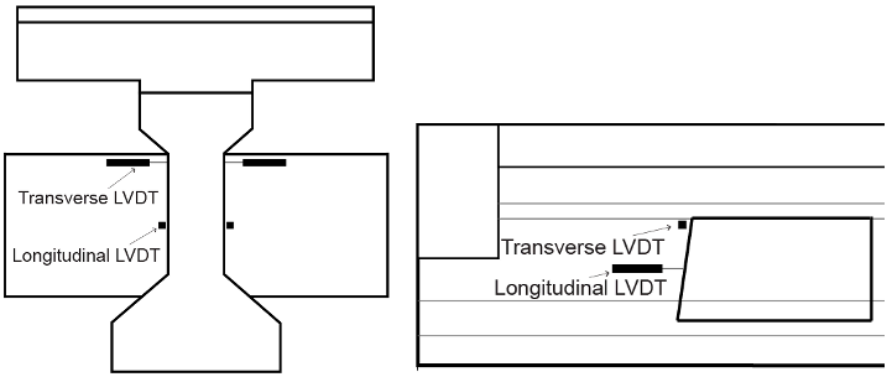

Figure 4.9. Locations of the LVDTs Behind the Anchor Blocks

4.5.3.2 Preliminary Strength Calculation for the Repaired Beams

Calculations of repaired strength were made for the two beams using the AASHTO simplified approach described in AASHTO LRFD article 5.6.3.1.3b which stated that the stress in the unbonded tensons can be taken as the effective stress in the prestressing steel after losses. Therefore, the repaired strength calculations were performed based on both the current condition, and the condition after 20 years, upon which the repair design was based. The results of these calculations are presented in Table 4.6. Note that based on the assumed future damage, the repair increases the strength to about 10% above the original strength. Based on current damage, the increase is much larger.

Table 4.6. Calculated Flexural Capacity

Beam	Undamaged Strength (k-ft)	Based on Assumed Damage over 20 years		Based on Current Observed Damage	
		Remaining Strength (k-ft)	Repaired Strength (k-ft)	Remaining Strength (k-ft)	Repaired Strength (k-ft)
I-Beam 1	1901	1398	2323	1752	2662

I-Beam 5	1901	1378	2318	1749	2656

The loading conditions for the two beams during testing are shown in Figure 4.10. Both beams were loaded using a spreader beam that applied two equal loads at a distance of 4 ft on each side of midspan. The predicted load and failure mechanism were calculated using these loading parameters and the estimated flexural strengths. Table 4.7 summarizes the findings.

Table 4.7. Predicted Failure Loads and Modes

Beam	Calculated Flexural Strength, k-ft	Mid-Span Self-Weight Moment, k-ft	Expected Applied Moment to Cause Failure, k-ft	Expected Applied Load to Cause Failure, kips	Expected Failure Mode
I-Beam 1	2662	208	2454	245	Concrete Crushing at the top
I-Beam 5	2656	208	2448	245	Concrete Crushing at the top

4.6 Experimental Test Methods

4.6.1 Test setup and Instrumentation

Both beams were tested in a simple span configuration, with one end supported by a roller and the other end supported by a pin. The flexural test setup is illustrated in Figure 4.10. Loads were applied using a 400-kip actuator.

The instrumentation plans for both beams were identical. Midspan and quarter point deflections were recorded, and arrays of strain gages were installed through the depth of the beams near midspan to determine strain distribution and the centroid location.

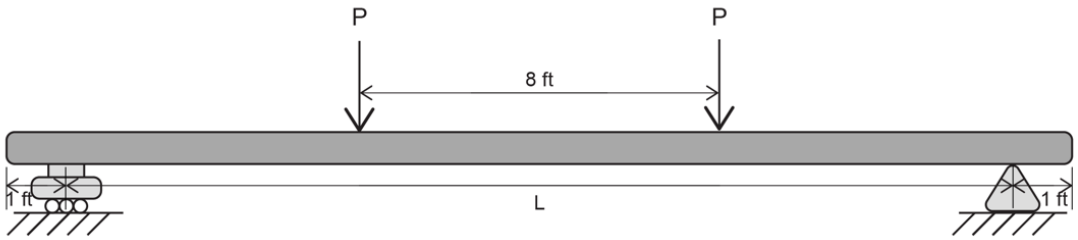

Figure 4.10. Flexural Test Set Up

4.7 Description, Discussion and Results of Tests

4.7.1 I-Beam 1 – Wax Filler

For this test, the beam was loaded in increments of 10 kips until the load reached 250 kips, at which point a displacement control was employed. During the loading process, the concrete ahead of the anchor block on the inland side at the live end began to crack, with shear cracks directed toward the load at 150 kips. At 160 kips, the first flexural crack formed, as indicated by the change in slope of the load-deflection plot (see Figure 4.11).

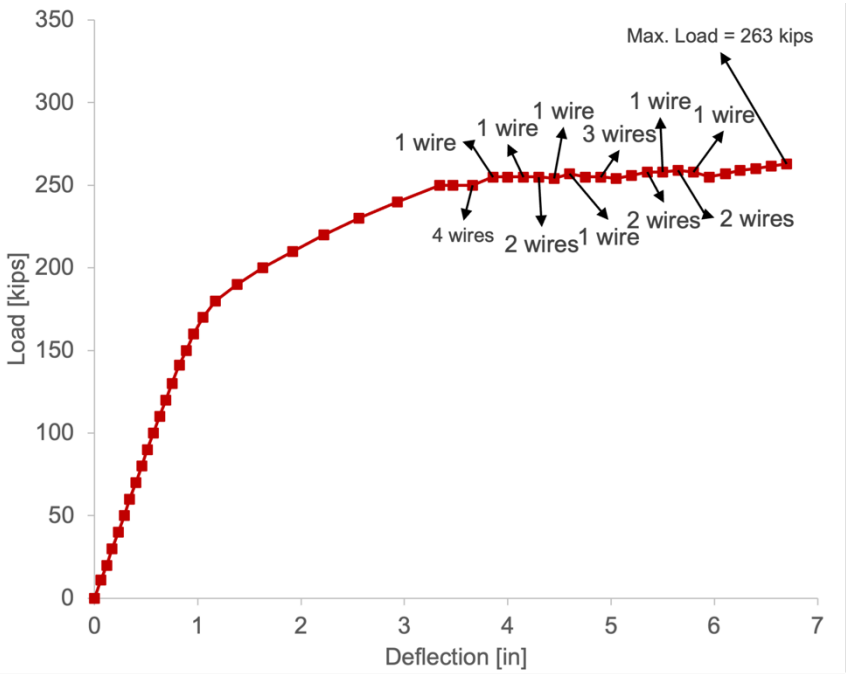

Figure 4.11. Load vs Deflection - I-Beam 1 - Repaired with Eternal PT – Wax

Continued loading resulted in further shear cracks in the web near the top side of each anchor block, oriented toward the support, as shown in Figure 4.12. Flexural cracks originated at the bottom flange and propagated up to the mid-height of the web within the constant moment region at the midspan. By 250 kips, there was a noise which was assumed to be one wire rupturing.

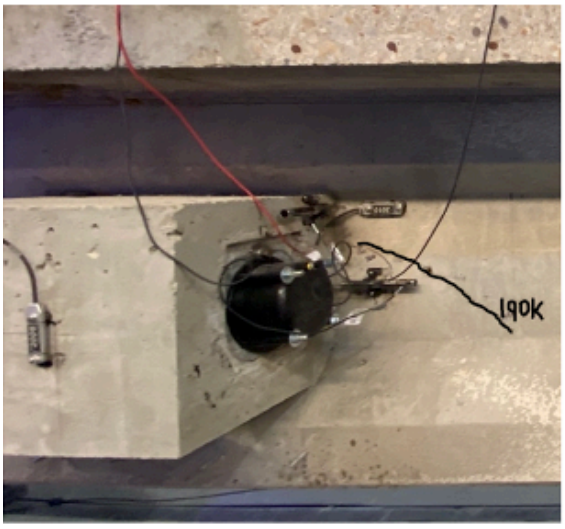

Figure 4.12. Shear Cracks at the Anchor Blocks

The number of broken wires during the test is shown in Figure 4.11. After 260 kips of load, the slope of the load-deflection plot began to flatten until the beam failed at 263 kips. The failure mechanism shown in Figure 4.13 is concrete crushing on the top of the beam that propagated to the bottom flange. It should be noted that there were no abnormal readings associated with the anchor blocks, confirming the effectiveness of the anchor block design.

Figure 4.13. Concrete Crushing at the Top of the Beam – I-Beam 1 - Repaired with External PT – Wax

The failure of the beam was quite explosive because, although the bonded pretensioned strands had yielded, the external post-tensioned strands were just at the beginning of the yielding phase. Upon crushing the concrete, the strands “snap back” to their original length and cause the explosive crushing of the entire cross-section.

String pots were used to measure the distance between each anchor block and the central diaphragm. Between the anchor block on the live end and the anchor block on the dead end, the elongation was 0.49 in. and 0.70 in., respectively (see Figure 4.14). As a result, the external PT experienced an ultimate stress of 251.5 ksi with additional average stress of 71.5 ksi. The movements of the anchors block were negligible, the largest was less than 0.01 in.

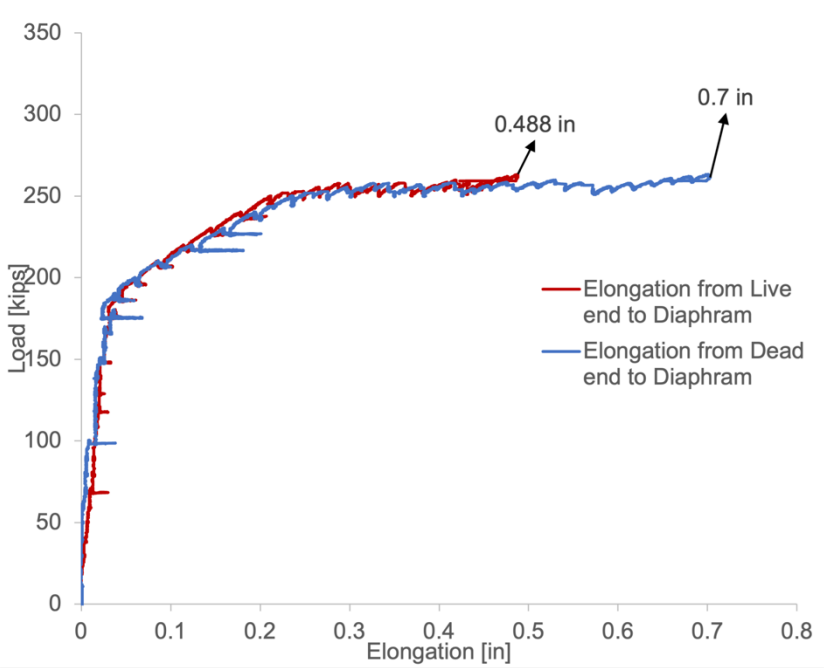

Figure 4.14. Elongation Between Anchor Blocks and Central Diaphragm – I-Beam 1

In Table 4.7, the predicted flexural strength with the external PT repair was 2662 k-ft. The self-weight moment is 208 k-ft, so the applied moment was expected to be 2454 k-ft. With a distance from the supports to the load points of 20 ft, this equates to an applied load of 245 kips. The actual failure load of 263 kips indicates that the assumption that the stress in the external tendons is the effective prestress is overly conservative.

4.7.2 I-Beam 5 – Grout Filler

The beam was loaded in 10-kip increments until the load reached 190 kips, and thereafter it was loaded in 5-kip increments. At a load of 100 kips, the first shear crack occurred ahead of the anchor block on the bay side at the live end. By a load of 120 kips, a shear crack had propagated ahead of each anchor block, and they continued to propagate with each load step until the load reached 160 kips. At 160 kips, a shear crack developed behind the anchor block towards the live end. As evidenced by the change in slope of the load-deflection plot, the first flexural

crack formed at load 170 kips (see Figure 4.15). With the increase in load, additional flexural cracks formed and propagated from the bottom flange to the top of the web.

Two wires from a deteriorated exposed strand ruptured at 195 kips (see Figure 4.15). Figure 4.16 shows the number of broken wires noted during the test. The cracks continued to grow, and the width of the existing cracks widened until the beam failed at 304 kips, with concrete crushing through the depth of the beam (see Figure 4.17).

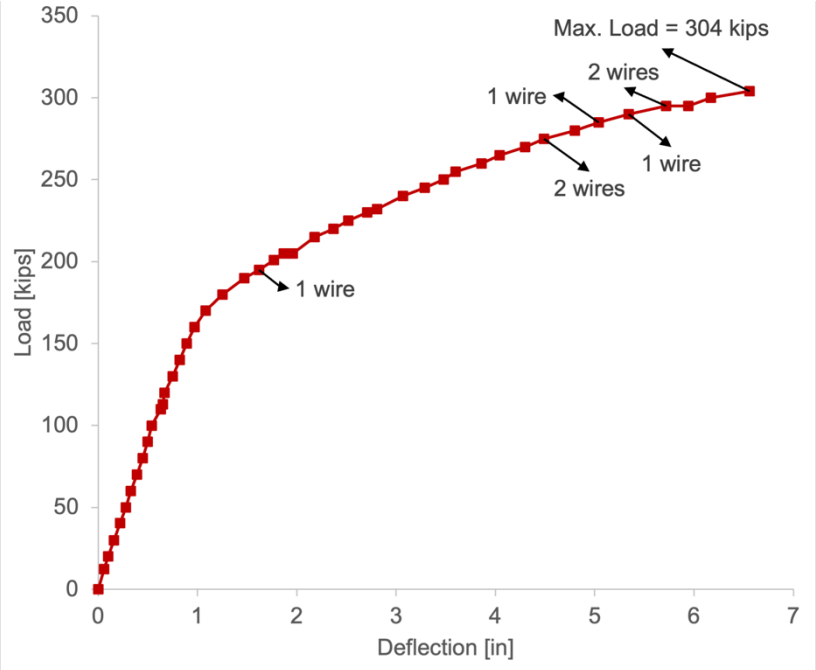

Figure 4.15. Load vs Deflection - I-Beam 5 - Repaired with External PT – Grout

As with the other beam repaired with external PT, the failure was quite explosive. String pots were used to record the elongation from each anchor block to the central diaphragm. The elongation between the anchor block from the live side and dead live were 0.58 in. and 0.6 in., respectively (see Figure 4.18). Therefore, the additional average stress in the external PT was 71.5 ksi.

Although there was some movement in the anchor blocks, it was still considered small. On the live end, the axial movement toward the center behind the anchor block was 0.05 in. On the other hand, the anchor block on the dead end shifted 0.13 in. The anchor blocks moved away from the web by 0.029 in. and 0.185 in. for the live end and dead end, respectively.

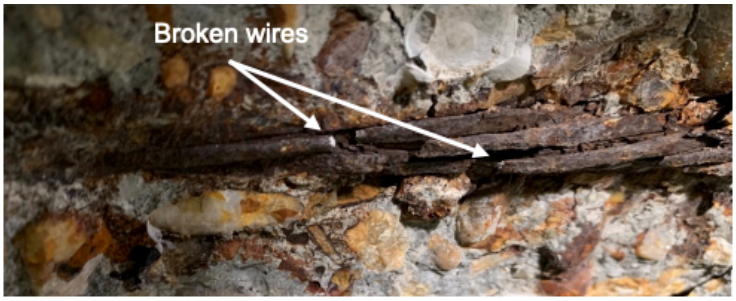

Figure 4.16. Broken Wires During the Test of I-Beam 5

Figure 4.17. Concrete Crushing at the Top of the Beam – I-Beam 5 - Repaired with External PT – Grout

In Table 4.7, the predicted flexural strength with the external PT repair was expected to be 2656 k-ft. Based on the known self-weight moment and loading arrangement, this equates to an applied load of 245 kips to fail the beam. The actual failure load of 304 kips indicates that the assumption that the stress in the external tendons is the effective prestress is overly conservative.

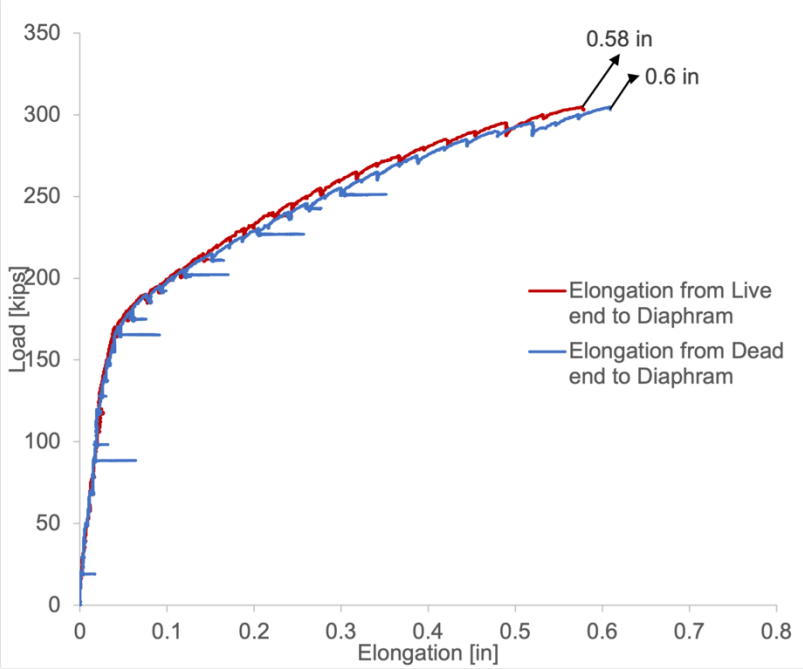

Figure 4.18. Elongation Between Anchor Blocks and Central Diaphragm – I-Beam 5

The failure loads of the two beams repaired with external PT were 263 kips for the beam with wax filler in the ducts and 304 for the beam with grout in the ducts. However, the filler material was not the reason for the difference. The beams had almost identical load-deflection behavior up to a load of 250 kips. After this load, the beam with wax had many more sounds of wires breaking compared to the beam with grout. So, the variation in strength is due to the state of the internal strands, not the filler material.

4.7.3 Discussion

Table 4.8 presents a summary of how the repaired beams performed. The AASHTO approach to calculating the flexural strength for beams strengthened with External PT, gave conservative flexural strength estimations. The additional ultimate stress in the unbonded external tendons for both beams was 95 ksi. Therefore, the ultimate stress in the I-Beam 1 and I-

Beam 5 is 262 ksi. The yield stress for the external tendons is 261 ksi, which means that the external tendons start had started to yield.

Also, there were no large movements in the anchor blocks, either laterally toward the center of the beam or away from the web, which confirmed that the specification in section 16.5 in (American Concrete Institute, 2019) provided appropriate design.

Table 4.8. Summary of Flexural Tests for I-Beam

Beam	Applied Load at Failure, kips	Moment					Failure Mode
		Total[1] Moment under Load at Failure, k-ft	AASHTO Simplified Method Calculated Flexural Strength, k-ft	M_{test}/M_{calc}	Calculated Flexural Strength Using Measured Tendon Stress Increase, k-ft	M_{test}/M_{calc}	
I-Beam 1	**263**	2832	2647	1.07	3133	0.9	Concrete Crush
I-Beam 5	**304**	3242	2626	1.23	3089	1.05	Concrete Crush

[1] Total moment includes self-weight, [2] Using experimental measured additional stress in external tendons

4.8 Analysis – Detailed method for estimating the ultimate stress in the external PT tendons in beams with bonded and unbonded prestressing strands.

In this section a proposed detailed approach is presented which can be used to calculate the ultimate stress in the external PT tendons. The effective prestress in the external PT must be calculated after all the losses occurred. An additional stress, caused by the external applied load during the test, is initially guessed. The initial total stress can be calculated by adding the effective prestress to the guessed additional stress. A moment-curvature diagram with an external axial PT force due to the initial total stress is required. Given the moment capacity, the self-weight moment and the external PT moment, the applied load that will cause the beam to fail can be determined. Based on the computed failure load, the total moment diagram, and the corresponding curvature along the beam at the level of the external PT can be created.

Subsequently, the elongation in the tendon can be obtained by integrating the strains along the length of the tendon and therefore the additional average strain can be calculated. The total strain is determined by adding the additional average strain to the strain obtained from the effective prestress. Then, using the total strain, the ultimate stress in the external PT can be determined from stress-strain curve of the external PT. The guessed additional stress is iteratively varied until the ultimate stress converges. Figure 4.20 shows the details in a flowchart format.

4.8.1 Example for Beam with Bonded and Unbonded Tendons – I-Beam 5

I-Beam 5 is used as example to explain the aforementioned analysis. Table 4.9 shows the required calculations to obtain the failure load and the ultimate stress in the external tendons. Also, Figure 4.19 presents the moment-curvature, moments, strain along the length of the beam and the external PT stress-strain graph.

Table 4.9. Sample Canulations to Obtain Ultimate Stress in the External PT and Failure Load for I-Beam 5

<table>
<tr><td colspan="2">1. Calculate effective prestress (AASHTO, 2017) and assume Δf_{avg} :</td></tr>
<tr><td rowspan="4">f_{pe} = 180 ksi
Assume Δf_{avg} = 72.5 ksi</td><td>Jacking stress = 216 ksi</td></tr>
<tr><td>Friction loss + seating loss = 30.5 ksi</td></tr>
<tr><td>Elastic shortening = 1.3 ksi</td></tr>
<tr><td>Creep and relaxation losses = 4.2 ksi</td></tr>
<tr><td colspan="2">2. Find moment-curvature diagram based on the assumed axial force:
Moment capacity at desired location = 2170 k-ft (see Figure 4.19a)</td></tr>
<tr><td colspan="2">3. Calculate total moments from external PT tendons and self-weight:</td></tr>
<tr><td colspan="2">$M_{ext\text{-}PT}$ = -750 k-ft and M_{self} = 201k-ft, M_{total} = -549 k-ft (see Figure 4.19b)</td></tr>
<tr><td colspan="2">4. Calculate load to cause failure: $M_{failure} = M_{ext+self} + M_{applied}$</td></tr>
<tr><td colspan="2">$M_{applied}$ = 2718 kip-ft, $P_{ultimate}$ = 272 kips, Figure 4.19b presents the total moment based on the applied moment.</td></tr>
<tr><td colspan="2">5. Calculate additional elongation Δu along the tendon: Δu = 1.5 in (see Figure 4.19c), Additional strain = 0.00338 which lead to a total strain = 0.00338 + (180/288000) = 0.0096</td></tr>
<tr><td colspan="2">6. $f_{avg\text{-}ultimate}$ = 252.5 ksi (from Figure 4.19d) and Δf_{avg} = 252.5 – 180 = 72.5 ksi , which is equal to our assumptions</td></tr>
<tr><td colspan="2">So, $P_{ultimate}$ = 272 kip and ultimate stress in the tendons f_{pe} = 252.5 ksi</td></tr>
</table>

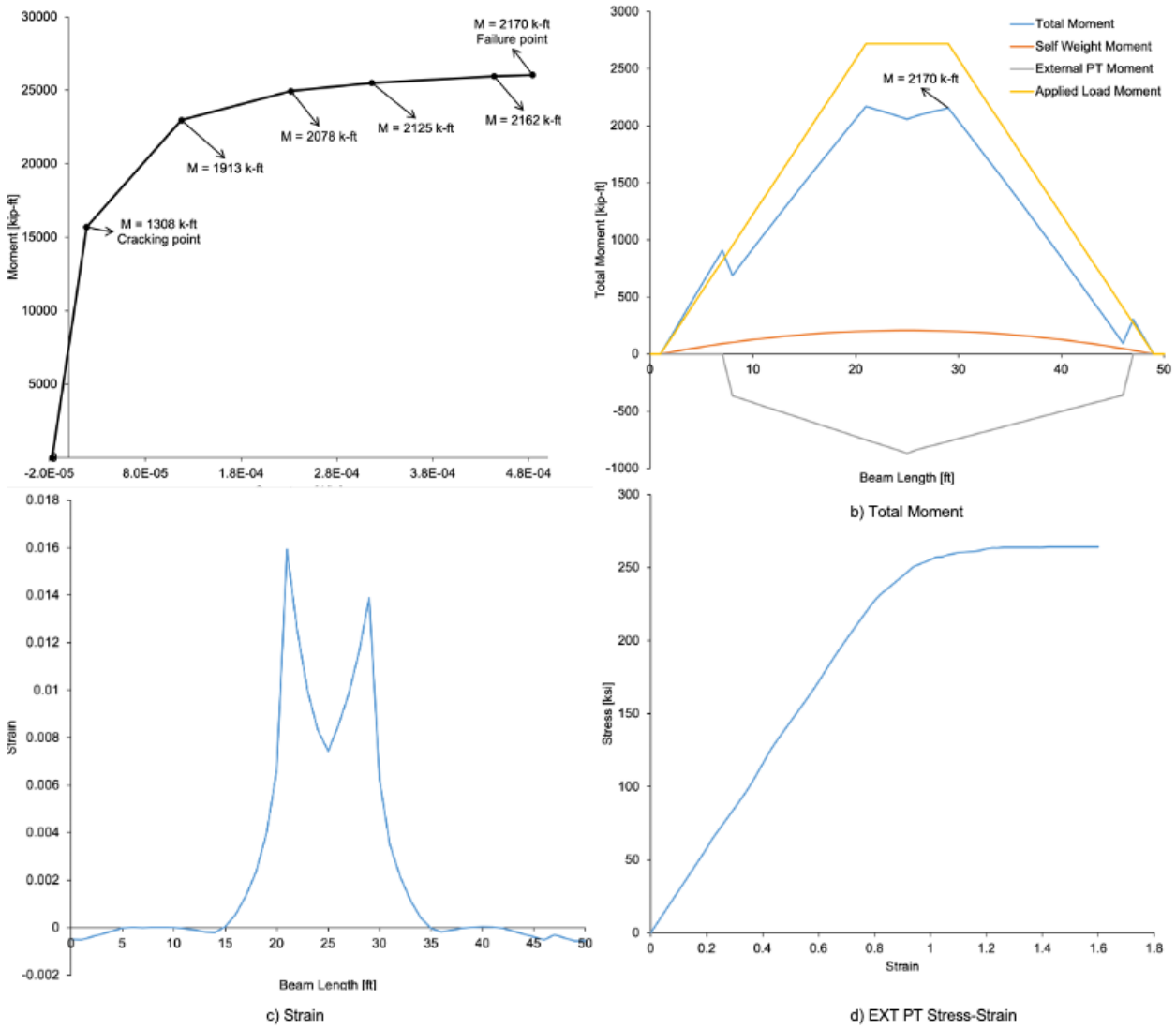

Figure 4.19. a) Moment-Curvature for I-Beam with Axial Load. b) Total Moment including Applied Moment, Self-weight Moment and External PT Moment. c) Strain Along the Length of the Beam. d) External PT Stress-Strain Graph.

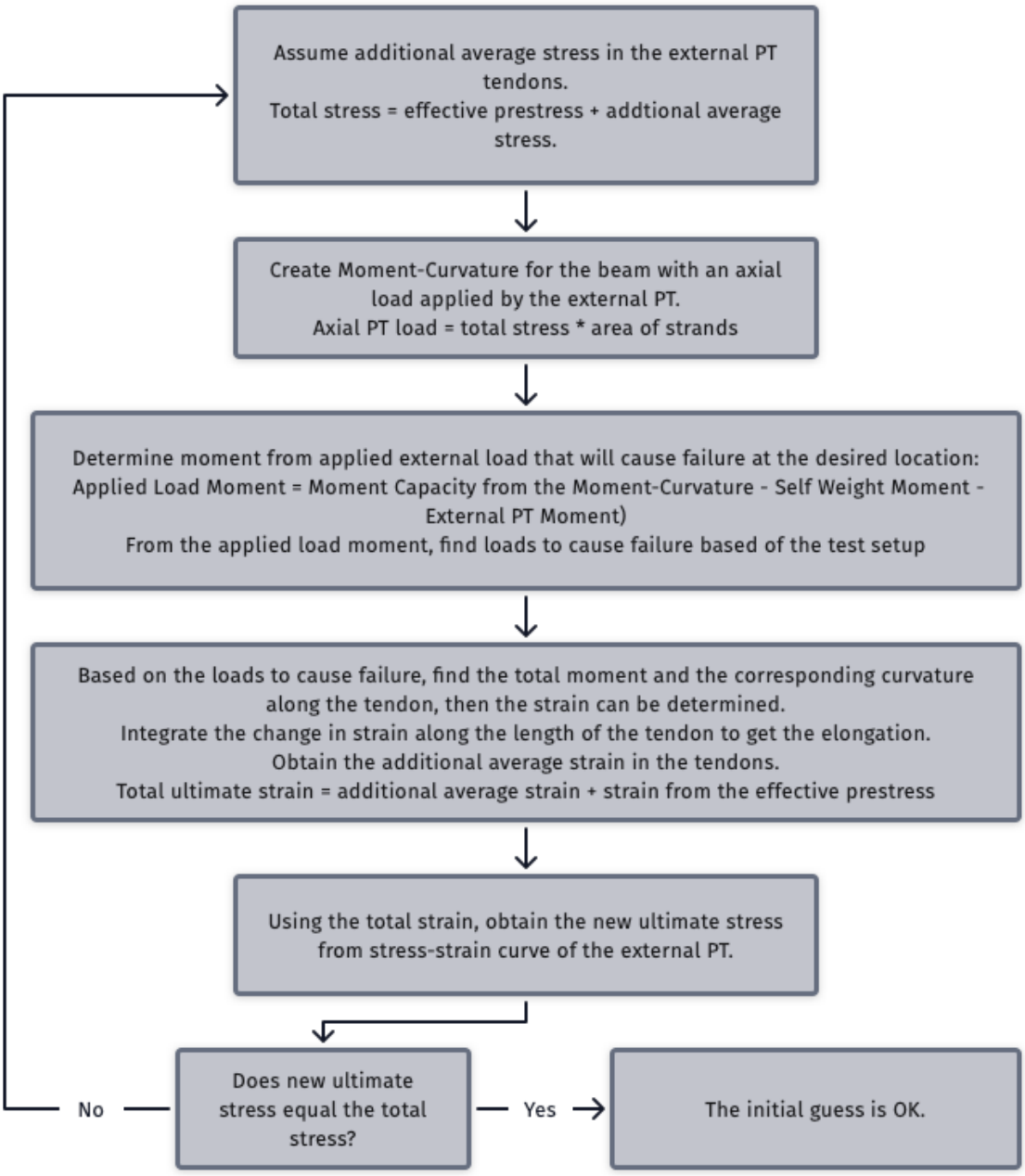

Figure 4.20. Detailed method to estimate the ultimate stress in the external PT tendons

Table 4.10 shows a comparison between the test results and the calculated stress and ultimate failure load. The difference between the additional load from the test and the calculation is 1% and 3% for I-Beam 5 and I-Beam 1, respectively. For I-Beam 5, the load achieved in the test was 304 kips, whereas the calculated load was 272 kips, a 10% difference and with

a conservative estimate. For I-Beam 1, the calculated ultimate load was 273 kips, while the test failure load was 263 kips, with a 4% difference.

The proposed approach predicts the ultimate stress and ultimate failure load quite good with 4-10% difference. The deflection was captured quite good using the proposed method (see Table 4.10).

Table 4.10. Comparison between Stress and Load from the Test and the Proposed Method

Beam	Additional Stress, ksi		Tested Stress / Calculated Stress	Ultimate Failure Load, kip		Tested Load / Calculated Load	Ultimate Deflection, in	
	From Test	Calculated		From Test	Calculated		From Test	Calculated
I-Beam 1	71.5	73.7	0.97	263	273	0.96	6.6	6.5
I-Beam 5	71.5	72.5	0.99	304	272	1.11	6.75	6.3

4.9 Summary and Conclusions

To correctly analyze a corrosion-damaged beam and create an external PT repair plan, it is necessary to first produce a detailed damage map of the beam to be repaired. This damage map should include longitudinal cracks, spalls, delaminations, and patches. Additionally, any exposed strands and their condition should be documented. The findings of half-cell and chloride content analysis did not contribute significantly to the strength calculation, which is consistent with Naito et al. (2010) and Alfailakawi et al., (2020). For the determination of flexural strength, using the reduced cross-sectional areas, a strain compatibility approach provides a good strength

estimate. However, the need of another method that calculate the strength capacity based on ultimate strain is recommended and needs to be further investigated.

The AASHTO simplified approach for estimating the flexural strength of beams containing bonded and unbonded tendons provides a conservative repair strength approximation. It can be used to determine the number and size of external strands required. The proposed detailed method provides a very good strength approximation. Also, it provides an excellent approximation for the ultimate stress in external tendons and the deflection of repaired beam.

The following recommendation shall be used if the external PT repair is chosen:

- The anchor blocks should be placed on the webs as close to the ends of the beams as is allowed by the construction and stressing process. The live-end anchor block may need to be placed farther from the end of the beam than the dead-end block to allow for access with the stressing ram.
- At the locations where anchor blocks and deviators are to be cast against the existing beam, the surface of the beam should be roughened with a chipping hammer to improve the bond of the new concrete to the old.
- The main flexural and shear friction reinforcement should be passed through slightly oversized holes in the webs and developed in the anchor block on the opposite side of the web. The bars should be epoxied into the holes for better development and to reduce the possibility of the anchor blocks moving relative to the beam's web during stressing.
- The deviation points should be placed at the existing interior diaphragms. The diaphragm walls should be extended downward, so the deviation point of the new

external tendons is as low as possible in the cross-section but not below the bottom of the bottom flange. The new lower part of the wall should be widened to accommodate a deviation saddle.

- Grout or wax may be used to fill the duct in an external PT repair. However, wax is more likely to prevent corrosion initiation in the tendons in the long term.

4.10 References

AASHTO, L. R. F. D. (1998). Bridge design specifications.

AASHTO, L. R. F. D. (2017). Specifications. *American Association of State Highway and*.

Alfailakawi, A., Roberts-Wollmann, C. L., Hebdon, M., & Koutromanos, I. (2020). Experimental and Analytical Evaluation of Residual Capacity of Corrosion-Damaged Prestressed Concrete Bridge Girders. https://rosap.ntl.bts.gov/view/dot/53953

American Concrete Institute, A. C. I. C. (2019). *Building code requirements for structural concrete (ACI 318-19) : an ACI standard; Commentary on building code requirements for structural concrete (ACI 318R-19)*.

ASTM-C876. (2015). Test Method for Corrosion Potentials of Uncoated Reinforcing Steel in Concrete. https://doi.org/10.1520/c0876-15

Balakumaran, S. S. G. (2010). *Influence of Bridge Deck Concrete Parameters on the Reinforcing Steel Corrosion*. Virginia Tech]. https://vtechworks.lib.vt.edu/bitstream/handle/10919/32665/GBalakumaran_SS_T_2010.pdf?sequence=2.

Bennitz, A., Schmidt, J. W., Nilimaa, J., Täljsten, B., Goltermann, P., & Ravn, D. L. (2012). Reinforced concrete T-beams externally prestressed with unbonded carbon fiber-reinforced

polymer tendons. *ACI Structural Journal*, *109*(4), 521. https://search.proquest.com/openview/a848a2dd02d26eb8e5d42dc1356d6478/1?pq-origsite=gscholar&cbl=36963

Harajli, M. H. (1993). Strengthening of concrete beams by external prestressing. *PCI journal*, *38*(6), 76-88.

Heo, S., Shin, S., & Lee, C. (2013). Flexural Behavior of Concrete Beams Internally Prestressed with Unbonded Carbon-Fiber-Reinforced Polymer Tendons. *Journal of Composites for Construction*, *17*(2), 167-175. https://doi.org/10.1061/(asce)cc.1943-5614.0000306

Khudeira, S. (2010). Strengthening of deteriorated concrete bridge girders using an external posttensioning system. *Practice Periodical on Structural Design and Construction*, *15*(4), 242-247. https://ascelibrary.org/doi/full/10.1061/(ASCE)SC.1943-5576.0000074

Lee, S.-H., Shin, K.-J., & Lee, H.-D. (2018). Post-Tensioning Steel Rod System for Flexural Strengthening in Damaged Reinforced Concrete (RC) Beams. *Applied Sciences*, *8*(10), 1763. https://doi.org/10.3390/app8101763

Leicht, L., Roberts-Wollmann, C. L., Koutromanos, I., Hebdon, M. H., & Mosig, O. (2022). Experimental and Analytical Investigation of a 64-Year-Old Prestressed Beam Retrofitted with External Posttensioning. *Journal of Bridge Engineering*, *27*(4). https://doi.org/10.1061/(asce)be.1943-5592.0001854

Naito, C., Jones, L., & Hodgson, I. (2010). Inspection methods & techniques to determine non visible corrosion of prestressing strands in concrete bridge components: task 3, forensic evaluation and rating methodology. https://rosap.ntl.bts.gov/view/dot/18121/dot_18121_DS1.pdf

Nassif, H., Ozkul, O., & Harajli, M. H. (2003). Flexural behavior of beams prestressed with bonded and unbonded. *PTI Journal*, *1*, 60-71.

Sayed-Ahmed, E. Y., Riad, A. H., & Shrive, N. G. (2004). Flexural strengthening of precast reinforced concrete bridge girders using bonded carbon fibre reinforced polymer strips or external post-tensioning. *Canadian Journal of Civil Engineering*, *31*(3), 499-512. https://doi.org/10.1139/l04-005

Suntharavadivel, T. G., & Aravinthan, T. (2005). *Overview of external post-tensioning in bridges*. In *Proceedings of the 2005 Southern Region Engineering Conference (SREC 2005)* (pp. 29-38). Engineers Australia, Toowoomba Local Group. https://eprints.usq.edu.au/2217

Zhang, X., Li, S., Zhang, W., Ikechukwu, O., Dai, L., & Wang, L. (2020). Second Remediation of Long-Term Deflection and Cracking of PT Box-Girder Bridge Using External Post-Tensioning. *Journal of Performance of Constructed Facilities*, *34*(5), 04020090. https://doi.org/10.1061/(asce)cf.1943-5509.0001491

CHAPTER 5: Large Scale Laboratory Testing – CFRP Repair Method

Chapter 5 consists of the manuscript: "Flexural Strengthening Repair of Corroded Damaged Bridge Girders Using CFRP Method" This paper is currently in preparation for submission to a journal.

Flexural Strengthening Repair of Corrosion Damaged Prestress Concrete Bridge Girders Using CFRP

Ali Alfailakawi[1]; Carin L. Roberts-Wollmann[2]; Matthew H. Hebdon, [3]; Ioannis Koutromanos, [4]

Virginia Tech, Blacksburg, VA

5.1 Abstract:

This paper presents the results of testing of three prestressed beams, with various levels of corrosion damage, which were repaired with Carbon Fiber Reinforced Polymer (CFRP) layups. Prior to testing, the beams were visually inspected, and the residual strength was evaluated based on two documented methods to quantify the effects of corrosion damage. The methods for damage estimation, which relied exclusively on visual inspections, were the method recommended by Naito et al., (2011), and the modified method developed by Alfailakawi et al., (2020). Based on the damage estimation, repairs were designed and implemented using CFRP to restore or increase the flexural strength. The beams were then tested in the lab to determine their flexural strength.

The tested strengths of the beams were compared to calculated strengths using the two methods for damage estimation and two different calculation approaches to account for the contribution of the CFRP. The two calculation approaches were those presented in ACI 440R (ACI 440, 2008) and in the AASHTO Guide Specifications for Design of Bonded FRP Systems

for Repair (AASHTO 2012). In addition, a parametric study was performed to determine the maximum reduction in flexural strength for which CFRP can be considered as a viable repair method to restore the lost capacity. Overall, the results yielded reasonable estimates of residual strength. Both methods for calculating strength appear to be valid. Plots based on the span length and beam spacing are provided to determine the maximum percentage of capacity reduction in order to allow the use of CFRP as a repair method.

5.2 Introduction

5.2.1 Background

Many research programs have carried out investigations into the condition of damaged corroded concrete beams. Naito et al. (2010) conducted a study on seven corroded segments of adjacent box beams to assess the condition of their prestressing strands. A method to calculate the residual capacity of damaged beams based on a reduction in the strand's cross-section was proposed, and this method is used in this study. Additionally, Alfailakawi et al. (2020) utilized a similar idea for strand cross-section reduction and provided more specific recommendations for calculating the residual capacity of corrosion-damaged prestressed AASHTO I-Beams.

If the method used to evaluate residual strength indicates that repair is required, several strategies can be used to restore the flexural capacity of a damaged beam such as external post tensioning, internal strand splices and welded steel jackets. However, these types of repairs can be labor intensive, and the beams can continue to experience corrosion (Klaiber et al., 2003). So, another alternative is FRP (Fiber Reinforced Polymer) laminates. This repair type is suggested because of the high strength to weight ratio of the material, excellent resistance to corrosion, good fatigue properties and ease of installation (Ali et al., 2014) (Klaiber et al., 2003). Many

research projects have been conducted and have proven that FRP can increase the capacity of concrete structures, reduce deflection and add more confinement to the concrete which delays future concrete spalling and cracking caused by the expansive forces of the corrosion (Rose et al., 2009) (Duthinh & Starnes, 2004) (Soudki, 2006) (Balasubramaniam et al., 2011).

Many experiments have tested the effect of the CFRP laminates on strengthening concrete bridge girders. For example, Isakveien Bridge in Oslo was demolished after 35 years in service, and four prefabricated prestressed concrete T-beams were preserved for testing (Takács & Kanstad, 2000). The flexural capacity increased by 28% and 37% in the beams with one and two CFRP layers, respectively. Also, Klaiber et al., (2003) tested the four-span Altoona Bridge, which is in Iowa. The bridge was damaged due to overhight vehicle. The authors concluded that flexural strengthening is feasible if 15% or less of the strands are damaged.

Ninety-four reinforced concrete beams were tested at the University of Waterloo (Soudki, 2006). All the specimens were subjected to an accelerated corrosion process which led to an approximately 15% loss in the steel. Tests showed that FRP reduced the cracks opening by 88%. The study concluded that FRP repair systems can recover the losses due to the corroded steel and can restore the strength, integrity, and serviceability of the structure.

Lee et al., (1997) tested four RC beams to verify the effectiveness of CFRP repair. The non-repaired beam had 10% loss in the steel cross section and failed at ultimate strength of 85% of the strength of the reference beam. While the two repaired beams failed with rupturing the CFRP sheets with an increase of 40% in the strength compared to the reference beam.

Nguyen et al., (2013) tested a total of 12 pretensioned concrete beams. The tests variables were level of damage, length of CFRP layups and number of CFRP plies. Results showed that the length of the sheets increased the stiffness by 10%. For example, the initial stiffness increased to 110% compared with the base beam, when the whole length of the span was bonded with CFRP sheet., but the ultimate loads were not affected. Additionally, the cracking load was significantly increased with the increase in number of CFRP layers. However, the beam , having 50% loss in strands compared to the base beam, repaired with three CFRP layers recovered strength to 91.5% of the control beam's strength. The trend of increasing strength did not continue with the beams that have four and five layers. The ultimate load for the beams strengthened with more than three layers shows a reduction compared to the one repaired with three layers and the debonding of CFRP sheets occurred earlier with these specimens. The cracks at midspan were well restrained and became smaller with the larger number of CFRP sheet layers.

Although studies showed how the CFRP increased the capacity strength, still there is a need to understand the correlation between the condition of the damaged corroded beams, especially those in service, and the CFRP as a repair method. So, more data with detailed non-destructive tests to assess deteriorated girders are required in order to decide their residual strength capacity and when CFRP repair can be used to restore the original flexural capacity.

5.2.2 Problem Statement

The calculation of the flexural capacity of prestressed concrete beams which have corrosion damage and are subsequently repaired, requires additional study. The research presented in this paper evaluated damaged beams using Alfailakawi et al., (2020) and Naito et al.'s (2011)

methods, developed CFRP repair schemes, repaired the beams, and tested the repaired beams. Improvements in methods to estimate the residual capacity and the repaired capacity of corrosion-damaged beams will help mitigate catastrophic bridge structural failure in the future. In addition, work was performed to provide a simple tool for designers to determine how much lost capacity can be restored with a CFRP repair, and when damage is so extensive that an alternative approach should be investigated.

5.2.2 Purpose and Scope

The overall purpose of this research was to evaluate recommendations for methods to calculate residual strength and to evaluate the repaired strength of corrosion damaged beams using CFRP. The capacities of repaired corrosion-damaged prestressed beams were determined using large-scale experimental tests. CFRP layups were used as a repair method and were evaluated to determine the resulting restoration of structural capacity. Beam testing included one beam each from three different bridges, the West Bound Hampton Roads Bridge Tunnel (HRBT) Bridge, the Lesner Bridge, and the Aden Road Bridge.

5.3 Description of Specimens

5.3.1 Hampton Road Bridge Tunnel Beams

The HRBT connects the cities of Hampton and Norfolk by crossing the Chesapeake Bay. The structure is made up of two independent bridges, each with a tunnel in the middle. The two bridges are of different ages: the older one (westbound structure) dates from 1956, while the younger one (eastbound structure) dates from 1976. This paper focuses on one of the beams that was cast to be used for rapid replacements for the westbound structure if it experienced damage, such as due to a ship impact. The beams were never needed, so they have been kept in a storage

location near the bridge. As a result, the beams did not exhibit any corrosion damage. However, the findings of the repair tests can still be used to understand the behavior of damaged beams with similar repairs.

The HRBT beams had a design concrete strength of 5000 psi and were prestressed with 29–3/8-in diameter, Grade 250, stress-relieved prestressing strands. The beams had a parabolically varying depth, from 46 in at the supports to 43 in at midspan. The thickness of the webs of the beams also varied over the first 9 ft-7.5 in at each end. The webs were 7 in wide over the support and 5 in wide over the middle section of the beam. Prior to repair and testing, a 48 in wide by 7 in thick slab was cast on top of the beam. Figure 5.1 shows the cross-section of HRBT beams. One HRBT beams with no repair was tested in a companion project (Alfailakawi et al ,2021) and the results of that test will be compared to the beam with CFRP repair presented herein. The beams will be referred to as HRBT beam and HRBT-CFRP beam, respectively, in this study.

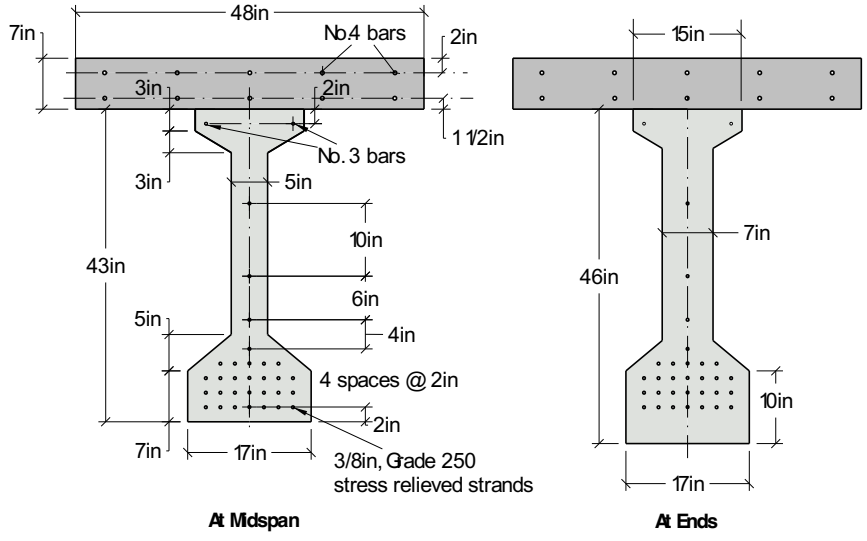

Figure 5.1. Cross-Section of Hampton Road Bridge-Tunnel Beams

5.2.2 Lesner Bridge Beams

The west bound lanes of the Lesner Bridge, also known as the Lynnhaven Inlet Bridge, were built in 1967. The approach spans were constructed using prestressed concrete beams, whereas the main spans were constructed with steel beams. The beams in the approach spans were 49 ft – 9 in long, 36 in deep prestressed I-beams (AASHTO Type II). The beams were specified to have 5000 psi concrete strength and were prestressed with 22 - 7/16-in Grade 270 stress-relieved prestressing strands. Each span included seven beams spaced 5 ft – 2.5 in center-to-center.

The bridge was demolished and rebuilt in 2016 after almost 50 years of service. Nine beams were recovered during the demolition phase and sent to Virginia Tech for testing. The slab between the beams was saw-cut to enable the beams to be retrieved, together with a part of their cast-in-place composite deck. Figure 5.2 illustrates the level of degradation in typical beams. The Lesner Bridge was repaired several times over the years, so patching is evident in many locations. The cross-section of the Lesner Bridge I-beams is shown in Figure 5.2. Note that the sides of the beam are labeled as “bay side” and “inland side.” As this suggests, when the beams were in-situ, the “bay side” faced the Chesapeake Bay, and the “inland side” faced the Lynnhaven Inlet. The bay side of the beams always exhibited a higher level of corrosion damage.

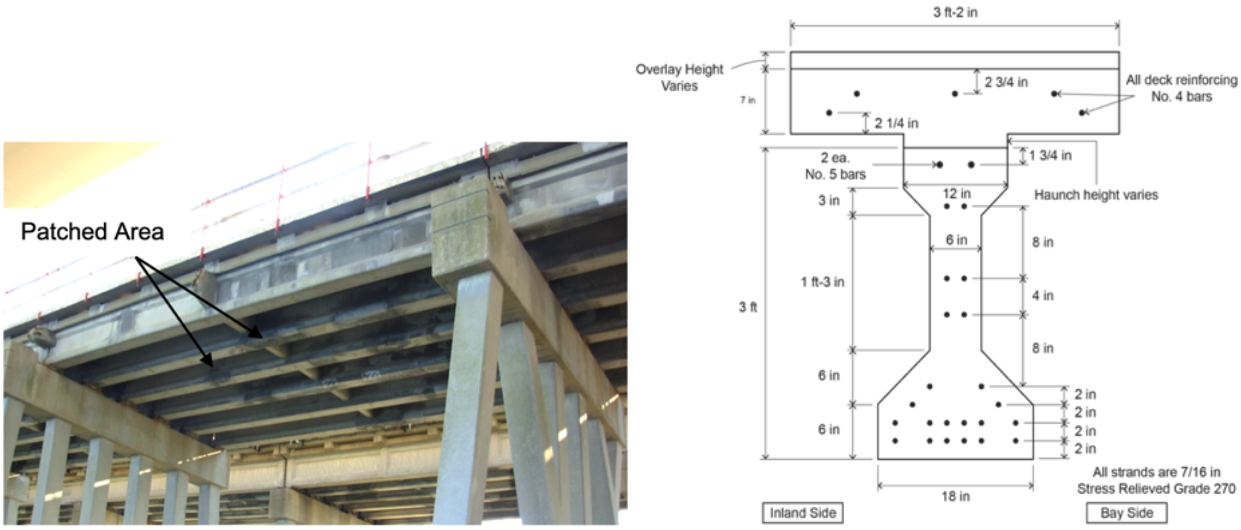

Figure 5.2. Typical Deterioration on the Lesner Bridge (left) Cross-section of Lesner Bridge I-Beams (Right)

For simplification purposes, the Lesner Bridge beam in this paper will be referenced as "I-Beam" which correspond to I-Beam 4 in Alfailakawi et al., (2022). More information regarding beam designations and the original locations can be found in (Alfailakawi et al., 2022).

5.3.1 Aden Road Bridge

The Aden Road Bridge was constructed in 1979. It was a three-span bridge with nine prestressed box beams per span. The fascia beams were 3 ft – 0 in wide by 27 in deep, and the seven interior beams were 4 ft – 0 in wide by 27 in deep. Only interior beams were used in this project. The beams were 55 ft long and were prestressed with 33 - 7/16-in diameter, Grade 270 stress-relieved strands. The beams were connected transversely with grouted 12-in deep shear keys and ½-in diameter Grade 270 prestressing strands at each quarter point of each span. The bridge had an asphalt wearing surface applied directly to the top of the box beams, which was removed prior to the demolition of the bridge.

After over 30 years of service the longitudinal joints had failed and the bridge showed signs of severe deterioration, including exposed and fractured prestressing strands (see Figure

5.3). In 2013, the bridge was demolished and replaced. During demolition, six of the interior beams were transported to Virginia Tech for future testing. One Aden Road Bridge beam will be evaluated in this study and will be referenced by the name Box Beam. This beam is referred to Box Beam 5 in (Alfailakawi et al., 2022). The cross-section of the Aden Road Bridge box beams is shown in Figure 5.3.

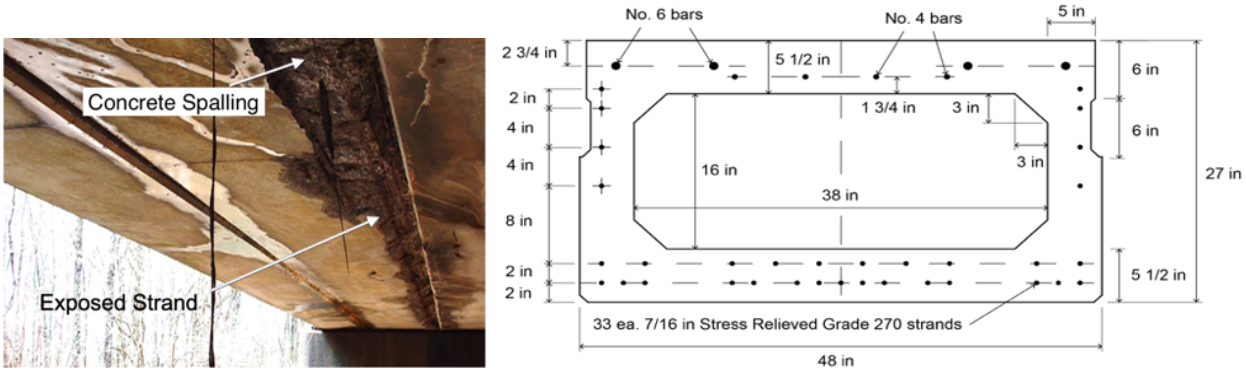

Figure 5.3. Typical corrosion damage on Aden Road Bridge (left), Cross-section of Aden Road Bridge Box Beams (right)

5.4 Evaluation of Corrosion Damage

Prior to designing the repair schemes for the beams, the beams were inspected to aid in the evaluation of the loss of flexural strength attributable to corrosion. Damage maps and half-cell heat maps were created based on visual inspection and half-cell tests, respectively. In addition, after the flexural strength tests powdered concrete samples were taken from the beams to evaluate chloride concentrations. Since HRBT Beams were undamaged, these techniques were performed only for Lesser and Aden Road beams.

5.4.1 Visual Inspection

The beams were examined, and each beam's existing condition was thoroughly documented. The documentation included the location of damage such as cracks, delaminations, spalling, patching, and strand exposure. Delaminations were located by tapping the sides of the

beams with a hammer and recording locations that had a hollow or dead sound. Detailed damage maps were created for each beam, indicating the size and location of each defect. Figure 5.4 and Figure 5.5 present damage maps for the I-Beam and the Box Beam, respectively

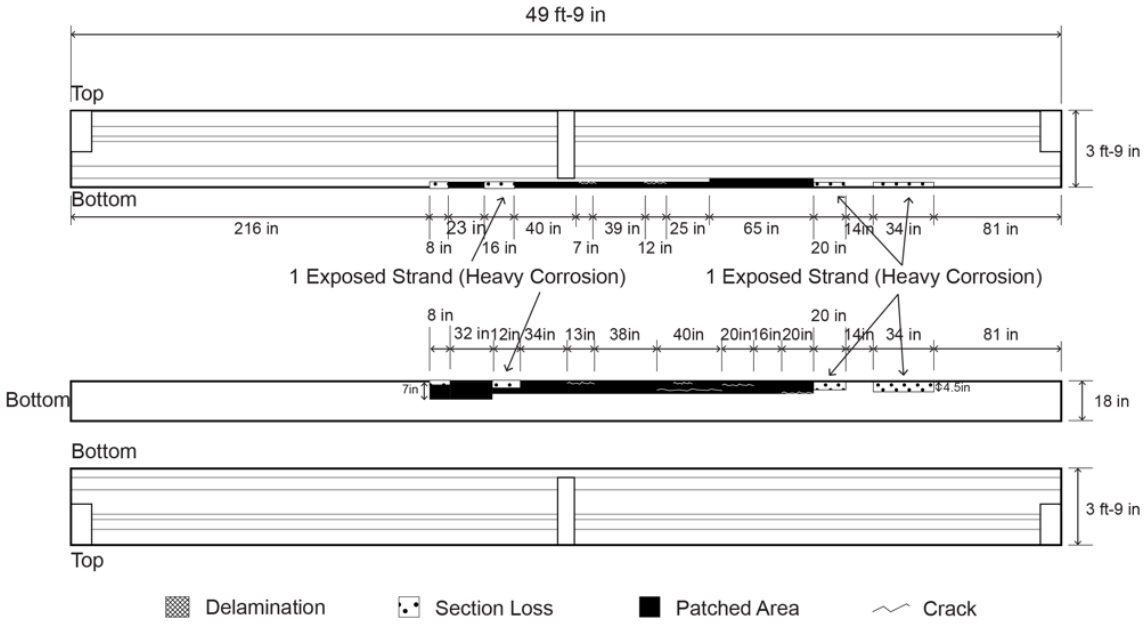

Figure 5.4. Damage Map for I-Beam

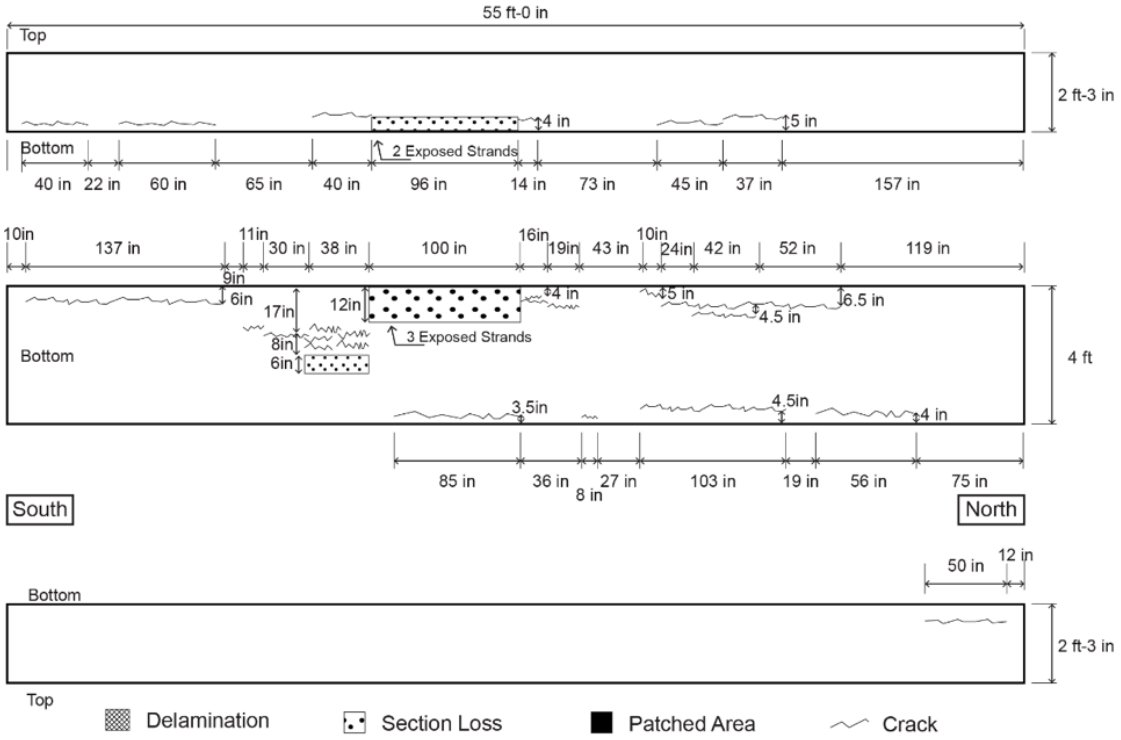

Figure 5.5. Damage Map for Box Beam

In Figure 5.4 and Figure 5.5, the top sketch is of one side, oriented right-side-up, the middle sketch is the bottom of the beam, and the bottom sketch is the other side of the beam, oriented up-side-down. This allows the reader to see how side and bottom face damage are related spatially.

5.4.2 Half-Cell Potential Tests

Half-cell readings were taken at 1283 points on all the sides of both beams. Figure 5.6 illustrates the potential mapping of an I-Beam and reveals that the beam has a low likelihood of corrosion in general. However, the beam has a high chance of corrosion at the middle of the beam on the bay side, quite similar to the damage maps generated. Similar potential mapping of the Box Beam and the visible damage can be found in (Alfailakawi et al., 2022).

As per ASTM C876, Table 5.1 shows the probability of corrosion for both beams. For instance, 294 half-cell readings were taken from the bay side of the I-Beam, 179 of which were more than -200mV, showing that 61% of the readings indicate that the probability of corrosion is less than 10%. In addition, 35% of readings indicate uncertainty (between -200mV and -350mV) and 4% of readings indicate 90% of corrosion (less than -350mV).

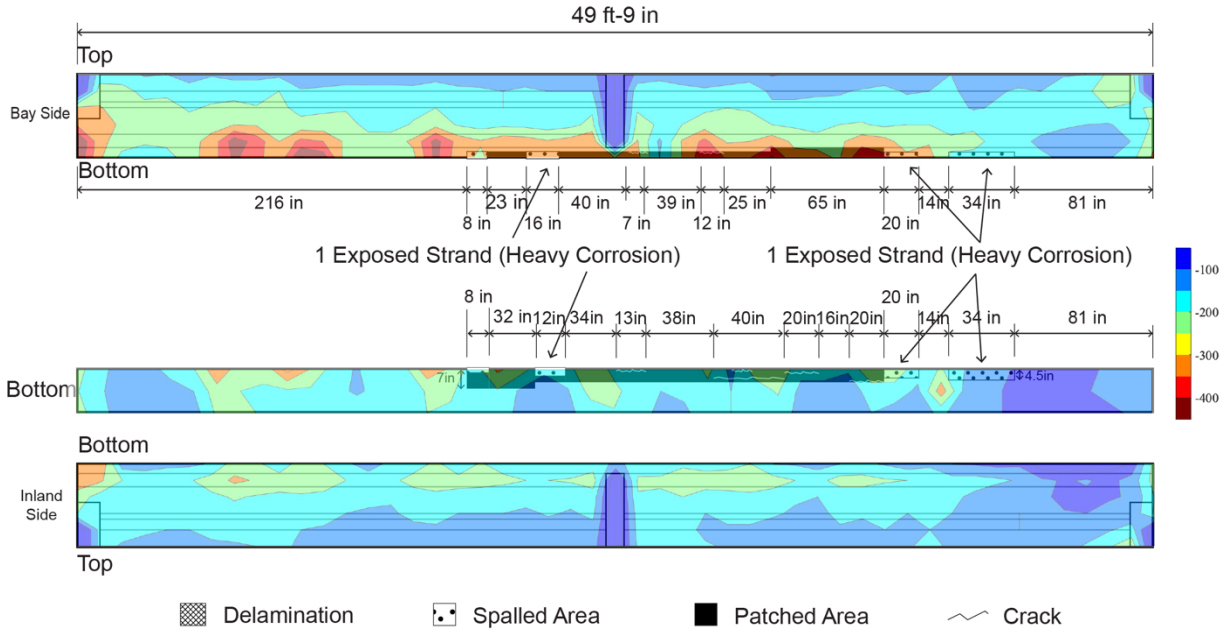

Figure 5.6. Heat Map for Half-Cell - I-Beam (in millivolts)

Table 5.1. Probability of Corrosion in the Beams

Beam	Side	10% Corrosion	Uncertain	90% Corrosion
I-Beam 4 - Repaired with CFRP	Bay	61%	35%	4%
	Bottom	80%	20%	0%
	Inland	87%	13%	0%
Box Beam 5 – Repaired with CFRP	East	26%	47%	27%
	Bottom	29%	57%	14%
	West	18%	56%	26%

5.4.3 Total Chloride Evaluation

This section summarizes the chloride concentration measurements performed on powdered samples taken from the tested beams. Table 5.2 compares the corrosion risk criteria for chloride concentration to the test findings.

Table 5.2. Risk of Corrosion Compared to Chloride Content (Balakumaran, 2010)

% Chloride by mass of sample (concrete)	Risk	Chloride content per volume of concrete (lb/yd3)
<0.03	Negligible	<1.17

0.03-0.06	Low	1.17-2.35
0.06-0.14	Medium	2.35-5.48
>0.14	High	>5.48

Similar to the damage maps and half-cell, chloride evaluation was done only for the I-Beam and Box Beams since HRBT Beams were undamaged. The chloride content testing results for the I-Beam and the Box Beam are presented in Figure 5.7. For the I-Beam, the penetration depth of 1 in had a greater chloride content than the initial depth of 0.5 in for the inland side and bay sides. This may be explained by the fact that water or rain might have washed away chloride from the surface of the concrete, resulting in a lower value. In general and aside from the surface, as the depth of the sample increased, the chloride content decreased on all sides. The only exception was the bay side – inclined on the I-Beam, which had an increase in the chloride content from 1.0 in to 1.5 in. The chloride concentration on the bay side was much greater than on the inland side at each depth point, most likely due to the bay side being exposed to a harsher environment than the inland side. Except for the horizontal bay side, the I-Beam may be judged to have negligible to low-risk conditions in accordance with Table 5.2.

For the Box Beam, as noted Figure 5.7, the top section of the box beam had a very low chloride. This outcome may be explained by the fact that the top of the box beam was covered with an asphalt overlay that served as a primary protector against chloride penetration. Additionally, cracks are known to form in the top surface and along the longitudinal joints between adjacent precast box beams due to differential movement of adjacent beams. These longitudinal cracks allow chloride-laden water to flow directly to the side and bottom of the beams. The Box Beam is classified as low to medium risk due to its chloride concentration of 2.57 lb/yd^3.

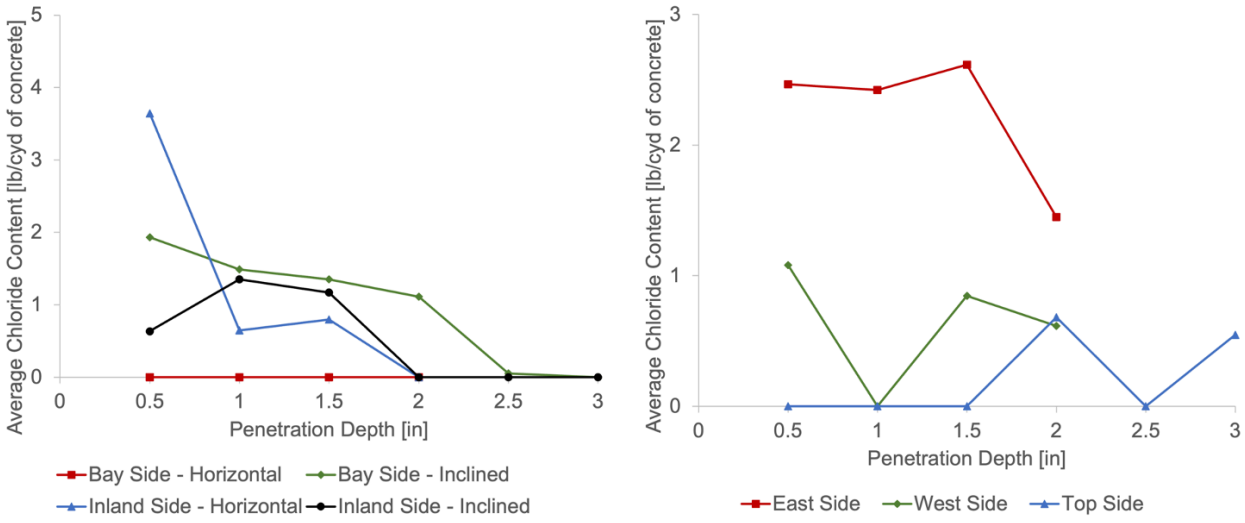

Figure 5.7. Results of Chloride Testing for I-Beam (Left) and Box Beam (Right)

5.4.4 Summary of Corrosion Evaluation

Correlations between the half-cell and damage maps clearly supported the location of the degradation and offer an indication of the beam's condition. Since samples were only obtained from the ends of the beam and not the entire length of the beam, the chloride content evaluation cannot be relied upon to estimate the residual strength for damaged beams, even if it does give some information on corrosion. Thus, given the unsatisfactory findings from the chloride evaluation and even with the confirmation of degradation from the half-cell, these techniques cannot be used to calculate the residual capacity of damaged beams. Only the visual inspection and damage maps offered a significant contribution to the calculations, which is in agreement with the recommendations of Naito et al., (2010). As a result, the next section evaluates residual strength only based on visual examination results.

5.5 Residual and Undamaged Strength Calculations

To design the necessary repairs, first the original undamaged strength and the residual flexural strength for each beam was calculated. As mentioned previously, the HRBT beam was not damaged, so only the original strength is determined. For the I-Beam and Box Beam specimens, the damage maps and the methods presented in Naito et al., (2011) and Alfailakawi et al., (2020) were used to account for the damage.

5.5.1 Tested Material Properties

The calculations presented in this section were performed using material properties based on samples taken from the beams after testing (see Table 5.3)

Table 5.3. Material Properties Based on Extracted Samples

Specimen	Beam Concrete Compressive Strength, psi	Deck Concrete Compressive Strength, psi	Prestressing Steel Breaking Strength, ksi
HRBT CFRP	5800	3600	258
I-Beam	7300	6300	275
Box Beam	6045	-	269

5.5.2 Evaluation of Corrosion Damage

Figure 5.8 presents cross-sections of the two beams repaired to return flexural strength. Each cross-section presents the damage that was present within one development length on each side of the midspan of the beam. Also shown in this figure is the assumed condition of strands based on their proximity to damage, such as a longitudinal crack, spall, or patch. The reduction in cross-sectional area of the strands that was used in the strength calculations is shown in the table within the figure.

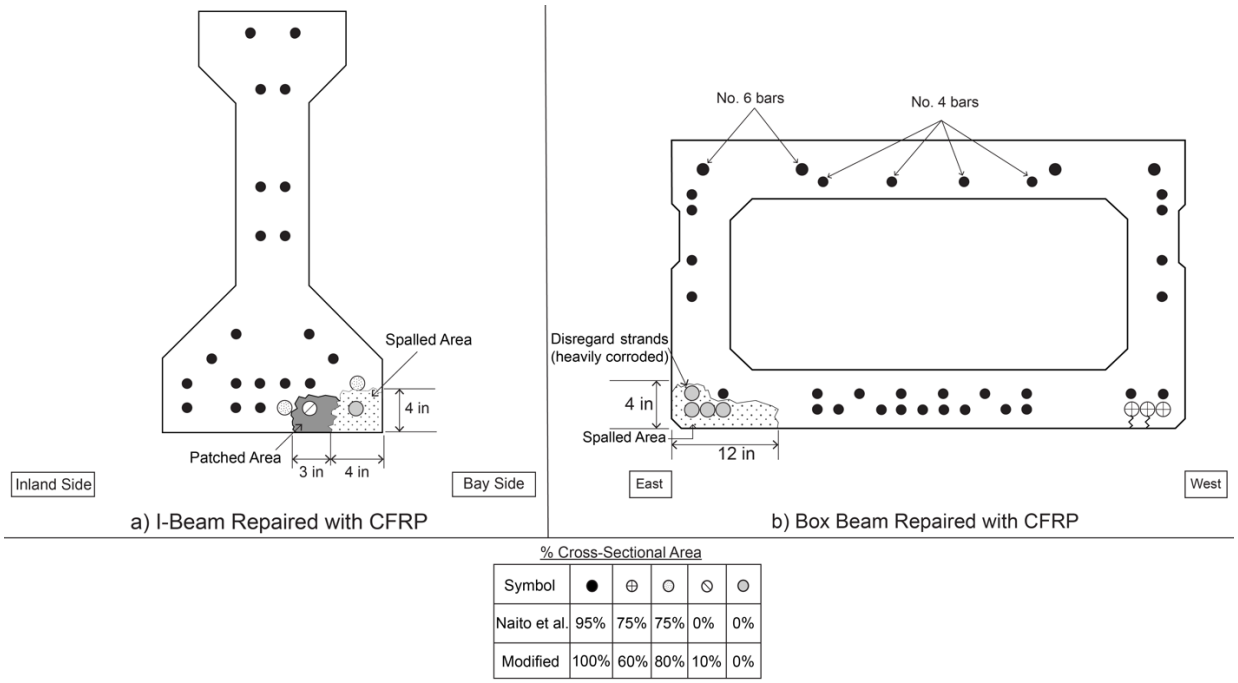

Figure 5.8. Beams Repaired with CFRP

The residual strength of the beams was calculated assuming that the repair would need to keep the beam in service for an additional 20 years. So, in addition to the currently observed damage, it was assumed that corrosion would continue to damage strands over an additional 20-year service life of the beam. If, at the time of a repair, only cosmetic repairs such as patching, were done to the beams, the corrosion would continue inside the beam. For example, Figure 5.8a shows the cross-section of I-Beam, with the current level of damage determined by the visual inspection. It was assumed that after an additional 20 years of service, the four interior strands adjacent to the affected area, within 2 in of the existing spall or patch, would also become damaged by corrosion.

To determine the residual strength of a beam with corrosion damage, modified method presented in Alfailakawi et al., (2020) was used to quantify damage for the I-Beam based on visual inspection information, while Naito et al (2011) recommendations was used for the Box Beam.

Based on these methods, the estimated residual strengths of the beams were calculated and are presented in Table 5.4. These calculations were first made based on an estimate of damage 20 years from now and then repeated based on the current condition of the beams. Also shown in Table 5.4 is the undamaged strength of the HRBT Beam. For all of the unrepaired beams, a strain compatibility approach was used to account for each layer of prestressing as well as the compression reinforcing in the deck.

Table 5.4. Estimated Strength Capacity of the Beams

Specimen	Undamaged Strength, k-ft	Strength with Current Corrosion Damage, k-f	Strength with Additional 20 years Corriosnion Damage, k-ft
HRBT-CFRP	1993		
I-Beam	1901	1718	1345
Box Beam	1481	1215	1168

5.5.3 Repairs

5.5.3.1 Hampton Road Bridge Tunnel Beam

The design of the CFRP repair was based on restoring strength to some of the very damaged beams in the actual HRBT bridge, but the tested beam had no damage. Figure 5.9 and Figure 5.10 show the details of the CFRP layups used to repair the HRBT-CFRP Beam. Three C400HM plies were attached to the soffit of the beam to increase the flexural strength. The breaking strength of the CFRP is 155 ksi. Each ply was 12 in wide and 0.08 in thick, so the total breaking strength of the three plies is 446 kips. However, failure could occur due to concrete crushing or debonding before the rupture of the CFRP. To enhance the bond of the longitudinal CFRP, one C200HM ply was wrapped around the bottom flange over 5 ft-6 in at the ends of the

beam as an anchorage system. The U-wrap plies were anchored with six CFRP anchors at each end, as shown in Figure 5.9 and Figure 5.10.

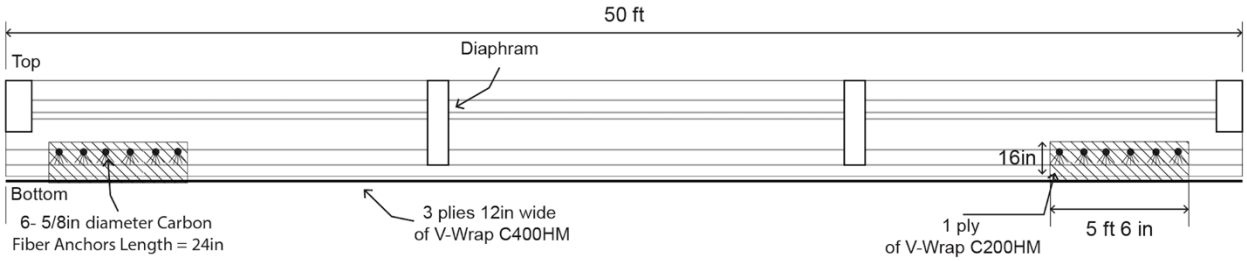

Figure 5.9. CFRP Layout for HRBT-CFRP Repair

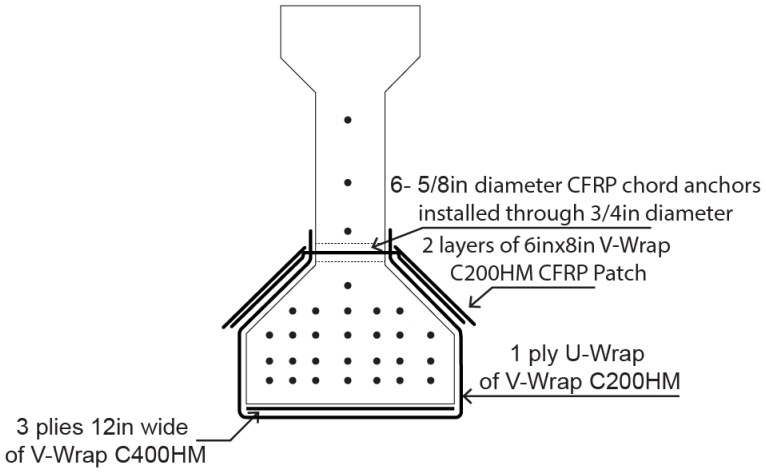

Figure 5.10. CFRP Repair Details for the HRBT-CFRP Beam

For the beam repaired with CFRP, two methods were used to calculate the flexural strength after repair: the method presented in ACI 440R (ACI 440, 2008) and the method in the AASHTO Guide Specifications for Design of Bonded FRP Systems for Repair (AASHTO, 2012) were used. For the calculation of flexural strength, several modes of failure must be considered: concrete crushing, CFRP rupture, and CFRP debonding.

5.5.3.2 Lesner and Aden Road Bridges

As mentioned before, I-Beam and Box beam were repaired using CFRP to restore the flexural strength. Based on the preliminary calculations, I-Beam required three C400HM plies 16

in wide. The anchorage system used for the I-Beam was the same as the one used for HRBT-CFRP Beam. While for the Box Beam, CFRP was attached only on the bottom flange, as only this face of the beam would be accessible in-situ. Box Beam required one C200HM ply, which contained three 12 in strips, to be attached to the 48 in wide bottom flange. The C400HM was as the one used for the flexural repair of the HRBT-CFRP beam. The C200HM has breaking stress of 155 ksi and a thickness of 0.04 in.

In order to get the maximum benefit from the CFRP repair, the weak surface of the concrete was removed using uniform mechanical chipping, and then it was washed with water. Locations with spalls were patched with high-strength concrete. Holes for the CFRP anchors were drilled through the webs of the I-beams. Finally, the CFRP sheets were applied using epoxy resin (see Figure 5.11).

Figure 5.11. CFRP Installation on I- Beams

5.3.3.3 Summary of Repaired Strengths and Expected Failure Loads

Calculations of repaired strength were made for the three beams using both the ACI 440 (ACI 440, 2008) and the AASHTO (AASHTO, 2012) methods. For the I-Beam and Box Beam, the repaired strength calculations were performed based on both the current condition, and the condition after 20 years, upon which the repair design was based. The results of these calculations are presented in Table 5.5.

Table 5.5. Calculated Flexural Capacity

Beam	CFRP Calculation Method	Undamaged Strength (k-ft)	Based on Assumed Damage over 20 years		Based on Current Observed Damage	
			Remaining Strength (k-ft)	Repaired Strength (k-ft)	Remaining Strength (k-ft)	Repaired Strength (k-ft)
HRBT-CFRP	ACI	1993	1993	2537	-	-
	AASHTO			2783		-
I-Beam	ACI	1901	1345	1851	1718	2272
	AASHTO			2026		2349
Box Beam	ACI	1481	1168	1501	1215	1549
	AASHTO			1277		1316

Figure 5.13 presents the loading conditions for the three beams during testing. All were loaded with a spreader beam which applied two equal loads at 4 ft each side of the centerline. Based on these loading conditions and the estimated flexural strengths, the anticipated load and failure mode were determined. The results are presented in Table 5.6.

Table 5.6. Predicted Failure Loads and Modes

Beam	CFRP Calc. Meth.	Calculated Flexural Strength, k-ft	Mid-Span Self-Weight Moment, k-ft	Expected Applied Moment to Cause Failure, k-ft	Expected Applied Load to Cause Failure, kips	Expected Failure Mode
HRBT CFRP	ACI	2537	215	2322	232	CFRP Debonding
	AASHTO	2783		2568	257	
I-Beam	ACI	2272	219	2053	207	CFRP Debonding
	AASHTO	2349		2130	215	
Box Beam	ACI	1549	253	1296	115	CFRP Debonding
	AASHTO	1315		1062	94.5	

5.6 Experimental Test Methods

5.6.1 Test setup and Instrumentation

All beams were tested in a simple span configuration, with one end supported by a roller and the other end supported by a pin. The flexural test setup is illustrated in Figure 5.12. The

span length for the HRBT beam and I-Beam was 48 ft, and the span length for the Box Beam was 53 ft. Loads were applied using a 400-kip actuator and a spreader beam, resulting in the application of two equal loads 8 ft apart, centered on the beam's midspan.

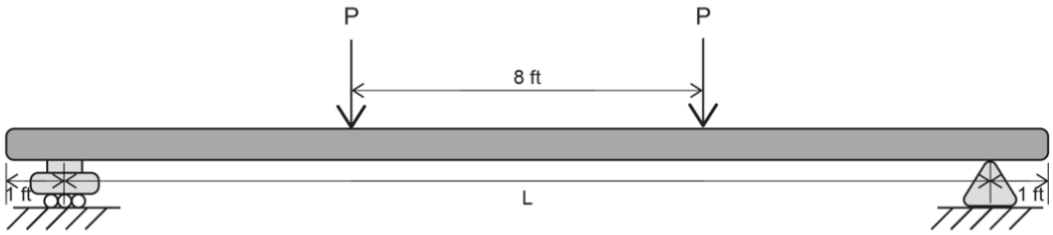

Figure 5.12. Flexural Test Set Up

All the beams had a similar instrumentation plan (Figure 5.13). Deflections were measured at midspan and the quarter points, and an array of strain gages was placed over the height of the beams near midspan to investigate strain distribution and the location of the centroid.

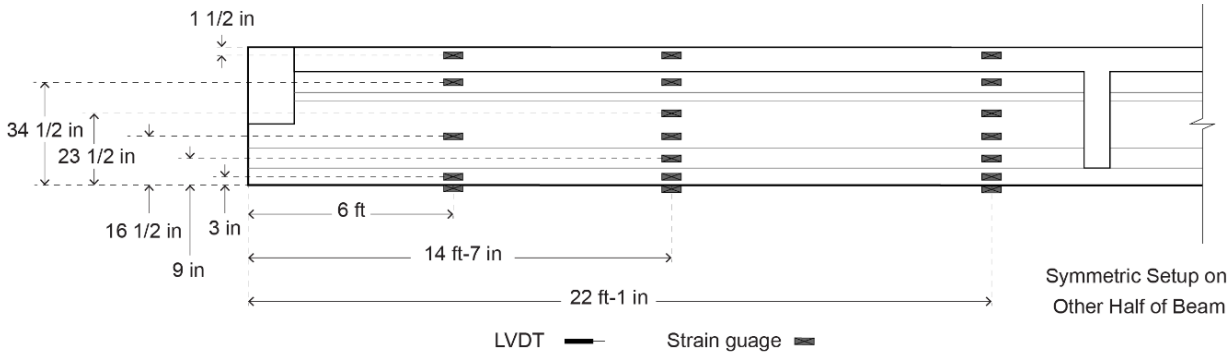

Figure 5.13. Instrumentation Plan

5.7 Description, Discussion and Results of Tests

5.7.1 Hampton Road Bridge Tunnel Beam

The load was applied in 10 kips increments, and at a load of 80 kips, the slope of the load vs deflection plot changed, as shown in Figure 5.16, indicating that cracks had begun to develop. Figure 5.16 also shows the load deflection behavior from an unrepaired HRBT beam tested in a companion study (Alfailakawi et al. 2022). Visible cracking was not evident until a load of 100 kips. When the load reached 215 kips, the CFRP began delaminating and debonding from the beam (see Figure 5.14). The beam continued to be loaded until it failed at 245 kips with a very wide, long flexural shear crack, as seen in Figure 5.15.

Figure 5.14. CFRP Debonded from the Soffit of the HRBT Beam

Figure 5.15. Flexural Shear Failure of the HRBT Beam Repaired with CFRP

The ultimate load of 245 kips was similar to the calculated load of 233 kips and 257 kips with the ACI and AASHTO method, respectively. Also, the assumed failure mode, debonding, was consistent with the observed mode. The premature loss of bond could have been due to poor preparation of the bottom surface of the beam, but it could also be related to the parabolic curve of the bottom flange.

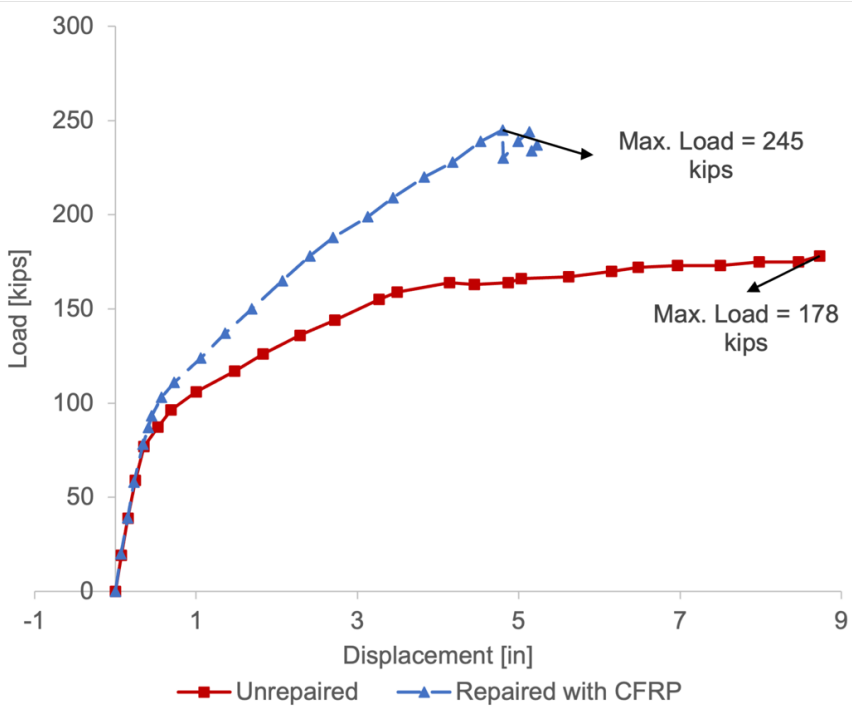

Figure 5.16. Load vs Deflection - HRBT Beams

5.7.1.1 Discussion

The load-deflection plots for the two beams are shown in Figure 5.16. The CFRP repair increased the flexural capacity by 37%, compared to the unrepaired beam that have tested by Alfailakawi et al., (2022). However, some ductility was sacrificed, and the repaired beam did not show an extended yield plateau.

The failures of the repaired beam were not a flexural failure but a more sudden shear failure. Figure 5.17 illustrates the computed shear capacity vs. the applied shear along the length

of the beam, calculated with the AASHTO sectional method. It is possible to demonstrate that the location where failure occurred was in the region on the graphs where the applied shear exceeded the capacity.

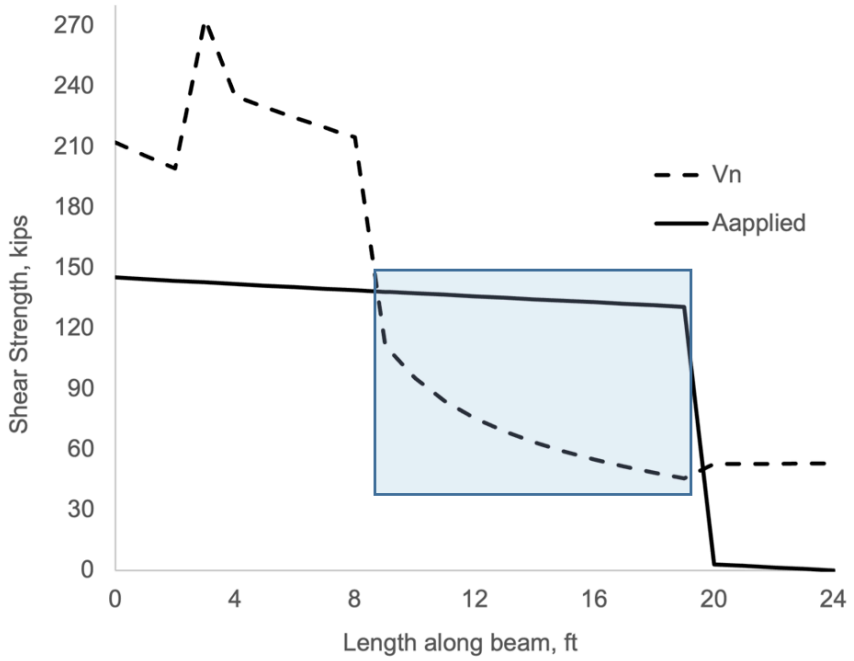

Figure 5.17. Shear Capacities along the Beam Repaired with CFRP

Although this beam failed in shear, it is important to note that this repair was somewhat unrealistic because the beam had no corrosion damage. In an actual repair scenario, if a beam is repaired to return it to its original strength, the shear strength should be adequate, assuming the original shear design was correct and there has been no shear-related damage.

5.7.2 Lesner Bridge I-Beam

Throughout this test, the beam was loaded in 10-kip increments. At a load of 75 kips, the first flexural crack was detected near the midspan of the beam on the bay side. The load was increased to 170 kips, and at that point, the popping of CFRP ruptering was audible. The load continued to be increased until it reached 230 kips, at which point the beam was unloaded to 192

kips due to a technical issue, and then reloaded. By the second attainment of 230 kips, the CFRP had failed and detached from the beam's soffit (see Figure 5.18).

Figure 5.18. CFRP Debonded

To determine the beam's capacity without the CFRP repair, the beam was unloaded to 130 kips, the CFRP was removed from the whole beam, and the beam was reloaded. After reaching 161 kips, the beam collapsed due to concrete crushing at the top, as shown in Figure 5.19. A load-deflection comparison between the undamaged and unrepaired I-Beam from the Lesner Bridge and the I-Beam repaired with CFRP is presented in Figure 5.20. More information about the unrepaired I-Beam can be found in (Alfailakawi et al., 2020).

Figure 5.19. Concrete Crushing Failure Mode and Cracking Pattern

In Table 5.6, the predicted flexural strength with the CFRP repair was expected to be 2272 k-ft using ACI and 2349 k-ft using the AASHTO method. As shown in the table this equates to applied loads of 207 and 215 kips for each method. The actual failure load of 234 kips indicates that both the methods used to calculate the repaired strength were conservative. Also, note in Table 5.5 that the unrepaired strength was estimated to be 1718 k-ft, which equates to an applied load of 150 kips. The actual strength after the CFRP was removed was slightly higher at 161 kips.

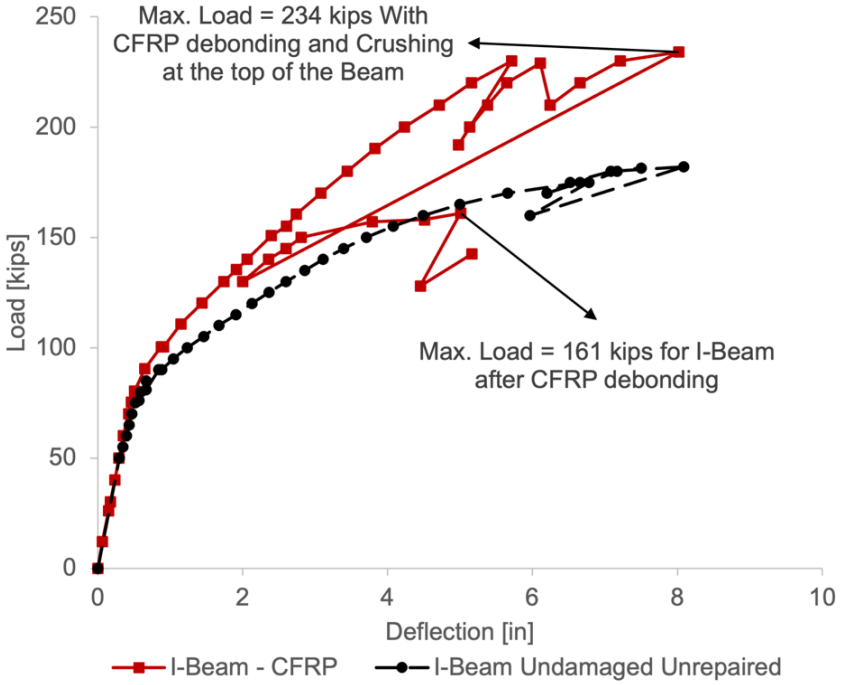

Figure 5.20. Load vs Deflection – I-Beam

5.7.3 Aden Road Box Beam

The beam was loaded in increments of 10 kips until it reached 40 kips, at which point the load increment was reduced to 5 kips. At a load of 50 kips, the first flexural crack was seen, corresponding to the change in slope of the load-deflection plot illustrated in Figure 5.21. More cracking noises continued to be heard, mostly in the patched regions used to cosmetically repair

the beam prior to repair with CFRP. At 50 kips, unexpected longitudinal cracks formed on both ends, which may be explained by a debonding between the concrete and the strands, rather than the CFRP. By 75 kips, CFRP debonding sounds were heard, but the location could not be determined. Additional sounds of concrete cracking and CFRP straining were heard, as well as the sound of a wire rupture at a load of 85 kips. The load was increased to 97 kips, at which point the test was interrupted due to technical issues.

The test proceeded with a 1.5 in residual deflection, and the load was increased until it reached 93 kips, at which point one of the three CFRP strips debonded and another ruptured (see Figure 5.22). When the load was reduced to 90 kips and then increased again, all the CFRP debonded off the beam's soffit. The beam was then unloaded to 54 kips, and the CFRP strips were removed, allowing the beam to be retested without repair to obtain a load-deflection plot for the beam in its damaged condition. The loading was continued until it reached 77 kips. Two wires broke in the beam's center, resulting in a very wide flexural crack. Finally, the beam collapsed due to concrete crushing at the top, with an ultimate load of 77 kips (see Figure 5.23).

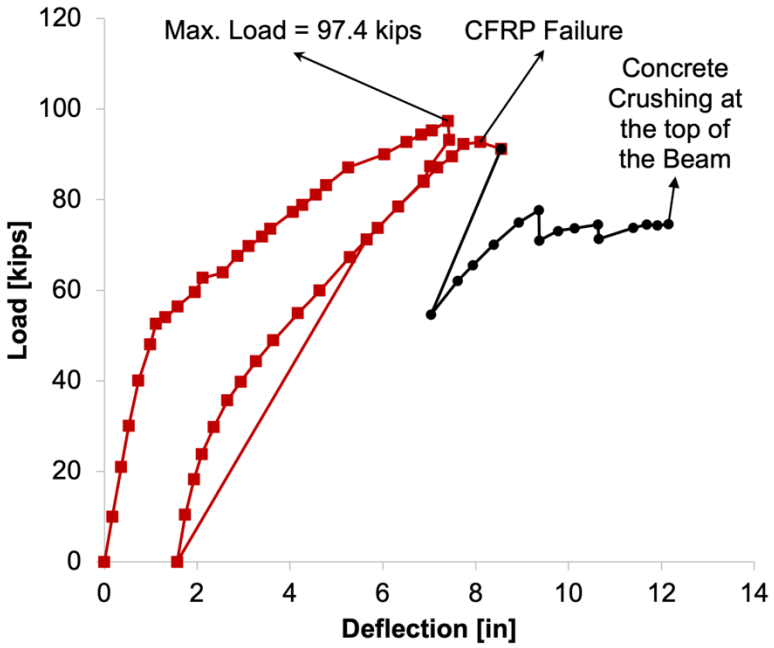

Figure 5.21. Load vs Deflection - Box Beam

Figure 5.22. CFRP Debonded and Ruptured on Bottom of Box Beam

Figure 5.23. Concrete Crushing Failure Mode

In Table 5.5, the predicted flexural strength with the CFRP repair was expected to be 1549 k-ft and 1316 k-ft with the ACI and AASHTO methods, respectively. These flexural strengths correspond to failure loads of 115 kips and 94.5 kips. The actual failure load of 97 kips indicates that the AASHTO method used to calculate the repaired strength was conservative while the ACI method was somewhat unconservative. Also, note in Table 5.5 that the unrepaired strength was estimated to be 1215 k-ft, which equates to an applied load of 85 kips. The actual strength after the CFRP was removed was somewhat less at 77 kips. The post-test forensic examination revealed that the cardboard void formers in the box beam were moist, indicating that there was trapped water in the box beam. This could have resulted in additional undetected corrosion of the prestressing. Previous tests have shown the reduction in cross-sectional area of the layer of strands next to the void is approximately 15% (Alfailakawi et al., 2020). Including the effect of water, the applied load calculated is 84 kips using AASHTO method and equal 102 kips using ACI method for the beam with CFRP repair.

5.7.4 Discussion

Table 4.8 presents a summary of the repaired beam performed. For the I-Beam, the AASHTO approach to calculating the flexural strength for beams strengthened with CFRP layups, gave conservative flexural strength estimations. For the Box Beam, water trapped in the can significantly decrease the strength capacity of the beam due to the chloride transport to the lower layer strands.

Table 5.7. Summary of Flexural Tests for I-Beam and Box Beam

Beam	Applied Load at Failure, kips	Moment				Failure Mode
		Total[1] Moment under Load at Failure, k-ft	Calc. Method	Calculated Flexural Strength, k-ft	M_{test}/M_{calc}	
HRBT CFRP	245	2665	ACI	2322	1.15	CFRP Debonding
			AASHTO	2568	1.04	

I-Beam	234	2542	ACI	2272	1.11	CFRP - Debonding
			AASHTO	2349	1.08	
Box Beam	97.5	1350	ACI	1549	0.87	CFRP - Debonding
			AASHTO	1316	1.03	
Box Beam - W/Water Effect -	97.5	1350	ACI	1399	0.96	CFRP - Debonding
			AASHTO	1200	1.12	

[1] Total moment includes self-weight

Alfailakawi et al., (2020) recommendations provide an excellent estimation for the residual capacity of the damaged I-Beam. This is critical in order to determine the needed repair capacity for the deteriorated beam. The test findings established that the estimate flexural capacity of the unrepaired damaged beam was accurate, and that the needed CFRP repair was determined appropriately. Combining these recommendations with the AASHTO approach, which produced more accurate results than ACI approach, will provide an a very good estimate of the flexural strength of a repaired damage beam.

For the Box Beam, Naito et al., (2011) recommendations combined with Alfailakawi et el., (2020) recommendations regarding the trapped water, should provide a good estimate of the residual capacity of the damaged Box Beam. Combining this with either the AASHTO or ACI methods should result in a reasonable estimate for the repaired beam.

5.8 CFRP Selection Repair - Parametric Study

It is essential to know for what level of corrosion damage CFRP is the best approach a repair method. Based on previous tests and the literature, the optimum number of CFRP layups that should be used is three plies; exceeding three plies will lead to earlier debonding failure. Therefore, in our study, three sheets of 400HM CFRP are used as a maximum number of plies and maximum strength properties.

So, the goal is to know the maximum reduction in the capacity of a beam that CFRP repair can recover from a damaged beam. To achieve the reduction in the capacity of a beam compared to its original capacity, a parametric study had been implemented to provide the bridge engineer with a convenient graph that can be used to determine this percentage based on the type and span length of the beam along with the spacing between the beams in a bridge. In this study, the method to calculate the capacity of a beam repaired with CFRP, which is presented in ACI 440R (ACI 440, 2008), was used since it gives more conservative results compared to AASHTO. However, both methods gave a good result in predicting the failure load in the beams, as we discussed earlier. The variables in our study were the span length, spacing between the beams in the bridge, and percentage loss in strength capacity. The analysis was performed investigating the span length, spacing, and the percentage of the capacity loss in the beam. Using the preliminary design data in the Bridge Design Manual, plots for AASHTO Beams type II, III, and IV were developed.

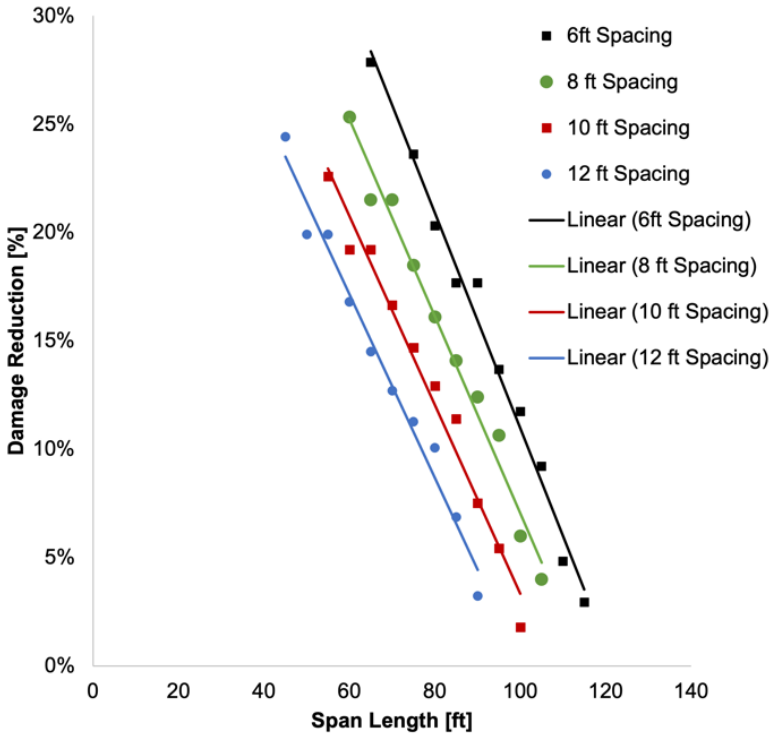

Figure 5.24. Original Data for AASHTO Type IV Beam

For example, Figure 5.24 shows the scatter points data for AASHTO type IV beam. These points are divided into four groups based on the spacing. For each group having the same spacing, the best fit linear is plotted. Then, regression tool was used to find a linear equation for all the samples in AASHTO Type IV beam and then been used to plot the data again as it shown in Figure 5.25. The maximum error found with this equation was not more than 2%.

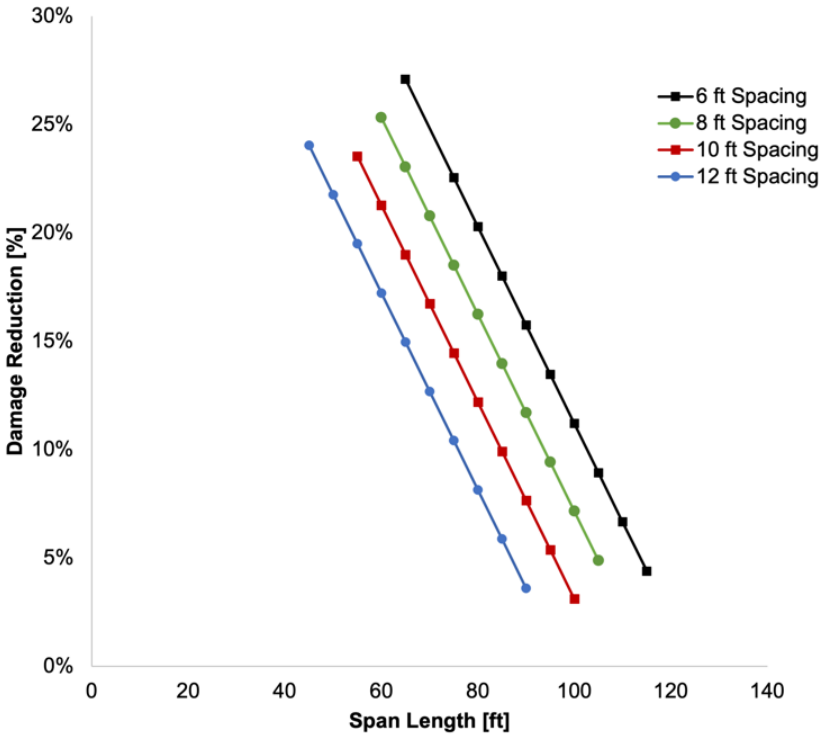

Figure 5.25. Data Regression for AASHTO Type IV Beam

Using the same procedure, Figure 5.26 shows the plots related to AASHTO II and III. I-Beam AASHTO II that was presented in this paper can be used as an example for this study. The span length is 50ft and the spacing is 6ft. From Figure 5.26, it can be shown that the maximum strength capacity loss percentage in the beam that can be recovered by the CFRP repair is 27%.

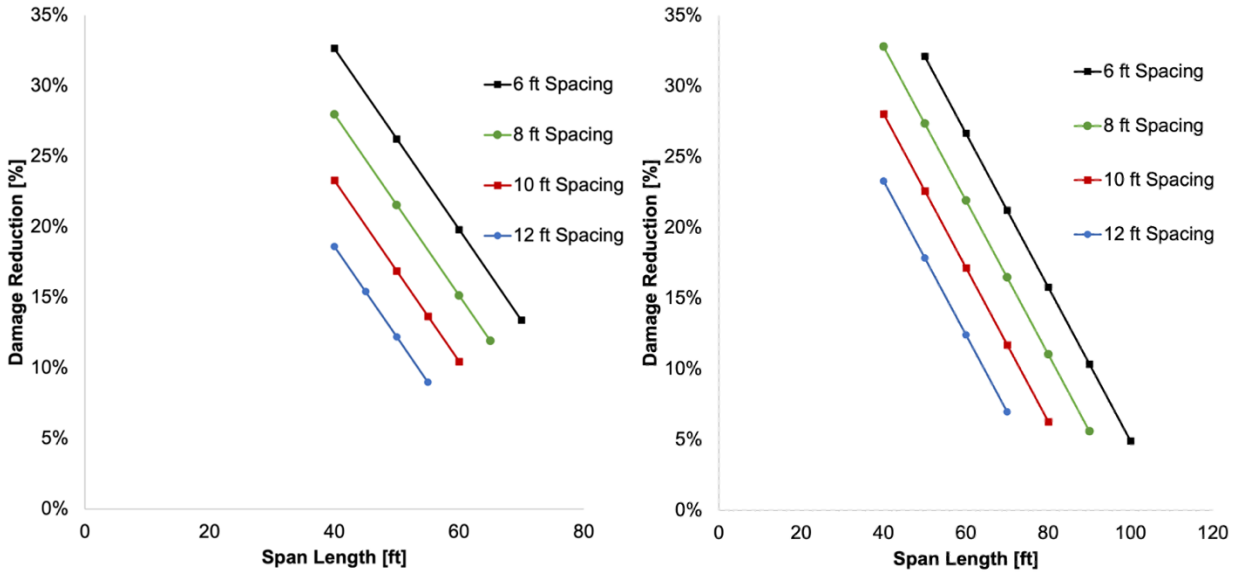

Figure 5.26. AASHTO type II (Left) and AASHTO type III (Right)

5.9 Summary and Conclusions

To properly evaluate a corrosion damaged beam and develop a CFRP repair design, a detailed damage map of the beam to be repaired must first be created. This damage map should detail the locations of longitudinal cracks, spalls, delaminations, and patches. Any exposed strands and their condition should also be recorded. Half-cell and chloride content results did not provide a valuable information to the strength calculation, and this is in agreement with Alfailakawi et al., (2020) and (Naito et al 2011).

For box beams, the recommendations of Naito et al. (2011) should be followed to assign a reduced cross-sectional area to strands in proximity to identified surface damage. For I-beams, the recommendations of Alfailakawi et al., (2020) should be used. For the determination of flexural strength, using the reduced cross-sectional areas, a strain compatibility approach provides an excellent strength estimate.

To select CFRP as a repair method, the condition of the concrete cover is very critical, particularly with I-beams. If more than 30% of the concrete cover is spalled in any one linear foot of the bottom flange, at a given section, it's not recommended to use CFRP as a repair method. Based on observations from the test of Box Beam, even if the CFRP adheres well to the soffit of the beam, a patched area that is added for cosmetic purposes may debond much sooner than the CFRP debonds from the beam's soffit.

For beams repaired with CFRP, the methods provided in ACI 440R (ACI 440, 2008) and The AASHTO Guide Specifications for Design of Bonded FRP Systems for Repair (AASHTO 2012) provide reasonable estimates of flexural strength.

5.10 References

1. Alfailakawi, A., Roberts-Wollmann, C.L., Hebdon, M., and Koutromanos, I. *Experimental and Analytical Evaluation of Residual Capacity of Corrosion Damaged Prestressed Concrete Bridge Girders.* VTRC 21-R6. Virginia Transportation Research Council, Charlottesville, VA, 2020.

2. Alfailakawi, A., Roberts-Wollmann, C.L., Hebdon, M., and Koutromanos, I. *Experimental and Analytical Evaluation of Repair Methods for Corrosion-damaged prestressed Concrete Bridge Beams.* VTRC 22-R1. Virginia Transportation Research Council, Charlottesville, VA, 2022.

3. Ali, A., Abdalla, J., Hawileh, R., & Galal, K. (2014). CFRP Mechanical Anchorage for Externally Strengthened RC Beams under Flexure. *Physics Procedia*, *55*, 10-16. https://doi.org/10.1016/j.phpro.2014.07.002

4. American Association of State Highway and Transportation Officials, *Guide Specifications for Design of Bonded FRP Systems for Repair and Strengthening of Concrete Bridge Elements*. AASHTO, Washington, D.C., 2012.

5. American Concrete Institute Committee 440. *Guide for the Design and Construction of Externally Bonded FRP Systems for Strengthening Concrete Structures*. ACI 440.2R-08, American Concrete Institute, Farmington Hills, MI, 2008.

6. Balakumaran, S. S. G. (2010). *Influence of Bridge Deck Concrete Parameters on the Reinforcing Steel Corrosion*. Virginia Tech]. https://vtechworks.lib.vt.edu/bitstream/handle/10919/32665/GBalakumaran_SS_T_2010.pdf?sequence=2.

7. Balasubramaniam, V., Raghunath, P. N., and Suguna, K. (2011). Performance of Corrosion-Damaged HSC Beams Strengthened with GFRP Laminates. *International Journal of Computer Science Engineering & Technology*, *1*(11).

8. Duthinh, D., and Starnes, M. (2004). Strength and ductility of concrete beams reinforced with carbon fiber-reinforced polymer plates and steel. Journal of composites for construction, 8(1), 59-69.

9. Klaiber, F. W., Wipf, T. J., and Kempers, B. J. (2003). *Repair of damaged prestressed concrete bridges using CFRP*. In *Proceedings of the 2003 mid-continental transportation research symposium, Ames, Iowa*. Citeseer.

10. Lee, H. S., Tomosawa, F., Masuda, Y., and Kage, T. (1997). *Effect of CFRP sheets on flexural strengthening of RC beams damaged by corrosion of tension rebar*. In *Proceedings of*

3rd International Symposium on Non Metallic (FRP) Reinforcement for Concrete Structures, Oct (pp. 23-23).

11. Naito, C., Jones, L., and Hodgson, I. Development of Flexural Strength Rating Procedures for Adjacent Prestressed Concrete Box Girder Bridges. *ASCE Journal of Bridge Engineering*, Vol. 61, No. 5, Sept/Oct 2011, pp. 662-670.

12. Nguyen, T. T. D., MATSUMOTO, K., IWASAKI, A., SATO, Y., & NIWA, J. (2013). *Performance of Pretensioning Prestressed Concrete Beams with Ruptured Strands Flexurally Strengthened by CFRP Sheets*. In *Proceedings of 3rd International Conference on Sustainable Construction Materials and Technologies, e-036, CD-ROM* (p. 10)

13. Rose, A. L., Suguna, K., and Ragunath, P. N. (2009). Strengthening of corrosion-damaged reinforced concrete beams with glass fiber reinforced polymer laminates. Journal of Computer Science, 5(6), 435.

14. Takács, P. F., & Kanstad, T. (2000). Strengthening prestressed concrete beams with carbon fiber reinforced polymer plates. *NORDIC CONCRETE RESEARCH-PUBLICATIONS*, *25*, 21-34.

CHAPTER 6: Conclusions, Recommendations, Future Work

Chapter 6 consists of conclusions from the results of experimental testing described in Chapters 3, 4, and 5. The conclusions and recommendations (section 6.1) have been provided in sequential order and split up accordingly based on the portion of the research they were completed in. Section 6.2 provides a list of potential future work.

6.1 Conclusions and Recommendations

6.1.1 Large Scale Laboratory Testing – Unrepaired Corrosion Damaged Girders

- For prestressed I-beams, with the (Naito et al., 2010a) method of damage estimation, either the AASHTO simplified method or strain compatibility approach can be used to calculate conservative estimates of flexural strength. The modified method for damage estimation, provides slightly more accurate estimates of residual strength compared to the (Naito et al., 2010a) method.
- The (Naito et al., 2010a) recommendations to estimate the residual cross-sectional area of prestressed strands in adjacent box beams result in reasonably accurate estimates of strength.
- The alternate method, which is based on strain limitation, produces satisfactory results, and accurately captures the failure mechanism.
- Poor drainage of water from the inside of box beams can lead to hidden damage, resulting in overly optimistic predicted flexural strength. Therefore, weep holes should be cleared to allow proper drainage of water.
- Data collected from visual inspections are the best inputs and are sufficient for estimating the remaining cross-sectional area of strands in prestressed concrete flexural members.

For unknown reasons, half-cell potentials and chloride concentration testing did not provide consistent results in this study.

6.1.2 Large Scale Laboratory Testing – External Post-Tensioning Repair Method

- To correctly analyze a corrosion-damaged beam and create an external PT repair plan, it is necessary to first produce a detailed damage map of the beam to be repaired. This damage map should include longitudinal cracks, spalls, delaminations, and patches. Additionally, any exposed strands and their condition should be documented. The findings of half-cell and chloride content analysis did not contribute significantly to the strength calculation, which is consistent with Naito et al. (2010) and Alfailakawi et al., (2020). For the determination of flexural strength, using the reduced cross-sectional areas, a strain compatibility approach provides a good strength estimate. However, the need of another method that calculates the strength capacity based on ultimate strain is recommended and needs to be further investigated.
- The AASHTO simplified approach for estimating the flexural strength of beams containing bonded and unbonded tendons provides a conservative repair strength approximation. It can be used to determine the number and size of external strands required. The proposed detailed method provides a very good strength approximation. Also, it provides an excellent approximation for the ultimate stress in external tendons and the deflection of repaired beams.
- The following recommendation shall be used if the external PT repair is chosen:
    - The anchor blocks should be placed on the webs as close to the ends of the beams as is allowed by the construction and stressing process. The live-end anchor block

may need to be placed farther from the end of the beam than the dead-end block to allow for access with the stressing ram.

- At the locations where anchor blocks and deviators are to be cast against the existing beam, the surface of the beam should be roughened with a chipping hammer to improve the bond of the new concrete to the old.
- The main flexural and shear friction reinforcement should be passed through slightly oversized holes in the webs and developed in the anchor block on the opposite side of the web. The bars should be epoxied into the holes for better development and to reduce the possibility of the anchor blocks moving relative to the beam's web during stressing.
- The deviation points should be placed at the existing interior diaphragms. The diaphragm walls should be extended downward, so the deviation point of the new external tendons is as low as possible in the cross-section but not below the bottom of the bottom flange. The new lower part of the wall should be widened to accommodate a deviation saddle.
- Grout or wax may be used to fill the duct in an external PT repair. However, wax is more likely to prevent corrosion initiation in the tendons in the long term.

6.1.3 Large Scale Laboratory Testing – CFRP Repair Method

- For box beams, the recommendations of Naito et al. (2011) should be followed to assign a reduced cross-sectional area to strands in proximity to identified surface damage. For I-beams, the recommendations of Alfailakawi et al., (2020) should be used. For the determination of flexural strength, using the reduced cross-sectional areas, a strain compatibility approach provides an excellent strength estimate.

- To select CFRP as a repair method, the condition of the concrete cover is very critical, particularly with I-beams. If more than 30% of the concrete cover is spalled in any one linear foot of the bottom flange, at a given section, it's not recommended to use CFRP as a repair method. Based on observations from the test of Box Beam, even if the CFRP adheres well to the soffit of the beam, a patched area that is added for cosmetic purposes may debond much sooner than the CFRP debonds from the beam's soffit.
- For beams repaired with CFRP, the methods provided in ACI 440R (ACI 440, 2008) and The AASHTO Guide Specifications for Design of Bonded FRP Systems for Repair (AASHTO 2012) provide reasonable estimates of flexural strength.

6.2 Future Work

Based on the author's experience in this study, the following items are proposed to be investigated by future researchers.

- Additional experimental tests data is needed to determine the capacity for beams that have different types and levels of damage other than other than those indicated in this research. In addition, more research is required to examine the impact of water trapped in box beams on their residual strength.

- Further research is needed to estimate the capacity of the corrosion damaged beams based only on the chloride concentration and the half-cell.

- More study is necessary to determine how corrosion affects the effective prestress of the strands. The majority of existing recommendations for corroded girders are aimed for determining the residual strength, not the cracking strength.

- Additional testing is necessary to examine the impact of external PT, with concrete anchor block, as a restoration method to recover the lost capacity in corrosion-damaged beams.

- Additional testing is required to confirm the detailed method presented in this study for calculating the ultimate stress in the external PT tendons in beams with bonded and unbonded tendons.

- Further research is needed to determine the impact of corrosion on external PT tendons, in long term, when ducts are filled with wax or grout.

- Further research of the bond between CFRP and curved surfaces is required.

References

AASHTO, L. R. F. D. (1998). Bridge design specifications.

AASHTO, L. R. F. D. (2017). Specifications. *American Association of State Highway and*.

AASHTO, T. P. (2011). 95-11 "Standard Method of Test for Surface Resistivity Indication of Concrete's Ability to Resist Chloride Ion Penetration.". *AASHTO Provisional Standards, 2011 Edition*.

Alfailakawi, A., Roberts-Wollmann, C. L., Hebdon, M., & Koutromanos, I. (2020). Experimental and Analytical Evaluation of Residual Capacity of Corrosion-Damaged Prestressed Concrete Bridge Girders. https://rosap.ntl.bts.gov/view/dot/53953

Ali, A., Abdalla, J., Hawileh, R., & Galal, K. (2014). CFRP Mechanical Anchorage for Externally Strengthened RC Beams under Flexure. *Physics Procedia*, *55*, 10-16. https://doi.org/10.1016/j.phpro.2014.07.002

American Concrete Institute, A. C. I. C. (2019). *Building code requirements for structural concrete (ACI 318-19) : an ACI standard; Commentary on building code requirements for structural concrete (ACI 318R-19)*.

ASTM-C876. (2015). Test Method for Corrosion Potentials of Uncoated Reinforcing Steel in Concrete. https://doi.org/10.1520/c0876-15

Balakumaran, S. S. G. (2010). *Influence of Bridge Deck Concrete Parameters on the Reinforcing Steel Corrosion*. Virginia Tech].

https://vtechworks.lib.vt.edu/bitstream/handle/10919/32665/GBalakumaran_SS_T_2010.pdf?sequence=2.

Balasubramaniam, V., Raghunath, P. N., & Suguna, K. (2011). Performance of Corrosion-Damaged HSC Beams Strengthened with GFRP Laminates. *International Journal of Computer Science Engineering & Technology*, *1*(11). https://pdfs.semanticscholar.org/83dc/fbdbe4a691d23194c67123862f7e12e6afa9.pdf

Bennitz, A., Schmidt, J. W., Nilimaa, J., Täljsten, B., Goltermann, P., & Ravn, D. L. (2012). Reinforced concrete T-beams externally prestressed with unbonded carbon fiber-reinforced polymer tendons. *ACI Structural Journal*, *109*(4), 521. https://search.proquest.com/openview/a848a2dd02d26eb8e5d42dc1356d6478/1?pq-origsite=gscholar&cbl=36963

Ceroni, F., Pecce, M., Matthys, S., & Taerwe, L. (2008). Debonding strength and anchorage devices for reinforced concrete elements strengthened with FRP sheets. *Composites Part B: Engineering*, *39*(3), 429-441. https://doi.org/10.1016/j.compositesb.2007.05.002

Chase, S. B., & Balakumaran, S. S. G. (2020). Magnetic Flux Leakage Device for Evaluation of Prestressed Concrete Box Bridges. https://trid.trb.org/view/1694895

Ciolko, A. T. (2005). *Corrosion and prestressed concrete bridges*. In *Structures Congress 2005: Metropolis and Beyond* (pp. 1-12). https://ascelibrary.org/doi/abs/10.1061/40753(171)17

Collins, M. P., & Mitchell, D. (1987). *Prestressed concrete basics*. Canadian Prestressed Concrete Institute.

Dasar, A., Hamada, H., Sagawa, Y., & Yamamoto, D. (2017). Deterioration progress and performance reduction of 40-year-old reinforced concrete beams in natural corrosion environments. *Construction and Building Materials*, *149*, 690-704. https://doi.org/10.1016/j.conbuildmat.2017.05.162

Dong, J., Wang, Q., & Guan, Z. (2013). Structural behaviour of RC beams with external flexural and flexural–shear strengthening by FRP sheets. *Composites Part B: Engineering*, *44*(1), 604-612. https://www.sciencedirect.com/science/article/pii/S1359836812001746

Duthinh, D., & Starnes, M. (2004). Strength and ductility of concrete beams reinforced with carbon fiber-reinforced polymer plates and steel. *Journal of composites for construction*, *8*(1), 59-69. https://ascelibrary.org/doi/abs/10.1061/(ASCE)1090-0268(2004)8:1(59)

Elsener, B., Andrade, C., Gulikers, J., Polder, R., & Raupach, M. (2003). Half-cell potential measurements—Potential mapping on reinforced concrete structures. *Materials and Structures*, *36*(7), 461-471.

Grelle, S. V., & Sneed, L. (2011). *An Evaluation of Anchorage Systems For Fiber-Reinforced Polymer (FRP) Laminates Bonded to Reinforced Concrete Elements*. In.

Grelle, S. V., & Sneed, L. H. (2013). Review of Anchorage Systems for Externally Bonded FRP Laminates. *International Journal of Concrete Structures and Materials*, *7*(1), 17-33. https://doi.org/10.1007/s40069-013-0029-0

Harajli, M. H., & Naaman, A. E. (1985). Evaluation of the inelastic behavior of partially prestressed concrete beams. *Report No. UMCE*, 85-82.

Harajli, M. H. (1990). Effect of span-depth ratio on the ultimate steel stress in unbonded prestressed concrete members. *Structural Journal*, *87*(3), 305-312. https://www.concrete.org/publications/internationalconcreteabstractsportal/m/details/id/2631

Harajli, M. H. (1993). Strengthening of concrete beams by external prestressing. *PCI journal*, *38*(6), 76-88.

Harries, K. A. (2009). Structural testing of prestressed concrete girders from the Lake View Drive Bridge. *Journal of Bridge Engineering*, *14*(2), 78-92. https://ascelibrary.org/doi/pdf/10.1061/(ASCE)1084-0702(2009)14:2(78)

Heejeong, S., & D., G. (2003). How Accurate Is Ground-Penetrating Radar for Bridge Deck Condition Assessment? *Transportation Research Record*, *1845*, 139 - 147.

Heo, S., Shin, S., & Lee, C. (2013). Flexural Behavior of Concrete Beams Internally Prestressed with Unbonded Carbon-Fiber-Reinforced Polymer Tendons. *Journal of Composites for Construction*, *17*(2), 167-175. https://doi.org/10.1061/(asce)cc.1943-5614.0000306

Hussien, O. F., Elafandy, T. H. K., Abdelrahman, A. A., Abdel Baky, S. A., & Nasr, E. A. (2012). Behavior of bonded and unbonded prestressed normal and high strength concrete beams. *HBRC Journal*, *8*(3), 239-251. https://doi.org/10.1016/j.hbrcj.2012.10.008

Imam, A., Department of Civil Engineering, S. H. U. O. A. T. A. S. F. A. A. I.-D. U., Allahabad - 211007, U.P, India, Mishra, S., & Kumar Bind, Y. (2018). Review study towards

corrosion mechanism and its impact on the durability of concrete structures. *AIMS Materials Science*, *5*(2), 276-300. https://doi.org/10.3934/matersci.2018.2.276

Khudeira, S. (2010). Strengthening of deteriorated concrete bridge girders using an external posttensioning system. *Practice Periodical on Structural Design and Construction*, *15*(4), 242-247. https://ascelibrary.org/doi/full/10.1061/(ASCE)SC.1943-5576.0000074

Kim, Y. J., Green, M. F., & Fallis, G. J. (2008). Repair of bridge girder damaged by impact loads with prestressed CFRP sheets. *Journal of Bridge Engineering*, *13*(1), 15-23. https://ascelibrary.org/doi/abs/10.1061/(ASCE)1084-0702(2008)13:1(15)

Kiviste, M., Tamme, V., Linnus, L., & Halgma, R. (2019). Half-cell potential mapping for corrosion risk evaluation of prestressed concrete ribbed panels from agricultural building after 20 years of service. https://dspace.emu.ee/bitstream/handle/10492/4784/BSE2019_Vol17SI1_Kiviste.pdf?sequence=4

Klaiber, F. W., Wipf, T. J., & Kempers, B. J. (2003). *Repair of damaged prestressed concrete bridges using CFRP*. In *Proceedings of the 2003 mid-continental transportation research symposium, Ames, Iowa*. Citeseer. https://citeseerx.ist.psu.edu/viewdoc/download?doi=10.1.1.564.8599&rep=rep1&type=pdf

Lee, H. S., Tomosawa, F., Masuda, Y., & Kage, T. (1997). *Effect of CFRP sheets on flexural strengthening of RC beams damaged by corrosion of tension rebar*. In *Proceedings of 3rd International Symposium on Non Metallic (FRP) Reinforcement for Concrete Structures, Oct* (pp. 23-23).

Lee, L.-H., Moon, J.-H., & Lim, J.-H. (1999). Proposed methodology for computing of unbonded tendon stress at flexural failure. *Structural Journal*, *96*(6), 1040-1048. https://www.concrete.org/publications/internationalconcreteabstractsportal/m/details/id/781

Lee, S.-H., Shin, K.-J., & Lee, H.-D. (2018). Post-Tensioning Steel Rod System for Flexural Strengthening in Damaged Reinforced Concrete (RC) Beams. *Applied Sciences*, *8*(10), 1763. https://doi.org/10.3390/app8101763

Leicht, L., Roberts-Wollmann, C. L., Hebdon, M. H., Koutromanos, I., & Mosig, O.

MacGregor, R. J. G. (1989). *Strength and ductility of externally post-tensioned segmental box girders*. PhD dissertation, The University of Texas at Austin].

Manning, D. G., & National, R. C. U. S. T. R. B. (1985). *Detecting defects and deterioration in highway structures*. Transportation Research Board, National Research Council.

Moawad, M., El-Karmoty, H., & El Zanaty, A. (2018). Behavior of corroded bonded fully prestressed and conventional concrete beams. *HBRC Journal*, *14*(2), 137-149. https://doi.org/10.1016/j.hbrcj.2016.02.002

Naaman, A. E., & Alkhairi, F. M. (1991). Stress at ultimate in unbonded post-tensioning tendons: Part 1--evaluation of the state of the art. *Structural Journal*, *88*(5), 641-651. https://www.researchgate.net/profile/Fadi_Alkhairi/publication/279903459_Stress_at_ultimate_in_unbonded_post-tensioning_tendons_Part_1_Evaluation_of_the_state-of-the-art/links/5ccfbcd3458515712e955c23/Stress-at-ultimate-in-unbonded-post-tensioning-tendons-Part-1-Evaluation-of-the-state-of-the-art.pdf

Naaman, A. E., & Alkhairi, F. M. (1992). Stress at ultimate in unbonded post-tensioning tendons: Part 2--proposed methodology. *Structural Journal*, *88*(6), 683-692. https://www.researchgate.net/profile/Fadi_Alkhairi/publication/279543485_Stress_at_ultimate_in_unbonded_post-tensioning_tendons_Part_2_Proposed_methodology/links/5ccfbcb292851c4eab861520/Stress-at-ultimate-in-unbonded-post-tensioning-tendons-Part-2-Proposed-methodology.pdf

Naito, C., Jones, L., & Hodgson, I. (2010a). Inspection methods & techniques to determine non visible corrosion of prestressing strands in concrete bridge components: task 3, forensic evaluation and rating methodology. https://rosap.ntl.bts.gov/view/dot/18121/dot_18121_DS1.pdf

Naito, C., Jones, L., & Hodgson, I. (2011). Development of Flexural Strength Rating Procedures for Adjacent Prestressed Concrete Box Girder Bridges. *Journal of Bridge Engineering*, *16*(5), 662-670. https://doi.org/10.1061/(asce)be.1943-5592.0000186

Naito, C., Sause, R., Hodgson, I., Pessiki, S., & Macioce, T. (2010b). Forensic Examination of a Noncomposite Adjacent Precast Prestressed Concrete Box Beam Bridge. *Journal of Bridge Engineering*, *15*(4), 408-418. https://doi.org/10.1061/(asce)be.1943-5592.0000110

Nassif, H., Ozkul, O., & Harajli, M. H. (2003). Flexural behavior of beams prestressed with bonded and unbonded. *PTI Journal*, *1*, 60-71.

Nguyen, T. T. D., MATSUMOTO, K., IWASAKI, A., SATO, Y., & NIWA, J. (2013). *Performance of Pretensioning Prestressed Concrete Beams with Ruptured Strands Flexurally*

Strengthened by CFRP Sheets. In *Proceedings of 3rd International Conference on Sustainable Construction Materials and Technologies, e-036, CD-ROM* (p. 10).

Ozbakkaloglu, T., & Saatcioglu, M. (2009). Tensile behavior of FRP anchors in concrete. *Journal of Composites for Construction*, *13*(2), 82-92. https://ascelibrary.org/doi/abs/10.1061/(ASCE)1090-0268(2009)13:2(82)

Papé, T. M., & Melchers, R. E. (2011). The effects of corrosion on 45-year-old pre-stressed concrete bridge beams. *Structure and Infrastructure Engineering*, *7*(1-2), 101-108. https://doi.org/10.1080/15732471003588411

Pape, T. M., & Melchers, R. E. (2013). Performance of 45-year-old corroded prestressed concrete beams. *Proceedings of the Institution of Civil Engineers - Structures and Buildings*, *166*(10), 547-559. https://doi.org/10.1680/stbu.11.00016

Pino, V., Nanni, A., Arboleda, D., Roberts-Wollmann, C., & Cousins, T. (2017). Repair of damaged prestressed concrete girders with FRP and FRCM composites. *Journal of Composites for Construction*, *21*(3), 04016111. https://ascelibrary.org/doi/abs/10.1061/(ASCE)CC.1943-5614.0000773

Roberts-Wollmann, C. L., Kreger, M. E., Rogowsky, D. M., & Breen, J. E. (2005). Stresses in external tendons at ultimate. *ACI Structural Journal*, *102*(2), 206. http://search.proquest.com/openview/1e58b980e3298dd0a88a8a744821b3aa/1?pq-origsite=gscholar&cbl=36963

Rodriguez, J., Ortega, L. M., & Casal, J. (1997). Load carrying capacity of concrete structures with corroded reinforcement. *Construction and Building Materials*

Corrosion and Treatment of Reinforced Concrete, *11*(4), 239-248. https://doi.org/10.1016/S0950-0618(97)00043-3

Rogers, R., Wotherspoon, L., Scott, A. N., & Ingham, J. M. (2012). Residual strength assessment and destructive testing of decommissioned concrete bridge beams with corroded pretensioned reinforcement. http://ir.canterbury.ac.nz/bitstream/handle/10092/10620/12655163_PCI Journal Scott_Rogers Residual Strength_2012.pdf?sequence=1

Rose, A. L., Suguna, K., & Ragunath, P. N. (2009). Strengthening of corrosion-damaged reinforced concrete beams with glass fiber reinforced polymer laminates. *Journal of Computer Science*, *5*(6), 435. http://citeseerx.ist.psu.edu/viewdoc/download?doi=10.1.1.165.9379&rep=rep1&type=pdf

Sayed-Ahmed, E. Y., Riad, A. H., & Shrive, N. G. (2004). Flexural strengthening of precast reinforced concrete bridge girders using bonded carbon fibre reinforced polymer strips or external post-tensioning. *Canadian Journal of Civil Engineering*, *31*(3), 499-512. https://doi.org/10.1139/l04-005

Shubinsky, G., & Northwestern University (Evanston, I. I. T. I. (1994). *Application of Optical Imaging Methods for Bridge Maintenance and Inspection*. Northwestern University Infrastructure Technology Institute. https://books.google.com/books?id=3z0dAQAAMAAJ

Soudki, K. A. (2006). FRP repair of corrosion-damaged concrete beams—Waterloo experience. In *Advances in Engineering Structures, Mechanics & Construction* (pp. 165-173). Springer. https://link.springer.com/chapter/10.1007/1-4020-4891-2_14

Suntharavadivel, T. G., & Aravinthan, T. (2005). *Overview of external post-tensioning in bridges*. In *Proceedings of the 2005 Southern Region Engineering Conference (SREC 2005)* (pp. 29-38). Engineers Australia, Toowoomba Local Group. https://eprints.usq.edu.au/2217

Takács, P. F., & Kanstad, T. (2000). Strengthening prestressed concrete beams with carbon fiber reinforced polymer plates. *NORDIC CONCRETE RESEARCH-PUBLICATIONS*, *25*, 21-34.

Tao, X., & Du, G. (1985). Ultimate stress of unbonded tendons in partially prestressed concrete beams. *PCI Journal*, *30*(6), 72-91. http://gateway.webofknowledge.com/gateway/Gateway.cgi?GWVersion=2&SrcApp=GSSearch&SrcAuth=Scholar&DestApp=WOS_CPL&DestLinkType=CitingArticles&UT=A1985C731300004&SrcURL=https://scholar.google.com/&SrcDesc=Back+to+Google+Scholar&GSPage=TC

Wight, J. K. (2013). Reinforced Concrete: Mechanics and Design : Mechanics and Design. http://www.myilibrary.com?id=535850

Zhang, X., Li, S., Zhang, W., Ikechukwu, O., Dai, L., & Wang, L. (2020). Second Remediation of Long-Term Deflection and Cracking of PT Box-Girder Bridge Using External Post-Tensioning. *Journal of Performance of Constructed Facilities*, *34*(5), 04020090. https://doi.org/10.1061/(asce)cf.1943-5509.0001491

Zou, T. (2014). *Non-Destructive Bridge Deck Condition Assessment with a Probability-Based Deterioration Threshold*. Virginia Tech]. https://vtechworks.lib.vt.edu/bitstream/handle/10919/49384/Zou_T_D_2014.pdf?sequence=1.

Appendix

Appendix A Results of Post-Tensioning

Appendix B Calculations

Appendix C Results of Flexural tests

Appendix A: Results of Post-Tensioning for I-Beam 1 and I-Beam 5

A.1 I-Beam 1 – Damaged and Repaired with External PT

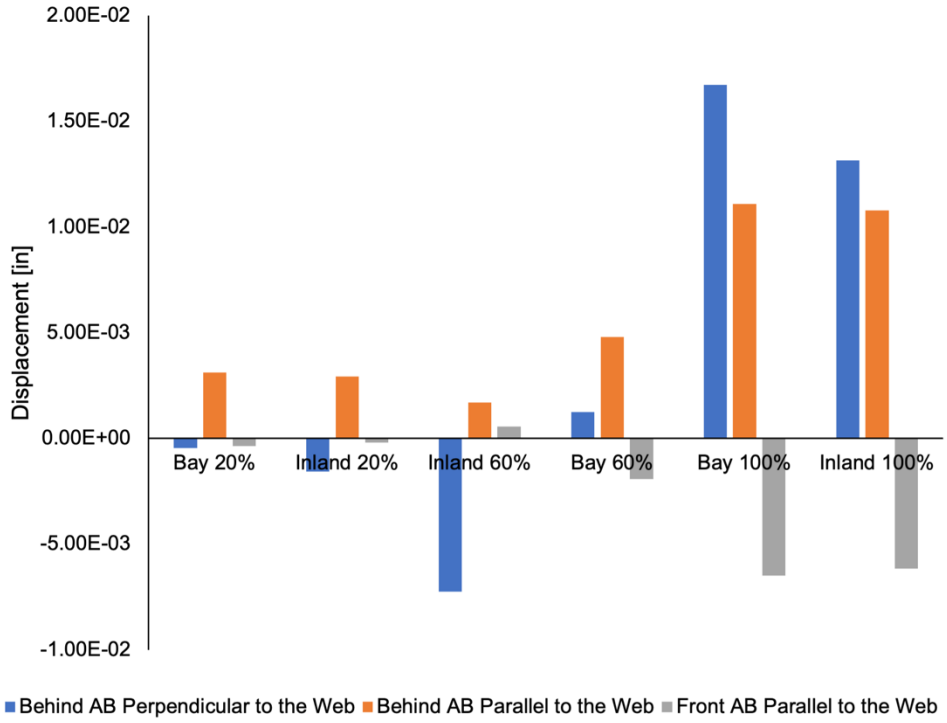

Figure A1.1. IB1 Displacement vs Stressing % "Live End - Bay Side"

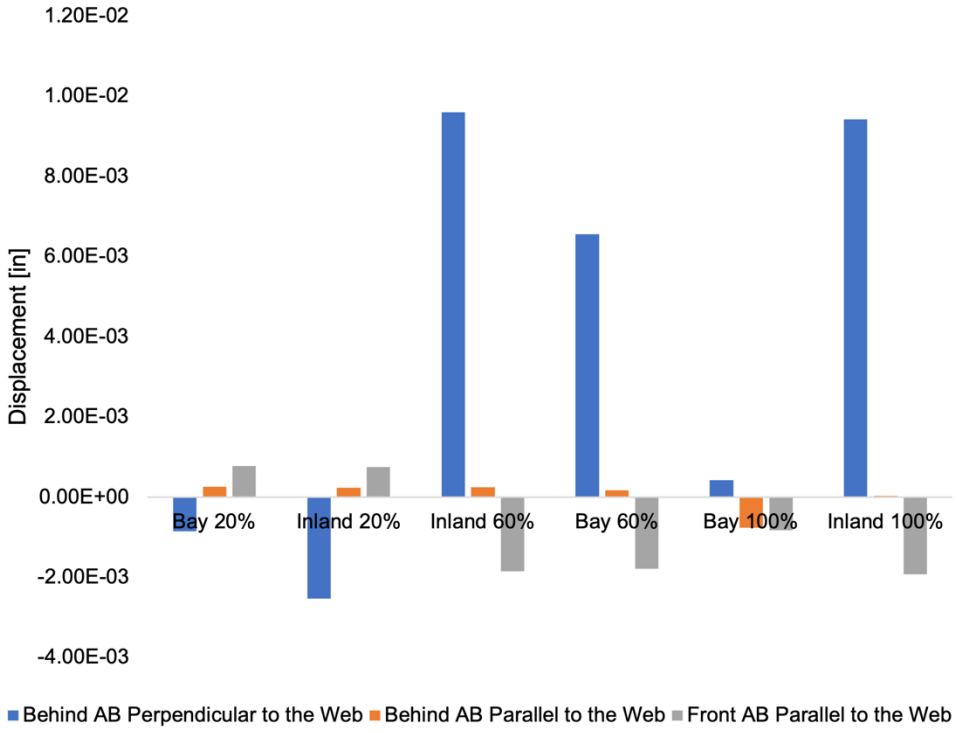

Figure A1.2. IB1 Displacement vs Stressing % "Live End - Inland Side"

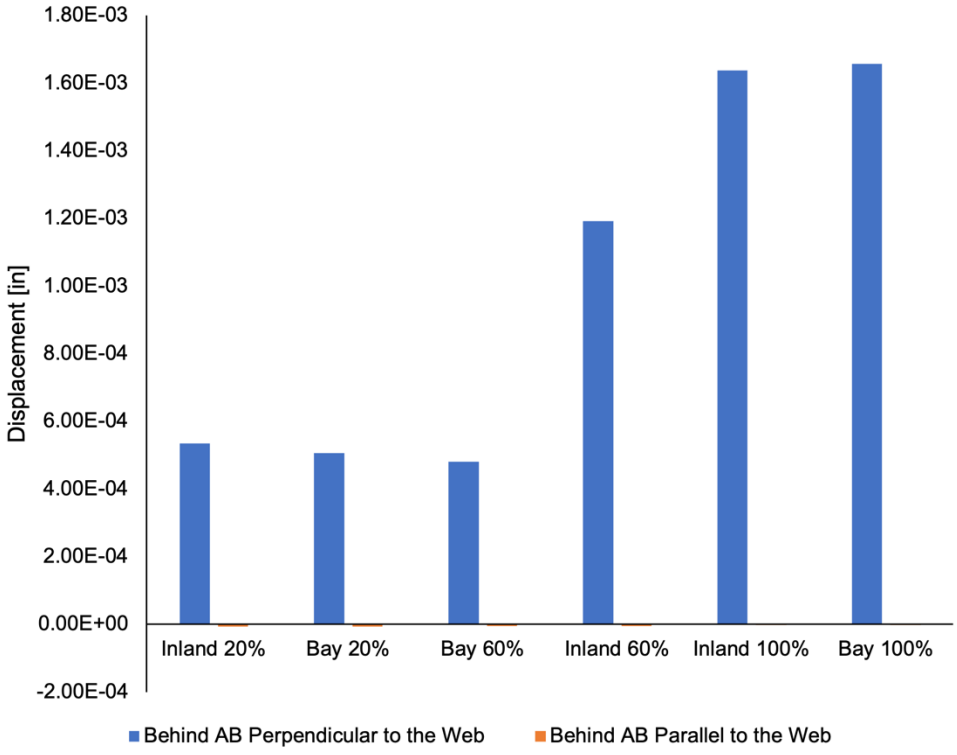

Figure A1.3. IB1 Displacement vs Stressing % "Dead End - Bay Side"

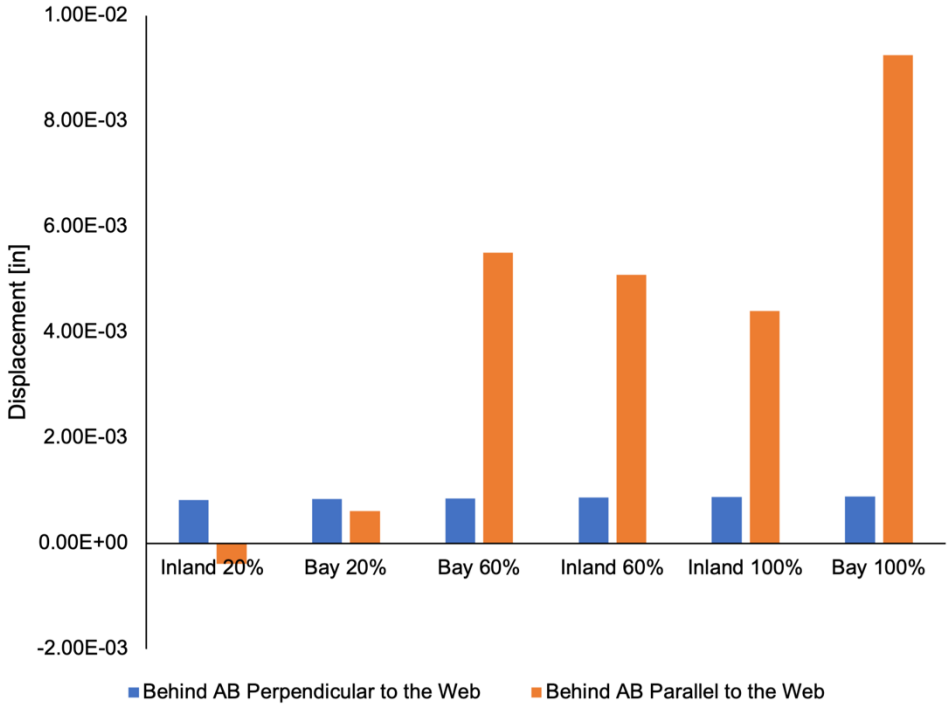

Figure A1.4. IB1 Displacement vs Stressing % "Dead End - Inland Side"

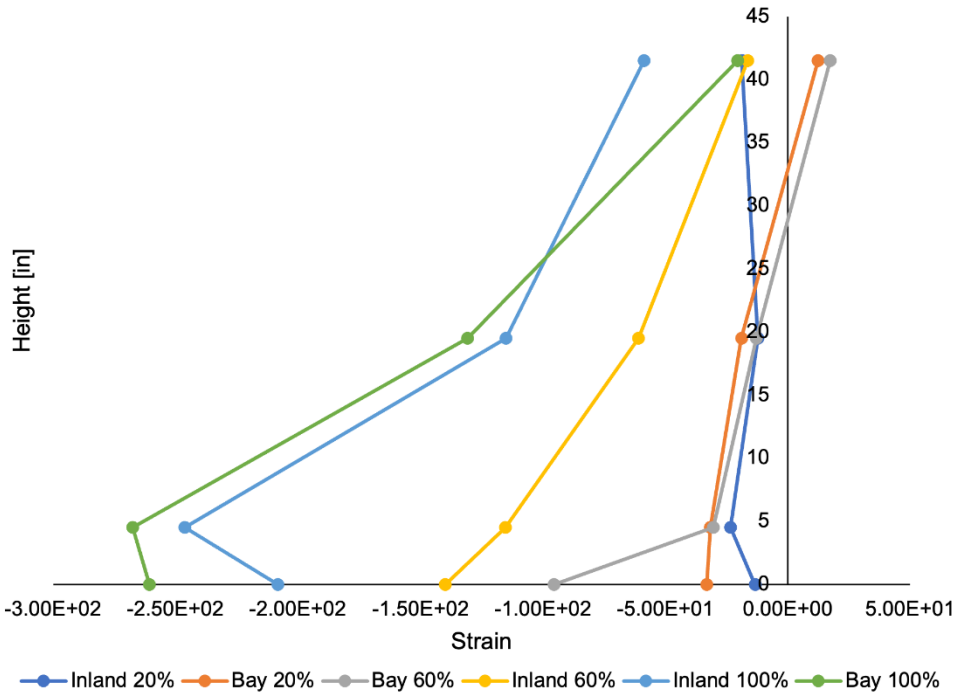

Figure A1.5. IB1 Strain vs Stressing % "Bay Side"

A.2 I-Beam 5 – Damaged and Repaired with External PT

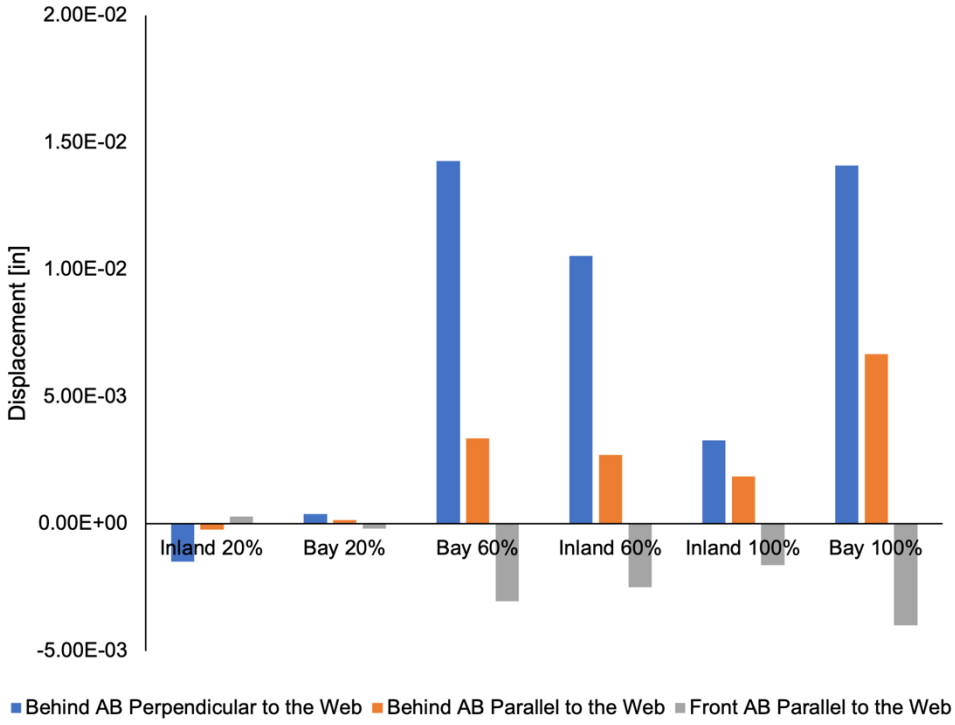

Figure A2.1. IB5 Displacement vs Stressing % "Live End - Bay Side"

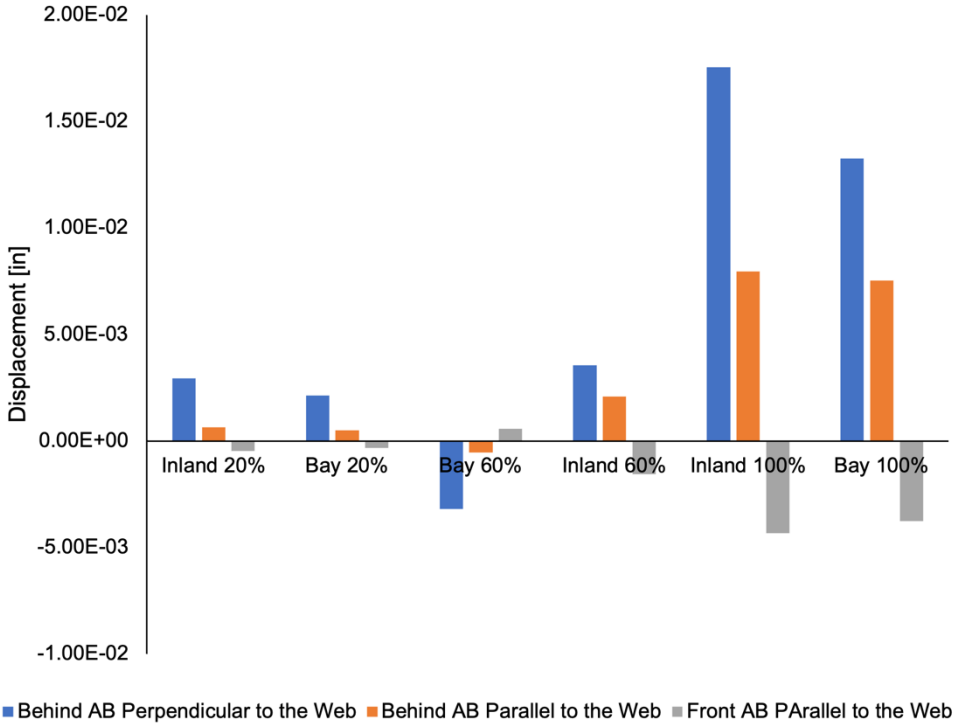

Figure A2.2. IB5 Displacement vs Stressing % "Live End - Inland Side"

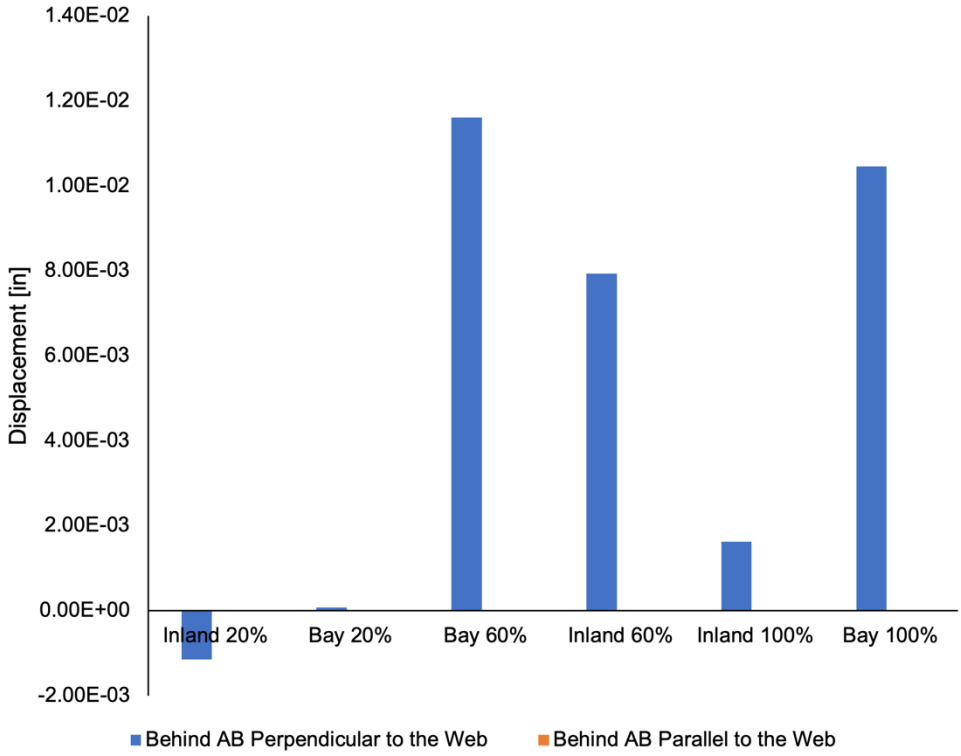

Figure A2.3. IB5 Displacement vs Stressing % "Dead End - Bay Side"

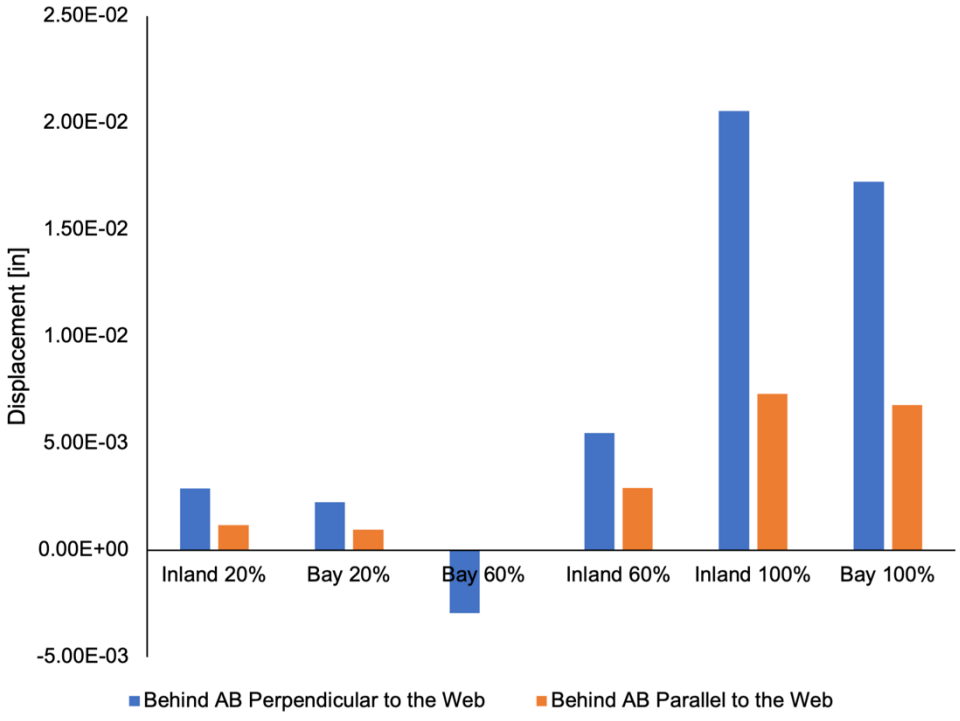

Figure A2.4. IB5 Displacement vs Stressing % "Dead End - Inland Side"

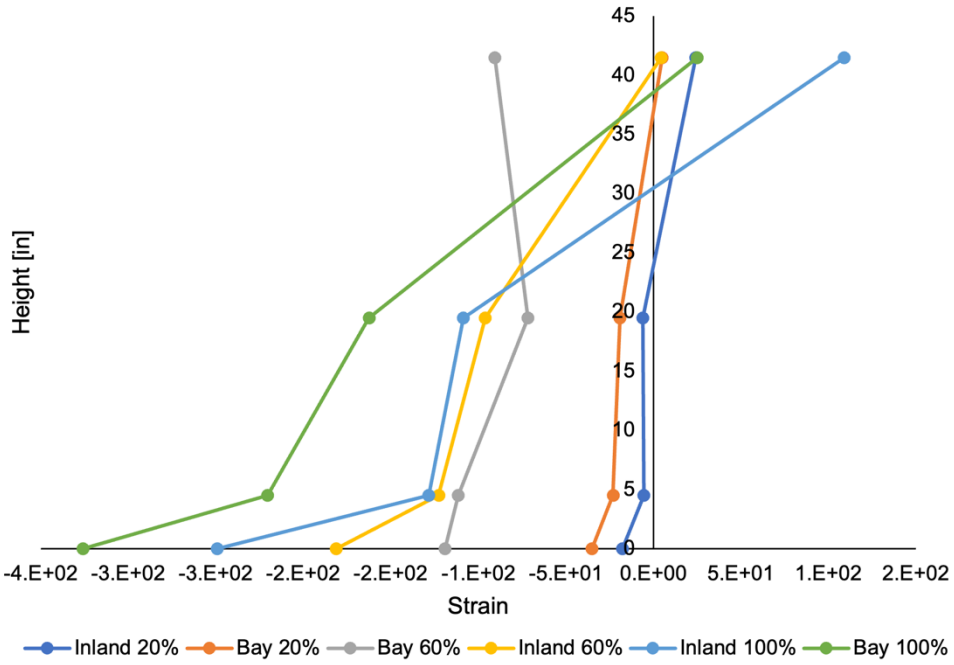

Figure A2.5. IB5 Strain vs Stressing % "Bay Side"

Appendix B: Equations and Calculations

B.1 Prestress Losses Equations from AASHTO

Losses: Time of Transfer to Time of Deck Placement

Shrinkage of Girder Concrete

$$\Delta f_{pSR} = \varepsilon_{bid} E_p K_{id} \qquad (5.9.3.4.2a-1)$$

$$K_{id} = \frac{1}{1+\frac{E_p A_{ps}}{E_{ci} A_g}\left(1+\frac{A_g e_{pg}^2}{I_g}\right)[1+0.7\psi_b(t_f,t_i)]} \qquad (5.9.3.4.2a-2)$$

Creep of Girder Concrete

$$\Delta f_{pCR} = \frac{E_p}{E_{ci}} f_{cqp} \psi_b(t_d, t_i) K_{id} \qquad (5.9.3.4.2b-1)$$

Relaxation of Prestressing Strands

$$\Delta f_{pk1} = \frac{f_{px}}{K_L}\left(\frac{f_{pk}}{f_{py}} - 0.55\right) \qquad (5.9.3.4.2c-1)$$

Losses: Time of Deck Placement to Final Time

Shrinkage of Girder Concrete

$$\Delta f_{pSD} = \varepsilon_{hdf} E_p K_{\mathrm{df}} \qquad (5.9.3.4.3a-1)$$

$$K_{df} = \frac{1}{1+\frac{E_p A_{pp}}{E_{ci} A_e}\left(1+\frac{A_e e_{pc}^2}{I_e}\right)[1+0.7\Psi_b(t_f,t_i)]} \qquad (5.9.3.4.3a-2)$$

Creep of Girder Concrete

$$\Delta f_{pCD} = \frac{E_p}{E_{ci}} f_{cgp}\left[\psi_b(t_f,t_i) - \psi_b(t_d,t_i)\right] K_{df} + \frac{E_p}{E_c} \Delta f_{cd} \psi_b(t_f,t_d) K_{df} \qquad (5.9.3.4.3b-1)$$

B.2 Flexural Capacity for Beam with Bonded Strands Equations from AASHTO

The average stress in prestressing steel, fps:

$$f_{ps} = f_{pu}\left(1 - k\frac{c}{d_p}\right) \qquad (5.6.3.1.1-1)$$

$$k = 2\left(1.04 - \frac{f_{py}}{f_{pu}}\right) \qquad (5.6.3.1.1-2)$$

For T-section behavior:

$$c = \frac{A_{ps}f_{pu} + A_s f_s - A_s' f_s' - \alpha_1 f_c'(b - b_w)h_f}{\alpha_1 f_c' \beta_1 b_w + kA_{ps}\frac{f_{pu}}{d_p}} \qquad (5.6.3.1.1-3)$$

For rectangular section behavior:

$$c = \frac{A_{ps}f_{pu} + A_s f_s - A_s' f_s'}{\alpha_1 f_c' \beta b + kA_{ps}\frac{f_{pu}}{d_p}} \qquad (5.6.3.1.1-4)$$

Table C5.6.3.1.1-1 -Values of k

Type of Tendon	f_{py}/f_{pu}	Value of k
Low relaxation strand	0.90	0.28
Type 1 high-strength bar	0.85	0.38
Type 2 high-strength bar	0.80	0.48

B.3 Simplified Flexural Capacity for Beam with Unbonded Tendons Equations from AASHTO

The depth of the neutral axis, c, for T-beams:

$$c = \frac{A_{psb}f_{pu} + A_{psu}f_{pe} + A_s f_s - A'_s f'_s - 0.85 f'_c (b - b_w) h_f}{0.85 f'_c \beta_1 b_w + k A_{ps} \frac{f_{pu}}{d_p}} \qquad (5.6.3.1.2 - 3)$$

The depth of the neutral axis, c, for rectangular beams:

$$c = \frac{A_{psb}f_{pu} + A_{psu}f_{pe} + A_s f_s - A'_s f'_s}{0.85 f'_c \beta_1 b + k A_{psb} \frac{f_{pu}}{d_p}} \qquad (5.6.3.1.2 - 4)$$

The stress in the bonded prestressing steel:

$$f_{ps} = f_{pu}\left(1 + 2\left(1.04 - \frac{f_{py}}{f_{pu}}\right)\frac{c}{d_p}\right) \qquad (5.6.3.1.1 - 1)$$

B.4 Flexural Capacity for Beam Repaired with Carbon Fiber Reinforced Polymer

Equations from ACI440.2R-08

The FRP-system design material properties:

$$f_{fu} = C_E f_{fu}^* \qquad \varepsilon_{fu} = C_E \varepsilon_{fu}^*$$

Area of FRP reinforcement:

$$A_f = n t_f w_f$$

Cross-sectional area:

$$A_{cg} = b_e h_f + b_w(h - h_f)$$

Distance from the top fiber to the section centroid:

$$y_t = \frac{b_f \frac{h_f^2}{2} + b_w(h-h_f)\left(h_f + \frac{(h-h_f)}{2}\right)}{A_{cg}}$$

Gross moment of inertia:

$$I_g = \frac{b_f h_f^3}{12} + b_f h_f \left(y_t - \frac{h_f}{2}\right)^2 + \frac{b_w(h-h_f)^3}{12} + b_w(h-h_f)\left(y_t - \frac{h-h_f}{2}\right)^2$$

Radius of gyration:

$$r = \sqrt{\frac{I_g}{A_{cg}}}$$

Effective prestressing strain:

$$\varepsilon_{pe} = \frac{f_{pe}}{E_p}$$

Effective prestressing force:

$$P_e = A_{ps} f_{pe}$$

Eccentricity of prestressing force:

$$e = d_p - y_t$$

Distance from extreme bottom fiber to the section centroid:

$$y_b = h - y_t$$

Initial strain in the beam soffit:

$$\varepsilon_{bi} = \frac{-p_e}{E_c A_{cg}}\left(1 + \frac{e y_b}{r^2}\right) + \frac{M_{DL} y_b}{E_c I_g}$$

The design strain of FRP accounting for debonding failure mode ε_{fd}:

$$\varepsilon_{fd} = 0.083\sqrt{\frac{f_c'}{n E_f t_f}} \leq 0.9\varepsilon_{fu}$$

The effective level of strain in the FRP reinforcement:

$$\varepsilon_{fe} = 0.003\left(\frac{d_f - c}{c}\right) - \varepsilon_{bi} \leq \varepsilon_{fd}$$

The strain in the existing prestressing steel:

$$\varepsilon_{pnet} = \left(\varepsilon_{fe} + \varepsilon_{bi}\right)\left(\frac{d_p - c}{d_f - c}\right)$$

The stress level in the prestressing steel and FRP:

$$f_{ps} = \begin{cases} 28{,}500\varepsilon_{ps} \text{ for } \varepsilon_{ps} \leq 0.0086 \\ 270 - \frac{0.04}{\varepsilon_{ps} - 0.007} \text{ for } \varepsilon_{ps} > 0.0086 \end{cases}$$

$$f_{fe} = E_f \varepsilon_{fe}$$

The strain in concrete at failure:

$$\varepsilon_c = \left(\varepsilon_{fe} + \varepsilon_{bi}\right)\left(\frac{c}{d_f - c}\right)$$

The strain ε_c' corresponding to f_c' :

$$\varepsilon_c' = \frac{1.7 f_c'}{E_c} \qquad \beta_1 = \frac{4\varepsilon_c' - \varepsilon_c}{6\varepsilon_c' - 2\varepsilon_c} \quad \alpha_1 = \frac{3\varepsilon_c'\varepsilon_c - \varepsilon_c^2}{3\beta_1 \varepsilon_c'^2}$$

B.5 Flexural Capacity Calculation

B.5.1 I-Beam 7 – Undamaged and Unrepaired

Beams' Information

General Information

Beam Information		
AASHTO Type II		
Area	369	in^2
MOI	50980	in^3
cb	15.83	in
f'c	5800	psi
wt/ft	384.4	lb/ft
span	48	ft
length	49.75	ft
height	36	in
Width		
Ec	4341	ksi
self wt mom	110.7	k-ft
Eci	4031	ksi
f'ci	5000	ksi

Slab information		
f'c	7200	psi
width	38	in
depth	7	in
overlay	2	in
total	9	in
slab weight	356.25	lb/ft
slab moment	102.6	k-ft

Bolster informarion		
f'c	7200	psi
width	12	in
height	1.5	in

Undamaged Strand Properties		
E	28000	ksi
Stress, ksi	strain	
0	0	
183	0.006535714	
229.5	0.01	
250	0.015	
270	0.06	

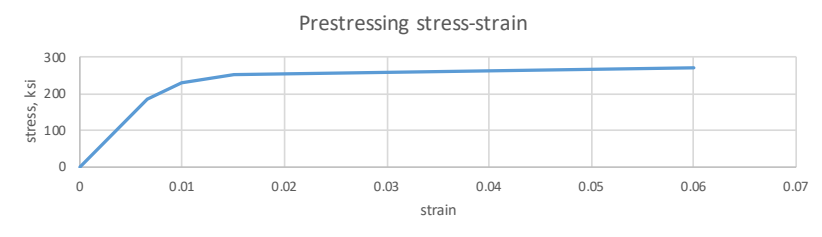

Prestress Strands Information

Damaged Strands				
Strand Pattern		All strands 7/16 in. SR Gr		270
Aps	0.117	in^2	cg	8.73
Row	dist from bott	No. of strands	area, in^2	area* dist
1	2	6	0.702	1.404
2	4	6	0.702	2.808
3	6	2	0.234	1.404
4	8	2	0.234	1.872
5	16	2	0.234	3.744
6	20	2	0.234	4.68
7	28	2	0.234	6.552
8	0	0	0	0
CRFP	0			
		22	2.574	22.464

Undamaged Strands (Original)				
Strand Pattern		All strands 7/16 in. SR Gr		270
Aps	0.117	in^2	cg	8.73
Row	dist from bott	No. of strands	area, in^2	area* dist
1	2	6	0.702	1.404
2	4	6	0.702	2.808
3	6	2	0.234	1.404
4	8	2	0.234	1.872
5	16	2	0.234	3.744
6	20	2	0.234	4.68
7	28	2	0.234	6.552
8	0	0	0	0
CFRP	0			
		22	2.574	22.464

Steel Information

	Bottom slab	Top slab	Top beam
As	0.4 in^2	0.6 in^2	0.62 in^2
d'	6.75 in	4.75 in	12.25 in
fy	40 ksi	40 ksi	60 ksi

Flexural Capacity

Strain Compatibility												
Neutral Axis	4.46	in										
Concrete												
a	3.07		beta 1	0.69		eps1	0.005349				arm, in	in-k
C	715.0485102	kips	esp u	0.003		Peff	385.5	kips			Moment	Moment

Strands Layer	Dist. From NA	eps 3	eps 2	total eps	stress1	stress2	stress 3	stress 4	STRESS	Force		
1	40.04	0.026959176	0.000412	0.03272	916.2	534.5	322.7	257.9	257.9	181.0	42.96	7777.5
2	38.04	0.025612696	0.000387	0.031349	877.8	516.1	317.0	257.3	257.3	180.6	40.96	7397.9
3	36.04	0.024266217	0.000362	0.029978	839.4	497.7	311.4	256.7	256.7	60.1	38.96	2340.0
4	34.04	0.022919737	0.000338	0.028607	801.0	479.3	305.8	256.0	256.0	59.9	36.96	2214.6
5	26.04	0.017533817	0.000239	0.023122	647.4	405.6	283.3	253.6	253.6	59.3	28.96	1718.8
6	22.04	0.014840858	0.000189	0.020379	570.6	368.8	272.1	252.4	252.4	59.1	24.96	1474.3
7	14.04	0.009454938	9.01E-05	0.014894	417.0	295.2	249.6	250.0	249.6	58.4	16.96	990.6
									SUM	658.4	24406.63	in-k
									C-T	0.0	2033.9	k-ft

Flexural Strength using AASHTO		
c	4.48	in
fps	257.3	ksi
dp	37.77	in
Mn	24208.6	in-k
	2017.4	k-ft

negative values means the bars are in compression

Rebars	Bottom slab		Top slab		Top beam	
eps	0.001544		0.00020		0.00525	
fs	40.0	ksi	5.7	ksi	60.0	ksi
Ts	16.00	kips	3.44	kips	37.20	kips
Mom arm	5.21	in	3.21	in	10.71	in
Moment	83.40253	in-k	11.06	in-k	398.51	in-k

B.5.2 I-Beam 3 – Damaged and Unrepaired

Beams' Information

General Information

Beam Information		
AASHTO Type II		
Area	369	in^2
MOI	50980	in^3
cb	15.83	in
f'c	5600	psi
wt/ft	384.4	lb/ft
span	48	ft
length	49.75	ft
height	36	in
Width		
Ec	4265	ksi
self wt mom	110.7	k-ft
Eci	4031	ksi
f'ci	5000	ksi

Slab information		
f'c	3500	psi
width	38	in
depth	7	in
overlay	2	in
total	9	in
slab weight	356.25	lb/ft
slab moment	102.6	k-ft

Bolster informarion		
f'c	3500	psi
width	12	in
height	1.5	in

Undamaged Strand Properties		
E	28000	ksi
Stress, ksi	strain	
0	0	
183	0.006535714	
229.5	0.01	
250	0.015	
270	0.06	

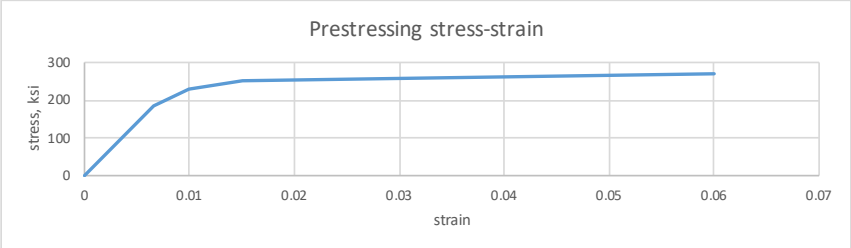

Prestress Strands Information

Damaged Strands				
Strand Pattern		All strands 7/16 in. SR Gr		270
Aps	0.117	in^2	cg	9.18
Row	dist from bott	No. of strands	area, in^2	area* dist
1	2	5	0.585	1.17
2	4	5.6	0.6552	2.6208
3	6	1.8	0.2106	1.2636
4	8	2	0.234	1.872
5	16	2	0.234	3.744
6	20	2	0.234	4.68
7	28	2	0.234	6.552
8	0	0	0	0
CRFP	0			
		20.4	2.3868	21.9024

Undamaged Strands (Original)				
Strand Pattern		All strands 7/16 in. SR Gr		270
Aps	0.117	in^2	cg	8.73
Row	dist from bott	No. of strands	area, in^2	area* dist
1	2	6	0.702	1.404
2	4	6	0.702	2.808
3	6	2	0.234	1.404
4	8	2	0.234	1.872
5	16	2	0.234	3.744
6	20	2	0.234	4.68
7	28	2	0.234	6.552
8	0	0	0	0
CFRP	0			
		22	2.574	22.464

Steel Information

	Bottom slab		Top slab		Top beam	
As	0.4	in^2	0.6	in^2	0.62	in^2
d'	6.75	in	4.75	in	12.25	in
fy	40	ksi	40	ksi	60	ksi

Flexural Capacity

Strain Compatibility												
Neutral Axis		6.33	in									
Concrete												
a	5.53		beta 1	0.875		eps1	0.005349				arm, in	in-k
C	625.6795842	kips	esp u	0.003		Peff	357.5	kips			Moment	Moment
Strands Layer	Dist. From NA	eps 3	eps 2	total eps	stress1	stress2	stress 3	stress 4	STRESS	Force		
1	38.17	0.018106096	0.000378	0.023834	667.4	415.2	286.2	253.9	253.9	148.5	41.73	6199.3
2	36.17	0.017157507	0.000357	0.022864	640.2	402.2	282.2	253.5	253.5	166.1	39.73	6599.2
3	34.17	0.016208918	0.000335	0.021893	613.0	389.1	278.3	253.1	253.1	53.3	37.73	2011.0
4	32.17	0.01526033	0.000313	0.020923	585.8	376.1	274.3	252.6	252.6	59.1	35.73	2112.4
5	24.17	0.011465976	0.000225	0.017041	477.1	324.0	258.4	250.9	250.9	58.7	27.73	1628.3
6	20.17	0.009568799	0.000182	0.0151	422.8	298.0	250.4	250.0	250.0	58.5	23.73	1388.6
7	12.17	0.005774444	9.4E-05	0.011218	314.1	245.8	234.5	248.3	234.5	54.9	15.73	863.3
									SUM	599.1	21138.25	in-k
									C-T	0.0	1761.5	k-ft

Flexural Strength using AASHTO		
c	6.34	in
fps	251.8	ksi
dp	37.32	in
Mn	20822.5	in-k
	1735.2	k-ft

negative values means the bars are in compression						
Rebars						
	Bottom slab		Top slab		Top beam	
eps	0.000201		-0.00075		0.00281	
fs	5.8	ksi	-21.7	ksi	60.0	ksi
Ts	2.34	kips	-13.00	kips	37.20	kips
Mom arm	3.98	in	1.98	in	9.48	in
Moment	9.308607	in-k	-25.77	in-k	352.76	in-k

B.5.3 I-Beam 6 – Damaged and Unrepaired

Beams' Information

General Information

Beam Information		
AASHTO Type II		
Area	369	in^2
MOI	50980	in^3
cb	15.83	in
f'c	6100	psi
wt/ft	384.4	lb/ft
span	48	ft
length	49.75	ft
height	36	in
Width		
Ec	4452	ksi
self wt mom	110.7	k-ft
Eci	4031	ksi
f'ci	5000	ksi

Slab information		
f'c	2900	psi
width	38	in
depth	7	in
overlay	2	in
total	9	in
slab weight	356.25	lb/ft
slab moment	102.6	k-ft

Bolster informarion		
f'c	2900	psi
width	12	in
height	1.5	in

Undamaged Strand Properties		
E	28000	ksi
Stress, ksi	strain	
0	0	
183	0.006535714	
229.5	0.01	
250	0.015	
270	0.06	

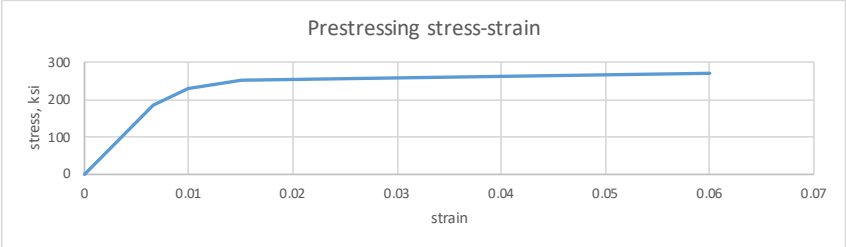

Prestress Strands Information

Damaged Strands				
Strand Pattern	All strands 7/16 in. SR Gr			270
Aps	0.117	in^2	cg	10.54
Row	dist from bott	No. of strands	area, in^2	area* dist
1	2	2.6	0.3042	0.6084
2	4	4.7	0.5499	2.1996
3	6	1.6	0.1872	1.1232
4	8	1.8	0.2106	1.6848
5	16	2	0.234	3.744
6	20	2	0.234	4.68
7	28	2	0.234	6.552
8	0	0	0	0
CRFP	0			
		16.7	1.9539	20.592

Undamaged Strands (Original)				
Strand Pattern	All strands 7/16 in. SR Gr			270
Aps	0.117	in^2	cg	8.73
Row	dist from bott	No. of strands	area, in^2	area* dist
1	2	6	0.702	1.404
2	4	6	0.702	2.808
3	6	2	0.234	1.404
4	8	2	0.234	1.872
5	16	2	0.234	3.744
6	20	2	0.234	4.68
7	28	2	0.234	6.552
8	0	0	0	0
CFRP	0			
		22	2.574	22.464

Steel Information

	Bottom slab		Top slab		Top beam	
As	0.4	in^2	0.6	in^2	0.62	in^2
d'	6.75	in	4.75	in	12.25	in
fy	40	ksi	40	ksi	60	ksi

Flexural Capacity

Strain Compatibility												
Neutral Axis		6.12	in									
Concrete												
a	5.54		beta 1	0.905		eps1	0.00535				arm, in	in-k
C	519.049597	kips	esp u	0.003		Peff	292.7	kips			Moment	Moment
				total								
Strands Layer	Dist. From NA	eps 3	eps 2	eps	stress1	stress2	stress 3	stress 4	STRESS	Force		
1	38.38	0.018803264	0.000273	0.024425	683.9	423.1	288.6	254.2	254.2	77.3	41.73	3226.7
2	36.38	0.017823342	0.000259	0.023432	656.1	409.8	284.6	253.7	253.7	139.5	39.73	5543.7
3	34.38	0.01684342	0.000245	0.022438	628.3	396.5	280.5	253.3	253.3	47.4	37.73	1789.1
4	32.38	0.015863498	0.000232	0.021445	600.4	383.1	276.4	252.9	252.9	53.3	35.73	1902.7
5	24.38	0.01194381	0.000177	0.01747	489.2	329.8	260.1	251.1	251.1	58.8	27.73	1629.3
6	20.38	0.009983966	0.00015	0.015483	433.5	303.1	252.0	250.2	250.2	58.6	23.73	1389.4
7	12.38	0.006064278	9.51E-05	0.011509	322.2	249.8	235.7	248.4	235.7	55.2	15.73	867.5
									SUM	490.0	16691.93	in-k
									C-T	0.0	1391.0	k-ft

Flexural Strength using AASHTO		
c	6.14	in
fps	251.7	ksi
dp	35.96	in
Mn	16383.0	in-k
	1365.2	k-ft

negative values means the bars are in compression						
Rebars						
	Bottom slab		Top slab		Top beam	
eps	0.000307		-0.00067		0.00300	
fs	8.9	ksi	-19.5	ksi	60.0	ksi
Ts	3.56	kips	-11.70	kips	37.20	kips
Mom arm	3.98	in	1.98	in	9.48	in
Moment	14.18226	in-k	-23.17	in-k	352.63	in-k

B.5.4 I-Beam 1 – Damaged and Repaired with External PT

Beams' Information

General Information

Beam Information		
AASHTO Type II		
Area	369	in^2
MOI	50980	in^3
cb	15.83	in
f'c	7455	psi
wt/ft	384.4	lb/ft
span	48	ft
length	49.75	ft
height	36	in
Width		
Ec	4922	ksi
self wt mom	110.7	k-ft
Eci	4031	ksi
f'ci	5000	ksi

Slab information		
f'c	6000	psi
width	38	in
depth	6.5	in
overlay	2	in
total	8.5	in
slab weight	336.458333	lb/ft
slab moment	96.9	k-ft

Bolster informarion		
f'c	6000	psi
width	12	in
height	1.5	in

Undamaged Strand Properties		
E	28000	ksi
Stress, ksi	strain	
0	0	
183	0.006535714	
229.5	0.01	
250	0.015	
270	0.06	

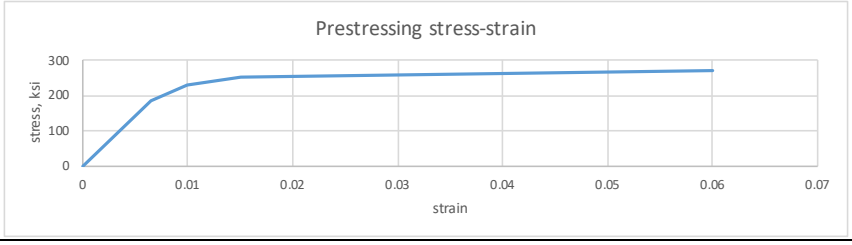

Prestress Strands Information

Damaged Strands				
Strand Pattern	All strands 7/16 in. SR Gr		270	
Aps	0.117	in^2	cg	9.49
Row	dist from bott	No. of strands	area, in^2	area* dist
1	2	3.9	0.4563	0.9126
2	4	5.8	0.6786	2.7144
3	6	2	0.234	1.404
4	8	2	0.234	1.872
5	16	2	0.234	3.744
6	20	2	0.234	4.68
7	28	2	0.234	6.552
unbonded	4.25	0	1.728	0
		19.7	2.3049	21.879

Undamaged Strands (Original)				
Strand Pattern	All strands 7/16 in. SR Gr		270	
Aps	0.117	in^2	cg	8.73
Row	dist from bott	No. of strands	area, in^2	area* dist
1	2	6	0.702	1.404
2	4	6	0.702	2.808
3	6	2	0.234	1.404
4	8	2	0.234	1.872
5	16	2	0.234	3.744
6	20	2	0.234	4.68
7	28	2	0.234	6.552
unbonded	4.25	0	1.728	7.344
		22	2.574	22.464

Steel Information

	Bottom slab	Top slab	Top beam
As	0.4 in^2	0.6 in^2	0.62 in^2
d'	6.75 in	4.75 in	11.75 in
fy	40 ksi	40 ksi	60 ksi

Corble Design

Corbel Information		
d	24	in
width	21	in
height	30	in
fy	60	ksi
f'c	4000	psi
Vu	145.152	kips
av	9	in
Compute the forces on the corbel		
Nuc	0	kips
Mu	1306.368	
Compute the shear friction steel Avf		
Avf	2.304	in2
Compute the flexural reinforcement Af		
Af	1.344	assume (d-a/2)=0.9d
a	1.12941176	
Af	1.23874699	based on new a
Compute the reinforcement An for direct tension		
An	0	
Compute the area of the tension-tie reinforcement Asc		
(Af+An)	1.23874699	take larger
(2Avf/3+An)	1.536	
0.04f'c/fy*bwd	1.344	Minimum
Asc	1.536	in2
use 5 No.5 bars	Asc 1.55	
Compute the area of horizontal stirrups		
0.5*(Asc-An)	0.768	use 4 No.4 and place them within (2/3)d measured from the tension tie.

Flexural Capacity – Simplified Method

Tendon Properties		
Eps	28000	ksi
# of strands (1 tendon)	4	
ApsOne	0.216	in^2
fpu (ksi)	270	ksi
jack stress (ksi)	216	ksi
anchor 1	9.25	ft
dev point 1	24.46	ft
dev point 2	25.29	ft
anchor 2	44.50	ft
Length	49.75	ft

Losses

Friction loss		
Angle1	0.043611111	rad
Angle2	0.034016667	rad
Δ angle	0.077627778	rad
μ	0.23	friction factor (Table 5.9.3.2.2b-1)
ΔfpF	5.765406568	ksi

Seating loss		
anchor set	0.046875	ft
L1	15.20833333	ft
L	0.833333333	ft
L2	19.20833333	ft
n	12.42055624	pick
area between cu	1031.315192	
area/EA	0.042630423	iterate

Elastic shortening	
N	2
CG from bottom (fron	4.2362
em	22.11
Aps	0.864
Ag	686.44
Ig	155318.0758
Ec	4031
fpbt	202.5
Mg	207.6
ΔfES (ksi)	1.311227279

Additional creep and relaxation loss		
ΔfLT	4.2	ksi

Seating Loss Details

Before anchor set			
Name	distance (ft)	stress (ksi)	force (kip)
end 1	0	0	0
anchor 1	9.25	216	186.624
dev point 1	24.45833333	216	186.624
dev point 2	25.29166667	210.2345934	181.6426887
anchor 2	44.5	210.2345934	181.6426887
end 2	49.75	0	0
slope (force)	5.977573529		

After anchor set			
Name	distance (ft)	force (kip)	Stress (ksi)
end 1	0	0	0
anchor 1	9.25	151.820265	175.7178993
dev point 1	24.45833333	151.820265	175.7178993
dev point 2	25.29166667	156.8015762	181.4833058
anchor 2	44.5	156.8015762	181.4833058
end 2	49.75	0	0
ΔfA (ksi)		34.51669416	Mid span

Strands Limits	
0	243
49.75	243
0	189
49.75	189
0	199.8
49.75	199.8

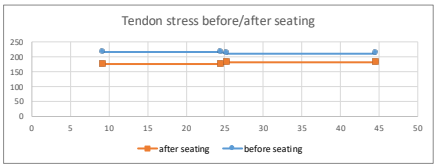

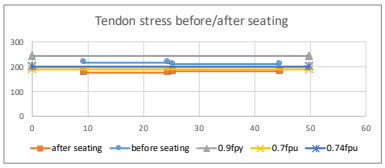

Stresses after all losses		
fpe	179.7	ksi

Service Strand Limit	
216	OK

Flexural Strength with AASHTO with Unbonded Tendons

Unbonded are 8 ea 0.6" diameter strands

	Apsu	1.728	in^2
	fpe	179.7	ksi
0.00	c	6.319355209	in
eq. 5.6.3.1.1-4	cg bott	4.2362	in
	dpu	40.2638	in
	a	4.739516406	in
	fps	252.240257	ksi
	T	891.9101685	kips
	C	918.5182796	kips
	Mn	31942.75449	in-k
	Mn	2661.896208	k-ft
	remaining	2454.3	
	load to kill	245.4296208	kips

assume rectangular

Bonded (New fps with updated C)
for bonded and unbonded tenden
for concrete block only

negative values means the bars are in compression AASHTOO Bonded and Unbonded

Rebars	Bottom slab	Top slab	Top beam
As	0.4 in^2	0.6 in^2	0.62 in^2
d'	6.75 in	4.75 in	11.75 in
eps	0.000204441	-0.00075	0.00258
fs	5.9 ksi	-21.6 ksi	60.0 ksi
Ts	2.37 kips	-12.96 kips	37.20 kips
Mom arm	4.38 in	2.38 in	9.38 in
Moment	10.38780432 in-k	-30.86 in-k	348.94 in-k

B.5.5 I-Beam 5 – Damaged and Repaired with External PT

Beams' Information

General Information

Beam Information		
AASHTO Type II		
Area	369	in^2
MOI	50980	in^3
cb	15.83	in
f'c	5700	psi
wt/ft	384.4	lb/ft
span	48	ft
length	49.75	ft
height	36	in
Width		
Ec	4303	ksi
self wt mom	110.7	k-ft
Eci	4031	ksi
f'ci	5000	ksi

Slab information		
f'c	5847	psi
width	38	in
depth	6.5	in
overlay	2	in
total	8.5	in
slab weight	336.458333	lb/ft
slab moment	96.9	k-ft

Bolster informarion		
f'c	4400	psi
width	12	in
height	1.5	in

Undamaged Strand Properties		
E	28000	ksi
Stress, ksi	strain	
0	0	
183	0.006535714	
229.5	0.01	
250	0.015	
270	0.06	

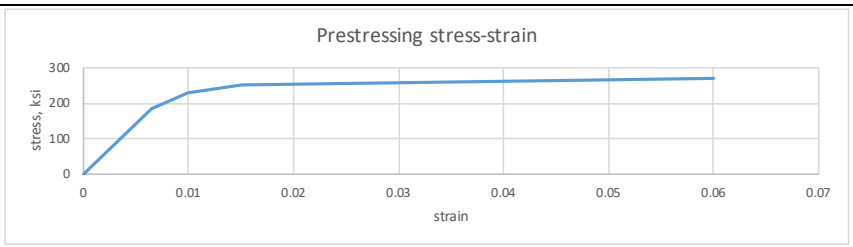

Prestress Strands Information

Damaged Strands				
Strand Pattern	All strands 7/16 in. SR Gr			270
Aps	0.117	in^2	cg	9.49
Row	dist from bott	No. of strands	area, in^2	area* dist
1	2	3.9	0.4563	0.9126
2	4	5.8	0.6786	2.7144
3	6	2	0.234	1.404
4	8	2	0.234	1.872
5	16	2	0.234	3.744
6	20	2	0.234	4.68
7	28	2	0.234	6.552
unbonded	4.25	0	1.728	0
		19.7	2.3049	21.879

Undamaged Strands (Original)				
Strand Pattern	All strands 7/16 in. SR Gr			270
Aps	0.117	in^2	cg	8.73
Row	dist from bott	No. of strands	area, in^2	area* dist
1	2	6	0.702	1.404
2	4	6	0.702	2.808
3	6	2	0.234	1.404
4	8	2	0.234	1.872
5	16	2	0.234	3.744
6	20	2	0.234	4.68
7	28	2	0.234	6.552
unbonded	4.25	0	1.728	7.344
		22	2.574	22.464

Steel Information

	Bottom slab	Top slab	Top beam
As	0.4 in^2	0.6 in^2	0.62 in^2
d'	6.75 in	4.75 in	11.75 in
fy	40 ksi	40 ksi	60 ksi

Corble Design

Corbel Information		
d	24	in
width	21	in
height	30	in
fy	60	ksi
f'c	4000	psi
Vu	145.152	kips
av	9	in
Compute the forces on the corbel		
Nuc	0	kips
Mu	1306.368	
Compute the shear friction steel Avf		
Avf	2.304	in2
Compute the flexural reinforcement Af		
Af	1.344	assume (d-a/2)=0.9d
a	1.12941176	
Af	1.23874699	based on new a
Compute the reinforcement An for direct tension		
An	0	
Compute the area of the tension-tie reinforcement Asc		
(Af+An)	1.23874699	take larger
(2Avf/3+An)	1.536	
0.04f'c/fy*bwd	1.344	Minimum
Asc	1.536	in2
use 5 No.5 bars	Asc 1.55	
Compute the area of horizontal stirrups		
0.5*(Asc-An)	0.768	use 4 No.4 and place them within (2/3)d measured from the tension tie.

Flexural Capacity – Simplified Method

Tendon Properties		
Eps	28000	ksi
# of strands (1 tendon)	4	
ApsOne	0.216	in^2
fpu (ksi)	270	ksi
jack stress (ksi)	216	ksi
anchor 1	9.25	ft
dev point 1	24.46	ft
dev point 2	25.29	ft
anchor 2	44.50	ft
Length	49.75	ft

Losses

Friction loss

Angle1	0.043611111	rad
Angle2	0.034016667	rad
Δ angle	0.077627778	rad
μ	0.23	friction factor (Table 5.9.3.2.2b-1)
ΔfpF	5.765406568	ksi

Seating loss

anchor set	0.046875	ft
L1	15.20833333	ft
L	0.833333333	ft
L2	19.20833333	ft
n	12.42055624	pick
area between cu	1031.315192	
area/EA	0.042630423	iterate

Elastic shortening

N	2	
CG from bottom (fron	4.2362	in
em	22.82	
Aps	0.864	
Ag	723.81	
Ig	162397.0444	
Ec	4031	
fpbt	202.5	
Mg	207.6	
ΔfES (ksi)	1.307900574	

Additional creep and relaxation los

ΔfLT	4.2	ksi

Seating Loss Details

Before anchor set

Name	distance (ft)	stress (ksi)	force (kip)
end 1	0	0	0
anchor 1	9.25	216	186.624
dev point 1	24.45833333	216	186.624
dev point 2	25.29166667	210.2345934	181.6426887
anchor 2	44.5	210.2345934	181.6426887
end 2	49.75	0	0
slope (force)	5.977573529		

After anchor set

Name	distance (ft)	force (kip)	Stress (ksi)
end 1	0	0	0
anchor 1	9.25	151.820265	175.7178993
dev point 1	24.45833333	151.820265	175.7178993
dev point 2	25.29166667	156.8015762	181.4833058
anchor 2	44.5	156.8015762	181.4833058
end 2	49.75	0	0
ΔfA (ksi)		34.51669416	Mid span

Strands Limits

0	243
49.75	243
0	189
49.75	189
0	199.8
49.75	199.8

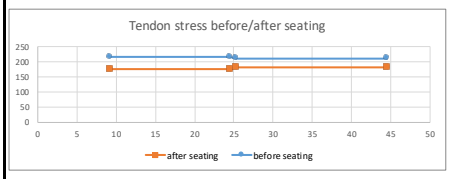

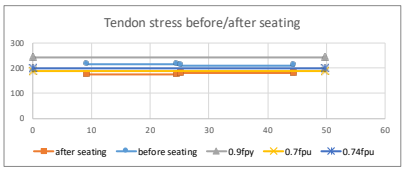

Stresses after all losses

fpe	179.7	ksi

Service Strand Limit

216	OK

Flexural Strength with AASHTO with Unbonded Tendons

Unbonded are 8 ea 0.6" diameter strands

	Apsu	1.728	in^2
	fpe	179.7	ksi
0.00	c	6.407857456	in
eq. 5.6.3.1.1-4	cg bott	4.2362	in
	dpu	40.2638	in
	a	4.854913201	in
	fps	251.9915327	ksi
	T	891.3368838	kips
	C	916.8896828	kips
	Mn	31866.74203	in-k
	Mn	2655.561836	k-ft
	remaining	2448.0	
	load to kill	244.7961836	kips

assume rectangular

Bonded (New fps with updated C) for bonded and unbonded tenden for concrete block only

negative values means the bars are in compression AASHTOO Bonded and Unbonded

Rebars	Bottom slab	Top slab	Top beam
As	0.4 in^2	0.6 in^2	0.62 in^2
d'	6.75 in	4.75 in	11.75 in
eps	0.000160183	-0.00078	0.00250
fs	4.6 ksi	-22.5 ksi	60.0 ksi
Ts	1.86 kips	-13.51 kips	37.20 kips
Mom arm	4.32 in	2.32 in	9.32 in
Moment	8.031799249 in-k	-31.37 in-k	346.80 in-k

B.5.6 I-Beam 4 – Damaged and Repaired with CFRP

Beams' Information

General Information

Beam Information		
AASHTO Type II		
Area	369	in^2
MOI	50980	in^3
cb	15.83	in
f'c	7320	psi
wt/ft	384.4	lb/ft
span	48	ft
length	49.75	ft
height	36	in
Width		
Ec	4877	ksi
self wt mom	110.7	k-ft
Eci	4031	ksi
f'ci	5000	ksi

Slab information		
f'c	6300	psi
width	38	in
depth	6.75	in
overlay	1.25	in
total	8	in
slab weight	316.666667	lb/ft
slab moment	91.2	k-ft

Bolster informarion		
f'c	5000	psi
width	12	in
height	1.25	in

Undamaged Strand Properties		
E	28000	ksi
Stress, ksi	strain	
0	0	
183	0.006535714	
229.5	0.01	
250	0.015	
270	0.06	

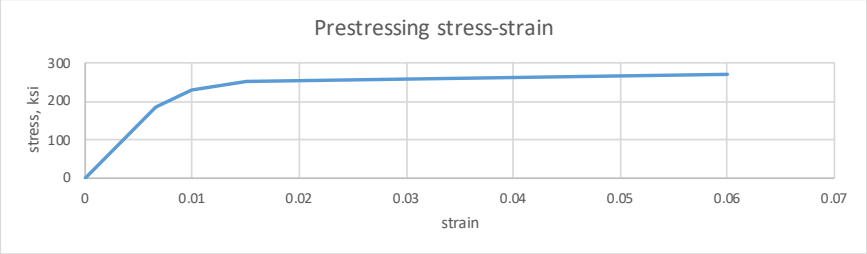

Prestress Strands Information

Damaged Strands				
Strand Pattern	All strands 7/16 in. SR Gr			270
Aps	0.117	in^2	cg	9.49
Row	dist from bott	No. of strands	area, in^2	area* dist
1	2	3.9	0.4563	0.9126
2	4	5.8	0.6786	2.7144
3	6	2	0.234	1.404
4	8	2	0.234	1.872
5	16	2	0.234	3.744
6	20	2	0.234	4.68
7	28	2	0.234	6.552
8	0	0	0	0
CRFP	0			
		19.7	2.3049	21.879

Undamaged Strands (Original)				
Strand Pattern	All strands 7/16 in. SR Gr			270
Aps	0.117	in^2	cg	8.73
Row	dist from bott	No. of strands	area, in^2	area* dist
1	2	6	0.702	1.404
2	4	6	0.702	2.808
3	6	2	0.234	1.404
4	8	2	0.234	1.872
5	16	2	0.234	3.744
6	20	2	0.234	4.68
7	28	2	0.234	6.552
8	0	0	0	0
CRFP	0			
		22	2.574	22.464

Steel Information

	Bottom slab		Top slab		Top beam	
As	0.4	in^2	0.6	in^2	0.62	in^2
d'	6.75	in	4.75	in	11	in
fy	40	ksi	40	ksi	60	ksi

CFRP Information

Ply Thickness	0.08	in/ply
Width	16	in
# of plies	3	
Ultimate Tnesile Strength	180000	ksi
Rupture Strain	0.0127	in/in
Modulus of elasticity of CFRP	14240	ksi

Flexural Capacity - ACI

Materials Properties		
ffu	171000	ksi
eps u	0.012065	
Af	3.84	in^2
Aslab	304	in^2
MOI	1621.333333	in^4
n	0.927715332	
Composite area	651.025461	in^2
Composite cg	26.30048971	in
Composite MOI	145867.6065	in^4
ROG	14.96857444	
eps effective	0.005347956	ksi
Pe	345.1420802	kip
eccentricity	16.81	in

Failrue Mode		
eps inial	-0.000233616	
eps fd	0.003841254	
eps fd new	0.003841254	
eps rupture	0.011569661	
eps fe new	0.003841254	
eps fe new	0.003841254	CFRP Debonding

Strain Compatibility

Neutral Axis	9.17	in

Concrete												
alpha - beam	0.506638344		beta - beam	0.692744		eps1	0.005347956				arm, in	in-k
alpha - slab	0.54		beta - slab	0.695123		Peff	345.1	kips			Moment	Moment
C	751.7983685	kips	eps u (CFM)	0.003		eps' c - slab	0.002367251	eps' c - beam	0.002552			
			eps u new	0.001036								

Strands Layer	Dist. From NA	eps 3	eps 2	total eps	stress1	stress2	stress 3	stress 4	STRESS	Force		
1	34.08	0.009001393	0.000313476	0.014663	404.5	289.2	247.7	249.8	247.7	168.1	38.06	6398.6
2	32.08	0.008801412	0.000295879	0.014445	398.4	286.2	246.8	249.7	246.8	57.8	36.06	2083.0
3	30.08	0.00860143	0.000278283	0.014228	392.3	283.3	245.9	249.6	245.9	57.6	34.06	1960.3
4	28.08	0.008401449	0.000260687	0.01401	367.9	271.6	242.4	249.2	242.4	56.7	26.06	1478.2
5	20.08	0.007601523	0.000190301	0.01314	355.7	265.8	240.6	249.0	240.6	56.3	22.06	1242.1
6	16.08	0.007201561	0.000155108	0.012705	331.4	254.1	237.0	248.6	237.0	55.5	14.06	780.0
7	8.08	0.006401635	8.47227E-05	0.011834	416.7	295.0	249.5	249.9	249.5	0.0	42.06	0.0
8	36.08	0.009201375	0.000331072	0.01488					54.7	210.0	42.06	8835.1
CFRP	36.08								SUM	775.4	27265.29	in-k
									C-T	0.0	2272.1	k-ft

negative values means the bars are in compression

Rebars	Bottom slab		Top slab		Top beam	
eps	-0.00079		-0.00145		0.00060	
fs	-23.0	ksi	-41.9	ksi	17.4	ksi
Ts	-9.18	kips	-25.16	kips	10.76	kips
Mom arm	6.48	in	4.48	in	10.73	in
Moment	-59.5272	in-k	-112.75	in-k	115.50	in-k

Flexural Capacity – AASHTO

AASHTO - CFRP Flexural Strength							
M	28187.71075	kip-in		2348.9759	k-ft		
Phi	0.000135861	1/in					
			eps 1	0.00534796		fps1	260.149073
eps 3	0.003710351		eps 2	0.00023273		fps2	219.983834
c	8.447792657					fps3	226.593257
eps top	0.001147729	eps	0.009291038	fps	219.9838339	fps4	247.462684
T	507.0407387	C-T	-2.01706E-05	Tcfrp	273.408		
y	epc	f'c	epsilon o	stress	b	C	M
0	0	6300	0.002381176	0	38	0	0
0.1	1.35861E-05	6300	0.002381176	0.06469989	38	0.245859571	0.02458596
0.2	2.71723E-05	6300	0.002381176	0.12938714	38	0.491671126	0.09833423
0.3	4.07584E-05	6300	0.002381176	0.19404913	38	0.737386679	0.221216
0.4	5.43446E-05	6300	0.002381176	0.25867324	38	0.982958308	0.39318332
0.5	6.79307E-05	6300	0.002381176	0.32324689	38	1.228338182	0.61416909
0.6	8.15168E-05	6300	0.002381176	0.38775753	38	1.473478598	0.88408716
0.7	9.5103E-05	6300	0.002381176	0.45219263	38	1.718332006	1.2028324
0.8	0.000108689	6300	0.002381176	0.51653975	38	1.962851043	1.57028083
0.9	0.000122275	6300	0.002381176	0.58078646	38	2.206988562	1.98628971
1	0.000135861	6300	0.002381176	0.64492044	38	2.450697662	2.45069766
1.1	0.000149448	6300	0.002381176	0.7089294	38	2.693931721	2.96332489
7.9	0.001073305	6300	0.002381176	4.24831894	38	16.14361198	127.534535
8	0.001086891	6300	0.002381176	4.28366645	38	16.2779325	130.22346
8.1	0.001100477	6300	0.002381176	4.31848071	38	16.4102267	132.922836
8.2	0.001114064	6300	0.002381176	4.35276304	38	16.54049954	135.632096
8.3	0.00112765	6300	0.002381176	4.38651487	38	16.66875651	138.350679
8.4	0.001141236	6300	0.002381176	4.4197378	38	8.026778515	67.4249395
8.44779266	0.003710351	6300	0.002381176	5.15462346	38	780.4487186	4278.50075
		7320	0.00256671			kip	kip-in

B.5.7 Box-Beam 1 – Damaged and Unrepaired

Beams' Information

General Information

Beam Information		
Box Beam		
Area	693	in^2
MOI	65941	in^3
cb	13.5	in
f'c	7250	psi
wt/ft	721.9	lb/ft
span	53	ft
length	55	ft
height	27	in
Width	48	in
Ec	4853	ksi
self wt mom	253.5	k-ft
Eci	3605	ksi
f'ci	4000	ksi

Slab information		
f'c	7250	psi
width	48	in
depth	0	in
overlay	0	in
total	0	in
slab weight	0	lb/ft
slab moment	0.0	k-ft

Bolster informarion		
f'c	5000	psi
width	0	in
height	0	in

Undamaged Strand Properties		
E	28000	ksi
Stress, ksi	strain	
0	0	
183	0.006535714	
229.5	0.01	
250	0.015	
270	0.06	

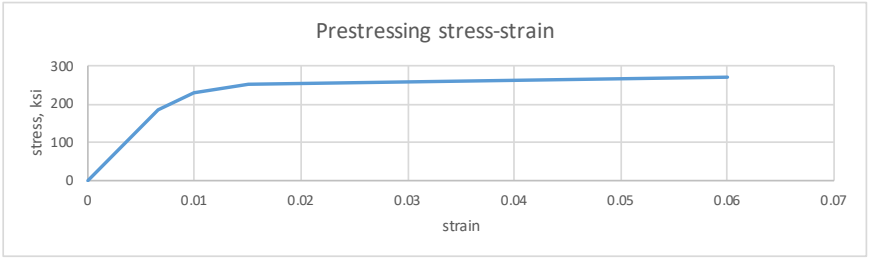

Prestress Strands Information

Damaged Strands				
Strand Pattern		All strands 7/16 in. SR Gr		270
Aps	0.115 in^2		cg	6.81
Row	dist from bott	No. of strands	area, in^2	area* dist
1	2	10.8	1.242	2.484
2	4	9.1	1.0465	4.186
3	12	1.7	0.1955	2.346
4	16	1.9	0.2185	3.496
5	20	1.7	0.1955	3.91
6	22	1.9	0.2185	4.807
7	0	0	0	0
8	0	0	0	0
CRFP	0			
		27.1	3.1165	21.229

Undamaged Strands (Original)				
Strand Pattern		All strands 7/16 in. SR Gr		270
Aps	0.115 in^2		cg	6.36
Row	dist from bott	No. of strands	area, in^2	area* dist
1	2	15	1.725	3.45
2	4	10	1.15	4.6
3	12	2	0.23	2.76
4	16	2	0.23	3.68
5	20	2	0.23	4.6
6	22	2	0.23	5.06
7	0	0	0	0
8	0	0	0	0
CFRP	0			
		33	3.795	24.15

Steel Information

	Bottom slab	Top slab	Top beam
As	0.8 in^2	1.76 in^2	0 in^2
d'	3.75 in	2.75 in	0 in
fy	60 ksi	40 ksi	0 ksi

Flexural Capacity

Strain Compatibility													
Neutral Axis		3.59	in										
Concrete													
a	2.47		beta 1	0.6875		eps1	0.005597					arm, in	in-k
C	730.1132321	kips	eps u	0.003		Peff	488.4	kips				Moment	Moment
Strands Layer	Dist. From NA	eps 3	eps 2	total eps	stress1	stress2	stress 3	stress 4	STRESS	Force			
1	21.41	0.017890167	0.000263	0.02375	665.0	414.1	285.9	253.9	253.9	315.3		23.77	7494.1
2	19.41	0.016218954	0.000242	0.022058	617.6	391.4	278.9	253.1	253.1	264.9		21.77	5765.9
3	11.41	0.0095341	0.000161	0.015292	428.2	300.5	251.2	250.1	250.1	48.9		13.77	673.2
4	7.41	0.006191674	0.00012	0.011908	333.4	255.1	237.3	248.6	237.3	51.9		9.77	506.4
5	3.41	0.002849247	7.89E-05	0.008525	238.7	209.7	223.5	247.1	209.7	41.0		5.77	236.4
6	1.41	0.001178033	5.85E-05	0.006834	191.3	187.0	216.5	246.4	187.0	40.9		3.77	153.9
7	23.41	0.019561381	0.000283	0.025441	712.4	436.8	292.8	254.6	254.6	0.0		25.77	0.0
									SUM	762.8		14783.33	in-k
									C-T	0.0		1231.9	k-ft

Flexural Strength using AASHTO		
c	3.69	in
fps	251.2	ksi
dp	20.19	in
Mn	14769.3	in-k
	1230.8	k-ft

negative values means the bars are in compression						
Rebars						
	Bottom slab		Top slab		Top beam	
eps	0.000134		-0.00070		-0.00300	
fs	3.9	ksi	-20.4	ksi	-87.0	ksi
Ts	3.10	kips	-35.83	kips	0.00	kips
Mom arm	2.52	in	1.52	in	-1.23	in
Moment	7.793606	in-k	-54.32	in-k	0.00	in-k

B.5.8 Box-Beam 2 – Damaged and Unrepaired

Beams' Information

General Information

Beam Information		
Box Beam		
Area	693	in^2
MOI	65941	in^3
cb	13.5	in
f'c	7100	psi
wt/ft	721.9	lb/ft
span	53	ft
length	55	ft
height	27	in
Width	48	in
Ec	4803	ksi
self wt mom	253.5	k-ft
Eci	3605	ksi
f'ci	4000	ksi

Slab information		
f'c	7100	psi
width	48	in
depth	0	in
overlay	0	in
total	0	in
slab weight	0	lb/ft
slab moment	0.0	k-ft

Bolster informarion		
f'c	5000	psi
width	0	in
height	0	in

Undamaged Strand Properties		
E	28000	ksi
Stress, ksi	strain	
0	0	
183	0.006535714	
229.5	0.01	
250	0.015	
270	0.06	

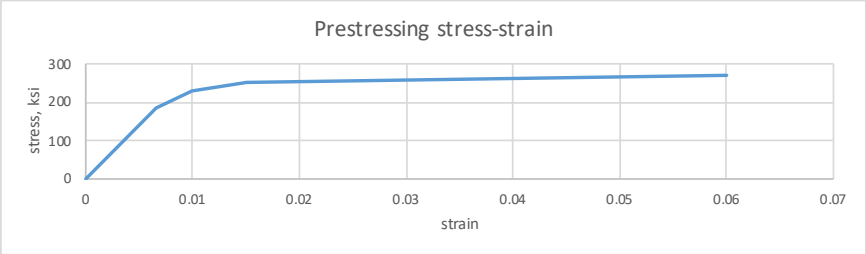

Prestress Strands Information

Damaged Strands				
Strand Pattern		All strands 7/16 in. SR Gr		270
Aps	0.115	in^2	cg	6.73
Row	dist from bott	No. of strands	area, in^2	area* dist
1	2	12.35	1.42025	2.8405
2	4	8.55	0.98325	3.933
3	12	1.9	0.2185	2.622
4	16	1.9	0.2185	3.496
5	20	1.9	0.2185	4.37
6	22	1.9	0.2185	4.807
7	0	0	0	0
8	0	0	0	0
CRFP	0			
		28.5	3.2775	22.0685

Undamaged Strands (Original)				
Strand Pattern		All strands 7/16 in. SR Gr		270
Aps	0.115	in^2	cg	6.36
Row	dist from bott	No. of strands	area, in^2	area* dist
1	2	15	1.725	3.45
2	4	10	1.15	4.6
3	12	2	0.23	2.76
4	16	2	0.23	3.68
5	20	2	0.23	4.6
6	22	2	0.23	5.06
7	0	0	0	0
8	0	0	0	0
CFRP	0			
		33	3.795	24.15

Steel Information

	Bottom slab		Top slab		Top beam	
As	0.8	in^2	1.76	in^2	0	in^2
d'	3.75	in	2.75	in	0	in
fy	60	ksi	40	ksi	0	ksi

Flexural Capacity

Strain Compatibility													
Neutral Axis		3.77	in										
Concrete													
a	2.62		beta 1	0.695		eps1	0.005597					arm, in	in-k
C	758.0973219	kips	eps u	0.003		Peff	513.6	kips				Moment	Moment
Strands Layer	Dist. From NA	eps 3	eps 2	total eps	stress1	stress2	stress 3	stress 4	STRESS	Force			
1	21.23	0.01691772	0.000281	0.022795	638.3	401.2	282.0	253.5	253.5	360.0		23.69	8528.5
2	19.23	0.015324302	0.000259	0.02118	593.0	379.6	275.3	252.7	252.7	248.5		21.69	5390.6
3	11.23	0.008950632	0.000171	0.014718	412.1	292.8	248.8	249.9	248.8	54.4		13.69	744.4
4	7.23	0.005763797	0.000127	0.011488	321.7	249.5	235.6	248.4	235.6	51.5		9.69	498.9
5	3.23	0.002576962	8.3E-05	0.008257	231.2	206.1	222.4	247.0	206.1	45.0		5.69	256.3
6	1.23	0.000983544	6.1E-05	0.006642	186.0	184.4	215.7	246.3	184.4	40.3		3.69	148.8
7	23.23	0.018511137	0.000302	0.024411	683.5	422.9	288.6	254.2	254.2	0.0		25.69	0.0
									SUM	799.7		15507.34	in-k
									C-T	0.0		1292.3	k-ft

Flexural Strength using AASHTO		
c	3.87	in
fps	250.4	ksi
dp	20.27	in
Mn	15470.7	in-k
	1289.2	k-ft

negative values means the bars are in compression						
Rebars						
	Bottom slab		Top slab		Top beam	
eps	-1.2342E-05		-0.00081		-0.00300	
fs	-0.4	ksi	-23.5	ksi	-87.0	ksi
Ts	-0.29	kips	-41.29	kips	0.00	kips
Mom arm	2.44	in	1.44	in	-1.31	in
Moment	-0.69908521	in-k	-59.52	in-k	0.00	in-k

B.5.9 Box-Beam 4 – Damaged and Unrepaired

Beams' Information

General Information

Beam Information		
Box Beam		
Area	693	in^2
MOI	65941	in^3
cb	13.5	in
f'c	6250	psi
wt/ft	721.9	lb/ft
span	53	ft
length	55	ft
height	27	in
Width	48	in
Ec	4506	ksi
self wt mom	253.5	k-ft
Eci	3605	ksi
f'ci	4000	ksi

Slab information		
f'c	6250	psi
width	48	in
depth	0	in
overlay	0	in
total	0	in
slab weight	0	lb/ft
slab moment	0.0	k-ft

Bolster informarion		
f'c	5000	psi
width	0	in
height	0	in

Undamaged Strand Properties		
E	28000	ksi
Stress, ksi	strain	
0	0	
183	0.006535714	
229.5	0.01	
250	0.015	
270	0.06	

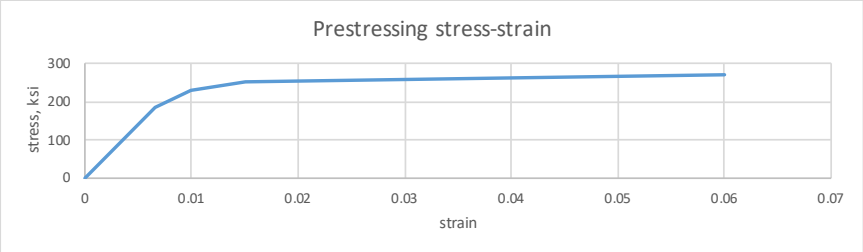

Prestress Strands Information

Damaged Strands				
Strand Pattern	All strands 7/16 in. SR Gr			270
Aps	0.115	in^2	cg	6.59
Row	dist from bott	No. of strands	area, in^2	area* dist
1	2	12.9	1.4835	2.967
2	4	9.1	1.0465	4.186
3	12	1.9	0.2185	2.622
4	16	1.9	0.2185	3.496
5	20	1.9	0.2185	4.37
6	22	1.9	0.2185	4.807
7	0	0	0	0
8	0	0	0	0
CRFP	0			
		29.6	3.404	22.448

Undamaged Strands (Original)				
Strand Pattern	All strands 7/16 in. SR Gr			270
Aps	0.115	in^2	cg	6.36
Row	dist from bott	No. of strands	area, in^2	area* dist
1	2	15	1.725	3.45
2	4	10	1.15	4.6
3	12	2	0.23	2.76
4	16	2	0.23	3.68
5	20	2	0.23	4.6
6	22	2	0.23	5.06
7	0	0	0	0
8	0	0	0	0
CFRP	0			
		33	3.795	24.15

Steel Information

	Bottom slab	Top slab	Top beam
As	0.8 in^2	1.76 in^2	0 in^2
d'	3.75 in	2.75 in	0 in
fy	60 ksi	40 ksi	0 ksi

Flexural Capacity

Strain Compatibility													
Neutral Axis		4.09	in										
Concrete													
a	3.02			beta 1	0.7375		eps1	0.005597				arm, in	in-k
C	769.6288201	kips		eps u	0.003		Peff	533.5 kips				Moment	Moment
Strands Layer	Dist. From NA	eps 3	eps 2	total eps	stress1	stress2	stress 3	stress 4	STRESS	Force			
1	20.91	0.01532661	0.000313	0.021237	594.6	380.3	275.6	252.8	252.8	375.0		23.49	8808.8
2	18.91	0.013860482	0.000289	0.019746	552.9	360.3	269.5	252.1	252.1	263.8		21.49	5670.0
3	10.91	0.007995966	0.000189	0.013782	385.9	280.3	245.0	249.5	245.0	53.5		13.49	722.2
4	6.91	0.005063709	0.00014	0.010801	302.4	240.2	232.8	248.1	232.8	50.9		9.49	482.7
5	2.91	0.002131451	9.02E-05	0.007819	218.9	200.2	220.6	246.8	200.2	43.7		5.49	240.2
6	0.91	0.000665322	6.55E-05	0.006328	177.2	180.2	214.4	246.1	177.2	38.7		3.49	135.1
7	22.91	0.016792739	0.000338	0.022728	636.4	400.3	281.7	253.4	253.4	0.0		25.49	0.0
									SUM	825.7		15983.75	in-k
									C-T	0.0		1332.0	k-ft

Flexural Strength using AASHTO		
c	4.21	in
fps	248.9	ksi
dp	20.41	in
Mn	15898.3	in-k
	1324.9	k-ft

negative values means the bars are in compression						
Rebars						
	Bottom slab		Top slab		Top beam	
eps	-0.00025		-0.00098		-0.00300	
fs	-7.3	ksi	-28.5	ksi	-87.0	ksi
Ts	-5.82	kips	-50.23	kips	0.00	kips
Mom arm	2.24	in	1.24	in	-1.51	in
Moment	-13.0498	in-k	-62.33	in-k	0.00	in-k

Strands Damage with Water Effect

Prestress Strands Information										
Damaged Strands					Undamaged Strands (Original)					
Strand Pattern		All strands 7/16 in. SR Gr		270	Strand Pattern		All strands 7/16 in. SR Gr		270
Aps	0.115	in^2	cg	7.07	Aps	0.115	in^2	cg	6.36
Row	dist from bott	No. of strands	area, in^2	area* dist	Row	dist from bott	No. of strands	area, in^2	area* dist
1	2	10.965	1.260975	2.52195	1	2	15	1.725	3.45
2	4	7.735	0.889525	3.5581	2	4	10	1.15	4.6
3	12	1.9	0.2185	2.622	3	12	2	0.23	2.76
4	16	1.9	0.2185	3.496	4	16	2	0.23	3.68
5	20	1.9	0.2185	4.37	5	20	2	0.23	4.6
6	22	1.9	0.2185	4.807	6	22	2	0.23	5.06
7	0	0	0	0	7	0	0	0	0
8	0	0	0	0	8	0	0	0	0
CRFP	0				CFRP	0			
		26.3	3.0245	21.37505			33	3.795	24.15

Flexural Capacity with Water Effect

Strain Compatibility													
Neutral Axis		3.71	in										
Concrete													
a	2.74		beta 1	0.7375		eps1	0.005597					arm, in	in-k
C	697.7197513	kips	eps u	0.003		Peff	474.0	kips				Moment	Moment
Strands Layer	Dist. From NA	eps 3	eps 2	total eps	stress1	stress2	stress 3	stress 4	STRESS	Force			
1	21.29	0.017215405	0.00027	0.023082	646.3	405.1	283.1	253.6	253.6	319.8		23.63	7556.9
2	19.29	0.015598173	0.000249	0.021445	600.4	383.1	276.4	252.9	252.9	224.9		21.63	4865.6
3	11.29	0.009129243	0.000167	0.014893	417.0	295.2	249.6	250.0	249.6	54.5		13.63	743.3
4	7.29	0.005894778	0.000126	0.011618	325.3	251.2	236.1	248.5	236.1	51.6		9.63	497.0
5	3.29	0.002660313	8.51E-05	0.008342	233.6	207.3	222.7	247.0	207.3	45.3		5.63	255.0
6	1.29	0.001043081	6.46E-05	0.006705	187.7	185.3	216.0	246.3	185.3	40.5		3.63	147.0
7	23.29	0.018832638	0.00029	0.02472	692.2	427.1	289.9	254.3	254.3	0.0		25.63	0.0
									SUM	736.6		14011.90	in-k
									C-T	0.0		1167.7	k-ft

Flexural Strength using AASHTO		
c	3.82	in
fps	250.3	ksi
dp	19.93	in
Mn	13974.4	in-k
	1164.5	k-ft

negative values means the bars are in compression						
Rebars						
	Bottom slab		Top slab		Top beam	
eps	3.23E-05		-0.00078		-0.00300	
fs	0.9	ksi	-22.5	ksi	-87.0	ksi
Ts	0.75	kips	-39.62	kips	0.00	kips
Mom arm	2.38	in	1.38	in	-1.37	in
Moment	1.785513	in-k	-54.76	in-k	0.00	in-k

B.5.10 Box-Beam 5 – Damaged and Unrepaired

Beams' Information

General Information

Beam Information		
Box Beam		
Area	693	in^2
MOI	65941	in^3
cb	13.5	in
f'c	6045	psi
wt/ft	721.9	lb/ft
span	53	ft
length	55	ft
height	27	in
Width	48	in
Ec	4432	ksi
self wt mom	253.5	k-ft
Eci	3605	ksi
f'ci	4000	ksi

Slab information		
f'c	6045	psi
width	48	in
depth	0	in
overlay	0	in
total	0	in
slab weight	0	lb/ft
slab moment	0.0	k-ft

Bolster informarion		
f'c	5000	psi
width	0	in
height	0	in

Undamaged Strand Properties		
E	28000	ksi
Stress, ksi	strain	
0	0	
183	0.006535714	
229.5	0.01	
250	0.015	
270	0.06	

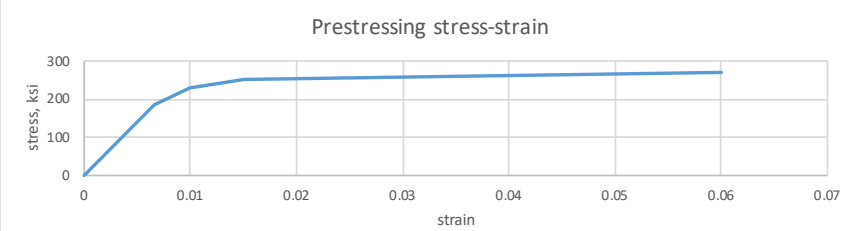

Prestress Strands Information

Damaged Strands				
Strand Pattern		All strands 7/16 in. SR Gr		270
Aps	0.115	in^2	cg	6.93
Row	dist from bott	No. of strands	area, in^2	area* dist
1	2	11.25	1.29375	2.5875
2	4	8.5	0.9775	3.91
3	12	1.9	0.2185	2.622
4	16	1.9	0.2185	3.496
5	20	1.9	0.2185	4.37
6	22	1.9	0.2185	4.807
7	0	0	0	0
8	0	0	0	0
CRFP	0			
		27.35	3.14525	21.7925

Undamaged Strands (Original)				
Strand Pattern		All strands 7/16 in. SR Gr		270
Aps	0.115	in^2	cg	6.36
Row	dist from bott	No. of strands	area, in^2	area* dist
1	2	15	1.725	3.45
2	4	10	1.15	4.6
3	12	2	0.23	2.76
4	16	2	0.23	3.68
5	20	2	0.23	4.6
6	22	2	0.23	5.06
7	0	0	0	0
8	0	0	0	0
CRFP	0			
		33	3.795	24.15

Steel Information

	Bottom slab		Top slab		Top beam	
As	0.8	in^2	1.76	in^2	0	in^2
d'	3.75	in	2.75	in	0	in
fy	60	ksi	40	ksi	0	ksi

CFRP Information

Ply Thickness	0.04	in/ply
Width	36	in
# of plies	1	
Ultimate Tnesile Strength	180000	ksi
Rupture Strain	0.0127	in/in
Modulus of elasticity of CFRP	14240	ksi

Flexural Capacity – ACI

Materials Properties		
ffu	171000	ksi
eps u	0.012065	
Af	1.44	in^2
Aslab	0	in^2
MOI	0	in^4
n	1	
Composite area	693	in^2
Composite cg	13.5	in
Composite MOI	65941	in^4
ROG	9.754637777	
eps effective	0.005560714	ksi
Pe	489.715425	kip
eccentricity	6.57	in

Failrue Mode		
eps inial	-0.000167606	
eps fd	0.008550495	
eps fd new	0.008550495	
eps fe new	0.008550495	CFRP Debonding

Strain Compatibility

Neutral Axis	5.02	in

Concrete								
alpha	0.82		beta 1	0.729973	eps1	0.005560714		
C	871.9314447	kips	eps u (CFM)	0.003	Peff	489.7	kips	
			eps u new	0.001915	eps' c	0.002318848		

Strands Layer	Dist. From NA	eps 3	eps 2	eps total	stress1	stress2	stress 3	stress 4	STRESS	Force	arm, in	in-k
				eps							Moment	Moment
1	19.98	0.013412616	0.000286093	0.019259	539.3	353.8	267.5	251.9	251.9	325.9	23.17	7550.0
2	17.98	0.012649811	0.000264069	0.018475	517.3	343.3	264.2	251.5	251.5	245.9	21.17	5204.7
3	9.98	0.00959859	0.000175973	0.015335	429.4	301.1	251.4	250.1	250.1	54.7	13.17	719.7
4	5.98	0.00807298	0.000131925	0.013766	385.4	280.0	244.9	249.5	244.9	53.5	9.17	490.6
5	1.98	0.006547369	8.78767E-05	0.012196	341.5	259.0	238.5	248.8	238.5	52.1	5.17	269.3
6	-0.02	0.005784564	6.58527E-05	0.011411	319.5	248.4	235.3	248.4	235.3	51.4	3.17	162.8
7	21.98	0.014175421	0.000308117	0.020044	561.2	364.3	270.7	252.2	252.2	0.0	25.17	0.0
8	21.98	0.014175421	0.000308117	0.020044	561.2	364.3	270.7	252.2	252.2	0.0	25.17	0.0
CFRP	21.98	0.013132592							121.8	175.3	25.17	4412.7
									SUM	958.8	18588.95	in-k
									C-T	0.0	1549.1	k-ft

negative values means the bars are in compression

Rebars	Bottom slab		Top slab		Top beam	
eps	-0.00076		-0.00136		-0.00300	
fs	-22.0	ksi	-39.3	ksi	-87.0	ksi
Ts	-17.62	kips	-69.25	kips	0.00	kips
Mom arm	3.34	in	2.34	in	-0.41	in
Moment	-58.8424	in-k	-162.06	in-k	0.00	in-k

Flexural Capacity – AASHTO

AASHTO - CFRP Flexural Strength					
M	15802.8337	kip-in	1316.90281	k-ft	
Phi	0.00094898	1/in			
eps 3	0.00351303				
c	3.70191124				
eps top	0.00079447	eps	0.00929395	fps	220.022902
T	692.027032	C-T	1.3227E-07	Tcfrp	102.528
y	eps	stress	b	C	M
0	0	0	48	0	0
0.1	9.4898E-05	0.48441781	48	2.32520551	0.23252055
0.2	0.0001898	0.94860718	48	4.55331447	0.91066289
0.3	0.00028469	1.3925681	48	6.68432688	2.00529806
0.4	0.00037959	1.81630057	48	8.71824273	3.48729709
0.5	0.00047449	2.21980459	48	10.655062	5.32753102
0.6	0.00056939	2.60308017	48	12.4947848	7.49687088
0.7	0.00066428	2.96612729	48	14.237411	9.9661877
0.8	0.00075918	3.30894597	48	15.8829407	12.7063525
0.9	0.00085408	3.6315362	48	17.4313738	15.6882364
1	0.00094898	3.93389798	48	18.8827103	18.8827103
1.1	0.00104388	4.21603132	48	20.2369503	22.2606453
1.2	0.00113877	4.4779362	48	21.4940938	25.7929125
1.3	0.00123367	4.71961264	48	22.6541407	29.4503829
1.4	0.00132857	4.94106063	48	23.717091	33.2039274
1.5	0.00142347	5.14228017	48	24.6829448	37.0244172
1.6	0.00151836	5.32327126	48	25.5517021	40.8827233
1.7	0.00161326	5.48403391	48	26.3233628	44.7497167
1.8	0.00170816	5.62456811	48	26.9979269	48.5962684
1.9	0.00180306	5.74487386	48	27.5753945	52.3932496
2	0.00189796	5.84495116	48	28.0557656	56.1115311
2.1	0.00199285	5.92480001	48	28.43904	59.7219841
2.2	0.00208775	5.98442042	48	28.725218	63.1954796
2.3	0.00218265	6.02381237	48	28.9142994	66.5028886
2.4	0.00227755	6.04297588	48	29.0062842	69.6150822
2.5	0.00237244	6.04191094	48	29.0011725	72.5029313
2.6	0.00246734	6.02061756	48	28.8989643	75.1373071
2.7	0.00256224	5.97909572	48	28.6996595	77.4890805
2.8	0.00265714	5.91734544	48	28.4032581	79.5291227
2.9	0.00275204	5.83536671	48	28.0097602	81.2283045
3	0.00284693	5.73315953	48	27.5191657	82.5574972
3.1	0.00294183	5.6107239	48	26.9314747	83.4875716
3.2	0.00303673	5.46805982	48	26.2466872	83.9893989
3.3	0.00313163	5.3051673	48	25.464803	84.03385
3.4	0.00322652	5.12204633	48	24.5858224	83.5917961
3.5	0.00332142	4.91869691	48	23.6097452	82.6341081
3.6	0.00341632	4.69511904	48	22.5365714	81.131657
3.7	0.00351122	4.45131273	48	0.40836152	1.51093763
3.70191124	0.00351303	4.446456	48	794.555032	1695.02844
				kip	kip-in

Strands Damage with Water Effect

Prestress Strands Information										
Damaged Strands					Undamaged Strands (Original)				
Strand Pattern		All strands 7/16 in. SR Gr		270	Strand Pattern		All strands 7/16 in. SR Gr		270
Aps	0.115	in^2	cg	7.42	Aps	0.115	in^2	cg	6.36
Row	dist from bott	No. of strands	area, in^2	area* dist	Row	dist from bott	No. of strands	area, in^2	area* dist
1	2	9.5625	1.0996875	2.199375	1	2	15	1.725	3.45
2	4	7.225	0.830875	3.3235	2	4	10	1.15	4.6
3	12	1.9	0.2185	2.622	3	12	2	0.23	2.76
4	16	1.9	0.2185	3.496	4	16	2	0.23	3.68
5	20	1.9	0.2185	4.37	5	20	2	0.23	4.6
6	22	1.9	0.2185	4.807	6	22	2	0.23	5.06
7	0	0	0	0	7	0	0	0	0
8	0	0	0	0	8	0	0	0	0
CFRP	0				CFRP	0			
		24.3875	2.8045625	20.817875			33	3.795	24.15

Flexural Capacity with Water Effect – ACI

Materials Properties		
ffu	171000	ksi
eps u	0.012065	
Af	1.44	in^2
Aslab	0	in^2
MOI	0	in^4
n	1	
Composite area	693	in^2
Composite cg	13.5	in
Composite MOI	65941	in^4
ROG	9.754637777	
eps effective	0.005560714	ksi
Pe	436.6703813	kip
eccentricity	6.08	in

Failrue Mode		
eps inial	-0.000124263	
eps fd	0.008550495	
eps fd new	0.008550495	
eps fe new	0.008550495	CFRP Debonding

Strain Compatibility													
Neutral Axis		4.75	in										
Concrete													
alpha	0.79			beta 1	0.724876		eps1	0.005560714				arm, in	in-k
C	793.9200533	kips		eps u (CFM)	0.003		Peff	436.7	kips			Moment	Moment
				eps u new	0.001801		eps' c	0.002318848					
					total								
Strands Layer	Dist. From NA	eps 3	eps 2	eps	stress1	stress2	stress 3	stress 4	STRESS	Force			
1	20.25	0.013426763	0.000246612	0.019234	538.6	353.4	267.4	251.9	251.9	277.0		23.28	6447.5
2	18.25	0.012669212	0.000228451	0.018458	516.8	343.0	264.2	251.5	251.5	209.0		21.28	4446.8
3	10.25	0.009639006	0.000155804	0.015356	430.0	301.4	251.5	250.2	250.2	54.7		13.28	725.7
4	6.25	0.008123904	0.000119481	0.013804	386.5	280.6	245.1	249.5	245.1	53.6		9.28	496.8
5	2.25	0.006608801	8.31577E-05	0.012253	343.1	259.7	238.7	248.8	238.7	52.2		5.28	275.3
6	0.25	0.005851249	6.49961E-05	0.011477	321.4	249.3	235.6	248.4	235.6	51.5		3.28	168.7
7	22.25	0.014184315	0.000264774	0.02001	560.3	363.9	270.5	252.2	252.2	0.0		25.28	0.0
8	22.25	0.014184315	0.000264774	0.02001	560.3	363.9	270.5	252.2	252.2	0.0		25.28	0.0
CFRP	22.25	0.014038171							121.8	175.3		25.28	4431.9
									SUM	873.2		16791.49	in-k
									C-T	0.0		1399.3	k-ft

negative values means the bars are in compression						
Rebars						
	Bottom slab		Top slab		Top beam	
eps	-0.00063		-0.00126		-0.00300	
fs	-18.4	ksi	-36.7	ksi	-87.0	ksi
Ts	-14.70	kips	-64.55	kips	0.00	kips
Mom arm	3.35	in	2.35	in	-0.40	in
Moment	-49.2866	in-k	-151.88	in-k	0.00	in-k

Flexural Capacity with Water Effect – AASHTO

AASHTO - CFRP Flexural Strength					
M	14409.0204	kip-in	1200.7517		
Phi	0.00102695	1/in			
eps 3	0.00343127				
c	3.34120951				
eps top	0.00070612	eps	0.00918069	fps	218.502711
T	612.804509	C-T	2.4177E-06	Tcfrp	102.528
y	eps	stress	b	C	M
0	0	0	48	0	0
0.1	0.0001027	0.52332226	48	2.51194686	0.25119469
0.2	0.00020539	1.02295523	48	4.91018509	0.98203702
0.3	0.00030809	1.49889889	48	7.19471469	2.15841441
0.4	0.00041078	1.95115326	48	9.36553565	3.74621426
0.5	0.00051348	2.37971833	48	11.422648	5.71132399
0.6	0.00061617	2.7845941	48	13.3660517	8.019631
0.7	0.00071887	3.16578057	48	15.1957467	10.6370227
0.8	0.00082156	3.52327774	48	16.9117331	13.5293865
0.9	0.00092426	3.85708561	48	18.5140109	16.6626098
1	0.00102695	4.16720418	48	20.0025801	20.0025801
1.1	0.00112965	4.45363345	48	21.3774406	23.5151846
1.2	0.00123234	4.71637343	48	22.6385925	27.1663109
1.3	0.00133504	4.9554241	48	23.7860357	30.9218464
1.4	0.00143774	5.17078548	48	24.8197703	34.7476784
1.5	0.00154043	5.36245756	48	25.7397963	38.6096944
1.6	0.00164313	5.53044034	48	26.5461136	42.4737818
1.7	0.00174582	5.67473382	48	27.2387223	46.3058279
1.8	0.00184852	5.795338	48	27.8176224	50.0717203
1.9	0.00195121	5.89225288	48	28.2828138	53.7373463
2	0.00205391	5.96547846	48	28.6342966	57.2685932
2.1	0.0021566	6.01501475	48	28.8720708	60.6313486
2.2	0.0022593	6.04086173	48	28.9961363	63.7914999
2.3	0.00236199	6.04301942	48	29.0064932	66.7149344
2.4	0.00246469	6.0214878	48	28.9031415	69.3675395
2.5	0.00256738	5.97626689	48	28.6860811	71.7152027
2.6	0.00267008	5.90735668	48	28.3553121	73.7238114
2.7	0.00277278	5.81475717	48	27.9108344	75.3592529
2.8	0.00287547	5.69846836	48	27.3526481	76.5874148
2.9	0.00297817	5.55849025	48	26.6807532	77.3741843
3	0.00308086	5.39482285	48	25.8951497	77.685449
3.1	0.00318356	5.20746614	48	24.9958375	77.4870962
3.2	0.00328625	4.99642013	48	23.9828166	76.7450133
3.3	0.00338895	4.76168483	48	9.4188806	31.082306
3.34120951	0.00343127	4.65805896	48	715.332512	1384.78345
				kip	kip-in

B.5.11 HRBT – Undamaged and Unrepaired

Beams' Information

General Information

Beam Information		
AASHTO Type II		
Area	374	in^2
MOI	79431.68	in^3
cb	18.73	in
f'c	5650	psi
wt/ft	389.6	lb/ft
span	48	ft
length	50	ft
height	43	in
Ec	4284	ksi
self wt mom	112.2	k-ft
Eci	3605	ksi
f'ci	4000	ksi

Slab information		
f'c	4500	psi
width	48	in
depth	7	in
overlay	0	in
total	7	in
slab weight	350	lb/ft
slab moment	100.8	k-ft

Bolster informarion		
f'c	4500	psi
width	12	in
height	0	in

Undamaged Strand Properties		
E	28000	ksi
Stress, ksi	strain	
0	0	
187.5	0.006696429	
212.5	0.01	
222.6	0.015	
250	0.06	

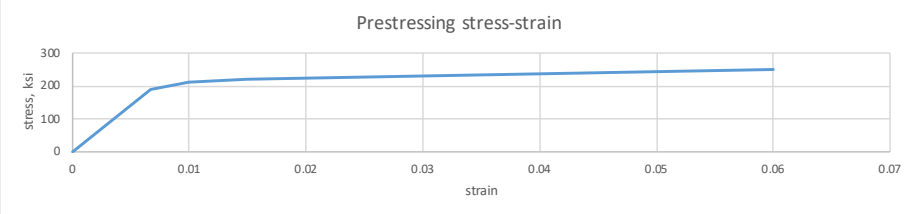

Prestress Strands Information

Damaged Strands				
Strand Pattern		All strands 3/8 in. SR Gr		250
Aps	0.08	in^2	cg	6.60
Row	dist from bott	No. of strands	area, in^2	area* dist
1	2	7	0.56	1.12
2	4	7	0.56	2.24
3	6	7	0.56	3.36
4	8	5	0.4	3.2
5	10	1	0.08	0.8
6	14	1	0.08	1.12
7	20	1	0.08	1.6
8	30	1	0.08	2.4
CFRP	0			
		30	2.4	15.84

Undamaged Strands (Original)				
Strand Pattern		All strands 3/8 in. SR Gr		250
Aps	0.08	in^2	cg	6.60
Row	dist from bott	No. of strands	area, in^2	area* dist
1	2	7	0.56	1.12
2	4	7	0.56	2.24
3	6	7	0.56	3.36
4	8	5	0.4	3.2
5	10	1	0.08	0.8
6	14	1	0.08	1.12
7	20	1	0.08	1.6
8	30	1	0.08	2.4
CFRP	0			
		30	2.4	15.84

Steel Information

	Bottom slab		Top slab		Top beam	
As	1.24	in^2	1.55	in^2	0	in^2
d'	5	in	2	in	0	in
fy	60	ksi	60	ksi	60	ksi

Flexural Capacity

Strain Compatibility													
Neutral Axis		3.62	in										
Concrete													
a	2.98		beta 1	0.825		eps1	0.004157					arm, in	in-k
C	547.9614097	kips	esp u	0.003		Peff	279.4	kips				Moment	Moment
Strands Layer	Dist. From NA	eps 3	eps 2	total eps	stress1	stress2	stress 3	stress 4	STRESS	Force			
1	44.38	0.036805139	0.000341	0.041303	1156.5	449.4	275.7	238.6	238.6	133.6		46.51	6214.6
2	42.38	0.035146591	0.000321	0.039625	1109.5	436.7	272.3	237.6	237.6	133.1		44.51	5921.9
3	40.38	0.033488044	0.000301	0.037946	1062.5	424.0	269.0	236.6	236.6	132.5		42.51	5631.4
4	38.38	0.031829496	0.000281	0.036268	1015.5	411.3	265.6	235.5	235.5	94.2		40.51	3816.6
5	36.38	0.030170949	0.000261	0.034589	968.5	398.6	262.2	234.5	234.5	18.8		38.51	722.5
6	32.38	0.026853854	0.000221	0.031232	874.5	373.2	255.4	232.5	232.5	18.6		34.51	641.8
7	26.38	0.021878212	0.000162	0.026197	733.5	335.1	245.2	229.4	229.4	18.4		28.51	523.2
8	16.38	0.013585475	6.21E-05	0.017805	498.5	271.6	228.3	224.3	224.3	17.9		18.51	332.1
									SUM	567.0		23918.12	in-k
									C-T	0.0		1993.2	k-ft

Flexural Strength using AASHTO		
c	4.00	in
fps	260.5	ksi
dp	43.40	in
Mn	26222.4	in-k
	2185.2	k-ft

negative values means the bars are in compression						
Rebars						
	Bottom slab		Top slab		Top beam	
eps	0.001146		-0.00134		-0.00300	
fs	33.2	ksi	-38.9	ksi	-87.0	ksi
Ts	41.22	kips	-60.30	kips	0.00	kips
Mom arm	3.51	in	0.51	in	-1.49	in
Moment	144.6006	in-k	-30.62	in-k	0.00	in-k

B.5.12 HRBT – Undamaged and Repaired with CFRP

Beams' Information

General Information

Beam Information		
AASHTO Type II		
Area	374	in^2
MOI	79431.68	in^3
cb	18.73	in
f'c	5650	psi
wt/ft	389.6	lb/ft
span	48	ft
length	50	ft
height	43	in
Ec	4284	ksi
self wt mom	112.2	k-ft
Eci	3605	ksi
f'ci	4000	ksi

Slab information		
f'c	5450	psi
width	48	in
depth	7	in
overlay	0	in
total	7	in
slab weight	350	lb/ft
slab moment	100.8	k-ft

Bolster informarion		
f'c	4500	psi
width	12	in
height	0	in

Undamaged Strand Properties	
E	28000 ksi
Stress, ksi	strain
0	0
187.5	0.006696429
212.5	0.01
222.6	0.015
250	0.06

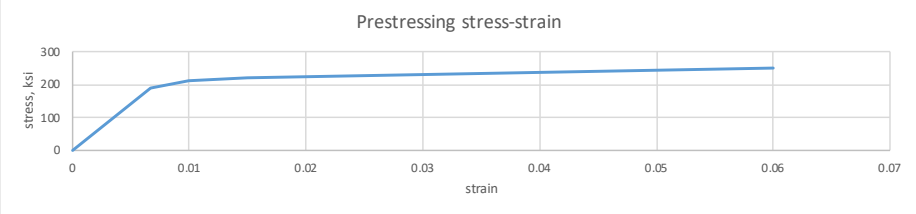

Prestress Strands Information

Damaged Strands				
Strand Pattern		All strands 3/8 in. SR Gr		250
Aps	0.08	in^2	cg	6.60
Row	dist from bott	No. of strands	area, in^2	area* dist
1	2	7	0.56	1.12
2	4	7	0.56	2.24
3	6	7	0.56	3.36
4	8	5	0.4	3.2
5	10	1	0.08	0.8
6	14	1	0.08	1.12
7	20	1	0.08	1.6
8	30	1	0.08	2.4
CFRP	0			
		30	2.4	15.84

Undamaged Strands (Original)				
Strand Pattern		All strands 3/8 in. SR Gr		250
Aps	0.08	in^2	cg	6.60
Row	dist from bott	No. of strands	area, in^2	area* dist
1	2	7	0.56	1.12
2	4	7	0.56	2.24
3	6	7	0.56	3.36
4	8	5	0.4	3.2
5	10	1	0.08	0.8
6	14	1	0.08	1.12
7	20	1	0.08	1.6
8	30	1	0.08	2.4
CFRP	0			
		30	2.4	15.84

Steel Information

	Bottom slab	Top slab	Top beam
As	1.24 in^2	1.55 in^2	0 in^2
d'	5 in	2 in	0 in
fy	60 ksi	60 ksi	60 ksi

CFRP Information

Flexural CFRP		
Ply Thickness	0.08	in/ply
Width	17	in
# of plies	3	
Ultimate Tnesile Strength	180	ksi
Rupture Strain	0.0127	in/in
Modulus of elasticity of CFRP	14240	ksi

Shear CFRP				
d	43.40	in	Ultimate Tensile Strength	180 ksi
dfv	19	in	Rupture Strain	0.0127 in/in
Width of each sheet wf	22	in	Modulus of Elasticity	14240 ksi
Spam between each sheet	22	in	# of plies	1
FRP strip length	66	in		
Ply thickness	0.08	in		

Flexural Capacity - ACI

Materials Properties		
ffu	171	ksi
eps u	0.012065	
Af	4.08	in^2
Aslab	336	in^2
MOI	1372	in^4
n	0.982141421	
Composite area	703.9995173	in^2
Composite cg	31.74717738	in
Composite MOI	215975.322	in^4
ROG	17.51523161	
eps effective	0.004157143	ksi
Pe	279.36	kip
eccentricity	25.15	in

Failrue Mode		
eps inial	-0.000245946	
eps fd	0.003374751	
eps fd new	0.003374751	
eps rupture	0.010963121	
eps fe new	0.003374751	
eps fe new	0.003374751	CFRP Debonding

Strain Compatibility

Neutral Axis	10.56	in

Concrete													
alpha - slab	0.394085655		beta - slab	0.685187		eps1	0.004157143					arm, in	in-k
alpha - beam	0.39		beta - beam	0.68482		Peff	279.4	kips				Moment	Moment
C	574.561691	kips	eps u (CFM)	0.003		eps' c - beam	0.002241807	eps' c - slab	0.002202				
			eps u new	0.000661									

Strands Layer	Dist. From NA	eps 3	eps 2	total eps	stress1	stress2	stress 3	stress 4	STRESS	Force		
1	37.44	0.007410832	0.000340921	0.011909	328.4	225.6	216.0	220.6	216.0	121.0	42.39	5126.8
2	35.44	0.007252184	0.000321006	0.01173	323.4	224.2	215.6	220.5	215.6	120.8	40.39	4876.7
3	33.44	0.007093536	0.000301092	0.011552	318.4	222.9	215.3	220.4	215.3	86.1	38.39	3305.3
4	31.44	0.006934888	0.000281178	0.011373	313.5	221.5	214.9	220.3	214.9	17.2	36.39	625.6
5	29.44	0.00677624	0.000261264	0.011195	303.5	218.8	214.2	220.1	214.2	17.1	32.39	554.9
6	25.44	0.006458944	0.000221436	0.010838	288.5	214.8	213.1	219.7	213.1	17.0	26.39	449.8
7	19.44	0.005983	0.000161693	0.010302	263.5	208.0	211.3	219.2	208.0	16.6	16.39	272.7
8	9.44	0.00518976	6.21223E-05	0.009409					48.1	196.1	46.39	9094.8
CFRP	39.44	0.011209067							SUM	740.6	30438.10	in-k
									C-T	0.0	2536.5	k-ft

negative values means the bars are in compression

Rebars	Bottom slab		Top slab		Top beam	
eps	-0.00158		-0.00243		-0.00300	
fs	-45.8	ksi	-70.5	ksi	-87.0	ksi
Ts	-56.78	kips	-109.30	kips	0.00	kips
Mom arm	4.81	in	1.81	in	-0.19	in
Moment	-272.904	in-k	-197.40	in-k	0.00	in-k

Flexural Capacity – AASHTO

Concrete Slab		Concrete Beam	
Et (ksi)	4307000	Et (ksi)	4399000
epsilon o	0.002214723	epsilon o	0.00225499
epsilon c	fc (ksi)	epsilon c	fc (ksi)
0	0	0	0
0.0005	2183.026066	0.0005	2227.77162
0.001	3810.496576	0.001	3899.98768
0.0015	4882.41153	0.0015	5016.64819
0.002	5398.770929	0.002	5577.75314
0.0025	5359.574772	0.0025	5583.30254
0.003	4764.82306	0.003	5033.29638

Mild Steel	
epsilon s	fs
0	0
0.002068966	60
0.02	60

AASHTO - CFRP Flexural Strength							
M	33392.36023	kip-in	2782.69669	kip-ft			
Phi	0.000119875	1/in					
			eps 1	0.00415714		fps1	241.590716
eps 3	0.004208824		eps 2	0.00026227		fps2	202.119112
c	8.28991818					fps3	209.729045
eps top	0.000993755	eps	0.00862824	fps	202.1191124	fps4	218.720306
T	485.0858698	C-T	-2.091E-05	Tcfrp	290.496		
y	epc	f'c	epsilon o	stress	b	C	M
0	0	5650	0.00225499	0	15	0	0
0.1	1.19875E-05	5650	0.00225499	0.05406201	15	0.08109301	0.0081093
0.2	2.3975E-05	5650	0.00225499	0.10811485	15	0.162172272	0.03243445
0.3	3.59625E-05	5650	0.00225499	0.16214936	15	0.243224045	0.07296721
0.4	4.795E-05	5650	0.00225499	0.2161564	15	0.324234604	0.12969384
0.5	5.99375E-05	5650	0.00225499	0.27012683	15	0.405190247	0.20259512
0.6	7.19251E-05	5650	0.00225499	0.32405154	15	0.486077303	0.29164638
0.7	8.39126E-05	5650	0.00225499	0.37792143	15	0.56688214	0.3968175
0.8	9.59001E-05	5650	0.00225499	0.43172745	15	0.647591171	0.51807294
0.9	0.000107888	5650	0.00225499	0.48546058	15	0.728190866	0.65537178
1	0.000119875	5650	0.00225499	0.53911184	15	0.808667753	0.80866775
1.1	0.000131863	5650	0.00225499	0.59267229	15	0.88900843	0.97790927
7.9	0.000947013	5450	0.00221472	3.54633094	48	17.02238853	134.476869
8	0.000959001	5450	0.00221472	3.577134	48	17.1702432	137.361946
8.1	0.000970988	5450	0.00221472	3.60751903	48	17.31609136	140.26034
8.2	0.000982976	5450	0.00221472	3.63748652	48	15.69965612	128.73718
8.28991818	0.004208824	5450	0.00221472	4.04270476	48	775.5818489	4244.34372
		5650	0.00225499			kip	kip-in

Appendix C: Results of Flexural Tests

C.1 I-Beam 7 – Undamaged and Unrepaired

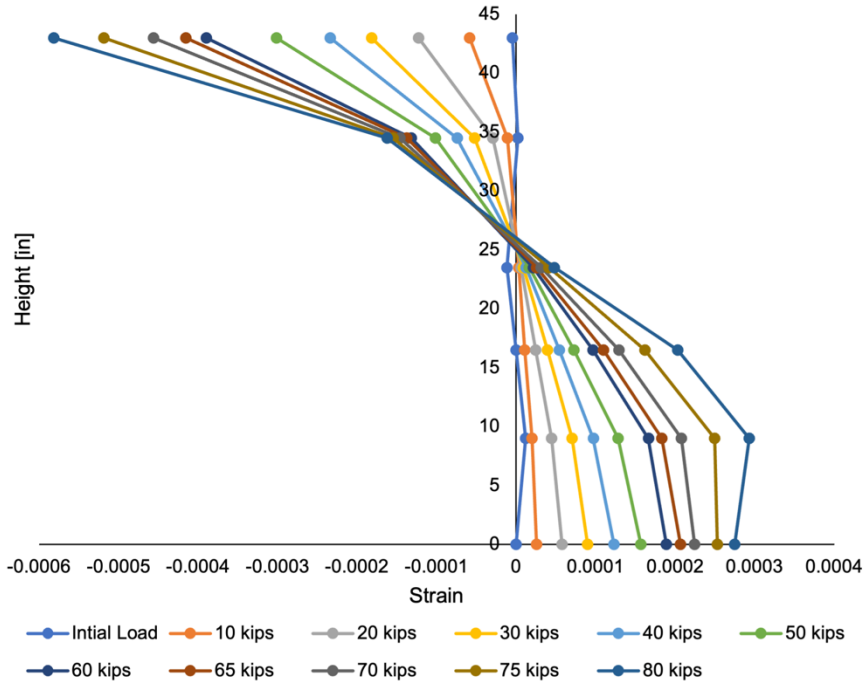

Figure C1.1. IB7 Height vs Strain

C.2 I-Beam 3 – Damaged and Unrepaired

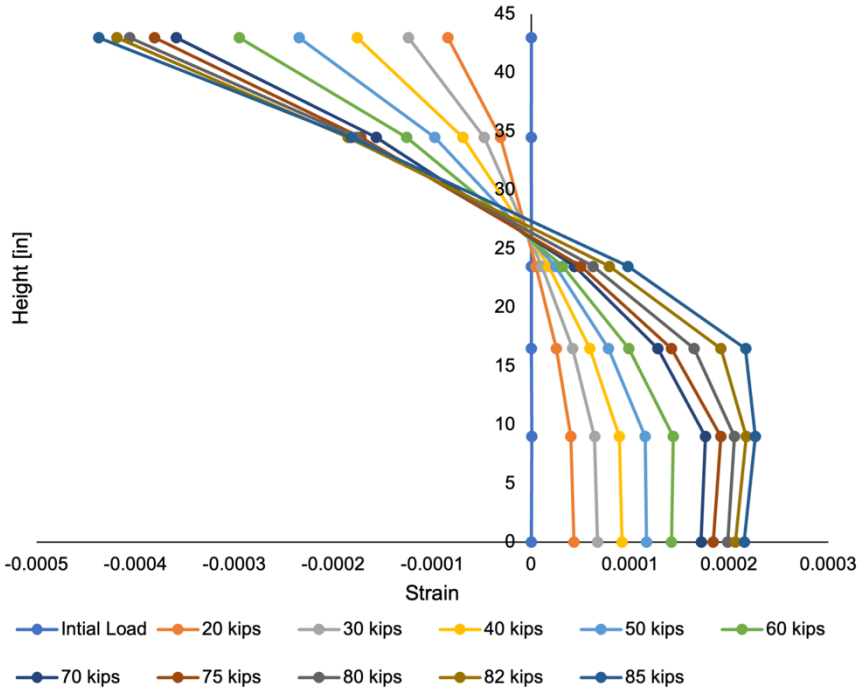

Figure C2.1. IB3 Height vs Strain

C.3 I-Beam 6 – Damaged and Unrepaired

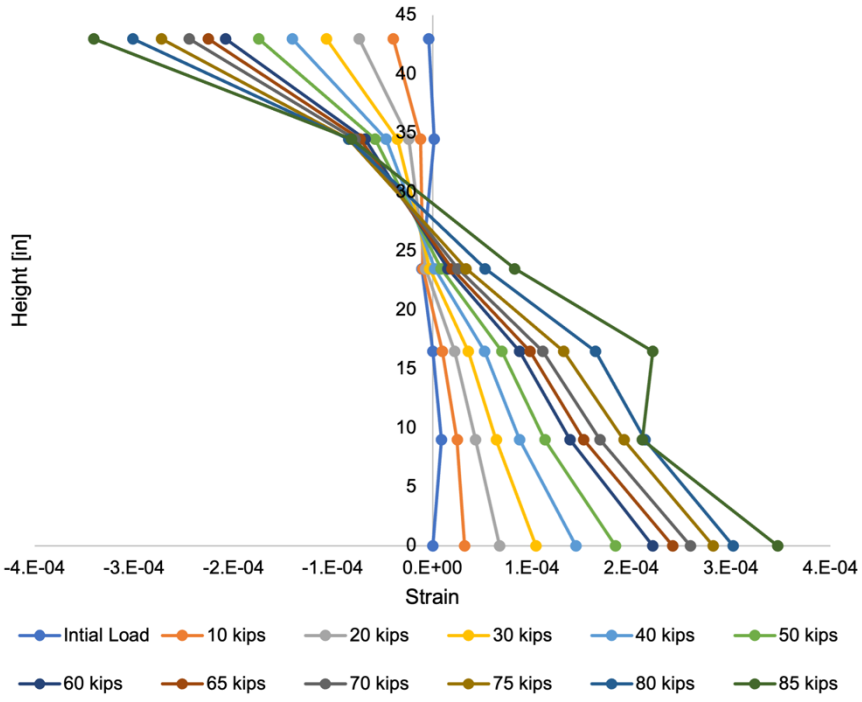

Figure C3.1. IB6 Height vs Strain

C.4 I-Beam 1 – Damaged and Repaired with External PT

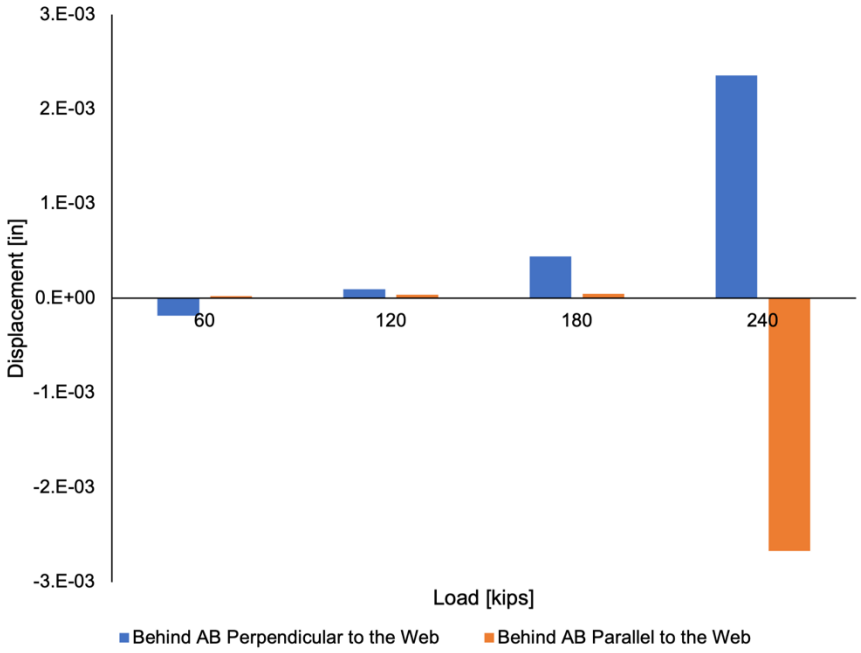

Figure C4.1. IB1 Displacement vs Stressing % "Live End - Bay Side"

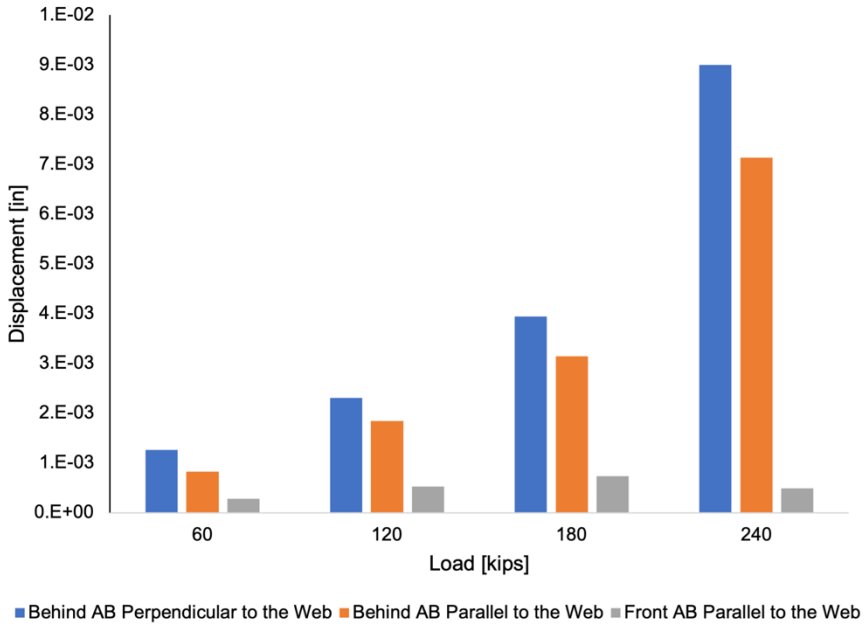

Figure C4.2. IB1 Displacement vs Stressing % "Live End - Inland Side"

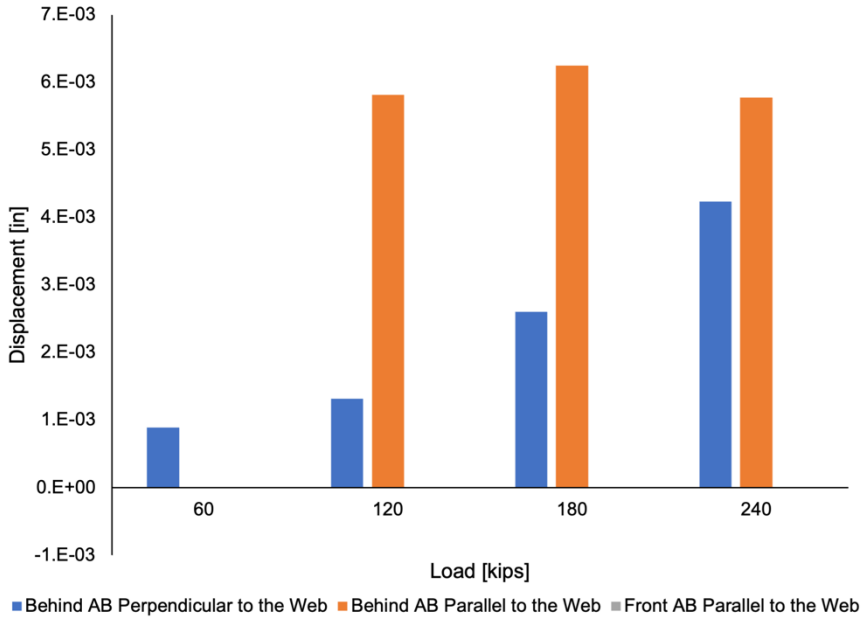

Figure C4.3. IB1 Displacement vs Stressing % "Dead End - Bay Side"

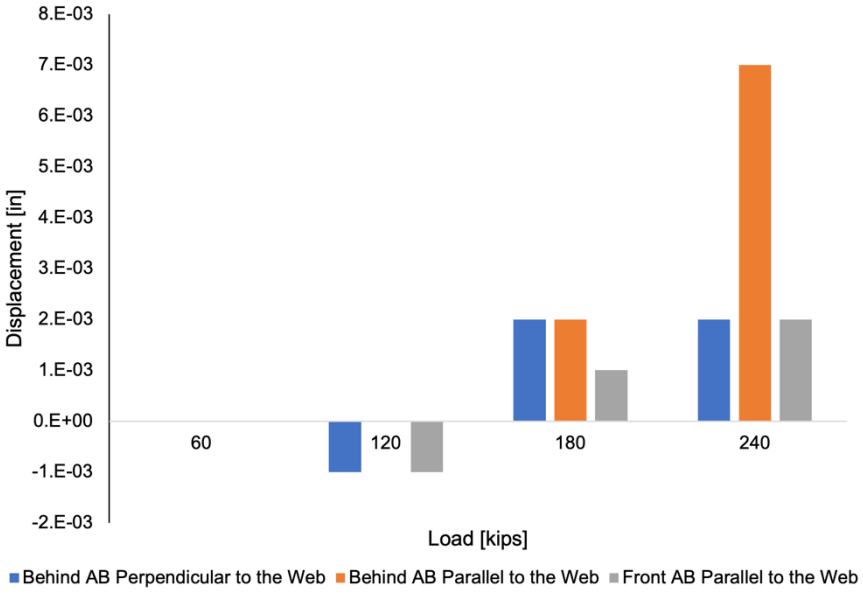

Figure C4.4. IB1 Displacement vs Stressing % "Dead End - Inland Side"

C.5 I-Beam 5 – Damaged and Repaired with External PT

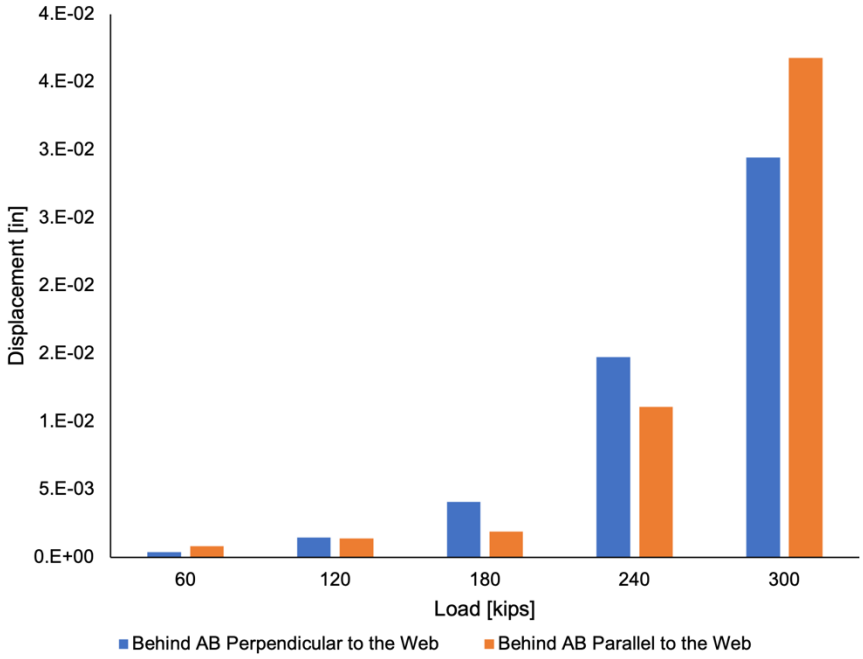

Figure C5.1. IB5 Displacement vs Stressing % "Live End - Bay Side"

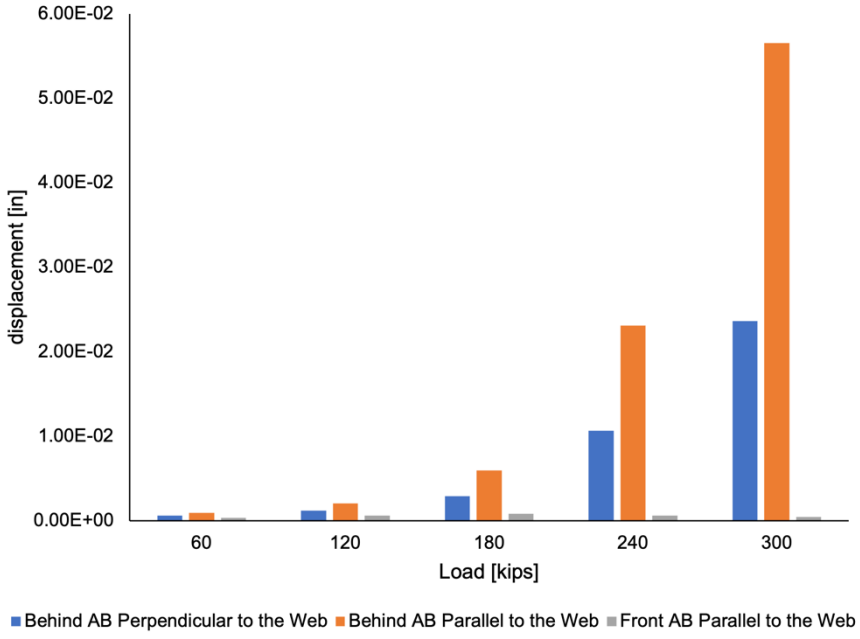

Figure C5.2. IB5 Displacement vs Stressing % "Live End - Inland Side"

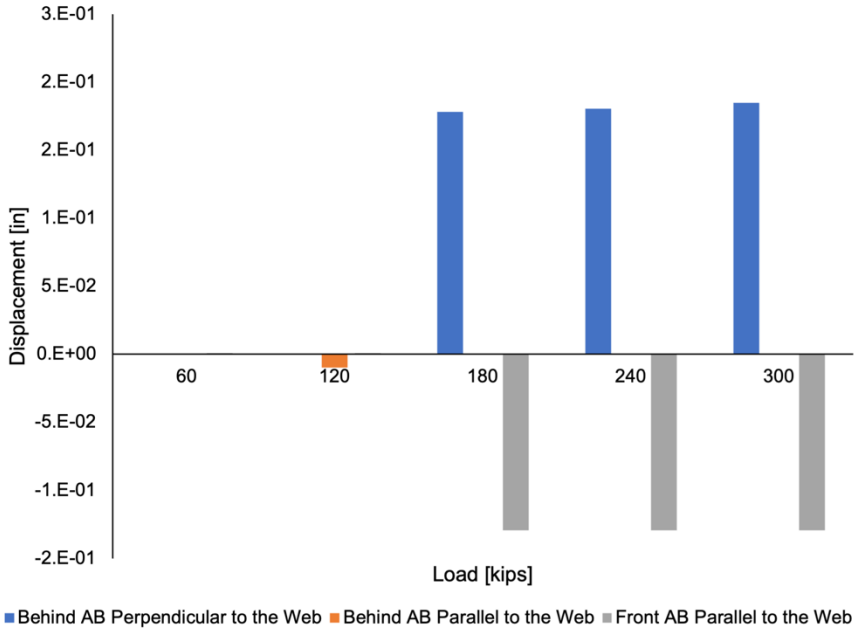

Figure C5.3. IB5 Displacement vs Stressing % "Dead End - Bay Side"

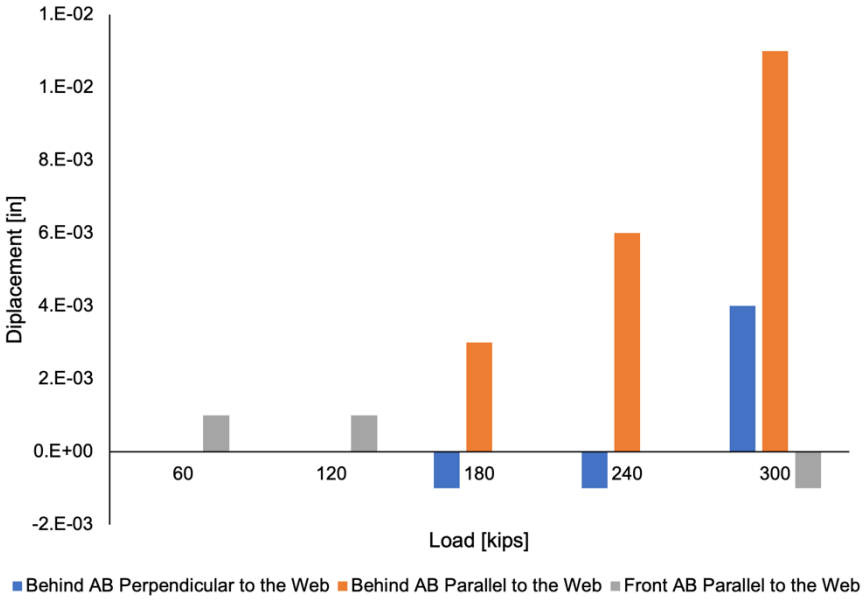

Figure C5.4. IB5 Displacement vs Stressing % "Dead End - Inland Side"

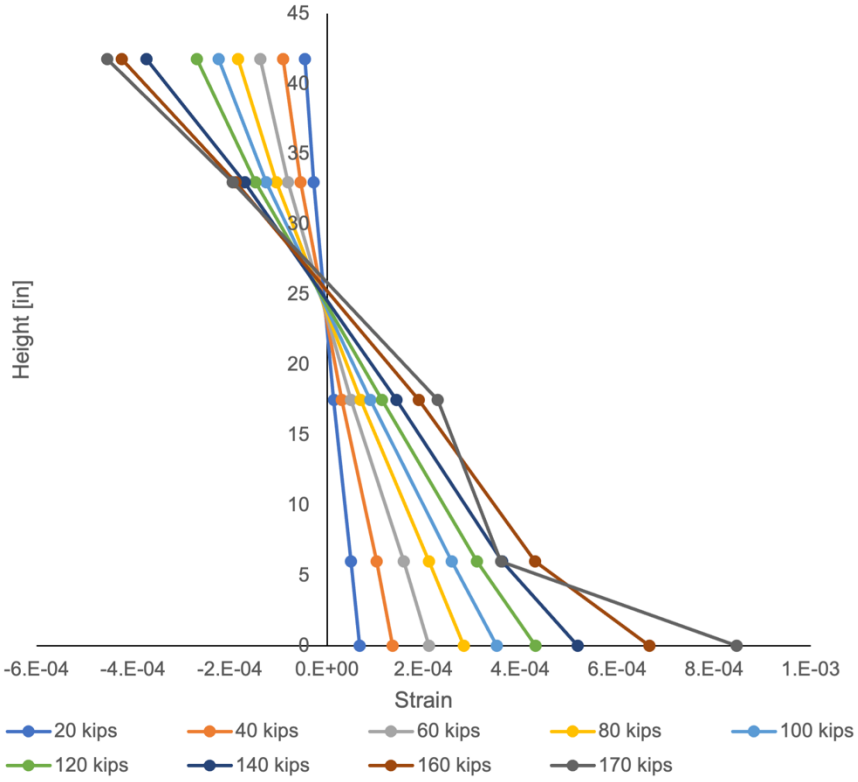

Figure C5.5. IB5 Strain vs Height

C.6 Box Beam 1 – Damaged and Unrepaired

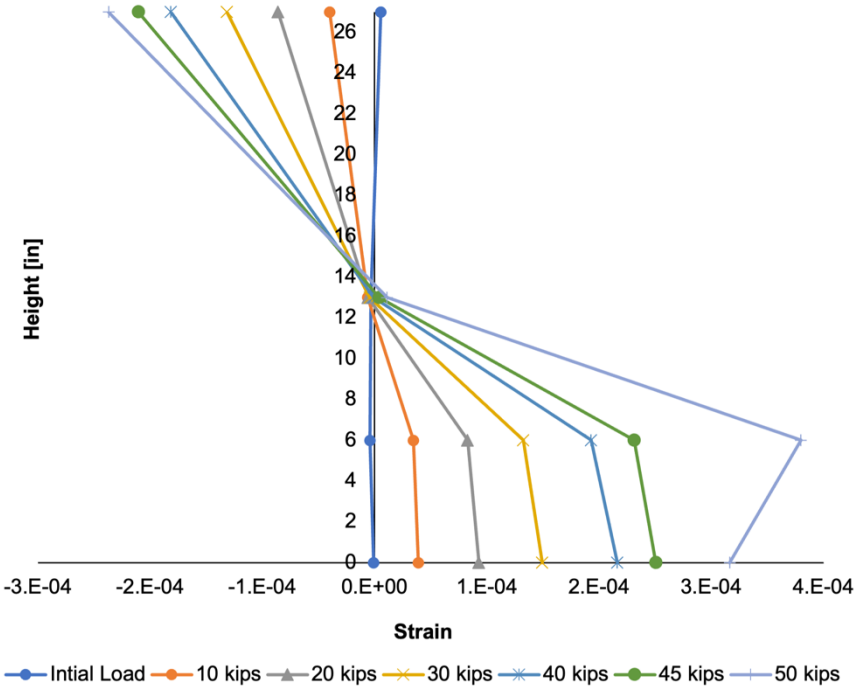

Figure C6. BB1 Strain vs Height

C.7 Box Beam 2 – Damaged and Unrepaired

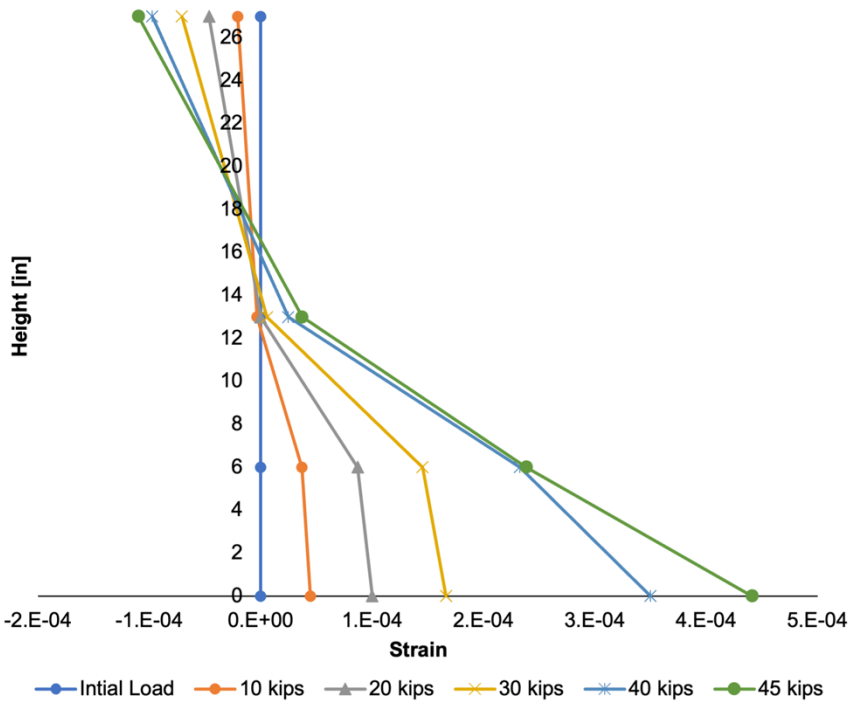

Figure C7. BB2 Strain vs Height